Mitochondrial DNA depletion mediated by herpes simplex virus type 1 UL12.5

by

Brett Adrian Kyle Duguay

A thesis submitted in partial fulfillment of the requirements for the degree of

Doctor of Philosophy

in

Virology

Department of Medical Microbiology and Immunology
University of Alberta

Abstract

Infection with herpes simplex virus type 1 (HSV-1) leads to the rapid and complete loss of mitochondrial DNA (mtDNA) and mitochondrial messenger RNA (mt-mRNA), effectively eliminating gene expression within mitochondria. Previous work determined that a unique 3' co-terminal transcript arising from within viral alkaline nuclease gene *UL12* produced an amino (N)-terminally truncated viral protein, termed UL12.5, which was responsible for mtDNA loss. The UL12 and UL12.5 proteins share the same open reading frame (ORF); however, translation initiation of UL12.5 occurs from the codon equivalent to UL12 M127. The N-terminal truncation of UL12.5 relative to UL12 unmasks a sequence which targets UL12.5 to mitochondria. My working hypothesis stated that UL12.5 localizes to the mitochondrial matrix, in close proximity to mtDNA, to nucleolytically degrade mitochondrial genomes. When I began this research it was clear that UL12.5 caused mtDNA loss by localizing to mitochondria. However, it was unclear how and why UL12.5-mediated mtDNA loss occurred. The data presented in this thesis firstly, support our earlier work and demonstrate that the mitochondrial localization of UL12.5 is controlled by an N-proximal mitochondrial localization sequence (MLS). Furthermore, while this MLS possesses many hallmarks of a mitochondrial matrix targeted protein, UL12.5 does not appear to simply translocate into the mitochondrial matrix. Secondly, inconsistent with the hypothesis, I observed that UL12.5 could cause mtDNA loss in the absence of its inherent nuclease activity, which suggested that cellular nucleases were involved in this process. In support of this revised hypothesis, I

discovered that mtDNA loss by UL12.5 was facilitated by the mitochondrial nucleases endonuclease G (ENDOG) and endonuclease G-like 1 (EXOG). Finally, following the construction of a UL12.5-null HSV-1 mutant virus impaired in the ability to cause mtDNA depletion, I observed that the elimination of mtDNA is not required for viral replication. Altogether, the research presented in this thesis support a unique and complex mechanism employed by the HSV-1 UL12.5 protein to destroy mtDNA. These data also leave open the possibility that mtDNA loss may have a significant role in HSV-1 replication *in vivo*.

To my daughters Amelia and Madeleine,

May your lives be enriched by science in the same way that mine has been.

Acknowledgements

I am very grateful to my Ph.D. advisor, Dr. Jim Smiley, for providing me with the opportunity to pursue a career in science. I have been fortunate to work with someone whose passion for science and teaching is both indisputable and infectious. I am proud at how much I learned through his guidance and am appreciative to him for his patience while I matured as a scientist. As well, I must acknowledge the guidance offered from my other supervisory committee members: Drs. Michele Barry and Bart Hazes.

I have worked with some truly amazing people both in and out of the lab over the years. Above all, I must thank Holly Bandi (née Saffran) for her invaluable technical assistance and her uncanny ability to locate just about anything in the lab. For being a great friend from the very beginning, I must thank Meaghan Hancock. Thank you to Rob Maranchuk for keeping the lab running smoothly during our time together. Thank you to all those who contributed to this work namely, Shayla Duley, Alina Ponomarev, Heather Eaton, and Jennifer Corcoran. Also, I must show my great appreciation for the continual support provided by the administrative staff of the Department of Medical Microbiology and Immunology. In particular, I thank Anne Giles for her thoughtful guidance.

Many individuals have contributed reagents for my research and as such I would like to thank Drs. Lori Frappier, Britt Glaunsinger, David Leib, Nikolaus Osterrieder, Gregory Smith, Graham Tipples, Roger Tsien, Sandra Weller, and John Wills for their kind contributions. I also wish to acknowledge the Government of the Province of Alberta and Alberta Innovates – Health Solutions for studentships that supported my work and the Canadian Institutes for Health Research for the operating grant which funded my lab.

My family has been very supportive of my desire to better myself through education. Although unfortunate that this journey has taken me so far from home the distance has never lessened their support.

Lastly, I lovingly thank my wife, Christine. I am incredibly blessed to have met her many years ago and even more blessed that she agreed to follow me across the country to Alberta. Christine has provided me with an immeasurable amount of support throughout this process. We have shared so many ups and downs and through them all she has always been there for me. My words will never fully express my gratitude to her.

Table of Contents

List of Tables

List of Figures

List of Abbreviations, Nomenclature, and Symbols

Δ	Delta (deletion)
APEX1/2	Apurinic/apyrimidinic endonuclease 1 and 2
BAC	Bacterial artificial chromosome
BCA	Bicinchoninic acid
ca.	Circa
CAPS	3-(Cyclohexylamino)-1-propanesulfonic acid
cDNA	Complementary DNA
CMV	Cytomegalovirus
CVSC	Capsid vertex-specific component
MT-CO2	Mitochondrially encoded cytochrome *c* oxidase subunit II gene
Cyto *c*	Cytochrome *c*
dH_2O	Distilled (Milli-Q) water
DMEM	Dulbecco's modified Eagle's medium
DMSO	Dimethylsulphoxide
DNA2	DNA replication helicase/nuclease 2
DNase	Deoxyribonuclease
DSP	Dithiobis(succinimidylpropionate)
DTT	Dithiothreitol
EBV	Epstein-Barr virus
EDTA	Ethylenediaminetetraacetic acid
EGFP	Enhanced green fluorescent protein
EGTA	Ethylene glycol-bis(2-aminoethylether)-*N,N,N′,N′*-tetraacetic acid
ENDOG	Endonuclease G
EXOG	Endonuclease G-like 1
F/L	M127F/M185L
F/L Res	M127F/M185L rescue
FBS	Fetal bovine serum
FEN1	Flap endonuclease 1
Fig.	Figure
GAPDH	Glyceraldehyde 3-phosphate dehydrogenase
gX	Glycoprotein (X = B, C, D, E, G, H, I, J, L, or M)
HCF-1	Host cell factor-1
HCMV	Human cytomegalovirus
HEL	Human embryonic lung
HHV	Human herpesvirus
hpi	Hours post-infection
hpt	Hours post-transfection
HSV	Herpes simplex virus
HSV-1	Herpes simplex virus type 1
HSV-2	Herpes simplex virus type 2
HVEM	Herpesvirus entry mediator
ICP	Infected cell protein
IF	Immunofluorescence
IP	Immunoprecipitation

IR	Inverted repeat
kbp	Kilobase pairs
KCl	Potassium chloride
KSHV	Kaposi's sarcoma-associated herpesvirus
LAT	Latency-associated transcript
LB	Lysogeny broth (also known as Luria-Bertani medium)
$MgCl_2$	Magnesium chloride
MLS	Mitochondrial localization sequence
MnSOD	Manganese superoxide dismutase
MOI	Multiplicity of infection
MOPS	3-(N-morpholino)propanesulfonic acid
mOrange	Monomeric orange fluorescent protein
miRNA	Micro-RNA
MRN	MRE11-RAD50-NBS1
mt-mRNA	Mitochondrial messenger RNA
mtDNA	Mitochondrial DNA
MTOC	Microtubule organizing centre
mtSSB	Mitochondrial single-stranded DNA binding protein
N.C.	Negative control
NaCl	Sodium chloride
NLS	Nuclear localization sequence
ORF	Open reading frame
PAA	Phosphonoacetic acid
PBS	Phosphate buffered saline
PFU	Plaque forming units
Pre-mRNA	Precursor messenger RNA
RIPA	Radioimmunoprecipitation assay
RNase	Ribonuclease
RNAi	Ribonucleic acid interference
ROS	Reactive oxygen species
RRL	Rabbit reticulocyte lysate
SDS	Sodium dodecyl sulphate
SDS-PAGE	Sodium dodecyl sulphate polyacrylamide electrophoresis
siRNA	Short interfering RNA
Sirt3	Sirtuin 3
SOX	Shutoff and exonuclease (encoded by KSHV ORF37)
SPA	Sequential peptide affinity
tGFP	Turbo green fluorescent protein
TIM	Translocase of the inner membrane
Tm	Melting temperature
TOM	Translocase of the outer membrane
TOM70	Translocase of outer mitochondrial membrane 70 homolog A
TR	Terminal repeat
U_L or UL	Unique long
U_S or US	Unique short
UV	Ultraviolet

vhs	Virion host shutoff
VP	Virion protein
VZV	Varicella-Zoster virus

The following nomenclature was used to describe genes and proteins in the text using *UL12.5* as an example:
UL12.5 gene (italicized)
UL12.5 protein (not italicized)

Chapter 1: Introduction

1.1 – *Herpesvirales*

The *Herpesvirales* is a large order of more than 100 species of viruses which infect a variety of animals, including: fish and amphibians (*Alloherpesviridae*), bivalves (*Malacoherpesviridae*), as well as birds, mammals, and reptiles (*Herpesviridae*) (1). In general, these viruses contain linear double-stranded DNA genomes encased within icosahedral capsids, which are surrounded by a proteinaceous layer, termed the tegument, and an outer envelope studded with glycoproteins (2). Viruses within this order contain genomes ranging from 124 to 295 kilobase pairs (kbp) in size and contain a series of core genes conserved among all herpesviruses that encode viral DNA replication proteins, structural virion proteins, and non-structural virion maturation proteins (2). In addition, viruses within the *Herpesvirales* encode a series of accessory genes that are involved in modulating the host cell environment (2). Herpesviruses will initially infect the host at a primary site, often as a result of close contact, which in some cases results in an asymptomatic infection. Subsequently, these viruses establish lifelong latency in the host which is characterized by an absence of viral progeny production and limited viral gene expression.

1.1.1 – The human herpesviruses

The focus of most herpesvirus research, including this study, has been on the nine human herpesviruses. These viruses are broadly classified into three subfamilies based on their tropism, growth, and characteristics of latency (Table 1.1). The human *Alphaherpesvirinae* contain the prototypical members herpes simplex virus types 1 (HSV-1) and 2 (HSV-2) in addition to Varicella-zoster virus

Table 1.1 – The human herpesviruses[a]

Subfamily – *Alphaherpesvirinae*				
Genus	Species (Official name)	Host range	Reproductive cycle	Latency cell type
Simplexvirus	Herpes simplex virus type 1 (Human herpesvirus 1)	Variable	Short	Neural
	Herpes simplex virus type 2 (Human herpesvirus 2)	Variable	Short	Neural
Varicellovirus	Varicella-zoster virus (Human herpesvirus 3)	Variable	Short	Neural
Subfamily – *Betaherpesvirinae*				
Genus	Species	Host range	Reproductive cycle	Latency cell type
Cytomegalovirus	Human cytomegalovirus (Human herpesvirus 5)	Restricted	Long	Multiple tissues
Roseolovirus	Human herpesvirus 6A	Restricted	Long	Leukocytic
	Human herpesvirus 6B	Restricted	Long	Leukocytic
	Human herpesvirus 7	Restricted	Long	Leukocytic
Subfamily – *Gammaherpesvirinae*				
Genus	Species	Host range	Reproductive cycle	Latency cell type
Lymphocryptovirus	Epstein–Barr virus (Human herpesvirus 4)	Restricted	Medium	B-cells
Rhadinovirus	Kaposi's sarcoma-associated herpesvirus (Human herpesvirus 8)	Restricted	Medium	Lymphoid

[a] Adapted from (1, 2)

(VZV). HSV-1 and HSV-2 are known as the causative agents of cold sores and genital herpes, respectively; however, in rare cases these viruses can infect brain tissue causing potentially lethal encephalitis (3). Primary infection with VZV often occurs during childhood or adolescence and results in varicella (chickenpox). Reactivation of VZV from latency results in herpes zoster (shingles) and is characterized by a painful self-limiting dermatomal rash. In some instances, nerve pain may persist long after the rash has subsided (postherpetic neuralgia); however, incidences of this complication and herpes zoster have declined due to the availability of effective VZV vaccines (4).

The *Betaherpesvirinae* contain four species known to infect humans. The prototypical member of this family is human cytomegalovirus (HCMV). This virus is prevalent within the population and is of significant concern for infants, where it can cause congenital abnormalities, and for older individuals who are immunocompromised. Human herpesvirus 6A (HHV-6A), 6B (HHV-6B), and 7 (HHV-7) are all highly related, T lymphotrophic viruses within the genus *Roseolovirus*. Recently, HHV-6A and HHV-6B were reclassified as distinct species due to their distinct epidemiological and biological characteristics (5, 6). The majority of HHV-6 infections occur early in life and proceed asymptomatically; however, some instances of HHV-6B infection can lead to roseola in infants (7). Interestingly, HHV-6 is one of a select group of human herpesviruses that is known to integrate into chromosomes with frequencies up to 1% (8, 9). HHV-7 is more distantly related to HHV-6A and HHV-6B, less well characterized, and has only been associated with a few clinical conditions (10).

The human gamma*herpesvirinae* are composed of two species: Epstein-Barr virus (EBV) and Kaposi's sarcoma-associated herpesvirus (KSHV). Both viruses primarily infect and establish latency in lymphoid cells. EBV is well known for its ability to cause infectious mononucleosis, which most often occurs in adolescents, and has been associated with numerous cancers (11). KSHV is the etiological agent of Kaposi's sarcoma (12), a common secondary infection in patients with acquired immunodeficiency syndrome. An interesting feature of these gammaherpesviruses is that after establishing latency the viral genome is maintained in the nucleus as episomes tethered to host chromosomes (13).

As the *Simplexviruses* HSV-1 and HSV-2 are the primary focus of this study, the introduction to the virion, the viral life cycle, and viral interactions with the host will focus primarily on data obtained using these two viruses.

1.2 – The herpes simplex virus virion

As mentioned above, the herpes simplex virus (HSV) virion is an enveloped virus containing an internal tegument layer and a nucleocapsid (Fig. 1.1A). The mature virion is roughly spherical and averages 186 nm in diameter with an estimated 595 to 758 viral glycoproteins protruding an additional ca. 20 nm from the surface (14). Under the surface, the tegument occupies roughly two-thirds of the total interior volume with the rest occupied by the icosahedral nucleocapsid (14).

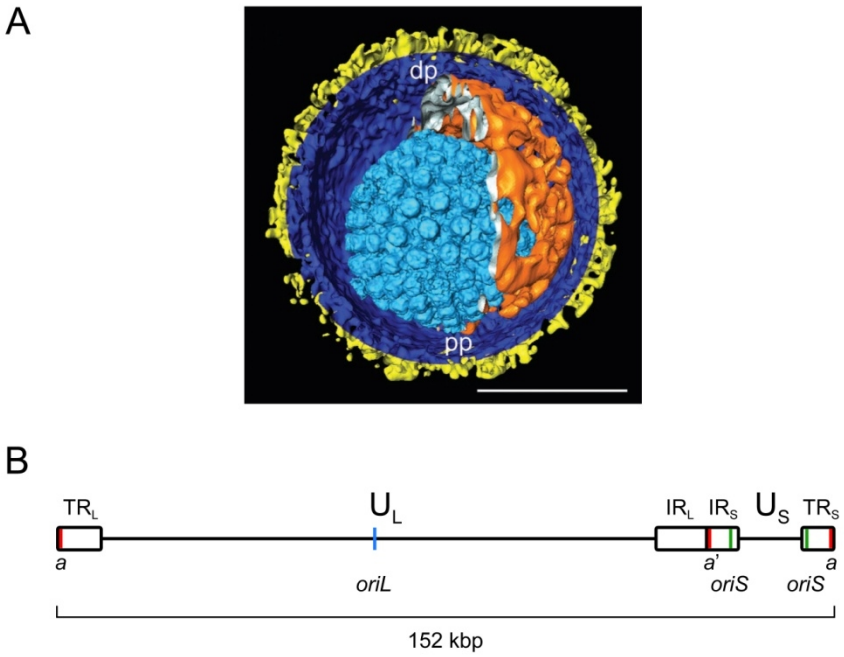

Figure 1.1. HSV-1 virion and genomic structure. (A) Cryo-electron tomography image of the HSV-1 virion. The glycoprotein spikes (yellow), envelope (blue), tegument (orange), and capsid (light blue) are indicated. dp, distal pole; pp, proximal pole. Scale bar = 100 nm. Image was adapted from **Grunewald** *et al*. 2003. Three-dimensional structure of herpes simplex virus from cryo-electron tomography. Science **302**:1396-1398. Reprinted with permission from AAAS. (B) Simplified schematic of the HSV-1 linear double-stranded DNA genome. U_L, unique long; U_S, unique short; TR_L, terminal repeat flanking U_L; IR_L, inverted repeat flanking U_L; IR_S, inverted repeat flanking U_S; TR_S, terminal repeat flanking U_S; *a*, *a* sequence (red, two copies); *a*', inverted *a* sequence (red); *oriL*, origin of replication within U_L (blue); *oriS*, origin of replication flanking U_S (green, two copies). Features are drawn to scale. Sequence information for HSV-1 strain 17 (reference sequence NC_001806.1) was obtained from the National Center for Biotechnology Information database.

1.2.1 – The viral genome

The viral genome of HSV is comprised of DNA and is linear and double-stranded (15). The approximate genome size of HSV-1 is 152 kbp (16-22) whereas HSV-2 is 154-155 kbp (23, 24). The physical organization of the genome is depicted in Fig. 1.1B and consists of unique long (U_L) and short (U_S) regions flanked by terminal repeat (TR) and inverted repeat (IR) regions (25). Within these repeat regions there exists one or more copies of the HSV *a* sequence (26, 27), a recombinogenic sequence (28) which mediates the inversion of the U_L and U_S regions during infection (29-31). The *a* sequence also contains the signals for viral DNA processing and packaging (32-35). The HSV genome also contains three origins of replication, one located within the U_L region (termed *oriL*) and two identical copies flanking the U_S region (both termed *oriS*) (36-39).

The HSV genome encodes approximately 85 proteins, 8 known non-coding RNAs, and a variety of microRNAs from both the sense and anti-sense strands of the genome (40). The majority of these genes encode single products and do not contain introns, however some exceptions exist (40). The HSV genome is also quite dense from a genetic standpoint in that some proteins are produced from clusters of 3' co-terminal transcripts, such as the region which encodes UL11, UL12.5, UL12, UL13, and UL14 (Fig. 1.2 and references 41, 42).

1.2.2 – The capsid

The capsid is a protein shell assembled within the nucleus from 162 individual subunits ordered in T=16 icosahedral symmetry which surrounds the viral genome (40). The outer portion of the mature capsid is comprised of

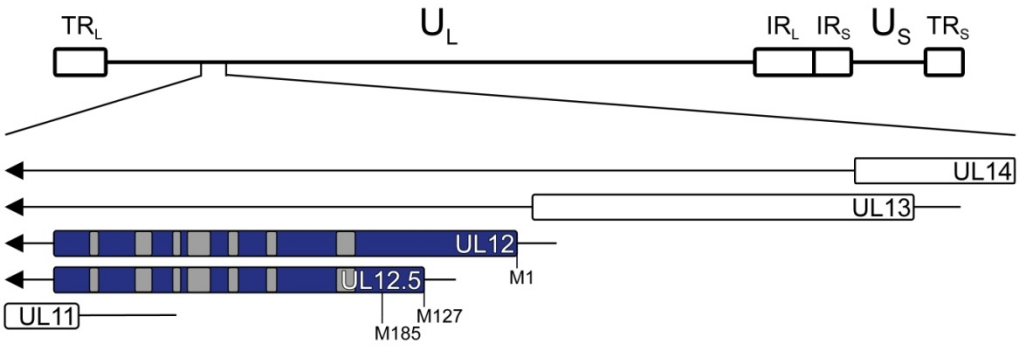

Figure 1.2. Physical location of the *UL12* and *UL12.5* loci in the HSV-1 genome. An expanded view of the U_L region spanning nucleotides 24800-28915 which encodes the overlapping, 3' co-terminal transcripts of *UL14*, *UL13*, *UL12*, *UL12.5*, and *UL11* is shown. Transcripts are indicated by lines with arrowheads. Open reading frames are indicated with boxes within the transcript. The proteins encoded by *UL12* and *UL12.5* (shown in blue) share the same open reading frame and contain seven nuclease motifs (shown in grey) conserved among all UL12 orthologs (43, 44). The positions of the initiator methionine for UL12 (M1), the initiator methionine of UL12.5 (M127), and the next in-frame methionine residue (M185) are indicated with all numbering relative to the UL12 protein. Features are drawn to scale. Sequence information for *UL14*, *UL13*, *UL12*, and *UL11* was obtained from the National Center for Biotechnology Information database (reference sequence NC_001806.1) and for *UL12.5* from (42).

multiple copies of six viral proteins: the major capsid protein virion protein 5 (VP5), the minor capsid proteins VP26, VP23, and VP19C (45), the DNA portal protein UL6 (46), and the scaffold-shaping protease VP24 (47, 48). The portal is comprised of twelve UL6 subunits, found only at a single vertex, and is the site of DNA packaging and release (46, 49). Additional viral proteins associated with the capsid include components of the terminase complex (UL15, UL28, and UL33) involved in DNA packaging (50) and the heterodimer of UL25 and UL17 which represent the capsid vertex-specific component (CVSC; (51)).

1.2.3 – The tegument

The tegument is acquired at various sub-cellular locations during nucleocapsid egress including the nucleus, the cytosol, and cytoplasmic membranes (52-60) and contains more than twenty viral proteins as well as some cellular proteins (61, 62). The tegument proteins are uniquely positioned to immediately influence both cellular and viral processes following virus entry by remaining near the plasma membrane, associated with the nucleocapsid, or within the cytosol (63-65). Examples of functions of tegument proteins include the activation viral gene expression (VP16 protein), the regulation of host and viral messenger RNA (mRNA) turnover (virion host shutoff (vhs) protein), and the modulation of host immune responses (viral protein kinases UL13 and US3 and infected cell protein 34.5 (ICP34.5)) (66). This semi-structured collection of proteins is held together through heteromeric associations (67) and is positioned within the virion through associations between nucleocapsid proteins UL36 and UL37 (68) and viral glycoproteins (69-71). Following virion release the tegument

undergoes a structural transformation to form a mature asymmetrical arrangement around the nucleocapsid (72).

1.2.4 – The virion envelope

The virion envelope has a phospholipid content similar to that of the Golgi network (73) and contains multiple copies of numerous viral proteins including: glycoprotein B (gB), glycoprotein C (gC), glycoprotein D (gD), glycoprotein E (gE), glycoprotein G (gG), glycoprotein H (gH), glycoprotein I (gI), glycoprotein K (gK), glycoprotein L (gL), glycoprotein M (gM), UL20, US9, and potentially UL24, UL34, and UL43 (40). As the nucleocapsid, tegument proteins, and glycoproteins congregate at cellular membranes, the process of final assembly and envelopment can occur (see section 1.3.1.8).

1.3 – The herpes simplex virus life cycle

Following primary infection of host cells, herpesviruses undergo tightly controlled, temporally-demarcated, waves of viral gene expression (74) that are followed by virion assembly and the release of progeny virions from the infected cell. At the site proximal to the primary infection, lytic replication will continue through cell to cell spread. Alternatively, progeny virus can travel to distal sites within the central nervous system to establish life-long latency within the host.

1.3.1 – HSV lytic replication: An overview

For HSV to infect cells, initial attachment to the host cell occurs through viral glycoproteins and their cognate cell surface receptors. Subsequently, fusion between the viral envelope and cellular membranes follows and the viral

nucleocapsid and tegument are released into the interior of the host cell. Once the capsid reaches the nucleus, the viral genome is injected into the nucleus where viral gene expression initiates. The immediate early (α) genes are transcribed first, followed by the early (β) genes, and subsequently the late (γ) genes (74). Replicated viral DNA is packaged into capsids in the nucleus, the nucleocapsid is transported to and enveloped in the cytoplasm, and the virion is released from the host cell following a membrane fusion event.

1.3.1.1 – HSV attachment and entry into the host cell

Attachment of HSV to host cells occurs initially through interactions between the viral proteins gC, and to a lesser extent gB, and the cell surface glycosaminoglycans heparan sulfate, chondroitin sulfate, and/or dermatan sulfate (75-81). Recently, gB has been shown to mediate subsequent virion "surfing" along plasma membrane filopodia until engagement with secondary receptors occurs (82). All of these initial interactions serve to tether the virion to the cell surface, placing the virion in a position conducive to initiating membrane fusion.

Following tethering, gD associates with either the herpesvirus entry mediator (HVEM) (83-85), nectin-1 (85, 86), nectin-2 (87, 88), or 3-O-sulfated heparan sulfate (89, 90). Interaction of gD with one of these receptors is a prerequisite for the initiation of membrane fusion, a process that is performed through the cooperation of glycoproteins gD, gB, gH, and gL (91). Crystal structures of free gD ectodomain as well as it bound to either HVEM or nectin-1 have demonstrated that these associations induce conformational changes in gD (92-95). This "activated" form of gD then modulates the activity of the

heterodimer gH/gL through an unknown mechanism, which in turn activates the trimeric class III membrane fusion protein gB (96-99). Recent work has also implicated gM and the small membrane-bound tegument protein UL11 (100) in enhancing the efficiency of viral entry (101). Much of the work outlined above has focused on HSV entry via fusion with the plasma membrane. Two alternative routes of entry for HSV have also been proposed involving the endosomal pathway (102, 103) and macropinocytosis (104).

1.3.1.2 – Transport of the nucleocapsid to the nucleus

In order to replicate within the cell, the viral genome must be transported into the nucleus. To reach its destination, the nucleocapsid exploits the cellular microtubule network (105, 106) and the dynein/dynactin minus-end-directed transport complex (107) to transit to the microtubule organizing centre (MTOC). How the nucleocapsid associates with dynein and/or dynactin still remains to be elucidated; however, the large tegument protein UL36 may be involved. After the initial stages of entry, UL36 disassociates from the viral envelope and maintains its association with the nucleocapsid throughout transport to the nuclear pore (108). Moreover, in the absence of UL36 nucleocapsids were no longer targeted to the nucleus (108). Once at the MTOC, the nucleocapsid shifts to plus-end-directed microtubule transport to finish the journey to the nuclear pore. At this point, the nuclear-localization signal (NLS) of UL36 appears to facilitate transport to and/or association with the nuclear pore since nucleocapsids containing UL36 ΔNLS mutants congregate at the MTOC (109).

The final role for the nucleocapsid during entry is to associate with the nuclear pore complex and release the genome into the nucleus. This process has been reconstituted *in vitro* and was shown to involve the cellular proteins importinβ and Ran-GTP (110). Moreover, *in vivo* studies have demonstrated the importance of the cellular nucleoporins Nup214 and Nup358 as well as the viral proteins UL36 and UL25 in uncoating (111-114). The UL25 protein associates with UL36 and UL6, and this complex is likely the link between incoming capsids and the nuclear pore (113, 115, 116). Subsequent proteolysis of UL25 and UL36 has been proposed to be a prerequisite for viral DNA release (49, 117). Once the viral genome enters the nucleus it adopts a compact and potentially circular form (118-120) and is immediately modified by cellular proteins involved in chromatinization (121, 122). Furthermore, compaction of the viral genome has also been recently observed *in vivo* using atomic force microscopy (123). Important to note is that it is currently unclear if circular genomes are competent for lytic phase replication (124).

1.3.1.3 – Initiation of viral gene expression: The α genes

At this point in the HSV life cycle, depending on the environment and cell type, the viral genome can continue on towards lytic replication and the production of progeny virus or it can enter a latent state marked by limited viral gene expression and no progeny virus production (discussed in section 1.3.2).

The initial activation of α gene synthesis is mediated by the viral tegument protein VP16 (125). Following release into the cytoplasm during virion entry, VP16 forms a complex with host cell factor-1 (HCF-1) and the cellular

transcription factor Oct-1 which initiates α gene transcription through recruitment of host RNA polymerase II (126-129). All α genes contain the *cis*-regulatory motif 5'TAATGARAT, which is crucial for VP16 transactivation of α gene expression (130-132). Of the six α genes which encode infected cell protein (ICP) 0, 4, 22, US1.5 (a truncated version of ICP22, 133), ICP27, and ICP47, all but ICP47 are required for the activation of β and/or γ gene expression (40). The α gene products also perform a variety of important functions outside their roles in viral gene expression however these are outside the scope of this review (40).

1.3.1.4 – Viral DNA replication: The β genes

The next group of viral genes which are expressed are the β genes. Activation of β promoters is dependent on ICP0 and ICP4 (134-139); however, ICP27 also has a role in modulating β gene expression (140, 141). The majority of β genes require α gene expression prior to their expression (74). A notable exception is the β gene *UL39* (which encodes ICP6) that has been shown to be minimally responsive to VP16; however, expression was upregulated by ICP0 (142). Some β genes encode proteins essential for viral DNA replication which include the DNA polymerase (*UL30*, *UL42*), the single-stranded DNA binding protein (*UL29*), the helicase/primase (*UL5*/*UL8*/*UL52*), and the origin binding protein (*UL9*) (143). The remainder of the proteins encoded by β genes are not essential for viral DNA replication and have roles in regulating the cellular nucleotide pool (deoxyuridine triphosphatase, *UL50*; thymidine kinase, *UL23*; and ribonucleotide reductase, *UL39*/*UL40* (144-148)), in promoting viral DNA maturation (alkaline nuclease, *UL12* (section 1.3.1.7 and references 149, 150)),

viral DNA maintenance (uracil N-glycosylase, *UL2* (151)), as well as in causing mtDNA depletion (*UL12.5* (see section 1.5.2.2 and reference 152)).

The generation of progeny genomes occurs in nuclear replication compartments which contain numerous viral and cellular proteins (153-157). At these sites, UL9 associates with *oriL* or either of the copies of *oriS* (158-160). This association then leads to unwinding of the DNA duplex by UL9 helicase activity, which is subsequently stimulated by the single-stranded DNA binding protein, ICP8 (161, 162). Next, the helicase/primase complex (163) further unwinds the duplex at the replication fork and creates 6-12 base oligoribonucleotide primers for DNA synthesis (164-166). These primers then serve as the template for viral DNA synthesis by the viral DNA polymerase complex, consisting of the DNA polymerase/proof-reading exonuclease/ ribonuclease (RNase) H (UL30; 167, 168) and the processivity factor (UL42; 169). It has also been demonstrated *in vitro* that the viral polymerase complex, helicase/primase complex, and ICP8 can mediate coordinated leading and lagging strand synthesis where the latter is impaired by high concentrations of ICP8 (170).

While the synthesis of viral DNA at the level of the replication fork appears relatively straight-forward, the overall mechanism of the replication of the entire viral genome is not as clear. Previous work has shown that HSV DNA forms “endless” structures following viral entry into the cell consistent with circularization of the genome (118-120). Subsequently, rolling circle replication leads to the formation of longer-than-unit-length concatemeric DNA. Recent work demonstrating that a host DNA ligase IV is involved in HSV DNA replication

supports the circularization model (171). However, it has also been proposed that these "endless" DNA structures may be formed through recombination (124). Interestingly, replication intermediates of HSV genomes have been shown to possess highly branched structures (172, 173). Moreover, cellular recombination and repair proteins are known to be involved in and recruited to sites of viral DNA replication (156, 157, 174, 175). It is still unclear what the initial fate of viral DNA is following entry into the nucleus; however, the unique viral DNA structures that occur during replication and the involvement of cellular proteins involved in DNA recombination and repair clearly demonstrate that DNA replication and recombination are tightly linked during HSV infection.

1.3.1.5 – Late gene expression: The γ genes

The products of the γ genes include proteins required for the assembly of the mature virion, such as tegument, capsid, and envelope proteins, in addition to some that disrupt cellular process during viral replication (40). The immediate-early protein ICP22 and the viral protein kinase UL13 appear to play a role in directing RNA polymerase II to transcribe γ genes (176). Moreover, work by Knipe and colleagues is supportive of a role for ICP8 as a regulator of γ gene transcription (177-180). While some γ gene expression is dependent on viral DNA replication having occurred (classified as true-late or γ_2 genes), some γ genes can be transcribed even when DNA synthesis is impaired (defined as leaky-late or γ_1 genes) (181). The distinct expression of γ_1 genes as compared to γ_2 genes is likely due to different *cis*-acting regulatory elements within their promoters (182-188).

1.3.1.6 – Capsid assembly

Once the viral genome has been replicated and the capsid proteins have been produced, assembly of the nucleocapsid proceeds in the nucleus. Initially, the capsid is assembled from the various capsid proteins (see section 1.2.1.2). It has been proposed that capsid assembly initiates from the portal complex to ensure the incorporation of a single portal in the mature capsid (189). As capsid assembly proceeds, four distinct types of HSV capsids have been observed in infected cells: the procapsid, A-capsid, B-capsid, and C-capsid, and these structures represent different maturational stages of virion assembly. The procapsid is the first and least stable capsid intermediate and, while it contains all capsid proteins, looks spherical as opposed to icosahedral (190). Both A- and B-capsids are icosahedral and lack DNA; however, B-capsids contain a cleaved form (VP22a) of the minor scaffold protein VP22 (45). A-capsids which contain no protein or DNA in their interiors are thought to be the by-products of aborted attempts to package viral DNA. C-capsids represent the mature form of the virion based on their similarity to capsids within enveloped virions and contain the full complement of viral DNA (45, 191). The breakdown of the interior scaffolding and the packaging of viral DNA have been proposed to be crucial steps in the stabilization of C-capsids (192).

1.3.1.7 – Processing and packaging of viral DNA

For DNA to be packaged into the capsid, the viral genome must be converted from a branched concatemeric structure to linear unit-length genomes. The resolution of DNA branches is thought to occur through the activity of the

viral alkaline nuclease, UL12, as viral replication defects and abnormal genome structures occur in cells infected with UL12-null mutant viruses (149, 150, 193, 194). UL12 has been demonstrated *in vitro* to nucleolytically degrade various branched DNA structures (195); however, it is also possible that the *in vivo* association of UL12 and ICP8 (196), which has been proposed to function as a resolvase (197-199), participates in the resolution of these viral DNA replication intermediates.

The processing of concatemeric viral DNA and packaging of unit-length genomes is a concerted process involving the viral proteins UL6, UL15, UL17, UL25, UL28, UL32, and UL33 (200). The HSV terminase complex and the portal protein UL6 associate (201-203) which is thought to bring the replicated DNA into close proximity with the capsid. The terminase complex then scans the concatemer for the site-specific cleavage sites termed *pac1* and *pac2* (35, 204), similar to the proposed scanning action of the bacteriophage λ terminase (205). The HCMV terminase complex protein UL89 (orthologous to HSV UL15) has been demonstrated to process DNA (206, 207) and the UL15 C-terminal domain has been demonstrated *in vitro* to possess nuclease activity (208) supportive of a role for HSV UL15 in concatemer cleavage during packaging. However it remains unclear how the site-specific cleavage required to create unit-length genomes is achieved.

1.3.1.8 – Nuclear egress and envelopment of HSV

Following assembly, the nucleocapsid must exit the nucleus and acquire the viral envelope. The most well-supported model for HSV envelopment

involves successive envelopment, de-envelopment, and re-envelopment steps at the inner nuclear membrane, outer nuclear membrane, and cytoplasmic membranes, respectively (40). Prior to budding through the nuclear membranes, the nuclear lamina is disrupted through the actions of the viral proteins UL31, UL34, US3 (209-211), and cellular kinases of the protein kinase C family (212, 213). The localization of UL31 and UL34 to the nuclear rim (214, 215) facilitates the recruitment of mature nucleocapsids through associations with the CVSC (216). These viral proteins are also required for efficient localization of gD and gM to the inner nuclear membrane (217). Subsequently, the nucleocapsid buds into the perinuclear space through the inner nuclear membrane (218, 219). Although it remains to be fully elucidated how nucleocapsids exit the nucleus, evidence suggests that this process involves de-envelopment at the outer nuclear membrane (220) which may be regulated by gB and gH (221).

The site of re-envelopment in the cytosol has been proposed to occur at the *trans*-Golgi network or endosomes (218, 222-225). This theory is consistent with the phospholipid content observed in virions (73). The viral glycoproteins gB, gD, gE, gI, gK, and gM as well as UL11, UL20, and UL37 have all been implicated in secondary cytoplasmic envelopment during egress (226-234). Cytoplasmic re-envelopment is thought to create a vesicular enveloped virion which is transported to the plasma membrane via exocytosis and ultimately released from the cell (40).

1.3.2 – HSV latency

Following primary lytic infections virions can travel to and infect sensory neurons which innervate the site of primary infection; these are often neurons of the trigeminal ganglion. Following HSV-1 infection, vesicle-contained virions (and to a lesser extent unenveloped nucleocapsids) then travel through the neuron cell body to the nucleus (235, 236). The subsequent expression of the latency-associated transcript (LAT), the repression of lytic gene expression, and the absence of viral progeny define the latent state (237-239).

The factors that lead to the establishment of latency are poorly understood. It has been proposed that an inability of VP16 to reach the nucleus (240) or the reduced availability of HCF-1 and Oct-1 (241, 242) in neurons may inhibit the induction of α gene expression thereby resulting in the establishment of latency. In the absence of α gene expression and the observation of euchromatic modifications at the *LAT* (243, 244), LAT can be expressed which supports the establishment of latency (245). Moreover, a progressive accumulation of heterochromatin has been observed on viral genomes during latency, which may be regulated by the expression of LAT (246, 247). In infections with LAT-null HSV-1 mutant viruses, the absence of LAT reduces the establishment of latency and results in increased neural cell death (248). Therefore, it is likely that a combination of viral and host proteins contribute to the establishment of latency.

The maintenance of latency is thought to be governed through the functions of LAT and cellular factors such as: repressive neuronal transcription factors (249, 250) and/or persistent inflammatory responses in trigeminal ganglia

(251-253). In humans, stressors such as infection, fever, ultraviolet (UV) exposure, tissue damage, and potentially emotional stress are thought to facilitate reactivation of latent HSV-1 (254). At a molecular level, HSV gene expression in acutely infected neurons does not appear to follow the same temporal cascade observed in other cells undergoing lytic replication (255, 256). While the viral proteins ICP0 (257, 258) and ICP4 (253) have been implicated in efficient reactivation, atypical regulation of the *UL48* gene (encoding VP16) and reduced reactivation of VP16 mutants *in vivo* also support a role for VP16 in initiating reactivation (259, 260).

1.4 – Herpesvirus modulation of host nuclear gene expression

Unlike during latency in which the host exerts control over viral gene expression, during productive infection herpesviruses must effectively compete for limited resources while counteracting host anti-viral defences to facilitate their replication. Global analyses of host gene expression during HSV-1, HSV-2, HCMV, and KSHV lytic infection have demonstrated that numerous host transcripts are up- and down-regulated following infection in cell culture (261-264), highlighting the dynamic interaction between virus and host.

1.4.1 – Messenger RNA processing, export, and silencing

At the transcriptional level, aberrant phosphorylation of RNA polymerase II by UL13 coordinated by ICP22 facilitates recruitment of the polymerase to viral genes (154, 176). Moreover, ICP22 also facilitates the sequestration of positive transcription elongation factor b which is then redirected to α gene

promoters in the presence of VP16 (265, 266). These events combine to result in a shift of RNA polymerase II directed transcription from host to viral genes.

Herpesviruses have also been observed to inhibit host gene expression post-transcriptionally within the nucleus (267-269). The processing of cellular precursor mRNAs (pre-mRNAs) is tightly regulated to ensure that only properly capped, spliced, and cleaved mRNAs are exported from the nucleus (270). However, the majority of herpesvirus transcripts lack introns (271-274) allowing these transcripts to bypass the splicing stage of mRNA processing. The inhibition of pre-mRNA splicing during infection is mediated through associations between ICP27 and splicing factors which inhibits spliceosome assembly (275-279). At later times post-infection ICP27 facilitates the export of intronless viral mRNAs by recruiting the RNA export factor Aly/REF to viral mRNAs and mediates their export through the TAP/NXF1 export machinery (280, 281).

Micro-RNAs (miRNAs) are another method used by herpesviruses to silence host gene expression. Numerous host transcripts have been demonstrated or predicted to be silenced by viral miRNAs produced by HSV-1, HCMV, EBV, and KSHV (282-288). Altogether, these viral miRNAs contribute to immune evasion, cell cycle regulation, inhibition of apoptosis, and promotion of viral gene expression.

1.4.2 – Cytoplasmic messenger RNA turnover

Within the cytoplasm, herpesviruses also facilitate the turnover of cytoplasmic mRNAs through orthologs of the HSV-1 endoribonuclease vhs (289-294). Following entry into the cell, vhs (a tegument protein) is released into the

cytosol where it causes accelerated mRNA turnover. The current view is that vhs targets actively translating mRNAs through its association with host translation initiation factors (295-297). A comprehensive understanding of all the cellular processes affected by vhs remains to be elucidated; however, vhs has been shown to inhibit the production of antiviral cytokines and chemokines (298-300), double-stranded RNA recognition (301, 302), NFκB activation (303), tetherin expression (304), and the activation of dendritic cells (303, 305, 306).

vhs also destabilizes viral transcripts during infection (307, 308); however, at late times post-infection vhs associates with VP16 and facilitates the translation of true-late viral transcripts ensuring adequate γ_2 gene expression (309-311). Altogether, these effects help redirect the cellular gene expression machinery toward the expression of viral genes.

1.5 – Herpesviruses and mitochondria

Disrupting host gene expression is one method used by herpesviruses to inhibit cellular functions. However, for important cellular processes such as those controlled by mitochondria, human herpesviruses have evolved multiple layers of regulatory control. These include the capacity to regulate the function of multiple nucleus-encoded mitochondrial proteins as well as the ability to disrupt mitochondrial gene expression (see sections 1.5.2 and 1.5.3.5).

1.5.1 – The mitochondrion

Mitochondria are small cytoplasmic organelles that are thought to have originated from the engulfment of an α-Proteobacterium by an amitochondriate

host cell (312). Through evolution, mitochondria have been established as integral components of higher eukaryotes and serve as key regulators of cellular energy production, apoptosis, anti-viral signalling, intermediary metabolism, and calcium homeostasis (313). Morphologically, these organelles are delineated by two membranes (termed the outer and inner mitochondrial membranes, in which the latter contains numerous invaginations termed cristae) that flank an intermembrane space and surround a central region termed the mitochondrial matrix (Fig. 1.3 and references 314, 315). The outer membrane is highly permeable and contains translocases, which facilitate the import of nuclear-encoded mitochondrial proteins translated in the cytosol (316, 317), and voltage dependent anion channels, which facilitate the passage of solutes through the outer membrane (Fig. 1.3 and references 318, 319). The inner mitochondrial membrane also contains translocases that direct mitochondrial protein import into the mitochondrial matrix (316, 317) as well as protein complexes involved in solute transport (320), the export of proteins from the matrix (321), and cellular ATP production (Fig. 1.3 and reference 322). The intermembrane space is important in redox control and mitochondrial protein sorting (323) in addition to containing various proteins important for apoptosis such as apoptosis inducing factor (324), cytochrome *c* (325-327), endonuclease G (ENDOG) (328-330), DIABLO (331, 332), and Omi (333-336). The mitochondrial matrix contains roughly two to four copies of mitochondrial DNA (mtDNA) (337-341), the proteins involved in its replication and transcription, and the factors required for the translation of mitochondrial messenger RNAs (mt-mRNAs) (Fig. 1.3).

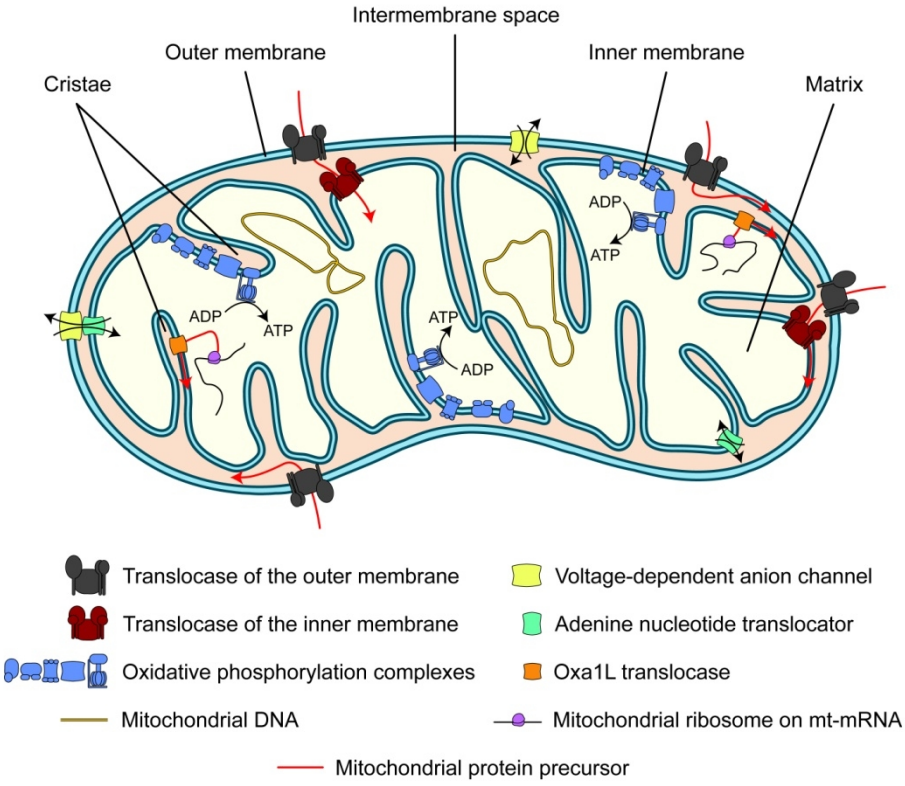

Figure 1.3. Mitochondrial structure and features. Shown is a simplified diagram of a mitochondrion. The outer membrane, inner membrane, intermembrane space, matrix, and various proteins and present in mitochondria are indicated. Mitochondrial DNA (gold lines) and mitochondrial messenger RNAs (mt-mRNAs, black lines associated with mitochondrial ribosomes (purple)) are found in the matrix. The passage of solutes through the outer and inner membranes is facilitated by the voltage-dependent anion channel (yellow) and the adenine nucleotide translocator (green), respectively. ATP production occurs in the matrix from the combined action of the oxidative phosphorylation complexes (blue). The paths followed by mitochondrial protein precursors (red arrows) during import from the cytosol through the translocases of the outer (grey) and inner (maroon) membranes or export from the matrix (following translation on mitochondrial ribosomes) through the Oxa1L translocase (orange) are shown.

1.5.2 – Herpesvirus modulation of mitochondrial function

By virtue of their importance in mediating cell death, mitochondria are targets of numerous human herpesvirus proteins which prevent the intrinsic apoptotic pathway during infection including HSV US3 and US11 (342-345), HCMV viral mitochondrion-localized inhibitor of apoptosis and the β2.7 RNA (346, 347), EBV BHRF1 (348-350), KSHV KSbcl-2, K7 and K15 (351-354). The HSV-1 US11 protein has also been shown to be important in down-regulating mitochondrial anti-viral signalling dependent on RIG-I-like receptors (355).

HSV and KSHV have also been demonstrated to inhibit aspects of oxidative phosphorylation (356-358) and mitochondrial calcium uptake (359) while also modulating reactive oxygen species (ROS) levels (360, 361). Interestingly, although HCMV infection leads to an increased flux through the tricarboxylic acid cycle and induction of mitochondrial biogenesis (362, 363), this virus ultimately inhibits mitochondrial ATP synthesis (364, 365). At a structural level, alterations in the morphology of mitochondria or the mitochondrial network are also known to occur following HSV, HCMV, HHV-6B, and EBV infection which are likely indicative of significant changes in mitochondrial function by this family of viruses (356, 366-369).

1.5.3 – Herpesvirus modulation of mitochondrial gene expression

In addition to inhibiting the expression and function of nuclear genome-encoded mitochondrial proteins, some human herpesviruses have been recently demonstrated to directly regulate gene expression within mitochondria. Although the vast majority of a eukaryotic cell's coding potential lies in DNA located

within the nucleus, mitochondrial genomes also have vital roles in overall mitochondrial function. As will be discussed in more detail, HSV and EBV disrupt mitochondrial gene expression as part of the global host shutoff mechanism during infection (see section 1.5.2.2).

1.5.3.1 – Mitochondrial gene expression

As endosymbiosis was established between the host cell and the α-Proteobacterium, much of the endosymbiont genome was transferred to the nucleus (370) resulting in the small, circular, double-stranded, mtDNA genome (Fig. 1.4 and reference 371). MtDNAs are transcribed and translated within mitochondria with the assistance of proteins encoded by nuclear genes, which are translated on cytoplasmic ribosomes and actively imported into mitochondria (Fig. 1.3 and reference 317). MtDNA genes are tightly packed into the human mitochondrial genome with only a few bases separating neighbouring genes (Fig. 1.4 and reference 372). As a result, the mitochondrial transcription apparatus generates polycistronic pre-mRNAs that are processed and modified to yield all thirteen mitochondrial mRNAs, two ribosomal RNAs, and twenty-two transfer RNAs (Fig. 1.4 and reference 373). To produce proteins, the mitochondrial translation apparatus within the matrix utilizes a unique genetic code to generate thirteen protein subunits of the oxidative phosphorylation machinery (372, 374-376). The regulation of mitochondrial gene expression involves transcriptional and post-transcriptional mechanisms similar to those that govern nuclear gene expression; however, mitochondrial gene expression is also influenced by mtDNA

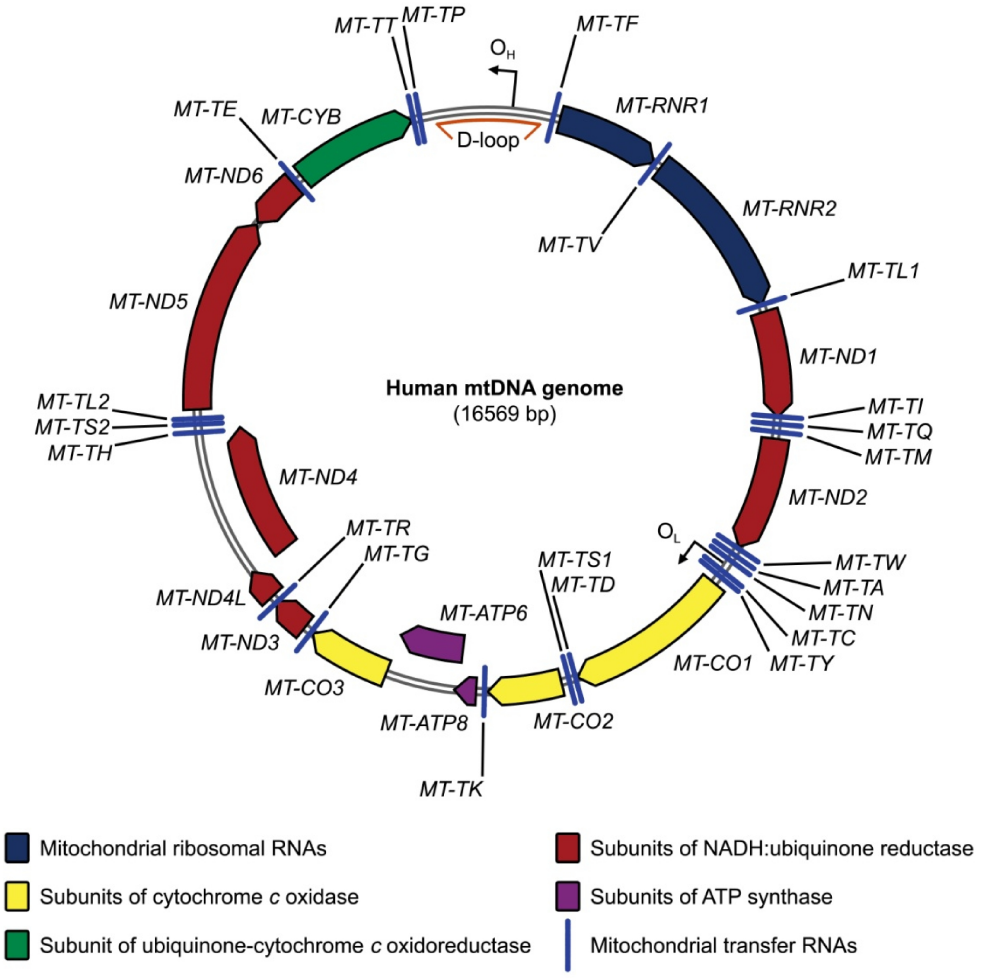

Figure 1.4. The human mitochondrial DNA genome. A map depicting the location of all mitochondria protein coding, ribosomal RNA, and transfer RNA genes as found in the human mitochondrial DNA genome is shown. The origins of heavy- (O_H) and light-strand (O_L) replication and the displacement loop (D-loop) are indicated. MT-TX, mitochondrially encoded transfer RNA (X = any amino acid); MT-RNR1-2, mitochondrially encoded ribosomal RNA; MT-ND1-6, mitochondrially encoded NADH-ubiquinone reductase subunits 1-6; MT-CO1-3, mitochondrially encoded cytochrome *c* oxidase subunits 1-3; MT-ATP6/8, mitochondrially encoded ATP synthase subunits; MT-CYB, mitochondrially encoded cytochrome *b*. Sequence information was obtained from the National Center for Biotechnology Information database (reference sequence NC_012920.1).

copy number (377). In this regard, tight control of mtDNA levels is important to maintain appropriate mitochondrial gene expression.

1.5.3.2 – Mitochondrial DNA replication

MtDNAs are associated with numerous proteins to form nucleoids similar to bacterial chromosomes (378) and are replicated independently of the cell cycle (379). Although still the subject of debate, mtDNA replication likely occurs through a mechanism with concurrent leading- and lagging-strand synthesis from independent origins of replication (380, 381) which may include RNA incorporation throughout the lagging strand (382). The minimal proteins needed for mtDNA replication have been identified *in vitro* as the mitochondrial DNA polymerase γ, the mitochondrial helicase Twinkle, and the mitochondrial single-stranded DNA binding protein (mtSSB) (383). Additional proteins also involved in replicating mtDNA include RNase H1 (384, 385), DNA ligase III (385, 386), mitochondrial topoisomerases I (387), and even the mitochondrial RNA polymerase (388). Evidence from different groups has also implicated the apoptotic nuclease ENDOG in mtDNA replication (389, 390).

1.5.3.3 – Mitochondrial DNA maintenance

Mitochondria are a major source of ROS which increases the risk for damage to mtDNA. Moreover, mtDNA has been observed to accumulate oxidative damage more readily than nuclear DNA (391, 392). To maintain mtDNA integrity, mitochondria utilize a variety of DNA repair pathways including mismatch repair, DNA strand break repair, and base excision repair. Mismatch repair in mitochondria is mediated by the Y-box-binding protein 1

(393, 394) while mtDNA strand breaks are resolved using aprataxin (395) and Cockayne syndrome proteins, CSA and CSB (396, 397). Mitochondrial base excision repair is the predominant and most thoroughly characterized repair mechanism in mitochondria and is mediated by various enzymes: uracil-DNA glycosylase 1 (398, 399), apurinic/apyrimidinic endonuclease 1 (APEX1) (400-403), flap endonuclease 1 (FEN1) (404, 405), DNA replication helicase/nuclease 2 (DNA2) (406, 407), tyrosyl-DNA phosphodiesterase (408, 409), and the mitochondrial endo/exonuclease endonuclease G-like 1 (EXOG) (410). DNA polymerase γ is responsible for all synthesis following DNA repair in addition to possessing lyase activity (411-413). The mitochondrial isoform of DNA ligase III appears to be the major contributor in lesion ligation in mitochondria (414-417). When persistent DNA damage overwhelms the repair machinery mtDNA is subsequently destroyed (418).

1.5.3.4 – Mitochondrial DNA in human disease and mitochondrial dysfunction

Since mitochondria cannot generate nucleotides *de novo*, nucleotides must either be imported from the cytosol (419, 420) or generated through the mitochondrial nucleotide salvage pathways (421, 422). As a result, mtDNA copy number is directly influenced by the availability of nucleotides in addition to the rate of replication. Mutations of proteins encoded by the nuclear genome involved in either of these two processes can cause mutations, deletions, or depletion of mtDNA, resulting in the collapse of oxidative phosphorylation and numerous debilitating or lethal diseases (423-425). At a molecular level, mtDNA depletion has been demonstrated to affect more than oxidative phosphorylation. For

example, the loss of mtDNA has also been observed to affect the regulation of apoptosis (426-436), cell cycle progression (437, 438), cancer development or progression (439-442), and insulin and glucose levels (443-446) in cell culture. Since alterations of mtDNA copy number is associated with human disease, it is important to also investigate what if any impact viral infection has on mtDNA and ultimately mitochondrial gene expression.

1.5.3.5 – Mitochondrial DNA depletion by HSV and EBV

As alluded to earlier, HSV-1, HSV-2, and EBV have evolved mechanisms to disrupt the expression of genes located in the mitochondrial genome (152, 447, 448). It was first observed by David Latchman that HSV-2 mediates a post-transcriptional decrease in mt-mRNA levels at early times post-infection (447). Almost twenty years after this initial observation, HSV-1 was demonstrated to cause a similar loss of mt-mRNA (152). Interestingly, HSV-1 and HSV-2 infected cells also displayed a coincident rapid and complete loss of mtDNA (152). A separate study also observed mtDNA loss during EBV lytic replication (448).

During EBV lytic infection, the multi-functional Zta transactivator protein (encoded by *BZLF1*) associates with the mtSSB and redirects a subset of the total pool of mtSSB to the nucleus, which was proposed to facilitate EBV replication (448). The retargeting of mtSSB to the nucleus also has a negative impact on mtDNA replication and ultimately results in mtDNA depletion during EBV lytic replication (448). However, it was noted that Zta was not sufficient to cause mtDNA loss in transfected EBV-negative cells indicating that additional viral proteins are likely involved in this process (448).

The depletion of mtDNA during HSV-1 infection is much more rapid than during EBV lytic replication, which suggested that HSV-1 mediated mtDNA loss is not the result of mtDNA replication inhibition but likely caused by active degradation of mtDNA (152). Human herpesviruses each encode PD-(D/E)XK-related deoxyribonucleases (449) referred to as alkaline nucleases (293, 450-456) due to their optimal activity in alkaline solutions (452, 457, 458). Therefore, it was plausible that a protein encoded by the HSV-1 alkaline nuclease gene, *UL12*, was involved in mediating mtDNA loss. In support of this hypothesis, no mt-mRNA or mtDNA loss was observed in cells infected with a UL12-null mutant virus (152). However, the *UL12* locus of HSV-1 encodes two highly-related proteins which are translated from two independent 3' co-terminal transcripts (Fig. 1.2 and references 41, 43). The resulting proteins, UL12 and the in-frame amino (N)-terminally truncated isoform UL12.5, share seven conserved nuclease motifs found in all UL12 orthologs (Fig. 1.2 and references 43, 44) and possess similar alkaline pH- and divalent cation-dependent 5'→3' exonuclease and endonuclease activities (458-461), with the exonuclease activity being the more robust of the two activities (452, 458, 462, 463).

1.5.3.5.1 – HSV-1 UL12: A nuclear recombinase

The UL12 protein is a phosphoprotein (464, 465) which contains an N-terminal nuclear localization sequence (196, 461). Once in the nucleus, UL12 participates in the maturation of viral DNA genomes during infection (150, 193, 194). UL12 may resolve branched viral DNA replication intermediates (150, 172, 173) through a recombination-mediated process since UL12 is capable of

mediating strand exchange in conjunction with ICP8 (197-199). In addition, UL12 associates with the host DNA damage machinery, MRE11, RAD50, NBS1, MSH3 and MSH6 (466, 467). These functions of UL12 are important for viral replication as cells infected with UL12-null mutant viruses are severely impaired (up to 1000-fold) in the generation of progeny virions and produce a disproportionately high amount of DNA-less A-capsids compared to wild-type virus infected cells (43, 149, 193, 194).

1.5.3.5.2 – HSV-1 UL12.5: The mediator of mitochondrial host shutoff

UL12.5 is expressed with β kinetics during infection comparable to UL12 (42, 459), and translation of UL12.5 initiates from UL12 codon M127 resulting in a protein lacking the N-terminal 126 amino acids of UL12 (Fig. 1.2 and references 42, 43, 468). Although this protein demonstrates similar nuclease and strand exchange activities as UL12 (461), UL12.5 cannot rescue the growth defect of UL12-null mutant viruses (43). Expression of UL12.5 is also not essential for viral replication as an HSV-1 mutant virus (M127F) with a substitution in the initiator methionine of UL12.5 reached viral titres comparable to wild-type virus (468). In contrast to the localization of UL12 to the nucleus, UL12.5 was observed to localize to the cytoplasm of transfected cells (461). Additional work by Saffran *et al*. demonstrated that UL12.5 colocalized with the mitochondrial network in both fixed and live cells (152). When UL12 and UL12.5 were tested for their ability to mediate mtDNA depletion in transfected cells, it was observed that while UL12 had little to no effect on mtDNA staining, expression of UL12.5 led to a dramatic and profound loss of mtDNA (152). Moreover, mtDNA

depletion by UL12.5 caused cells to become auxotrophic for uridine and pyruvate after two days indicative of a collapse of oxidative phosphorylation (152). These observations were similar to results obtained using mtDNA-less (rho^0) cells that were generated following long-term treatment with ethidium bromide (469). Altogether, these data indicate that UL12.5 is both necessary and sufficient to mediate mtDNA loss. By extension, UL12.5 is likely the viral protein responsible for mtDNA and mt-mRNA depletion in infected cells.

1.6 – Thesis objectives

Currently, HSV-1, HSV-2, and EBV are the only viruses known to cause mtDNA depletion of infected cells. However, the molecular basis for this process and its role in viral pathogenesis is largely unknown. To investigate these concepts further, I was tasked with elucidating the mechanism of HSV-1 UL12.5-mediated mtDNA loss and to examine the role of mtDNA depletion in HSV-1 infection. This research was divided into the following three objectives:

1) To investigate the mitochondrial localization of UL12.5. We initially hypothesized that UL12.5 localizes to the mitochondrial matrix based on its ability to mediate mtDNA depletion. However, our initial experiments did not identify a classical mitochondrial matrix targeting sequence. Therefore, I performed experiments to determine how UL12.5 localizes to mitochondria by utilizing mutagenesis to map the mitochondrial localization sequence of UL12.5 and through sub-cellular fractionation techniques.

2) To elucidate the mechanism of mtDNA loss mediated by UL12.5. The classification of UL12.5 as a nuclease led us to hypothesize that UL12.5 causes mtDNA loss by directly degrading mtDNA. To address this question, I investigated whether UL12.5 nuclease activity was required for mtDNA loss by examining the effect of various nuclease-inactivating mutations on the ability of UL12.5 to mediate mtDNA loss. The outcome of these experiments directed additional research that investigated the contribution of cellular proteins in this process.

3) To determine if mtDNA depletion is required for HSV-1 replication. Studying the role of mtDNA depletion during HSV-1 infection has been difficult due to the overlapping nature of *UL12* and *UL12.5* in the viral genome and the importance of UL12 during viral replication. To circumvent this issue, various mutations to the *UL12* gene were examined that were predicted to abrogate the expression of mtDNA depleting viral proteins while preserving UL12 function. Ultimately, an HSV-1 mutant virus was identified that was significantly impaired in its ability to cause mtDNA depletion and was used to determine whether mtDNA loss was essential for viral replication in cell culture.

Chapter 2: Materials and Methods

2.1 – List of buffers

1X Tris, acetic acid, EDTA (TAE) buffer
40 mM Tris (Invitrogen, 15504-020)
20 mM Sodium acetate trihydrate (EMD, SX0255-3)
1 mM Ethylenediaminetetraacetic acid (EDTA) dihydrate (EMD, EX0539-1)

5X Protein sample buffer
200 mM Tris-Cl (pH 6.8)
5% (w/v) Sodium dodecyl sulphate (SDS) (BIORAD, 161-0302)
50% (v/v) Glycerol (Fisher, BP229-4)
1.43 M 2-mercaptoethanol (Sigma, M3148)

10X DNA loading dye
100 mM Tris-Cl (pH 8.0)
10 mM EDTA
50% Glycerol
0.02 g (w/v) Bromophenol blue (Sigma, B6896)
0.02 g (w/v) Xylene cyanol (Sigma, X-4126)

Acid wash buffer (pH 3.0)
40 mM Citric acid (Fisher, A940)
10 mM Potassium chloride (KCl) (Caledon, 5920-1)
135 mM Sodium chloride (NaCl) (Fisher, BP358-10)

Annealing buffer (1X)
10 mM Tris-Cl (pH 8.0)
50 mM NaCl
1 mM EDTA

CAPS transfer buffer (pH 11)
10 mM 3-(Cyclohexylamino)-1-propanesulfonic acid (CAPS) (Sigma, C-2632)
10% (v/v) Methanol (Fisher, A452-4)

Digitonin lysis buffer
1 mM Sodium phosphate monobasic (NaH_2PO_4) (BDH, ACS795)
8 mM Sodium phosphate dibasic (Na_2HPO_4) (Caledon, 8120-1)
75 mM NaCl
250 mM Sucrose (EMD, SX1075-3)
190 μg/mL Digitonin (Sigma, D141)
1X cOmplete (EDTA-free) protease inhibitor cocktail (Roche, 11873580001)

Immunoprecipitation (IP) lysis buffer
50 mM Tris-Cl (pH 7.5)
150 mM NaCl
1 mM Ethylene glycol-bis(2-aminoethylether)-N,N,N',N'-tetraacetic acid (EGTA) (pH 8.0) (Caledon, 4040-5)
1% (v/v) IGEPAL CA-630 (Sigma, I-8896)
0.25% (w/v) Sodium deoxycholate (Sigma, D-6750)
1X cOmplete (EDTA-free) protease inhibitor cocktail

Luria-Bertani (LB) medium
1% (w/v) Bacto-tryptone (BD, 211705)
0.5% (w/v) Yeast extract (BD, 212750)
1% (w/v) NaCl

Luria-Bertani (LB)/agar plates
LB medium
15 g/L agar (BD, 214010)
Appropriate antibiotic: 50-100 μg/mL ampicillin (Sigma, A-9518), 30 μg/mL chloramphenicol (Sigma, C-1919), or 30 μg/mL kanamycin (Sigma, K-4000)

Mitochondria isolation buffer
10 mM HEPES (pH 7.5) (Caledon, 4080-5)
200 mM D-Mannitol (Sigma, M9546)
70 mM Sucrose
1 mM EGTA (pH 8.0)

MOPS buffer (1X) (pH 7.0)
20 mM 3-(N-morpholino)propanesulfonic acid (MOPS) (BioShop, MOP001.500)
5 mM Sodium acetate trihydrate
1 mM EDTA
0.1% (v/v) Diethyl pyrocarbonate (DEPC) (Sigma, D-5758)

Nick translation reaction buffer
33 mM Tris-Cl (pH 7.9)
10 mM Magnesium chloride ($MgCl_2$) (Caledon, 4720-1)
50 mM NaCl
33 μM dATP/dGTP/dTTP (Invitrogen)
20 μCi [α-^{32}P]-dCTP (PerkinElmer)
5U *Escherichia coli* DNA polymerase I (New England Biolabs, M0209S)

Nuclease assay buffer
50 mM Tris-Cl (pH 8.8)
10 mM $MgCl_2$
5 mM 2-mercaptoethanol

Oligo labelling buffer
44 mM Tris-Cl (pH 8.0)
4.4 $MgCl_2$
9 mM 2-mercaptoethanol
17.6 µM dATP/dGTP/dTTP
50 µCi [α-^{32}P]-dCTP (PerkinElmer)
181 mM HEPES (pH 6.6)

Phosphate buffered saline (PBS) (pH 7.4)
137 mM NaCl
2.7 mM KCl
8.3 mM Sodium phosphate dibasic (Na_2HPO_4) (Caledon, 8120-1)
1.7 mM Potassium phosphate monobasic (KH_2PO_4) (Caledon, 6660-1)

Radioimmunoprecipitation assay (RIPA) buffer
50 mM Tris-Cl (pH 8.0)
150 mM NaCl
1 mM EDTA
1% (v/v) IGEPAL CA-630
0.1% (w/v) SDS
0.5% (w/v) Sodium deoxycholate
1X cOmplete (EDTA-free) protease inhibitor cocktail

Resolving gel buffer
375 mM Tris-Cl (pH 8.8)
7.5, 10%, or 12.5% Acrylamide:Bis-Acrylamide (37.5:1) (Fisher, BP1410-1)
0.1% (w/v) SDS
0.05% (w/v) Ammonium persulfate (BIORAD, 161-0700)
0.05% (v/v) Tetramethylethylenediamine (TEMED) (EMD, 8920)

SDS-PAGE running buffer (pH 8.3)
25 mM Tris
192 mM Glycine (Roche, 03117251001)
0.1% (w/v) SDS

Stacking gel buffer
125 mM Tris-Cl (pH 6.8)
4% Acrylamide:Bis-Acrylamide (37.5:1)
0.1% (w/v) SDS
1% (w/v) Ammonium persulfate
0.1% (v/v) TEMED

Stripping buffer
62.5 mM Tris-Cl (pH 6.7)
2% (w/v) SDS
0.8% (v/v) 2-mercaptoethanol

Super Optimal broth with Catabolite-repression (SOC) medium
2% (w/v) Bacto-tryptone
0.5% (w/v) Yeast extract
8.6 mM NaCl
2.5 mM KCl
10 mM $MgCl_2$
20 mM D-Glucose (BDH, ACS369)
Tris/glycine transfer buffer (pH 8.3)
25 mM Tris
192 mM Glycine
20% (v/v) Methanol

Urea/SDS buffer
10 mM Tris-C1 (pH 7.8)
7 M Urea (GE, 17-1319-01)
350 mM NaCl
10 mM EDTA
1% (w/v) SDS

2.2 – Cell culture

All cells were maintained at 37°C with 5% CO_2 in 75 cm^2 or 150 cm^2 tissue culture flasks (Corning). Vero (African green monkey kidney epithelial) and HeLa (human cervical carcinoma (470)) cells were grown in complete media comprised of Dulbecco's modified Eagle's medium (DMEM) supplemented with 5% or 10% heat-inactivated fetal bovine serum (FBS) (Sigma, F1051), respectively. Human embryonic lung (HEL) fibroblasts were grown in DMEM supplemented with 10% FBS and 1 mM sodium pyruvate (Gibco, 11360-070). MRC-5 (human fetal lung) fibroblasts (471) were grown in DMEM supplemented with 5% FBS, 1 mM sodium pyruvate, and 0.1 mM non-essential amino acids (Gibco, 11140-050). The EBV-positive cell line B95-8 (marmoset leukocyte, 472) was maintained in HEPES-buffered RPMI 1640 medium (Gibco, 22400-089)

supplemented with 10% FBS and 2 mM L-glutamine (Gibco, 25030-081). The cell line Cre-Vero, which stably expresses the Cre recombinase (473), was grown similarly to Vero cells, except for supplementation with 400 μg/mL hygromycin B (Invitrogen) at every fifth passage to maintain the transgene. The UL12 complementing cell line 6-5 (193) was maintained in complete Vero medium supplemented with 250 ug/mL G418 (Gibco). Vero cells and 6-5 cells were also supplemented with 100U/mL penicillin/streptomycin (Gibco). Cell lines were obtained from the following sources: American Type Culture collection (HEL, HeLa, MRC-5, and Vero), Dr. David Leib (Cre-Vero), Dr. Jutta Prieksatis (B95-8), and Dr. Sandra Weller (6-5).

Cells were grown in culture flasks until confluency was reached. Once confluent, cells were washed once with phosphate buffered saline (PBS), followed by one wash with Trypsin-EDTA (Gibco), and then incubated at 37°C for approximately five minutes. The cells were resuspended in the appropriate growth medium and reseeded between 10-20% confluency with the addition of growth medium up to 12.5 mL (75 cm^2 flask) or 25 mL (150 cm^2 flask). B95-8 cells were grown until confluency was reached and then processed for DNA isolation. No passaging of this cell line was performed.

Prior to seeding cells in dishes or plates for experiments, the concentration of cells was determined using a hemocytometer (Hausser). Cells were mixed 1:1 with 0.4% trypan blue solution (Sigma, T8154). The number of viable cells was determined from the mean of two counts, multiplied by both the hemocytometer conversion ($1x10^4$) and the dilution factor of 2.

2.3 – DNA methods and techniques

2.3.1 – Polymerase chain reactions

All standard polymerase chain reactions (PCRs) were performed using Platinum *Pfx* DNA Polymerase (Invitrogen) under the following conditions: 1X *Pfx* Amplification Buffer (Invitrogen), 0.3 mM each of deoxyadenosine triphosphate (dATP), deoxycytidine triphosphate (dCTP), deoxyguanosine triphosphate (dGTP), and deoxythymidine triphosphate (dTTP), 0.25-2.5 mM $MgCl_2$, 0.3 μM of each primer, 10-100 ng template DNA, 1-2.5 units (U) *Pfx* polymerase, 0-3X Enhancer solution (Invitrogen), with distilled water (dH_2O) to adjust to a final volume of 50 μL. Following an initial denaturation step at 94°C for up to 5 minutes, three-step cycling (95°C for 15 seconds (denaturation), lowest primer melting temperature (Tm) minus ≤5°C for 30 seconds (annealing), 68°C for 1 minute per kbp of DNA (extension)) was performed for a total of 25-35 cycles followed by incubation at 4°C.

Site-directed mutagenesis was performed in two ways. The first method used the QuikChange site-directed mutagenesis kit (II or XL, Stratagene) and PCR to mutate the desired open reading frame (ORF) using complementary primers containing the desired mutations according to the manufacturer's guidelines, unless otherwise indicated. The second method used overlap PCR as previously described (474). Briefly, to generate the desired mutation, the ORF of interest was amplified using *Pfx* DNA polymerase in two separate reactions that generate overlapping portions of the ORF where the internal primers contain the mutated sequence. The resulting overlapping PCR products are then combined in

equimolar ratios and reamplified using external primers to generate the full-length mutagenized ORF.

PCRs products were examined using agarose gel electrophoresis to determine if the appropriate product was present (section 2.3.4). When one product was present, the DNA was purified using the QIAquick PCR Purification Kit (QIAGEN). When multiple products were present, the appropriate DNA was isolated by gel extraction (section 2.3.4).

2.3.2 – Restriction endonuclease digestions

All restriction endonuclease digestions were performed with commercially available enzymes using the conditions recommended by the manufacturer. Double digestions were performed concurrently when both enzymes displayed optimal activity in a common reaction buffer. For sequential restriction digestions, the first digestion reaction was performed followed by purification of the DNA using a QIAquick PCR Purification Kit (QIAGEN) prior to the subsequent digestion reaction. Typically, digestion reactions were performed for one hour at the temperature recommended by the manufacturer.

2.3.3 – Isolation of total cellular DNA

Cells for DNA isolation were lysed in Urea/SDS lysis buffer. Total cellular DNA was first sheared using QIAshredder columns (QIAGEN), followed by two extractions with phenol:chloroform:isoamyl alcohol (25:24:1) (Sigma), one chloroform extraction, and subsequent precipitation with 95% ethanol. The precipitated DNA was resuspended in 0.3 M sodium acetate, treated with 10

mg/mL RNase A for 45 minutes at 37°C, followed by precipitation in 95% ethanol, and resuspension in dH_2O.

2.3.4 – Agarose gel electrophoresis and gel extraction of DNA

Agarose gels were made by dissolving 0.5-2% (w/v) agarose in 1X TAE buffer followed by the addition of 0.5 μg/mL ethidium bromide (Sigma, E-8751). The agarose gels were submerged in 1X TAE buffer and DNA samples containing 1X DNA loading dye (diluted from a 10X stock) were loaded into the well. The GeneRuler 1kb DNA Ladder Plus (Fermentas, SM1333) was used approximate the size of the DNA fragments. Agarose gels were run between 70-80V (small gels) or 80-120V (large gels) for up to two hours. For some applications, DNA in gels lacking ethidium bromide was stained following electrophoresis in 1X TAE containing 0.5 μg/mL ethidium bromide for 30 minutes at room temperature. All ethidium bromide stained DNA was visualized using an ImageQuant 300 imager (GE Healthcare). When additional sensitivity was required, DNA in gels was stained with SYBR Gold (used as 20000X stock, Invitrogen, S11494) diluted in 1X TAE buffer for 15-40 minutes and the DNA signal visualized using a FLA-5100 imager (Fujifilm).

When required, DNA bands were excised from the agarose gel and processed using a Gel Extraction Kit (QIAGEN) following the manufacturer's guidelines. All DNA samples were resuspended in 10 mM Tris-Cl (pH 8.5).

2.3.5 – Plasmids

All plasmids used over the course of this study are listed in Table 2.1. The pEGFP-C1 mammalian expression vector was obtained from Clontech. The

Table 2.1 – Expression plasmids used in this study

Plasmid	Description	Source
pEGFP-C1	CMV promoter; kanamycin resistance; expresses EGFP; for expression *in vivo*	Clontech
pOP1EGFP	Derived from pEGFP-C1; expresses residues M185 to L214 of the UL12.5 MLS fused to a C-terminal EGFP	This study (2.3.8.1)
pOP2EGFP	Derived from pEGFP-C1; expresses residues M215 to R245 of the UL12.5 MLS fused to a C-terminal EGFP	This study (2.3.8.1)
pOP1OP2EGFP	Derived from pEGFP-C1; expresses residues M185 to R245 of the UL12.5 MLS fused to a C-terminal EGFP	This study (2.3.8.1)
pSAK	Derived from pEGFP-C1; lacks *EGFP* ORF; for expression *in vivo*	S. Weller (461)
pSAK tGFP	Expresses turbo GFP (tGFP); epitope control for experiments using tGFP fusion proteins	This study (2.3.8.2)
pSAK MnSOD-tGFP	Expresses MnSOD fused to a C-terminal tGFP	This study (2.3.8.2)
pSAK Sirt3-H248Y-tGFP	Expresses a catalytically-inactive version of sirtuin 3 fused to a C-terminal tGFP	This study (2.3.8.2)
pSAK UL12/12.5	Expresses wild-type UL12 derived from HSV-1 KOS	S. Weller (461)
pSAK UL12.5	Expresses wild-type UL12.5 derived from HSV-1 KOS	S. Weller (461)
pSAK UL12.5-ΔN	Expresses UL12.5 lacking residues W128-R148; nuclease-deficient	This study (2.3.8.2)
pSAK UL12.5-EGFP	Expresses UL12.5 fused to a C-terminal EGFP	S. Weller (461)
pSAK UL12.5-R→A-EGFP	Expresses UL12.5 containing R188A/R192A/R196A/ R199A/R200A mutations within the MLS which is fused to a C-terminal EGFP	This study (2.3.8.2)
pSAK UL12.5-R→N-EGFP	Expresses UL12.5 containing R188N/R192N/R196N/ R199N/R200N mutations within the MLS which is fused to a C-terminal EGFP	This study (2.3.8.2)
pSAK UL12.5-ΔMLS-EGFP	Expresses UL12.5 lacking residues R188-R212 of the MLS fused to a C-terminal EGFP	This study (2.3.8.2)
pSAK $UL12_{M185}$-EGFP	Expresses $UL12_{M185}$ fused to a C-terminal EGFP	This study (2.3.8.2)
pSAK $UL12_{M215}$-EGFP	Expresses $UL12_{M215}$ fused to a C-terminal EGFP	This study (2.3.8.2)
pSAK UL12.5-D340E-mOrange	Expresses UL12.5 containing the D340E mutation fused to a C-terminal mOrange protein; nuclease-deficient	J. Corcoran (475)
pSAK UL12.5-G336A/S338A-mOrange	Expresses UL12.5 containing the G336A/S338A mutations fused to a C-terminal mOrange protein; nuclease-deficient	J. Corcoran (475)
pSPUTK	*In vitro* expression vector; ampicillin resistance; contains SP6 promoter and the *Xenopus* β-globin 5' untranslated region	Stratagene
pSPUTK UL12.5 ΔC	Expresses UL12.5 lacking residues P578-R626; nuclease-deficient; *in-vitro* transcription only	This study (2.3.8.3)
pcDNA-Orange	Expresses monomeric Orange (mOrange) protein from the pcDNA3.1(-) vector	H. Saffran (152)

Table 2.1 – Expression plasmids used in this study, *continued*

Plasmid	Description	Source
pcDNA3.1/*myc*-His(-) version A	CMV and T7 promoters; ampicillin resistance; used to generate fusion proteins with C-terminal c-myc/6x His tags; for expression *in vitro* or *in vivo*	Invitrogen
pcDNA3.1(-) UL12	Expresses UL12	This study (2.3.8.4)
pcDNA3.1(-) UL12.5	Expresses UL12.5	This study (2.3.8.4)
pcDNA3.1(-) UL12.5-L150K	Expresses UL12.5 containing the L150K mutation; nuclease-deficient	This study (2.3.8.4)
pcDNA3.1(-) UL12.5-ΔN	Expresses UL12.5 lacking residues W128-R148; nuclease-deficient	This study (2.3.8.4)
pcDNA3.1(-) UL12.5-ΔMLS	Expresses UL12.5 lacking residues R188-R212; nuclease-deficient	This study (2.3.8.4)
pcDNA3.1(-) UL12.5-ΔC	Expresses UL12.5 lacking residues P578-R626; nuclease-deficient	This study (2.3.8.4)
pcDNA3.1(-) UL12.5-D340E	Expresses UL12.5 containing the D340E mutation; nuclease-deficient	This study (2.3.8.4)
pcDNA3.1(-) UL12.5-G336A/S338A	Expresses UL12.5 containing the G336A/S338A mutations; nuclease-deficient	This study (2.3.8.4)
pcDNA3.1(-) $UL12_{M185}$	Expresses UL12M185; nuclease-deficient	This study (2.3.8.4)
pcDNA3.1(-) ENDOG-myc-His	Expresses ENDOG fused to a C-terminal c-myc/6x His tag	This study (2.3.8.4)
pcDNA3.1(-) ENDOG-H141A-myc-His	Expresses ENDOG containing the H141A mutation fused to a C-terminal c-myc/6x His tag; nuclease-deficient	This study (2.3.8.4)
pcDNA3.1(-) EXOG-myc-His	Expresses EXOG fused to a C-terminal c-myc/6x His tag	This study (2.3.8.4)
pcDNA3.1(-) EXOG-H140A-myc-His	Expresses EXOG containing the H140A mutation fused to a C-terminal c-myc/6x His tag; nuclease-deficient	This study (2.3.8.4)
pMZS3F	CMV promoter; ampicillin resistance; used to generate fusion proteins with C-terminal sequential peptide affinity (SPA) tags	L. Frappier (476)
pMZS3F UL12-SPA	Expresses UL12 fused to a C-terminal SPA tag. Note: Generated from KOS37 SPA which contains a recoded 3' end of UL12 (see Fig. 6.8)	This study (2.3.8.5)
pMZS3F UL12.5-SPA	Expresses UL12.5 fused to a C-terminal SPA tag. Note: Generated from KOS37 SPA which contains a recoded 3' end of UL12.5 (see Fig. 6.8)	This study (2.3.8.5)
pMZS3F UL12.5-L150K-SPA	Expresses UL12.5 containing the L150K mutation fused to a C-terminal SPA tag; nuclease-deficient	This study (2.3.8.5)
pMZS3F UL12.5-D340E-SPA	Expresses UL12.5 containing the D340E mutation fused to a C-terminal SPA tag; nuclease-deficient	This study (2.3.8.5)
pMZS3F UL12.5-G336A/S338A-SPA	Expresses UL12.5 containing the G336A/S338A mutations fused to a C-terminal SPA tag; nuclease-deficient	This study (2.3.8.5)
pMZS3F UL12.5-ΔN-SPA	Expresses UL12.5 lacking residues W128-R148 fused to a C-terminal SPA tag; nuclease-deficient	This study (2.3.8.5)
pMZS3F UL12.5-ΔMLS-SPA	Expresses UL12.5 lacking residues R188-R212 fused to a C-terminal SPA tag; nuclease-deficient	This study (2.3.8.5)
pMZS3F UL12.5-ΔC-SPA	Expresses UL12.5 lacking residues P578-R626 fused to a C-terminal SPA tag; nuclease-deficient	This study (2.3.8.5)

Table 2.1 – Expression plasmids used in this study, *continued*

Plasmid	Description	Source
pMZS3F UL12$_{M185}$-SPA	Expresses UL12$_{M185}$ fused to a C-terminal SPA tag; nuclease-deficient. Note: Generated from KOS37 SPA which contains a recoded 3' end of UL12$_{M185}$ (see Fig. 6.8)	This study (2.3.8.5)
pMZS3F UL12$_{M185}$-D340E-SPA	Expresses UL12$_{M185}$ containing the D340E mutation fused to a C-terminal SPA tag; nuclease-deficient	This study (2.3.8.5)
pMZS3F UL12$_{M185}$-G336A/S338A-SPA	Expresses UL12$_{M185}$ containing the G336A/S338A mutations fused to a C-terminal SPA tag; nuclease-deficient	This study (2.3.8.5)
pMZS3F EBV-BGLF5-SPA	Expresses EBV BGLF5 fused to a C-terminal SPA tag	This study (2.3.8.5)
pMZS3F HCMV-UL98-SPA	Expresses HCMV UL98 fused to a C-terminal SPA tag	L. Frappier
pMZS3F HSV2-UL12-SPA	Expresses HSV-2 UL12 fused to a C-terminal SPA tag	This study (2.3.8.5)
pMZS3F HSV2-UL12$_{M117}$-SPA	Expresses HSV-2 UL12 lacking residues M1-P116 fused to a C-terminal SPA tag	This study (2.3.8.5)
pMZS3F KSHV-SOX-SPA	Expresses KSHV SOX (ORF37) fused to a C-terminal SPA tag	This study (2.3.8.5)
pMZS3F VZV-ORF48-SPA	Expresses VZV ORF48 fused to a C-terminal SPA tag	This study (2.3.8.5)
pcDNA3.1(+)	CMV and T7 promoters; ampicillin resistance; for expression *in vitro* or *in vivo*	Invitrogen
pcDNA3.1(+) HCMV-MLS-UL98-SPA	Expresses HCMV UL98 with an N-terminal MLS and a C-terminal SPA tag	This study (2.3.8.6)
pcDNA3.1(+) KSHV-MLS-SOX-SPA	Expresses KSHV SOX with an N-terminal MLS and a C-terminal SPA tag	This study (2.3.8.6)
pcDNA3.1(+) VZV-MLS-ORF48-SPA	Expresses VZV ORF48 with an N-terminal MLS and a C-terminal SPA tag	This study (2.3.8.6)
pcDNA4-Myc-HisA-H248Y-Sirt3	CMV promoter; ampicillin resistance; expresses a catalytically-inactive version of sirtuin 3 fused to a C-terminal c-myc/6x His tag	T. Finkel (477)
pCMV6-AC ENDOG-tGFP	CMV promoter; ampicillin resistance; expresses ENDOG fused to a C-terminal tGFP tag	OriGene
pCMV6-AC EXOG-tGFP	CMV promoter; ampicillin resistance; expresses EXOG fused to a C-terminal tGFP tag	OriGene
pUC119-AK	Contains a 3.2-kbp *Sph*I fragment of the larger *Eco*RI D fragment of HSV-1 KOS ligated into pUC119	S. Weller (43)
pF1'-CMV-AK(M127F/M185L)	Contains a UL12 gene with mutations which prevent UL12.5 (M127F) and UL12$_{M185}$ (M185L) expression	S. Weller
p*galK*	Expresses galactokinase from the prokaryotic em7 promoter	D. Court (478)

vectors pSAK, pSAK UL12/12.5, pSAK UL12.5, and pSAK UL12.5-EGFP were obtained from Sandra Weller and were created as previously described (461). The plasmids pcDNA-Orange, pSAK UL12.5-mOrange, pSAK UL12.5-D340E-mOrange, and pSAK UL12.5-G336A/S338A-mOrange were created as previously described (152). The *in vitro* transcription vector pSPUTK was obtained from Stratagene. The mammalian expression vector pcDNA3.1/*myc*-His(-) version A was obtained from Invitrogen. The plasmid pcDNA4-Myc-HisA-H248Y-Sirt3 was purchased from Addgene (plasmid 24917) (477). The plasmids pMZS3F (476) and pMZS3F HCMV-UL98-SPA were both obtained from Lori Frappier. The plasmids pCMV6-AC ENDOG-tGFP (RG205089) and pCMV6-AC EXOG-tGFP (RG224222) were purchased from Origene. The construction of the remaining plasmids is described in section 2.3.8.

2.3.6 – Ligation of plasmid DNA

Cohesive ends of plasmid DNA and PCR products were created by digestion with restriction endonucleases (section 2.3.2). For the creation of blunt ends, either DNA Polymerase I, Large (Klenow) Fragment (Invitrogen, 18012-021) or T4 DNA polymerase (Invitrogen, 18005-017) was used. Briefly, the digested DNA was incubated with 0.5 U Klenow in 50 mM Tris-Cl (pH 8.0), 10 mM $MgCl_2$, 50 mM NaCl with 17 μM dATP/dCTP/dGTP/dTTP for 15 minutes at room temperature. Alternatively, the digested DNA was incubated with 10U T4 DNA polymerase in T4 DNA Polymerase Buffer (Invitrogen; 33 mM Tris-acetate (pH 7.9), 66 mM sodium acetate, 10 mM magnesium acetate, 1 mM Dithiothreitol (DTT)) with 100 μM dATP/dCTP/dGTP/dTTP for 15 minutes at 11°C. To

prevent the recircularization of vector DNA, the 5' phosphates were removed using 1U Antarctic Phosphatase (New England Biolabs) in Antarctic Phosphatase Reaction Buffer (New England Biolabs; 50 mM Bis-Tris-Propane-Cl (pH 6.0), 1 mM $MgCl_2$, 0.1 mM $ZnCl_2$) incubated for 15 minutes at 37°C. Following either fill-in reactions or dephosphorylation reactions, the QIAquick PCR Purification Kit (QIAGEN) was used followed by elution in 10 mM Tris-Cl (pH 8.5) to remove enzymes and to exchange buffers.

Insert and vector DNAs were quantitated using a spectrophotometer prior to performing the ligation reaction. All ligations were performed using T4 DNA Ligase. For regular T4 DNA Ligase reactions, vector DNA (50-100 ng) was combined with the appropriate amount (ng) of insert DNA (ng) in 1:3 or 1:6 vector to insert ratios. The amount of insert DNA required was determined using the Ligation Calculator available at: http://www.insilico.uni-duesseldorf.de/Lig_Input.html. The insert and vector DNAs were incubated in Ligase Reaction Buffer (Invitrogen) with 1U T4 DNA Ligase (Invitrogen) overnight at 14°C for both cohesive and blunt end ligations. For Quick Ligase (New England Biolabs) reactions, similar ratios of insert to vector DNA were used as described above. The DNAs were incubated in 1X Quick Ligase Buffer (New England Biolabs; 66 mM Tris-Cl (pH 7.6), 10 mM $MgCl_2$, 1 mM DTT, 1 mM ATP, 7.5% polyethylene glycol-6000) and incubated with 2000 U Quick Ligase (New England Biolabs) at room temperature for 5 minutes. Following the ligation reactions, drop-dialysis was performed to reduce the salt concentration of each sample prior to electroporation. Briefly, each ligation reaction was placed on a 0.05 μm filter

(Millipore) floating on 500 mL 10 mM Tris-Cl (pH 8.0) which was agitated gently with a stir bar for 15 minutes.

2.3.7 – Plasmid manipulation

For transformations, plasmid DNA (ca. 1-50 ng) was diluted in 10 µL dH_2O and combined with 40 µL *Escherichia coli* (*E. coli*) strain DH5α and electroporated using a 0.1 cm cuvette and a Gene Pulser II (BIORAD). The settings used for electroporation were: 200 ohms, 25 µfaraday, and 1.8 volts. Following electroporation, bacteria were removed from the cuvette, placed into 1 mL of SOC medium, and allowed to recover for 1 hour at 37°C in a shaking incubator set at 225 rpm. An aliquot of the recovered bacteria were then plated onto Luria-Bertani (LB) agar plates containing the appropriate antibiotic and allowed to form colonies overnight at 37°C.

Colonies picked from plates were expanded in LB medium containing the appropriate antibiotic at 37°C overnight in a shaking incubator set at 225 rpm as 3-5 mL (miniprep), 50 mL (midiprep), or 100 mL (maxiprep) cultures. For long term storage, aliquots of LB bacterial cultures were mixed with glycerol to achieve a final concentration of 15% glycerol and stored at -80°C. Plasmid DNA was isolated using QIAGEN Spin Miniprep, Plasmid Midi, or Plasmid Maxi kits following the manufacturer's guidelines. All DNAs were resuspended in 10 mM Tris-Cl (pH 8.5).

2.3.8 – Construction of plasmids

All primers required for plasmid construction were synthesized by Integrated DNA Technologies and are listed in Table 2.2. All mammalian

Table 2.2 – Primers used in plasmid construction

Primer name	Sequence (5'→3')[a]
JRS77	GGAATTCCGCCACC***ATG***GAGTCCACGGGAGGCC
JRS83	GGGGTACC***TCA***GCGAGACGACCTCCCCG
JRS86	GGAATTCCGCCACC***ATG***TGGTCGGCGTCGGTGAT
JRS93	GGAATTCCGCCACC***ATG***GTGGACCGCGGACTCGG
JRS94	GGAATTCCGCCACC***ATG***GGGTTTTACGAGGCGGCC
JRS102	C***ATG***GTGGACCGCGGACTCGGTCGGCACCTATGGCGCCTGACGCGCCGC GGGCCCCCGGCCGCCGCGGACGCCGTGGCGCCCCGGCCCCT
JRS103	CATGAGGGGCCGGGGCGCCACGGCGTCCGCGGCGGCCGGGGGCCCGCG GCGCGTCAGGCGCCATAGGTGCCGACCGAGTCCGCGGTCCAC
JRS104	C***ATG***GGGTTTTACGAGGCGGCCACGCAAAACCAGGCCGACTGCCAGCTA TGGGCCCTGCTCCGGCGGGGCCTCACGACCGCATCCACCCTCCG
JRS105	CATGCGGAGGGTGGATGCGGTCGTGAGGCCCCGCCGGAGCAGGGCCCA TAGCTGGCAGTCGGCCTGGTTTTGCGTGGCCGCCTCGTAAAACCC
JRS114	C***ATG***GTGGAC**GC**CGGACTCGGT**GC**GCACCTATGG**GC**CCTGACG**GCCGC** CGGGCCCCCGG
JRS115	CCGGGGGCCCG**GC**G**GC**CGTCAGG**GC**CCATAGGTGC**GC**ACCGAGTCCG**G C**GTCCAC***CAT***G
JRS143	GGAATTCCGCCACC***ATG***GCGGCCGCCGCAACACC
JRS145	GGAATTCCGCCACC***ATG***GCACGATCGGGATTGG
JRS149	GGTCGACTCTAGGGTACCGCGAGACGACCTCC
JRS154	GGAATTCCGCCACC***ATG***GCCGACGTGGATGAGCTCG
JRS158	GGCACAGCCTCAGGTCA***CTA***CTTGTCATCGTCATCC
JRS205	GGT***ATG***GTGGAC**AA**CGGACTCGGT**AACC**ACCTATGG**AA**CCTGACG**AACA** **A**CGGGCCCCC
JRS206	GGGGGCCCG**TT**G**TT**CGTCAGG**TT**CCATAGGTG**GTT**ACCGAGTCCG**TT**GT CCAC***CAT***ACC
JRS515	GGT**ATG**GTGGAC**GCATATGCA**CCCCTCATGGGG
JRS516	CCCCATGAGGGG**TGCATATGC**GTCCAC**CAT**ACC
JRS533	CGAGACGTTCGAGCGCCAC**AAA**CGCGGGTTGCTGC
JRS534	GCAGCAACCCGCG**TTT**GTGGCGCTCGAACGTCTCG
JRS535	CGAATTCCGCCACC***ATG***CACCTGCGCGGG
JRS536	CCCGCGCAGGTG***CAT***GGTGGCGGAATTCG
JRS538	CCGATATC**TCA**ATCGATGCGGACGGGGGTAATG
JRS574	CCTCTAGAGC***CTA***CTTGTCATCGTCATCCTTGTAGTCG
JRS606	GGGGTACCGCGAGACGACCTCCCCGTCGTCGGTG
JRS607	GGGGTACCATCGATGCGGACGGGGGTAATGATCAGGGCGATCG
JRS608	AGAATTCCGCCACC***ATG***CACCTGCGCGG
JRS623	GGAATTCCGCCACC***ATG***TGGTCGGCGTCGGCGATCCCC
JRS624	GGGGTACCGCGAGACGACCTCCCCGCCGTCG
JRS625	GGGGTACCAAGCAACGGTTTCTCCGTTGC
JRS627	GGGGTACCTGGAGTTGACTCGTCGTCGGCAAAGAG
JRS628	GGAATTCCGCCACC***ATG***GAGGCCACCCCCACACC
JRS629	GGGGTACCCGGGCTGTGAGGGACGTTTGCAG
JRS714	CGAATTCCGCCACC***ATG***GAGAGCGACGAGAGCG
JRS715	GCGGTACCTTAAACTCTTTCTTCACCGGCATCTGCA
JRS719	CTAGCCTCGAGAATTCGCCACC***ATG***CTGTTTAATCTGAGGATCCTGTTAA ACAATGCAGCTTTTAGAAATGGTCACAACTTCATGGTTCGAAATTTTCGG TGTGGACAACCACTACAA

Table 2.2 – Primers used in plasmid construction, *continued*

Primer name	Sequence (5'→3')[a]
JRS720	TTGTAGTGGTTGTCCACACCGAAAATTTCGAACCATGAAGTTGTGACCAT TTCTAAAAGCTGCATTGTTTAACAGGATCCTCAGATTAAACAG***CAT***GGTG GCGAATTCTCGAGGCTAG
JRS721	GGACAACCACTACAA***ATG***GCACGATCGGGATTGG
JRS723	GGACAACCACTACAA***ATG***GAGGCCACCCCC
JRS724	GAAGGCACAGCCTCA***CTA***CTTGTCATCGTCATCCTTGTAG
JRS734	GGACAACCACTACAA***ATG***TGGGGCGTCTCGAG
JRS736	TCGAGAATTCGCCACC***ATG***
JRS737	ATTGCGGCCGC***CTA***CTTGTCATCGTCATCCTTGTAGT
JRS764	TAGTCGAATTCCGCCACC***ATG***CGGGCGCTGCG
JRS765	TACAAGCTTCGCCACC***ATG***GCTATCAAGAGTATCGCTTCCCG
JRS766	TGCGGATCCTTAAACTCTTTCTTCACCGGCATCTGCA
JRS767	AGCAAGCTTCTTACTGCCCGCCGTGATGG
JRS768	TACGGATCCCGCCACC***ATG***GCTATCAAGAGTATCGCTTCCCG
JRS769	TGCAAGCTTGGATGGCTTTCTTATCTGGGTTCCTGA
JRS770	CCGCGGT**GC**CCTGGCC
JRS771	GGCCAGG**GC**ACCGCGG
JRS772	GTCACGAGGA**GC**CATGGCTCCAG
JRS773	CTGGAGCCATG**GC**TCCTCGTGAC
JRS775	CGTACGATAT***C****TA*CTTGTCATCGTCATCCTTGTAGT
JRS870	CGACTCGAGCGCCACC***ATG***TTGAGCCGGGCAGT
JRS872	TCGAAAGCTTCCTTTTTGCAAGCCATGTATCTTTCAGTTACAT
JRS873	CGACTCGAGCGCCACC***ATG***GCGTTC
JRS874	TCGAGAATTCAGTTTGTCTGGTCCATCAAGCTTC

[a] Start/stop codons are indicated in bold italics, point mutations/insertions are indicated in bold, and restriction sites are underlined.

expression plasmids were generated to contain the Kozak consensus sequence for optimal translation initiation (CCACC; reference 479). Codon and amino acid numbering of all HSV-1 UL12.5 mutants is indicated relative to that of the HSV-1 UL12 protein.

2.3.8.1 – pEGFP-C1 plasmids

The plasmid pEGFP-C1 (Clontech) is a mammalian expression vector which expresses enhanced green fluorescent protein (EGFP) using the CMV promoter. Plasmids encoding portions of the UL12.5 mitochondrial localization sequence (MLS) (M185 to L214, M215 to R245, or M185 to R245) fused to the N-terminus of EGFP in pEGFP-C1 were constructed as follows: The *EGFP* sequence was removed from pEGFP-C1 following digestion with *Age*I and *Bgl*II, blunt ends were created for both the *EGFP* fragment and vector using Klenow, and *EGFP* was cloned into *Sma*I-digested pUC19 (Invitrogen) to create pUC19EGFP. The pEGFP-C1 vector lacking *EGFP* was religated to create pEMPTY. Pairs of complementary oligonucleotides, JRS102/JRS103 (encoding M185 to L214) and JRS104/JRS105 (M215 to R245), were incubated in equimolar ratios in annealing buffer (1X final concentration), heated to 95°C, then cooled to room temperature to generate ligation-ready duplexes with *Nco*I sites at their termini. The pUC19EGFP vector was digested with *Nco*I and the MLS encoding duplexes OP1 or OP2 were ligated in-frame with EGFP to create the intermediate plasmids pUC19OP1EGFP or pUC19OP2EGFP, respectively. The intermediate plasmid pUC19OP1OP2EGFP encoding the M185 to R245 sequence was made by ligating the OP1 duplex into *Nco*I digested pUC19OP2EGFP. The

OP1EGFP, OP2EGFP, and OP1OP2EGFP ORFs were then cloned into pEMPTY using *Hind*III and *Kpn*I sites to create pOP1EGFP (encodes M185-L214-EGFP), pOP2EGFP (encodes M215-R245-EGFP), and pOP1OP2EGFP (encodes M185-R245-EGFP), respectively.

2.3.8.2 – pSAK plasmids

The pSAK plasmid was derived from pEGFP-C1 (Clontech) through the removal of the *EGFP* ORF as previously described (461). The plasmids pSAK UL12/12.5, which contains wild-type *UL12* sequence, pSAK UL12.5, which contains wild-type *UL12.5* sequence, and pSAK UL12.5-EGFP, which encodes UL12.5 fused to a C-terminal enhanced green fluorescent protein (EGFP), were derived from HSV-1 strain KOS and have been previously described (461). The pSAK vectors encoding UL12.5-D340E-mOrange and UL12.5-G336A/S338A-mOrange also have been previously described (475).

The plasmids pSAK $UL12_{M185}$-EGFP and pSAK $UL12_{M215}$-EGFP were created by PCR using the primers JRS93/JRS149 ($UL12_{M185}$) or JRS94/JRS149 ($UL12_{M215}$) with pUC119-AK as the template. The resulting PCR products were digested with EcoRI and KpnI and ligated into pSAK UL12.5-EGFP digested with the same enzymes to create plasmids encoding $UL12_{M185}$-EGFP or $UL12_{M215}$-EGFP fusion proteins. The plasmid pSAK M185-R245-R→A-EGFP which encodes a M185-R245-EGFP fusion protein containing arginine to alanine substitutions (R188A, R192A, R196A, R199A, and R200A) within the UL12.5 MLS was created from pOP1OP2EGFP using the QuikChange II site-directed mutagenesis kit and primers JRS114/JRS115. The plasmids pSAK UL12.5-R→A-

EGFP, which encodes UL12.5-EGFP containing R188A, R192A, R196A, R199A, and R200A substitutions, and pSAK UL12.5-R→N-EGFP, which encodes UL12.5-EGFP containing arginine to asparagine substitutions (R188N, R192N, R196N, R199N, and R200N), were created from pSAK UL12.5-EGFP using the QuikChange II site-directed mutagenesis kit and primers JRS114/JRS115 or JRS205/JRS206, respectively. The plasmid pSAK UL12.5-ΔMLS-EGFP lacking in the MLS of UL12.5 (ΔMLS, deletes residues R188-R212) was introduced into pSAK UL12.5-EGFP using the QuikChange XL site-directed mutagenesis kit with primers JRS515 and JRS516. A plasmid containing the UL12 nuclease-inactivating ΔN mutation (deletes residues W128-R148 (460)) was introduced into pSAKUL12.5 using the QuikChange XL site-directed mutagenesis kit with primers JRS535 and JRS536 to create pSAK UL12.5-ΔN.

Plasmids encoding turbo green fluorescent protein (tGFP) only or C-terminal tGFP tagged proteins in the pSAK backbone were generated using PCR. A control plasmid expressing tGFP was generated by amplified the *tGFP* ORF from pCMV6-AC ENDOG-tGFP using the primers JRS714 and JRS715. The primers incorporated start and stop codons as well as restriction sites, which allowed the ORF to be ligated into *Eco*RI/*Kpn*I-digested pSAK to create pSAK tGFP. The ENDOG-tGFP ORF was amplified from pCMV6-AC ENDOG-tGFP using primers JRS764 and JRS715 and ligated into *Eco*RI/*Kpn*I-digested pSAK to generate pSAK ENDOG-tGFP. The EXOG-tGFP ORF was amplified from pCMV6-AC EXOG-tGFP using primers JRS765 and JRS766 and ligated into *Hind*III/*Bam*HI-digested pSAK to generate pSAK EXOG-tGFP. A pcDNA4

plasmid expressing a catalytically-inactive, myc-tagged version of sirtuin 3 (Sirt3-H248Y-myc) (477) was obtained from Addgene (Plasmid 24917), used as a template to amplify the Sirt3-H248Y ORF lacking the *myc* tag using primers JRS873 and JRS874, and ligated into *Xho*I/*Eco*RI-digested pSAK tGFP to create pSAK Sirt3-H248Y-tGFP. A plasmid expressing manganese superoxide dismutase (MnSOD)-tGFP was generated by PCR using pBI-EGFP-MnSOD (480) (16612, Addgene) as a template. This plasmid was amplified with primers JRS870 and JRS872 and ligated into *Xho*I/*Hind*III-digested pSAK tGFP which created pSAK MnSOD-tGFP.

2.3.8.3 – pSPUTK plasmids

The pSPUTK vector (Stratagene) is designed for efficient *in vitro* protein expression using the SP6 promoter and the *Xenopus* β-globin 5' untranslated region linked to an optimized translation initiation site (ACCAUGG) (481). A plasmid containing the UL12 nuclease-inactivating ΔC mutation (deletes residues P578-R626 from the UL12.5 protein, (460)) was created by PCR using primers JRS86 and JRS538 using pcDNA3.1(-) UL12.5 (see section 2.3.5) as a template. The PCR product was digested with *Eco*RI and *Eco*RV and ligated into pSPUTK to create pSPUTK UL12.5-ΔC.

2.3.8.4 – pcDNA3.1(-) plasmids

Plasmids expressing UL12.5 and the UL12.5 nuclease-deficient mutants UL12.5-L150K, UL12.5-ΔN, UL12.5-ΔMLS, and UL12.5-ΔC were generated in the mammalian expression vector pcDNA3.1/*myc*-His(-) version A (Invitrogen). The UL12.5 ORF was amplified by PCR from pSAK12/UL12.5 by PCR using

primers JRS86 and JRS83. The PCR product was digested with *Eco*RI and *Kpn*I and ligated into pcDNA3.1/*myc*-His(-) version A to create pcDNA3.1(-) UL12.5. The L150K mutation (460) was introduced into pcDNA3.1(-) UL12.5 using a modified QuikChange II site-directed mutagenesis protocol (482) with primers JRS533 and JRS534. To generate a pcDNA plasmid encoding UL12.5 containing the ΔN mutation, the plasmid pSAK UL12.5-ΔN was digested with *Eco*RI and *Kpn*I and the fragment coding for the ΔN mutation was ligated into pcDNA3.1(-) UL12.5 to create pcDNA3.1(-) UL12.5-ΔN. To generate a pcDNA plasmid encoding UL12.5 containing the ΔMLS mutation, the plasmid pSAK UL12.5-ΔMLS-EGFP was digested with *Eco*RI and *Age*I and the fragment coding for the ΔMLS mutation was ligated into pcDNA3.1(-) UL12.5-L150K to create pcDNA3.1(-) UL12.5-ΔMLS. To generate a pcDNA plasmid encoding UL12.5 containing the ΔC mutation, pSPUTK UL12.5-ΔC was digested with *Xba*I and *Eco*RV and UL12.5-ΔC ORF was then ligated into pcDNA3.1/*myc*-His(-) version A creating pcDNA3.1(-) UL12.5-ΔC. Cloning the UL12.5 and the UL12.5 nuclease-deficient mutant genes into pcDNA3.1/*myc*-His(-) version A in the manner described places a stop codon upstream of the *myc*-His tag coding sequence which results in the expression of untagged proteins.

Plasmids encoding C-terminally myc-tagged ENDOG and EXOG were generated by PCR amplification of pCMV6-AC-ENDOG-tGFP or pCMV6-AV-EXOG-tGFP. These PCRs introduced a 5' *Eco*RI site (ENDOG) or 5' *Bam*HI site (EXOG), and 3' *Hind*III sites to the ORFs. Amplification of the ENDOG ORF used primers JRS764 and JRS767. Amplification of the EXOG ORF used primers

JRS768 and JRS769. Plasmids encoding nuclease-deficient versions of ENDOG (ENDOG-H141A (483)) and EXOG (EXOG-H140A (484)) were generated using overlap PCR. Briefly, the ENDOG ORF was amplified by PCR using primers JRS764 and JRS771 or JRS770 and JRS767. The resulting overlapping PCR products were combined in equimolar ratios and reamplified using primers JRS764 and JRS767 to generate the ENDOG-H141A ORF. Similarly, the EXOG-H140A ORF was amplified by PCR using primers JRS768 and JRS773 or JRS772 and JRS769 and the overlapping PCR products were reamplified using primers JRS768 and JRS769. All ENDOG and EXOG ORFs were ligated into pcDNA3.1/*myc*-His(-) to create pcDNA3.1-ENDOG-myc-His, pcDNA3.1-ENDOG-H141A-myc-His, pcDNA3.1-EXOG-myc-His, and pcDNA3.1-EXOG-H140A-myc-His.

A pcDNA3.1 plasmid expressing monomeric orange (mOrange (485)) fluorescent protein (pcDNA-Orange) has been previously described (152). A pcDNA4 plasmid expressing a catalytically-inactive, myc-tagged version of sirtuin 3 (Sirt3-H248Y-myc) (477) was obtained from Addgene (Plasmid 24917).

2.3.8.5 – pMZS3F plasmids

The pMZS3F mammalian expression vector contains the CMV immediate-early promoter and encodes the sequential peptide affinity (SPA) tag composed of a calmodulin binding peptide and three modified FLAG sequences separated by a tobacco etch virus protease cleavage site (476). The UL12-SPA, UL12.5-SPA, and $UL12_{M185}$-SPA ORFs were amplified by PCR using DNA isolated from Vero cells infected with KOS37 SPA which is a mutant virus that

expresses C-terminal SPA-tagged UL12 and UL12.5 proteins (see section 2.7.4). The PCRs introduced a 5' *Eco*RI restriction site, and either a 3' *Xba*I or 3' *Bsu*36I site to the ORFs using primers JRS77 and JRS574 (UL12-SPA), JRS86 and JRS158 (UL12.5-SPA), JRS93 and JRS574 ($UL12_{M185}$-SPA). Restriction digested PCR products were ligated into pMZS3F to create pMZS3F UL12-SPA, pMZS3F UL12.5-SPA, and pMZS3F $UL12_{M185}$-SPA.

The vectors pcDNA3.1(-) UL12.5-L150K, pcDNA3.1(-) UL12.5-ΔN, pcDNA3.1(-) UL12.5-ΔMLS, pcDNA3.1(-) UL12.5-ΔC, pSAK UL12.5-D340E-mOrange, and pSAK UL12.5-G336A/S338A-mOrange were used as templates for PCRs that added 5' *Eco*RI and 3' *Kpn*I sites using the following primers: L150K, ΔMLS, UL12.5-D340E, UL12.5-G336A/S338A (JRS86 and JRS606), ΔN (JRS608 and JRS606), ΔC (JRS86 and JRS607), and $UL12_{M185}$-D340E or $UL12_{M185}$-G336A/S338A (JRS93 and JRS606). To fuse the various ORFs in-frame with the SPA tag coding sequence an intermediate cloning vector (pcDNA3.1 UL12.5-SPA) was used. This intermediate vector was created by digesting pMZS3F UL12.5-SPA with *Bsu*36I, treating with T4 DNA polymerase (Invitrogen), followed by digestion with *Eco*RI, and ligation of the UL12.5-SPA ORF into an *Eco*RI/*Sma*I digested pcDNA3.1/*myc*-His(-) version A creating pcDNA3.1 UL12.5-SPA. All PCR products were digested with *Eco*RI and *Kpn*I and ligated into the intermediate vector which contains a *Kpn*I site immediately upstream of the SPA tag coding sequence. All intermediate vectors encoding SPA-tagged proteins were digested with *Eco*RI and *Bsu*36I and ligated into the final expression vector pMZS3F to generate: pMZS3F UL12.5-L150K-SPA,

pMZS3F UL12.5-D340E-SPA, pMZS3F UL12.5-G336A/S338A-SPA, pMZS3F UL12.5-ΔN-SPA, pMZS3F UL12.5-ΔMLS-SPA, pMZS3F UL12.5-ΔC-SPA, pMZS3F $UL12_{M185}$-D340E-SPA, and pMZS3F $UL12_{M185}$-G336A/S338A-SPA.

To generate plasmids encoding SPA tagged UL12 orthologs, total DNA was isolated from Vero cells infected with HSV-2, MRC-5 cells infected with VZV, or B95-8 cells latently infected with EBV as described in section 2.3.3. The viral genes were amplified by PCR using the following primers: HSV-2 *UL12* (JRS143 and JRS624), HSV-2 $UL12_{M117}$ (JRS623 and JRS624), VZV *ORF48* (JRS145 and JRS625), and EBV *BGLF5* (JRS154 and JRS627). The plasmid pcDEF3 ORF37 (293), kindly provided by Dr. Britt Glaunsinger, was used to amplify Kaposi's sarcoma-associated herpesvirus (KSHV) *ORF37* (also known as shutoff and exonuclease (*SOX*)) using primers JRS628 and JRS629. All *UL12* orthologs were first digested with *Eco*RI and *Kpn*I and cloned into pcDNA3.1(-) UL12.5-SPA which placed the ortholog ORFs in-frame with the SPA tag coding sequence. The intermediate pcDNA3.1(-) vectors were double digested with *Eco*RI/*Bsu*36I or *Nhe*I (VZV ORF48 only) and subcloned into the expression vector pMZS3F.

2.3.8.6 – pcDNA3.1(+) plasmids

Plasmids encoding SPA-tagged UL12 orthologs containing the human ornithine transcarbamylase MLS (486) were made using overlap PCR. First, complementary oligonucleotides JRS719/JRS720 (encoding the ornithine transcarbamylase MLS) were incubated in equimolar ratios in annealing buffer (1X final concentration), heated to 95°C, then cooled to room temperature. Next,

pMZS3F plasmids encoding ORF48, UL98, and SOX were used as templates for PCR using the following primers: *ORF48* (JRS721 and JRS724), *UL98* (JRS734 and JRS724), and *SOX* (JRS723 and JRS724). The resulting PCR products, which contained 5' sequences which overlapped with the 3' sequence encoding the MLS, and the MLS duplex were combined in equimolar ratios and reamplified using primers JRS736 and JRS737 (*MLS-ORF48-SPA* and *MLS-SOX-SPA*) or JRS736 and JRS775 (MLS-*UL98-SPA*). Finally, the resulting PCR products were ligated into pcDNA3.1 (+) to create pcDNA3.1(+) VZV-MLS-ORF48-SPA, pcDNA3.1(+) HCMV-MLS-UL98-SPA, and pcDNA3.1(+) KSHV-MLS-SOX-SPA.

2.3.9 – DNA sequencing and analysis

Sequencing of DNA was performed by the Molecular Biology Service Unit in the Faculty of Science (University of Alberta) or The Applied Genomics Centre in the Faculty of Medicine & Dentistry (University of Alberta). Chromatograms were analyzed using FinchTV (Geospiza). ABI sequences generated by TAGC were processed through the basecaller PeakTrace (Nucleics) prior to sequence analysis. DNA sequences were compared to reference sequences using the ClustalW or Clustal Omega multiple sequence alignment programs or the Nucleotide Basic Local Alignment Search Tool (BLASTn).

2.3.10 – Generation of radiolabelled probes for Southern blotting

To generate end-labelled probes for Southern blotting, an oligonucleotide complementary to the mitochondrially encoded cytochrome *c* oxidase subunit

II gene (5'-GGAGTCGAAGGTCTCCTGGGTTTAAGAATAATGGGGG) was incubated with 50 μCi [γ-^{32}P]-ATP (PerkinElmer) and 20U T4 polynucleotide kinase (New England Biolabs) in 1X T4 Polynucleotide Kinase Reaction Buffer (New England Biolabs, 70 mM Tris-Cl (pH 7.6), 10 mM $MgCl_2$, 5 mM DTT) for 90 minutes at 37°C. The reaction was diluted 1:1 with 1X TAE, phenol/chloroform extracted once, and passed through an illustra NAP-5 column (GE, 17-0853-01).

To generate random-primed probes for Southern blotting, the *UL12* gene was restriction digested from pSAK UL12/12.5 using *Eco*RI and *Kpn*I. The oligonucleotide was combined with 2 μg/μL random hexamers, heated at 95°C for five minutes, and then cooled on ice. The oligonucleotide/hexamers were then incubated with oligo labelling buffer, bovine serum albumin (New England Biolabs), and Klenow for 30 minutes at 37°C. The reaction was diluted 1:1 with 1X TAE, phenol/chloroform extracted once, and passed through an illustra NICK column (GE, 17-0855-01). All radiolabelled products were quantitated using a LS6500 scintillation counter (Beckman).

2.3.11 – Southern blotting

To visualize mtDNA remaining in infected cells (Chapter 6), equivalent amounts of DNA were treated with *Hpa*I and subjected to agarose gel electrophoresis (section 2.3.4) at 70V for approximately four hours. The DNA was subsequently stained with SYBR Gold and visualized (see section 2.3.4). The gel was washed sequentially with 0.25 M HCl, 0.5 M NaOH, 1 M Tris-Cl (pH 7.4)/1.5 M NaCl, and 150 mM sodium citrate (pH 7.0)/1.5 M NaCl prior to

transferring the DNA to a GeneScreen Plus (PerkinElmer) membrane overnight followed by cross-linking with a UV Stratalinker 2400 (Stratagene). Radiolabelled probes were hybridized with membranes using ExpressHyb hybridization solution (Clontech) following the manufacturer's guidelines. Radiolabelled signals were visualized using film or a FLA-5100 imaging system (Fujifilm) following exposure to a phosphor screen. To measure mtDNA content, an oligonucleotide derived from the mitochondrially encoded cytochrome *c* oxidase subunit II gene was end-labelled using [γ-^{32}P]-ATP. The percentage of mtDNA remaining in infected cells is represented by the mtDNA:DNA ratio (*MT-CO2*/SYBR Gold) of a given sample normalized to the mtDNA:DNA ratio of mock at four hours post-infection from at least three independent Southern blots.

To visualize genetic alterations to the *UL12* gene (Fig. 6.2), equivalent amounts of DNA were treated with *Tfi*I and subjected to agarose gel electrophoresis in the presence of ethidium bromide (section 2.3.4) at 60V for five hours. The DNA signal visualized using a gel imaging system. The gel was process for Southern blotting as indicated above. Hybridization was performed using the *UL12* gene labelled with [α-^{32}P]-dCTP by random-priming.

2.3.12 – Transfection of plasmid DNA into mammalian cells

Transient transfection of plasmid DNA was performed using Lipofectamine 2000 (Invitrogen) following the manufacturer's guidelines. Both plasmids and Lipofectamine 2000 were diluted in Opti-MEM I Reduced Serum Medium (Gibco, 31985-070), incubated separately for five minutes at room temperature, and subsequently combined for twenty minutes at room temperature.

Cells were transfected between 60-80% confluency, the culture medium and transfection mix containing plasmid DNA and transfection reagent was removed five hours post-transfection, and the culture medium was replaced with the appropriate pre-warmed medium. For transfections which result in mtDNA depletion, the culture medium added at five hours post-transfection was supplemented with 50 μg/ml uridine (to compensate for the defect in pyrimidine biosynthesis) and 1 mM sodium pyruvate (a hydrogen acceptor used to regenerate oxidized nicotinamide adenine dinucleotide during anaerobic glycolysis) (469).

2.4 – RNA methods and techniques

2.4.1 – Agarose gel electrophoresis of RNA

Denaturing agarose gels were made by dissolving 1-2% (w/v) agarose in 1X MOPS buffer containing 2% (v/v) formaldehyde (Fluka, 47629) and 0.5 μg/mL ethidium bromide. RNA samples were combined with 1X MOPS, 17% formaldehyde (Sigma, F-8775), and 50% formamide (Fisher, BP227-500) and incubated at 60°C for 15 minutes. The denaturing gel was submerged in 1X MOPS and the samples were separated at 100 V for up to two hours. The RNA standard Millennium Marker-Formamide (Ambion, AM7151) was used to approximate the size of the RNA fragments. The stained RNA was visualized using a UV transilluminator.

2.4.2 – In vitro transcription

To generate DNA templates for *in vitro* transcription, plasmids encoding the protein of interest were first linearized using *Xba*I (pMZS3F UL12-SPA

plasmid), *Bsu*36I (pMZS3F plasmids encoding UL12.5 and UL12.5/UL12$_{M185}$ mutants), *Kpn*I (pcDNA3.1(-) plasmids encoding UL12, UL12.5, UL12$_{M185}$, UL12.5-ΔN, UL12.5-L150K, and UL12.5-ΔMLS), or *Eco*RV (pcDNA3.1(-) UL12.5-ΔC) to prevent run-on transcription. Using the T7 promoter present within the pMZS3F and pcDNA3.1(-) plasmids, RNA was generated using the MAXIscript T7 *In Vitro* Transcript Kit (Ambion) supplemented with 1 mM DTT and 1 U RNaseOUT recombinant ribonuclease inhibitor (Invitrogen, 10777-019) as per the manufacturer's guidelines. RNA was treated with deoxyribonuclease (DNase) I (Ambion) for 15 minutes at 37°C followed by the addition of Ammonium Acetate Stop Solution (Ambion) prior to phenol/chloroform and chloroform extractions. RNA was precipitated using isopropanol at -20°C for 15 minutes and centrifuged at 20800 × *g* for 15 minutes at 4°C. All RNAs were resuspended in dH_2O, quantitated using a spectrophotometer, and visualized in denaturing agarose gels (section 2.4.1) to verify transcript sizes.

2.5 – Protein methods and techniques

2.5.1 – Cell lysis and protein quantitation for western blotting

Transfected or infected cells were washed in PBS and lysed in RIPA buffer for 20-30 minutes on ice. Lysates were cleared by centrifugation at 20800 × *g* for five minutes at 4°C. Lysate protein concentration was determined using the Bicinchoninic Acid (BCA) Protein Assay Kit (Pierce). Briefly, 5 µL of each cell lysate or standards containing 0-40 µg bovine serum albumin were combined with 0.5 mL working reagent (Pierce) and made up to 1 mL with dH_2O. All

lysates and standards were incubated at 37°C for 30 minutes and then measured at 562 nm using a spectrophotometer. All lysates were mixed with 5X protein sample buffer prior to storage at -20°C.

2.5.2 – SDS-polyacrylamide gel electrophoresis

Proteins were separated in 7.5%, 10%, or 12.5% acrylamide gels by SDS-polyacrylamide gel electrophoresis (SDS-PAGE) using the Mini-PROTEAN Tetra Cell system (BIORAD). Protein samples containing protein sample buffer were incubated at 95°C for five minutes prior to loading. The PageRuler Prestained Protein Ladder (Fermentas, SM0671) was used as a protein ladder for each gel. Proteins were separated at approximately 150 V in SDS-PAGE running buffer until adequately resolved.

2.5.3 – Western blotting

Proteins were transferred to nitrocellulose membranes (Hybond ECL, GE Healthcare) via wet or semi-dry transfer apparatuses. All filter papers, membranes, and gels were incubated in transfer buffer for five minutes prior to transfer. For wet transfer of proteins, the sandwich consisting of filter paper, membrane, and gel were placed in a Mini Trans-Blot Cell (BIORAD) and transferred at 150 mA for two hours (CAPS transfer buffer) or 100 V for one hour (tris/glycine transfer buffer). For semi-dry transfer of proteins, the sandwich consisting of filter paper, membrane, and gel were placed in a semi-dry transfer apparatus (Tyler) and transferred at 450 mA for ca. 50 minutes.

Membranes for chemiluminescent detection were blocked in PBS containing 5% skim milk powder for one hour at room temperature. Primary

antibodies were incubated with membranes overnight at 4°C and horseradish peroxidase-conjugated goat anti-mouse or goat anti-rabbit secondary antibodies were incubated with membranes for one hour at room temperature. All antibodies were diluted in PBS containing 1% skim milk. Proteins were visualized using ECL Plus (GE Healthcare) or ECL2 (Pierce).

Membranes for infrared imaging were blocked in 1:1 Odyssey Blocking Buffer (LI-COR):Tris-buffered saline containing 0.1% Tween-20 (OBBT) for one hour at room temperature. Primary antibodies were incubated overnight at 4°C and secondary antibodies (Alexa Fluor 680 goat anti-rabbit (Invitrogen, A21076) and IRDye800 donkey anti-mouse (Rockland, 610-732-124)) were incubated for one hour at room temperature. All antibodies were diluted in OBBT. Proteins were detected using the Odyssey Infrared Imaging System (LI-COR).

For some membranes, antibodies were removed by incubation in stripping buffer at 65°C for 30 minutes. The membranes were washed with dH_2O and tris-buffered saline containing 0.1% Tween-20 then blocked prior to reprobing.

2.5.4 – Immunoprecipitations

For immunoprecipitations, transfected cells were harvested at 48 hours post-transfection, lysed with IP lysis buffer, and cleared by centrifugation at 20800 × *g* for 15 minutes. All incubations were carried out at 4°C. Antibody-protein G-agarose conjugates were formed overnight in PBS and washed three times with IP lysis buffer before use. Transfected cell lysates were incubated for 30 minutes with protein G-agarose (Roche, 05015952001) prior to incubating

with the antibody-agarose conjugates for two hours. The immunoprecipitates were washed three times in IP lysis buffer.

For immunoprecipitations following chemical cross-linking, transfected cells were harvested at 24 hours post-transfection, washed with PBS, and treated with dimethylsulphoxide (DMSO) or dithiobis(succinimidylpropionate) (DSP) in DMSO at a final concentration of 1 mM. The cells were washed with 20 mM Tris-Cl (pH 7.5) to quench the reaction. After another wash in PBS, the cells scrapped, and lysed with IP lysis buffer. Pre-clearing and the creating of antibody-protein G-agarose conjugates were performed as indicated above. Immunoprecipitations were performed overnight at 4C. The immunoprecipitates were washed three times in IP lysis buffer.

Immunoprecipitates for western blotting were resuspended in RIPA buffer containing 5X protein sample buffer and subjected to SDS-PAGE. For *in vitro* nuclease assays, after the washes in IP lysis buffer the immunoprecipitates were subsequently washed three times with 50 mM Tris-Cl (pH 8.8) prior to being resuspended in 50 mM Tris-Cl (pH 8.8) containing protease inhibitors. 5X protein sample buffer was added to an aliquot of each immunoprecipitate and subjected to infrared western blotting using rabbit anti-FLAG (Sigma, F7425) for quantitation prior to performing nuclease assays.

2.5.5 – Protein sequence analyses

The algorithm MitoProt II (version 1.101) (487) was used to determine the probability of export to mitochondria for the protein sequences of interest. This algorithm can be accessed at ihg.gsf.de/ihg/mitoprot.html. To determine the

predicted secondary structure of protein sequences of interest the algorithm PredictProtein (488) was used. The PredictProtein algorithm can be accessed at www.predictprotein.org. Helical wheel diagrams were generated using the University of Virginia Helical Wheel Applet (cti.itc.virginia.edu/~cmg/Demo/wheel/wheelApp.html).

2.6 – *In vitro* nuclease assays

2.6.1 – In vitro nuclease assays using in vitro translated proteins

SPA-tagged proteins were synthesized *in vitro* using Nuclease-treated Rabbit Reticulocyte Lysates (Promega, L4960) containing 20.4 μCi L-^{35}S-methionine (PerkinElmer), 1 U RNaseOUT (Invitrogen), and *in vitro* transcribed RNA substrates (section 2.4.3) as per the manufacturer's guidelines. Untagged UL12, UL12.5, and UL12.5 mutant proteins were synthesized using the same procedure albeit in the absence of L-^{35}S-methionine according to the manufacturer's guidelines. Following synthesis, ^{35}S-containing proteins were subjected to electrophoresis through a 7.5% polyacrylamide gel. The polyacrylamide gel was fixed with successive incubations in 50% methanol-10% glacial acetic acid for 30 minutes and 7% glacial acetic acid-7% methanol-1% glycerol for five minutes followed by drying for one hour at 80°C in a Drygel Sr. (Hoefer). The ^{35}S-methionine-containing proteins were then visualized by autoradiography.

To assay for *in vitro* exonuclease activity of the SPA-tagged proteins, 5 μL programmed rabbit reticulocyte lysate was incubated with 85 ng *Eco*RI-

linearized pUC19 and nuclease assay buffer (50 mM Tris-Cl (pH 8.8), 10 mM $MgCl_2$, 5 mM β-mercaptoethanol) for 2 h at 37°C. To assay for *in vitro* endonuclease activity, 5 μL programmed rabbit reticulocyte lysate was incubated with 150 ng pUC19 (uncut) and nuclease assay buffer for 2 h at 37°C. To assay for *in vitro* exonuclease or endonuclease activity using untagged proteins, 10 μL programmed rabbit reticulocyte lysate was incubated as indicated above with 10 ng *Eco*RI-linearized pEGFP-C1 or 10 ng pEGFP-C1 (uncut), respectively.

Following the incubations, the nuclease assays were treated in succession with 0.25 mg/mL RNase A (DNase and protease free; Fermentas, EN0531) for up to 10 minutes at 37°C, 0.5 % SDS, and 0.2 mg/mL proteinase K (Fungal; Invitrogen, 25530-015) for up to 10 minutes at 37°C. The remaining linear and circular DNA was resolved by 0.75 % agarose gel electrophoresis. For assays using SPA-tagged proteins, the DNA was electrophoresed in the presence of ethidium bromide and visualized as described in section 2.3.4. For assays using untagged proteins, the DNA was stained using SYBR Gold and visualized as described in section 2.3.4.

2.6.2 – In vitro nuclease assays using immunoprecipitated proteins

Immunoprecipitates were incubated with *Eco*RI-linearized pUC19 DNA or uncut pEGFP-C1 DNA in nuclease assay buffer for two hours at 37°C. The remaining pUC19 DNA was resolved by agarose gel electrophoresis and visualized following SYBR Gold staining (see section 2.3.4). Immunoprecipitates incubated with circular pEGFP-C1 were processed by SYBR Gold staining (see section 2.3.4) to visualize DNA quantity and migration or by nick translation to

visualize endonuclease activity. For nick translation, the immunoprecipitates were removed by centrifugation and the supernatants were incubated at room temperature for one hour in nick translation reaction buffer. DNA was isolated by phenol/chloroform extraction and resolved by agarose gel electrophoresis without ethidium bromide (section 2.3.4). The agarose gel was dried overnight, exposed to a phosphor screen, and radiolabelled DNA was visualized using a FLA-5100 imaging system.

To evaluate for the presence of topoisomerase contamination, immunoprecipitates were incubated with uncut pEGFP-C1 DNA in nuclease assay buffer for one hour at 37°C. The remaining DNA was isolated by extractions with phenol:chloroform:isoamyl alcohol (25:24:1) (Sigma) and chloroform. To each sample 20 µg of transfer RNA (tRNA) (Sigma) was added as a carrier and all nucleic acids were precipitated as indicated in section 2.3.3. The DNA/tRNA solutions were divided equally and incubated at 37°C for one hour in the presence or absence of *Eco*RI. The remaining DNA was separated by agarose gel electrophoresis, stained with SYBR Gold and visualized as described in section 2.3.4.

2.7 – Construction and manipulation of herpesviruses

Two wild-type HSV-1 strains were used in this study: the infectious bacterial artificial chromosome (BAC) derived strain KOS37 (473) obtained from David Leib and strain KOS. The HSV-2 strain HG52 was used for plasmid generation and was provided by the MRC Virology Group. The

UL12/UL12.5/UL12$_{M185}$-null virus AN1, which possesses a deletion/insertion mutation within the *UL12* ORF, was obtained from Sandra Weller (149). The parental strain of VZV-Oka was kindly provided by Graham Tipples.

2.7.1 – Infection of cells with HSV-1, HSV-2, and VZV

Cells were infected at a multiplicity of infection (MOI) of 5 or 10 with virus diluted in a small volume of serum-free medium. Adsorption was allowed to occur for one hour at 37°C in an atmosphere containing 5% CO_2. The plates, dishes, or flasks used for infection were rocked every 15 minutes to ensure even coverage of the cell monolayer with virus. After one hour, the medium was replaced with pre-warmed DMEM containing the appropriate supplementation depending on the cell type (see section 2.2). Infected cells were harvested between 4-60 hours post-infection depending on the experiment.

2.7.2 – Generating virus stocks

To generate virus stocks, Vero cells (or 6-5 cells for AN1 virus stocks) were infected at an MOI of 0.01 or 0.05 following the protocol in section 2.7.1. Once total cytopathic effect was achieved, the infected cells were detached from the surface into the growth medium and pelleted at 2000 rpm for five minutes at 4°C in a GS-6R centrifuge (Beckman). The cell pellet containing cell-associated virus was resuspended in 1 mL of serum-free DMEM per 150 cm^2 flask. The cells were subjected to three freeze (-80°C) and thaw (37°C) cycles followed by sonication three times in 20 second intervals at level 7 using a Model 550 Sonic Dismembrator (Fisher). Samples were cooled on ice between sonication steps. Debris was removed from the suspension by centrifugation for 10 minutes at 4°C

and 3000 rpm using a GS-6R centrifuge. The supernatants containing virus were aliquoted and stored at -80°C.

2.7.3 – Single-step and multi-step growth curves

Vero cells were infected at a MOI of 5 (single-step) or 0.1 (multi-step) for one hour at 37°C as described in section 2.7.1. After one hour, the monolayers were washed twice with PBS, twice with acid wash buffer, twice with DMEM, and replaced with complete Vero medium for the duration of the infection. Infected cells were harvested in the growth medium at 1.5, 4, 8, 12, 24, and 36 hours post-infection (single-step) or 4, 12, 24, 36, 48, and 60 hours post-infection (multi-step). Small virus stocks were prepared as described in section 2.7.2. Each sample was titred on UL12 complementing cell line 6-5.

2.7.4 – Construction of UL12 mutant viruses

KOS37-derived viruses KOS37 M127F/M185L (F/L), KOS37 M127F/M185L Rescue (F/L Res), and KOS37 SPA (SPA) were generated in *E. coli* strain SW102 using lambda Red-mediated homologous recombination (478; protocol available at http://ncifrederick.cancer.gov/research/brb/protocol/Protocol3_SW102_galK_v2.pdf). All primers required for virus construction were synthesized by Integrated DNA Technologies and are listed in Table 2.3.

To generate the F/L BAC, *galK* was amplified by PCR from p*galK* (478) using primers JRS199 and JRS200 and inserted into the KOS37 BAC between *UL12* codons 126 and 186 (Fig. 6.1). Next, the plasmid pF1'-CMV-AK(M127F/M185L) was used to generate a PCR product using primers JRS201 and JRS202 to replace *galK* seamlessly with the desired mutated *UL12* sequence. The F/L Res

Table 2.3 – Primers used in virus construction

Primer name	Sequence (5'→3')[a]
JRS199	CCCACGCCCGCGACCCGGACGCCGATCCCGACTCCCCGGACCTTGACTC TCCTGTTGACAATTAATCATCGGCA
JRS200	GGCCCGCGGCGCGTCAGGCGCCATAGGTGCCGACCGAGTCCGCGGTCCA CTCAGCACTGTCCTGCTCCTT
JRS201	CCCACGCCCGCGACCCGG
JRS202	GGCCCGCGGCGCGTCAGG
JRS203	CCGCAGACGAAAAGCCCCGG
JRS204	CCTCGTAAAACCCCATGAGGGGCC
JRS451	GGGCCAAGTACGCTTTCGACCCCATGGACCCCAGCGACCCCACGGCCTC CCCTGTTGACAATTAATCATCGGCA
JRS452	AATGCCCGGAACGCCTCCGGGGACCGGTGTGCCATCAAGTCCTCGTACG CTCAGCACTGTCCTGCTCCTT
JRS453	GGGCCAAGTACGCTTTCGACCCCATGGACCCCAGCGACCCCACGGCCTC CGCCTATGAAGATTTGATGGCTCATCG
JRS454	AATGCCCGGAACGCCTCCGGGGACCGGTGTGCCATCAAGTCCTCGTACG C***CTA***CTTGTCATCGTCATCCTTGTAGTC
JRS455	GGGACATTCACGGCTACCTGG
JRS456	CTTGCGTGACGAGAGCCTCC
JRS804	GCTGCGGGCCCACGGTACGCCAGTAGCCGAGGACTTTATGACGCGCGTG GCCGCGTTGGCTTAGGGATAACAGGGTAATCGATTT
JRS805	ACCGTGGGCCCGCCAGTGTTACAACCAATTAACC
JRS822	GTTCACCCGGCGGCGCGCTCAACCACCGCTCCCCCCACGTCGTCTCGGA A***ATG***TGGGGCGTCTCGAG
JRS823	AATGCCCGGAACGCCTCCGGGGACCGGTGTGCCATCAAGTCCTCGTACG C***CTA***CTTGTCATCGTCATCCTTGTAGTCG
JRS825	GCGAGTTTCTGCTTTCGCACG

[a] Start/stop codons are indicated in bold italics, restriction sites are underlined, and HSV-1 homology regions are highlighted in grey.

BAC was created from the F/L BAC using the same protocol outlined above with the exception that *galK* was replaced with a wild-type *UL12* PCR product amplified from pUC119-AK using primers JRS201 and JRS202. To construct the SPA BAC, a duplicated 3' portion of *UL12* was recoded and the SPA tag coding sequence was fused to the 3' end of *UL12* (Figs. 6.5 and 6.8). This recoding involved placing silent mutations in 208 of 242 codons of the 3' 726 bp of *UL12* to avoid recombination and the disruption of the overlapping *UL11* gene (Fig. 6.8). A *galK* cassette amplified from p*galK* using primers JRS451 and JRS452 was inserted between nucleotides 1152 and 1153 of *UL12* in the KOS37 BAC. A plasmid containing the recoded region of the *UL12* gene fused in-frame to the SPA tag coding sequence was synthesized by GeneArt. This synthesized *UL12* sequence was amplified using the primers JRS453 and JRS454 and used to replace *galK* generating the SPA BAC. This *UL11* locus in this BAC is positioned similarly to the *UL11* locus in the KOS37 UL98 BAC (Fig. 6.6).

A UL98 expressing KOS37 BAC (UL98) was created using *en passant* mutagenesis in the *E. coli* strain GS1783 (489). The kanamycin resistance gene, *aphAI*, and an I-*Sce*I endonuclease site were amplified from the vector pEPKan-S using the primers JRS804 and JRS805 and cloned into the pMZS3F UL98-SPA vector using the *Apa*I site. The resulting *UL98* sequence containing *aphAI*, an I-*Sce*I site, and a sequence duplication was amplified by PCR using primers JRS822 and JRS823 and targeted into the KOS37 BAC. This recombination event deleted nucleotides 1-1152 of *UL12*, preventing UL12, UL12.5, and $UL12_{M185}$ expression, while leaving *UL11* intact. A subsequent recombination event

removed the *UL98* sequence duplication, *aphA1* gene, and I-*Sce*I site resulting in the UL98 BAC (Fig. 6.5). In this BAC the *UL11* transcript is no longer transcribed from within the *UL12*/*UL12.5* ORF (Fig. 6.6).

All mutant BACs were screened by PCR using the primers: JRS203 and JRS204 (F/L, F/L Res), JRS455 and JRS456 (SPA), or JRS825 and JRS456 (UL98). Wild-type and mutated BACs were propagated in *E. coli*, isolated using a Large-Construct Kit (QIAGEN), and transfected into Cre-Vero cells to generate infectious viral particles. Additional passaging through Cre-Vero cells was performed to remove the BAC sequence from the viral DNA.

2.8 – Small interference RNA methods and techniques

2.8.1 – siRNAs

All small interfering RNAs (siRNAs) were obtained from Ambion. The siRNAs used in this study targeted: ENDOG (s707), EXOG (s19298), or a non-targeting control (hereafter referred to as N.C. siRNA, 4390847).

2.8.2 – siRNA knockdown of EXOG and ENDOG

Endogenous EXOG knockdown was evaluated using HeLa cells transfected for 48 hours with 10 nM total siRNA (10 nM negative control (N.C.) siRNA, 5 nM EXOG + 5 nM N.C. siRNAs, or 5 nM ENDOG + 5 nM N.C. siRNAs) using DharmaFECT 1. Total cell lysates were prepared and processed for infrared western blotting using rabbit anti-EXOG (Invitrogen) and mouse anti-actin (Sigma) primary antibodies. Alternatively, siRNA transfected cells were lysed for 10 minutes on ice with digitonin lysis buffer and centrifuged at 20800 ×

g for five minutes at 4°C. To the supernatants (cytoplasmic fractions) 5X protein sample buffer was added. The pellets (mitochondrial fractions) were resuspended in 25 mM Tris-Cl (pH 8.0), 0.1% Triton X-100 to which 5X protein sample buffer was added. Lysates were processed for infrared western blotting using rabbit anti-EXOG (Invitrogen), mouse anti-glyceraldehyde 3-phosphate dehydrogenase (GAPDH) (Biodesign International), mouse anti-MnSOD (Stressgen), and mouse anti-cytochrome *c* (556433, BD Biosciences).

SiRNAs were also evaluated for their ability to suppress overexpression of the desired protein. HeLa cells were transfected with both 10 nM total siRNA (as indicated above) and 1 μg plasmid DNA (pcDNA3.1-EXOG-myc or pcDNA3.1-ENDOG-myc) using DharmaFECT Duo. Lysates were prepared at 48 hpt and processed for infrared western blotting using mouse anti-c-myc (Sigma) and rabbit anti-actin (Sigma).

2.9 – Microscopy methods and techniques

2.9.1 – Live cell fluorescence imaging

HeLa cells grown in chambered coverglass dishes (Nunc, 155383) were used for all live cell imaging. Cells were transfected with the indicated EGFP or tGFP expression plasmids for the times indicated, stained with 50 nM MitoTracker Red CMXRos (Invitrogen, M7512) for 30 minutes, washed three times, and covered with warm HeLa medium unless otherwise stated. All images were obtained using an Axiovert 200M fluorescence microscope (Zeiss). An ApoTome optical sectioning device (Zeiss) was used where indicated.

2.9.2 – Immunofluorescence microscopy

HeLa cells were grown on coverslips, transfected for 24 or 48 hours, and processed for immunofluorescence as previously described (461). Briefly, the cells were washed with PBS, fixed with 4% (w/v) paraformaldehyde (Marivac, 0171) in PBS for ten minutes, washed again with PBS, then permeabilized in 1% Triton X-100 (Fisher, BP151) in PBS for ten minutes. Blocking was performed using 3% (v/v) normal goat serum (Gibco, PCN5000) in PBS overnight at 4°C. Mouse anti-cytochrome *c* (BD Biosciences, 556432) and either rabbit anti-FLAG (Sigma, F7425) or rabbit anti-c-myc (Sigma, C3956) were used as primary antibodies. Alexa Fluor 555-conjugated goat anti-rabbit (Invitrogen, A21428) and Alexa Fluor 488-conjugated goat anti-mouse (Invitrogen, A11001) were used as secondary antibodies. All antibodies were diluted in 3% (v/v) normal goat serum in PBS and incubated for 1.5 h at room temperature. Stained cells were mounted onto slides using VECTASHIELD (Vector Laboratories, H-1000) containing 1 mg/mL 4',6-diamidino-2-phenylindole (DAPI; Molecular Probes, D1306). Alternatively, stained cells were stained with 1 mg/mL DAPI for 10 minutes then mounted on slides using Mowiol 4-88 (Sigma, 81381). All images were obtained with an Axiovert 200M fluorescence microscope using an ApoTome optical sectioning device.

2.9.3 – PicoGreen live cell imaging of mtDNA depletion

Chambered coverglass dishes were used for all PicoGreen (Invitrogen) mtDNA depletion assays. To quantitate mtDNA depletion by UL12, UL12.5, UL12.5 mutants, or UL12 orthologs, 200 ng of plasmid DNA was co-transfected

with 100 ng pcDNA-Orange. To assess the effect of ENDOG and/or EXOG overexpression on mtDNA depletion by $UL12_{M185}$-G336A/S338A-SPA two plasmid combinations were used: 1) 2:1:1, 200 ng total pcDNA3.1 plasmid DNA (empty vector alone, empty vector and ENDOG/EXOG/Sirt3 plasmid DNA, or ENDOG and EXOG plasmid DNA) was co-transfected with 100 ng of pMZS3F plasmid DNA (empty vector or $UL12_{M185}$-G336A/S338A-SPA) and 100 ng pcDNA-Orange or 2) 5:1:1, 500 ng total pcDNA3.1 plasmid DNA (empty vector alone, empty vector and ENDOG or EXOG plasmid DNA, or ENDOG and EXOG plasmid DNA) was co-transfected with 100 ng of pMZS3F plasmid DNA (empty vector or $UL12_{M185}$-G336A/S338A-SPA) and 100 ng pcDNA-Orange.

To determine if ENDOG-mediated mtDNA depletion could be inhibited by ENDOG siRNA, 300 ng of plasmid DNA (empty vector or a plasmid encoding ENDOG-myc) was co-transfected with either 10 nM N.C. or ENDOG siRNA and 100 ng pcDNA-mOrange.

To determine if ENDOG and/or EXOG knockdown had any effect on mtDNA depletion, HeLa cells were first seeded into 24-well plates and transfected with 10 nM total siRNA using DharmaFECT 1 (Thermo Scientific, T-2001) for 48 hours. These cells were trypsinized and reverse transfected into chambered coverglass dishes for an additional 24 hours with the indicated siRNAs, 100 ng pcDNA-Orange, and 100 ng of empty vector or a plasmid expressing UL12.5-SPA or $UL12_{M185}$-G336A/S338A-SPA using DharmaFECT Duo (Thermo Scientific, T-2010).

For all live cell imaging, cells were stained with 3 μL/mL PicoGreen for 1 hour at 37°C and mtDNA was visualized in mOrange-positive cells. Images were obtained using an Axiovert 200M fluorescence microscope using a 40X oil immersion objective.

2.10 – Mitochondria methods and techniques

2.10.1 – Crude isolation of mitochondria

HeLa cells were transfected or infected for the indicated times and scraped into growth medium. The cells were pelleted at 1000 × *g* for five minutes at 4°C. The cell pellet was washed with PBS, resuspended in mitochondria isolation buffer containing protease inhibitors, and rocked at 4°C for up to twenty minutes. Cells were disrupted with fifty up/down strokes through a 22 gauge needle or fifty up/down strokes with a dounce homogenizer. The lysate was centrifuged at 1000 × *g* for at least five minutes at 4°C to pellet unlysed cells and debris. The supernatant was transferred to a new tube and centrifuged at 8000 × *g* for at least fifteen minutes at 4°C to obtain the crude mitochondria-containing pellet. The pellet was washed then resuspended in mitochondria isolation buffer.

2.10.2 – Mitochondrial proteinase K protection assays

HeLa cells grown in 100 mm dishes were transfected with 20 μg of plasmid DNA or mock infected or infected with KOS37 SPA at a MOI of five for twenty-four hours and mitochondria were isolated as described in section 2.10.1. The total protein concentration of the isolated mitochondria was determined using a BCA protein assay as described in section 2.5.1. First, 8 μg of mitochondria

were left untreated or treated with detergent (1% final IGEPAL CA-630 (Sigma)) on ice for ten minutes. Next, the same isolated mitochondria were incubated in the presence or absence of proteinase K (Invitrogen, 25530-031) at a final concentration of 200 μg/mL for fifteen minutes at 37°C. Phenylmethylsulfonyl fluoride (ICN, 800263) was added to all samples at final concentration of 5mM to inhibit proteinase K activity. Finally, 5X protein sample buffer was added to all samples prior to analysis using infrared western blotting (see sections 2.5.2 and 2.5.3). The following primary antibodies were used: Rabbit α-FLAG (to detect all SPA-tagged proteins), mouse α-translocase of outer mitochondrial membrane 70 homolog A (TOM70) (Abcam, ab89624), and the MitoProfile Membrane Integrity WB Antibody Cocktail (MitoSciences; MS620, comprised of α-Ubiquinol-Cytochrome *c* Reductase Core Protein I (Core 1), mouse α-ATP5A (CVa), mouse α-voltage dependent anion channel 1/Porin, mouse α-Cyclophilin D, and mouse α-Cytochrome *c*).

2.11 – Image processing and statistical analyses

All microscopy images were acquired with an Axiovert 200M fluorescence microscope using the AxioVision 4.5 program (Zeiss). All graphs and statistical analyses (two-tailed *t*-tests with equal variance) were performed with Microsoft Excel 2007. Image processing was performed using Illustrator CS2 and Photoshop CS2 (Adobe).

Chapter 3

Identification of the mitochondrial localization sequence of HSV-1 UL12.5

Portions of figures 3.4 and 3.6 have been published in:

Corcoran JA, Saffran HA, Duguay BA, Smiley JR. 2009. Herpes simplex virus UL12.5 targets mitochondria through a mitochondrial localization sequence proximal to the N terminus. J Virol **83:**2601-2610.

All experiments presented within this chapter were performed by B. Duguay.

3.1 – Preface

The HSV-1 UL12 and UL12.5 proteins provide an interesting example of two highly related viral proteins with distinct functions; UL12 functions in viral DNA maturation (150, 193, 194) and UL12.5 mediates the rapid loss of mtDNA (152). The distinct localization of these two proteins offers the principle basis for their unique functions, as UL12 is targeted to the nucleus (196, 461) and UL12.5 co-localizes with mitochondria (152). While the localization of UL12 to the nucleus is known to be determined by the N-terminal 126 residues (461), residues absent from UL12.5, the determinants required to direct UL12.5 to mitochondria have not been elucidated. While there are a large variety of MLSs, many of those which direct proteins to the mitochondrial matrix are N-terminal and generally contain amphipathic α-helices with a positively-charged face (317, 490). Subsequent sequence analyses led us to hypothesize that the MLS of UL12.5 was positioned in an atypical, internal location. The data presented in this chapter support this hypothesis and demonstrate that a subset of UL12.5 is fully imported into mitochondria using a MLS positioned 58 residues downstream of the N-terminus which contains many of the hallmarks of other classical matrix-targeting MLSs.

3.2 – Results

3.2.1 – Localization of UL12.5 is controlled by an N-proximal mitochondrial localization sequence

Our recently published data demonstrated that unlike the related nuclear protein, UL12, the UL12.5 protein co-localized with the mitochondrial protein cytochrome *c* and the mitochondrial stain MitoTracker Red (152) while also causing mtDNA loss in the absence of other viral proteins (152). Initial work by Jennifer Corcoran and Holly Saffran involved creating progressive N-terminal truncation mutants through deletions of the *UL12* and *UL12.5* ORFs to roughly define the MLS of UL12.5 (475). Data accumulated using these mutants demonstrated that a MLS was present downstream of residue D125 and upstream of residue M215 (475). Moreover, as more of the N-terminus of UL12 was removed up to residue M127 (the initiation codon of UL12.5; see Fig. 1.2), the mtDNA depletion activity of these mutants increased (475). Interestingly, truncation of the UL12.5 protein to the next in-frame methionine (M185; see Fig. 1.2) downstream of the initiation codon of UL12.5 had a positive impact on mitochondrial localization and no significant impact on mtDNA depletion compared to UL12.5 (475). Significant truncation of the UL12/UL12.5 N-terminus to M390 also uncovered an additional MLS however this mutant was unable to cause mtDNA loss (475). Altogether, these results support the conclusion that UL12.5 is a mitochondrial protein and demonstrated that the MLS is located in the N-terminus of UL12.5. However, subsequent experiments performed by Jennifer Corcoran and Holly Saffran using the M127F virus (which

expresses $UL12_{M185}$ but no UL12.5) (468) and their observation that the $UL12_{M185}$ protein also causes mtDNA depletion demonstrated that the extreme N-terminus of UL12.5 was not required for translocation to mitochondria or mtDNA deletion (475).

To extend the work performed by Jennifer Corcoran and Holly Saffran which examined the mechanism of UL12.5 mitochondrial localization, I created N-terminal truncation mutants of UL12.5 fused to a C-terminal enhanced green fluorescent protein (EGFP) tag (Fig. 3.1). When expressed in HeLa cells, EGFP demonstrated a diffuse localization throughout the cell with no detectable co-localization with MitoTracker Red (Fig. 3.2A). In contrast, UL12.5-EGFP localized both to the nuclei and mitochondria in transfected cells, similar to our previously published results with both untagged and EGFP-tagged proteins (Figs. 3.2A and references 152, 475). When I examined the localization of the $UL12_{M185}$-EGFP, I observed clear co-localization with mitochondria and an absence of nuclear staining (Fig. 3.2A). This observation was in good agreement with immunofluorescence data using an untagged version of $UL12_{M185}$ (Fig. 4.5 and reference 475). When translation was directed to begin at the subsequent in-frame methionine codon, M215, the resulting protein could no longer localize to mitochondria and instead was targeted to the nucleus (Fig. 3.2A). My data presented here further support our additional data (475) and further indicates that the mitochondrial localization of UL12.5 is directed by residues within the N-terminus of the protein.

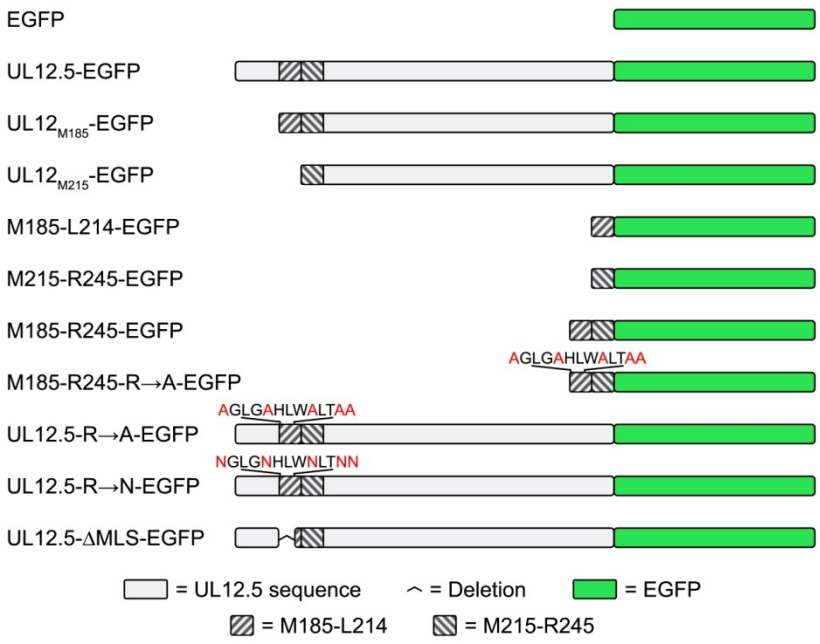

Figure 3.1. EGFP-tagged UL12.5 mutants used to study mitochondrial localization of UL12.5. Schematics of C-terminal EGFP-tagged proteins used in this study. The position of the UL12.5 mitochondrial localization sequence (comprising residues M185-R245 of the full-length protein) or portions thereof (M185-L214 or M215-R245) is indicated. The R→A and R→N substitution mutations are shown in red above the respective proteins. The location of the ΔMLS depletion mutation is also indicated. All residue numbering is relative to the UL12 protein. All schematics are drawn to scale. EGFP, enhanced green fluorescent protein; R→A, arginine to alanine substitution mutations at residues 188, 192, 196, 199, and 200; R→N, arginine to asparagine substitution mutations at residues 188, 192, 196, 199, and 200.

A

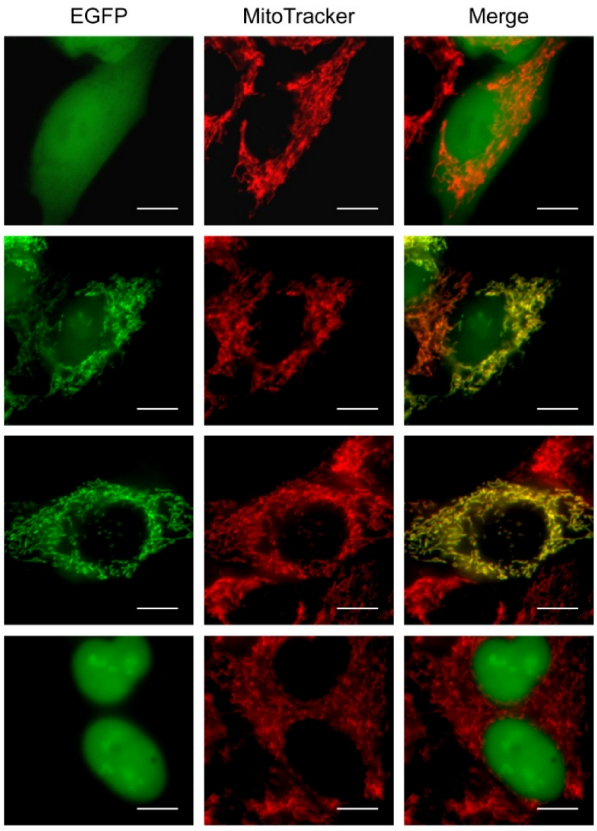

B

Protein	N-terminal sequence	Probability of export to mitochondria
EGFP	MADYDQLSRS GGSRARGTVD CRIRSLSSRS ESGLVQLVHA	0.1674
UL12.5	MWSASVIPNA LPSHILAETF ERHLRGLLRG VRAPLAIGPL	0.2100
$UL12_{M185}$	MVDRGLGRHL WRLTRRGPPA AADAVAPRPL MGFYEAATQN	0.8496
$UL12_{M215}$	MGFYEAATQN QADCQLWALL RRGLTTASTL RWGPQGPCFS	0.0306

Figure 3.2. Subcellular localization of EGFP-tagged UL12.5 and N-terminally truncated derivatives. (A) HeLa cells expressing EGFP or EGFP-tagged proteins for 48 hours were stained with 100 nM MitoTracker Red for 20 minutes and visualized by live cell fluorescence microscopy using a 40X objective. Scale bars = 10 μm. (B) The N-terminal 40 amino acids of EGFP, UL12.5, $UL12_{M185}$, and $UL12_{M215}$ are displayed with + signs indicated above positively charged residues. The probability of each protein localizing to mitochondria as predicted by MitoProt II is indicated.

A variety of signals can contribute to mitochondrial localization and some of the best characterized are N-terminal presequences. While these sequences vary in both sequence and length, they are generally between 15-55 amino acids long with a net positive charge of +3 to +6 (491). When the mitochondrial targeting sequence prediction algorithm MitoProt II (487) was used to assess the likelihood of the extreme N-terminus of UL12.5 functioning as a MLS, the probability was low (21%) despite the presence of a cluster of positively charged residues (Fig. 3.2B). Since truncating the UL12.5 protein to M185 did not affect mitochondrial localization or mtDNA depletion (Fig. 3.2A and reference 475), it was plausible that residues near M185 formed the UL12.5 MLS. Using the MitoProt II algorithm, it was observed that the N-terminus of $UL12_{M185}$ had a high probability (85%) of directing $UL12_{M185}$ to mitochondria (Fig. 3.2B). Conversely, EGFP and $UL12_{M215}$-EGFP were not predicted to localize to mitochondria, with probabilities of export to mitochondria of 17% and 3%, respectively; which was consistent with the presented microscopy data (Fig. 3.2A).

3.2.2 – Residues downstream of M185 are crucial for mitochondrial localization of UL12.5

I next examined if the N-terminus of UL12.5 contained the common structural characteristics of MLSs. The PredictProtein algorithm revealed that a significant portion of the N-terminus is predicted to be α-helical (Fig. 3.3A). Interestingly, of the four predicted helical regions within the UL12.5 N-terminus, only the region downstream of M185 (R188-G201) is expected to form an

A

127 MWSASVIP NALPSHILAE TFERHLRGLL RGVRAPLAIG PLWARLDYLC SLAVVLEEAG 184

185 MVDRGLGRHL WRLTRRGPPA AADAVAPRPL MGFYEAATQN QADCQLWALL RRGLTTASTL 244

B

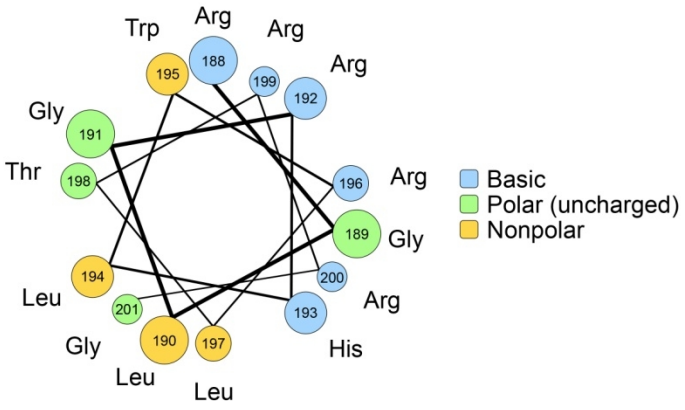

Figure 3.3. Secondary structure prediction of the N-terminus of UL12.5. (A) The primary amino acid sequence of UL12.5 from the initiator methionine (M127) to leucine 244 is shown. Highlighted in red are sequences predicted by PredictProtein to be helical in nature. (B) The amphipathic nature of the predicted α-helix spanning residues arginine 188 to glycine 201 is depicted using a helical wheel diagram.

amphipathic α-helix with a positively-charged face (Fig. 3.3B). Earlier experiments demonstrated that the region between M127 and P160 could not function as a MLS and mutagenesis of positively-charged arginine residues R148, R151, R155, and R158 did not have any impact on mtDNA depletion by UL12.5 (Jennifer Corcoran, unpublished data). These data were consistent with additional work by Jennifer Corcoran and Holly Saffran (475) and my data (Figs. 3.2A and 4.5) which together demonstrate that the N-terminal 58 residues are not required for mitochondrial localization. In light of the above mentioned data and bioinformatic analyses that suggest the residues downstream of M185 possess the hallmarks of mitochondrial matrix targeted proteins (Figs. 3.2B and 3.3), I next tested the ability of residues downstream of M185 to redirect a non-mitochondrial protein, EGFP, to mitochondria. To perform these experiments, thirty to sixty residue portions of the M185-R245 protein sequence were fused to the N-terminus of EGFP (Fig. 3.1). Using live cell imaging it was observed that residues M185-L214 were moderately capable of redirecting EGFP to mitochondria, while residues M215-R245 had no effect on EGFP localization, to the extent that the localization of M215-R245-EGFP was indistinguishable from EGFP (Fig. 3.4). However, when the entire sixty residue sequence was present (M185-R245-EGFP), the EGFP fusion protein was efficiently targeted to mitochondria similarly to that observed for UL12.5 and $UL12_{M185}$ (Fig. 3.4), indicating that residues M185-R245 function as a bona fide MLS.

The region spanning residues M185-R245 of UL12.5 contains a net positive charge of +5 where the majority of the basic residues are tightly clustered

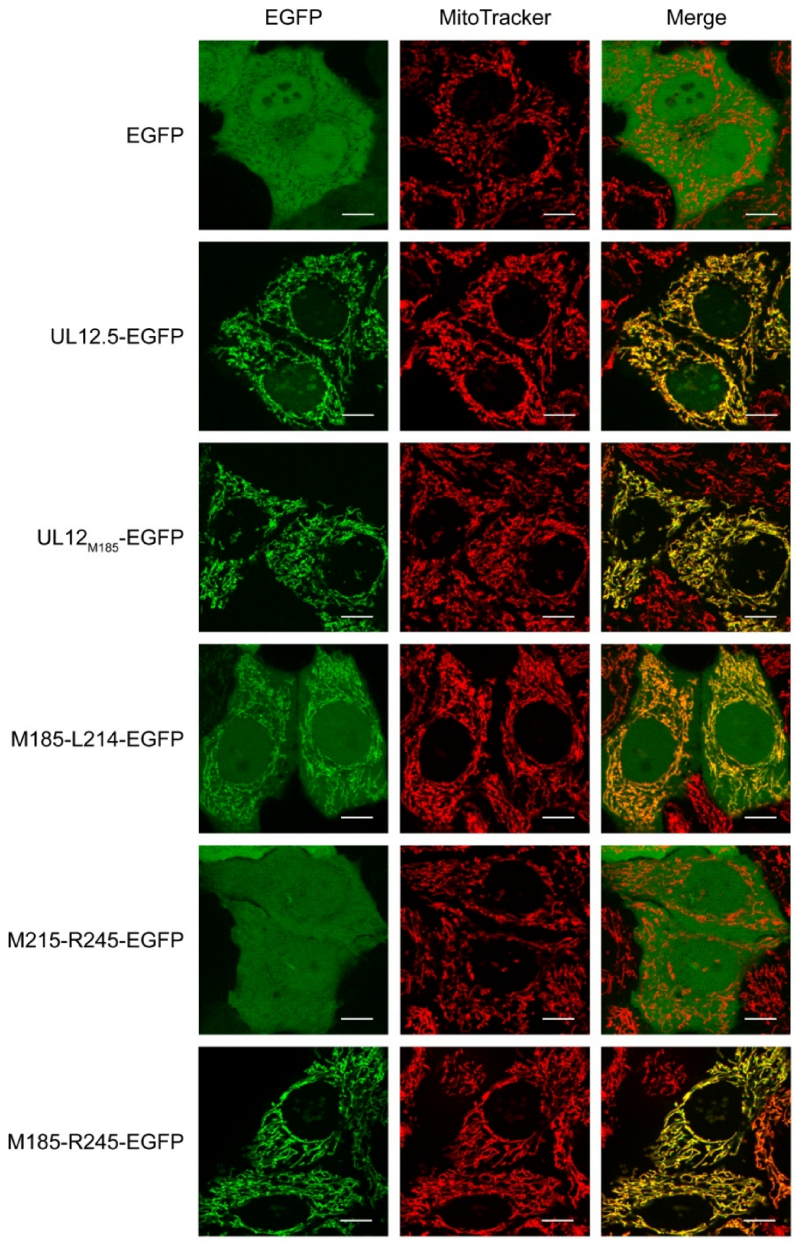

Figure 3.4. Residues downstream of M185 are crucial for mitochondrial localization of UL12.5. HeLa cells transfected with plasmids encoding EGFP or the indicated EGFP fusion proteins for 24 hours were stained with MitoTracker Red and imaged by live cell fluorescence microscopy using a 63X objective with an ApoTome. All residue numbering is relative to the UL12 protein. Scale bars = 10 μm.

within residues 188-200. To examine the importance of this polybasic region in mitochondrial localization, I mutated five arginine residues (188, 192, 196, 199, and 200) to alanines in both M185-R245-EGFP and UL12.5-EGFP (Fig. 3.1). These five substitution mutations significantly impaired the ability of M185-R245-R→A-EGFP to localize to mitochondria (Fig. 3.5). Furthermore, when the identical substitution mutations were present in the full-length UL12.5 protein mitochondrial localization was similarly disrupted (Fig. 3.5). However, since the arginine to alanine substitutions disrupt both the charge and the amphipathicity of the predicted helical region of the UL12.5 MLS, I examined the effect of more conservative arginine to asparagine substitutions on mitochondrial localization. Interestingly, the loss of the cluster of basic amino acids in UL12.5-R→N-EGFP (Fig. 3.1) did not remarkably effect the mitochondrial localization of this protein when compared to UL12.5-EGFP (Fig. 3.6). This observation would suggest that the hydrophilic character of this region of UL12.5 rather than the positive charge is most important to direct UL12.5 to mitochondria. In another test of the importance of these N-proximal residues of UL12.5 for mitochondrial localization, I created a deletion mutant lacking residues 188 to 212 which includes six of the nine arginine residues present within the M185-R245 region of UL12.5 (Fig. 3.1). UL12.5-ΔMLS-EGFP was not observed to have any significant co-localization with MitoTracker during live cell imaging experiments (Fig. 3.7). Similarly, both untagged and C-terminally tagged versions of UL12.5-ΔMLS did not co-localize with the mitochondrial protein cytochrome *c* in immuno-fluorescence experiments (Figs. 4.3 and 4.5). Altogether, these data demonstrate

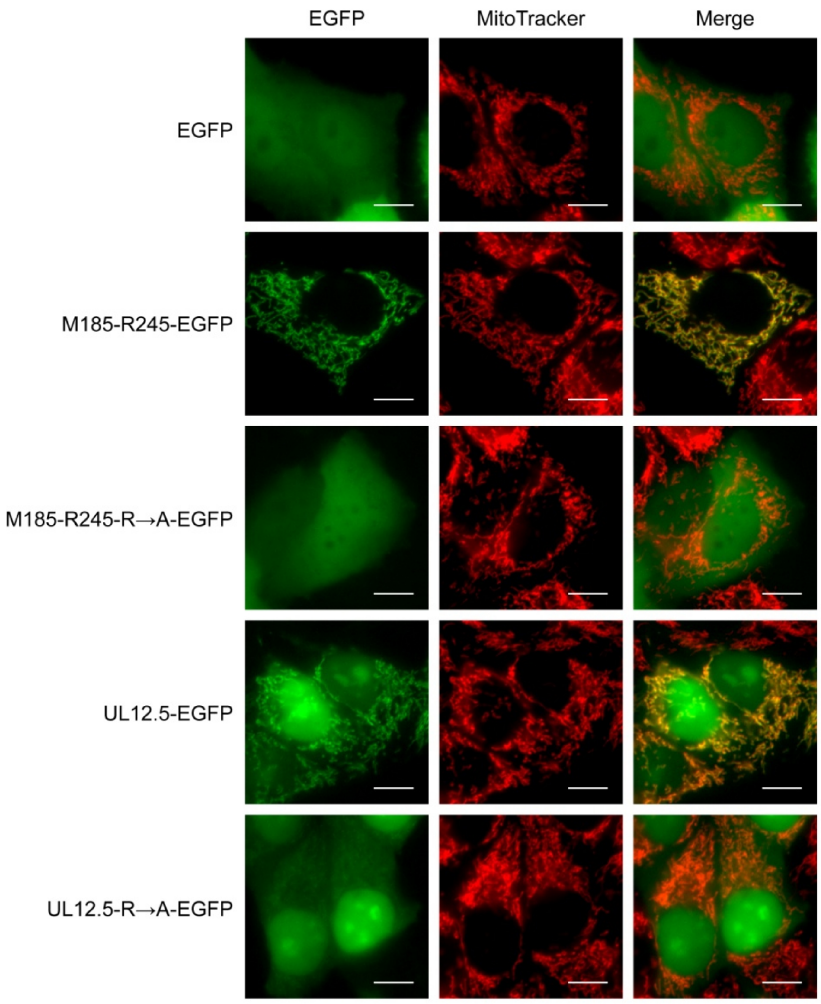

Figure 3.5. Arginines within the UL12.5 mitochondrial localization sequence are crucial for mitochondrial localization. HeLa cells were transfected for 48 hours with plasmids encoding EGFP or the indicated EGFP fusion proteins were stained with 100 nM MitoTracker Red for 20 minutes and imaged by live cell fluorescence microscopy using a 40X objective. R→A, arginine to alanine substitution mutations at residues 188, 192, 196, 199, and 200. All residue numbering is relative to the UL12 protein. Scale bars = 10 μm.

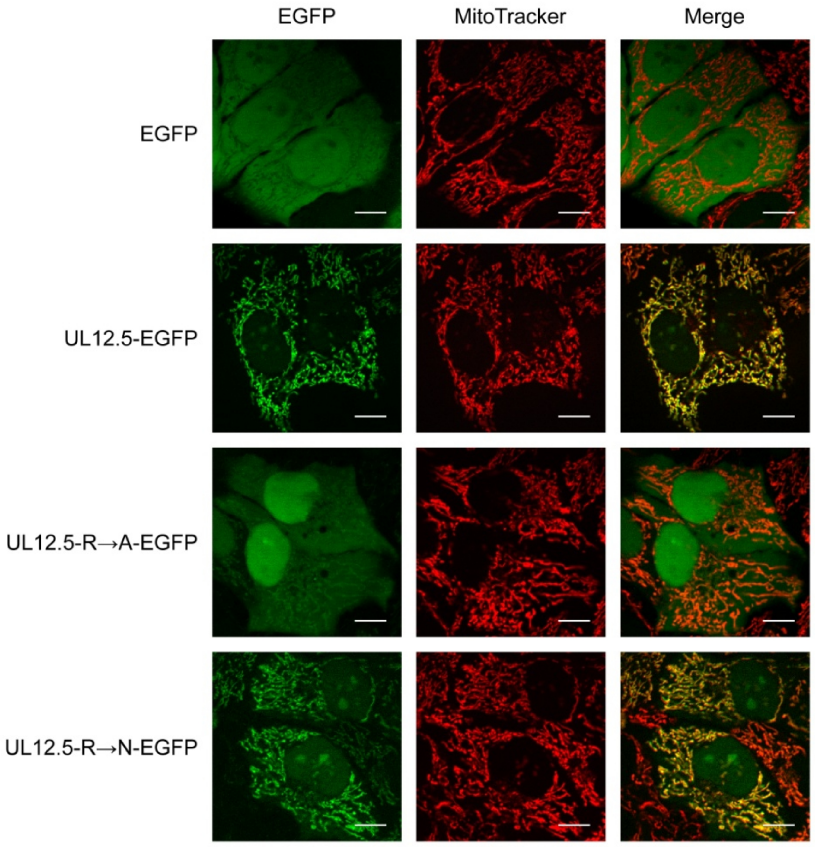

Figure 3.6. Hydrophilicity and not charge of N-proximal residues facilitate the mitochondrial localization of UL12.5. HeLa cells were transfected for 24 hours with plasmids encoding EGFP or the indicated EGFP fusion proteins were stained with MitoTracker Red and imaged by live cell fluorescence microscopy using a 63X objective with an ApoTome. R→A, arginine to alanine substitution mutations at residues 188, 192, 196, 199, and 200; R→N, arginine to asparagine substitution mutations at residues 188, 192, 196, 199, and 200. All residue numbering is relative to the UL12 protein. Scale bars = 10 μm.

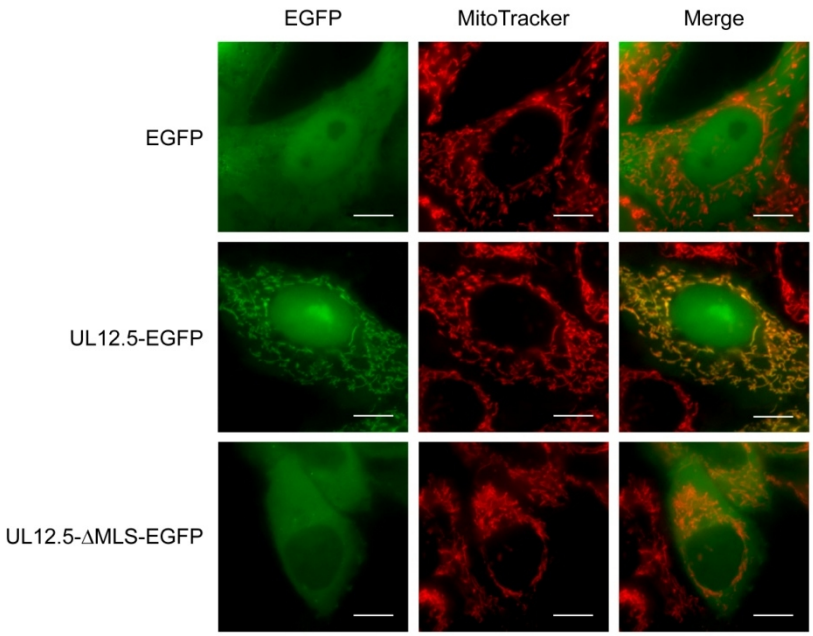

Figure 3.7. Residues 188-212 are a major determinant for the mitochondrial localization of UL12.5. HeLa cells transfected with plasmids encoding EGFP or the indicated EGFP fusion proteins for 36 hours were stained with MitoTracker Red and examined by live cell fluorescence microscopy using a 63X objective. UL12.5-ΔMLS-EGFP; UL12.5-EGFP lacking residues arginine 188 to arginine 212. All residue numbering is relative to the UL12 protein. Scale bars = 10 μm.

that mitochondrial localization of UL12.5 is directed by residues downstream of M185. While this region contains characteristics common to other MLSs (i.e. amphipathic, helical, net positive charge), the internal location of these residues and the dispensability of the positively charged arginines suggests that this is an atypical MLS.

3.2.3 – A fraction of total UL12.5 and UL12$_{M185}$ is fully imported into mitochondria

For mtDNA depletion to occur, the simplest hypothesis is that UL12.5 must localize to the mitochondrial matrix to be in close proximity to mtDNA to facilitate its degradation. The MLS of UL12.5 does have characteristics of a matrix-targeting MLS yet its internal placement is not common to most mitochondrial matrix proteins. Data generated by Jennifer Corcoran using fractionated and digitonin treated mitochondria provided evidence to suggest that UL12.5 localizes to the mitochondrial matrix; however, these studies could not indicate whether UL12.5 is fully or partially imported into the mitochondrial matrix (475).

To more accurately determine in which sub-mitochondrial compartment UL12.5 resides, I performed proteinase K protection assays using mitochondria isolated from cells expressing UL12.5-SPA or UL12$_{M185}$-SPA. The UL12.5-SPA and UL12$_{M185}$-SPA proteins used in these experiments are fusion proteins with a sequential peptide affinity (SPA) tag appended to their respective C-termini. The SPA tag is comprised of a calmodulin binding peptide and three modified FLAG sequences separated by a TEV protease cleavage site (476) and was used to

facilitate protein detection in transfected cells. Additional characterization of these fusion proteins is described in Chapter 4. Following transfection of HeLa cells for twenty-four hours with a control plasmid (pMZS3F) or UL12.5-SPA or $UL12_{M185}$-SPA expressing plasmids, mitochondria were crudely isolated (along with lysosomes and microbodies) using differential centrifugation. Untreated mitochondria (- Detergent, - Proteinase K) isolated from cells transfected with UL12.5-SPA or $UL12_{M185}$-SPA expressing plasmids contained full-length proteins of ca. 70 kDa or ca. 68 kDa, respectively, as well as numerous smaller C-terminal protein fragments (Fig. 3.8A). The apparent molecular masses of the full-length proteins were similar to those observed in whole cell lysates (Fig. 4.1B). Many of the protein fragments can also be observed in whole cell lysates containing SPA-tagged (Fig. 4.2) or untagged versions of UL12.5 and $UL12_{M185}$ (475). The increased intensity of the C-terminal protein fragments is likely due to the increased concentration of these proteins in isolated mitochondria (Fig. 3.8A) compared to their concentration in whole cell lysates (Fig. 4.2). When the isolated mitochondria were treated with proteinase K (- Detergent, + Proteinase K) to degrade any cytoplasm-exposed peripheral or integral outer mitochondrial membrane proteins, I observed that some full-length UL12.5-SPA or $UL12_{M185}$-SPA could be observed (Fig. 3.8A) supporting the conclusion that UL12.5-SPA and $UL12_{M185}$-SPA can be fully imported into mitochondria. However, it is important to note that protease-protected full-length UL12.5-SPA and $UL12_{M185}$-SPA only represent a minority of the total SPA-tagged protein species present within mitochondria (Fig. 3.8A). The treatment with proteinase K was sufficient

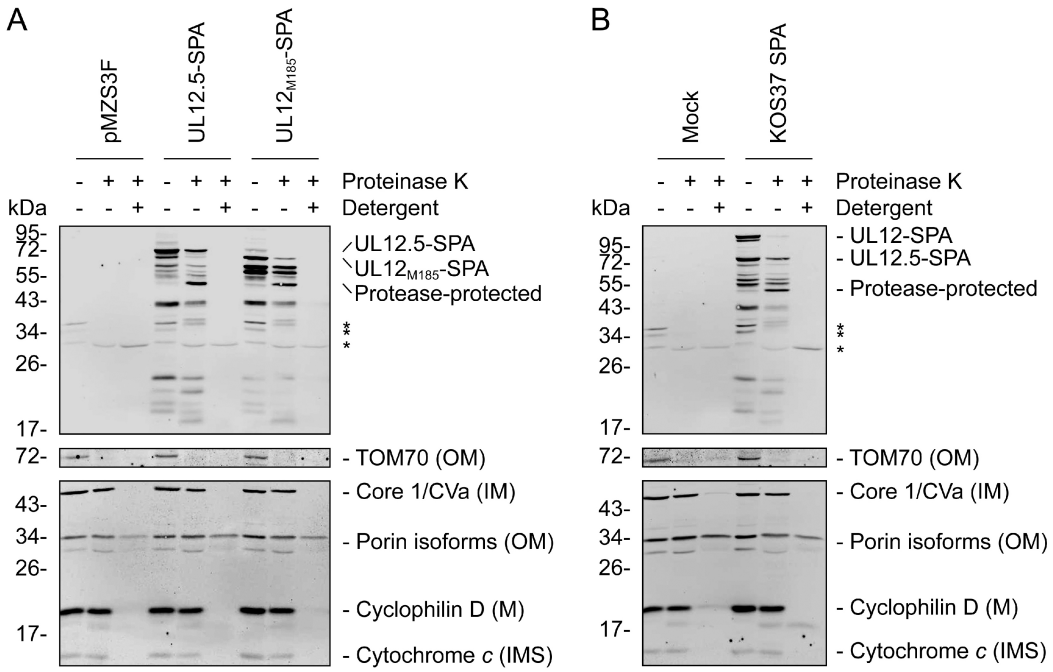

Figure 3.8. A subset of full-length UL12.5 and UL12$_{M185}$ proteins is fully imported into mitochondria in transfected and infected cells. Mitochondria from HeLa cells transfected with the indicated plasmids (A) or either mock infected or infected with KOS37 SPA (B) were isolated and subjected to proteinase K protection assays. Mitochondrial proteins were visualized following immunodetection with anti-FLAG (top), anti-TOM70 (middle), and the Membrane Integrity WB Antibody Cocktail (bottom). Protein species are identified to the right. Molecular mass is indicated in kilodaltons (kDa). Non-specific bands are indicated with asterisks. The submitochondrial localization of each control protein is indicated in brackets (OM, outer mitochondrial membrane; IM, inner mitochondrial membrane; M, mitochondrial matrix; IMS, mitochondrial intermembrane space).

to degrade the outer mitochondrial membrane protein TOM70 while not harsh enough to disrupt outer mitochondrial membrane integrity as determined by the presence of the soluble intermembrane space protein, cytochrome *c* (Fig. 3.8A). The porin (voltage-dependent anion channel 1) isoforms were not affected by proteinase K treatment alone (Fig. 3.8A) due to the known protease-resistance of this protein following insertion into the outer mitochondrial membrane (492, 493). Interestingly, although intact UL12.5-SPA and $UL12_{M185}$-SPA were detectable in mitochondria following proteinase K treatment, a notable protease-protected fragment (ca. 50 kDa) common to both proteins was created (Fig. 3.8A). Furthermore, numerous C-terminal fragments (cluster of three bands ≥ 55 kDa, a single band of ca. 43 kDa, and a cluster of bands < 26 kDa) of both UL12.5-SPA and $UL12_{M185}$-SPA were unaffected by proteinase K treatment, indicating that these too are inside mitochondria (Fig. 3.8A). When the isolated mitochondria were treated with IGEPAL CA-630, to disrupt the outer and inner mitochondrial membranes, prior to treatment with proteinase K (+ Detergent, + Proteinase K), all SPA-tagged proteins, TOM70, cytochrome *c*, the inner mitochondrial membrane protein Core 1/CVa, and the mitochondrial matrix protein cyclophilin D were no longer visible indicating their susceptibility to proteinase K when in solution (Fig. 3.8A). The porin isoforms were also reduced in abundance following treatment of mitochondria with detergent and proteinase K (Fig. 3.8A) suggesting that some of the porin isoforms were solubilised by treatment with detergent.

To determine if mitochondrial localization of UL12.5-SPA during infection was consistent with my observations in transfected cells, I also performed proteinase K protection assays on mitochondria isolated from cells infected with HSV-1 mutant virus expressing C-terminally SPA-tagged versions of UL12 and UL12.5 (see Chapter 6). Following mock or KOS37 SPA infection, mitochondria were again isolated by differential centrifugation. While samples of untreated isolated mitochondria from infected cells contained the nuclear protein UL12-SPA (Fig. 4.3), this protein was essentially absent from isolated mitochondria following treatment with proteinase K (Fig. 3.8B), indicating that the presence of UL12-SPA was likely a contaminant of this crude isolation method. More importantly, the results obtained using mitochondria isolated from infected cells were virtually identical to those obtained using mitochondria isolated from cells transiently expressing UL12.5-SPA, both in the observation of a fraction of protease-protected full-length UL12.5-SPA protein and the numerous C-terminal protease-protected fragments (compare Figs. 3.8A and B).

3.3 – Conclusions

Altogether, these results indicate that the N-proximal MLS present between residues M185 and R245 is sufficient to direct UL12.5 to mitochondria. However, following import UL12.5 appears to adopt multiple isoforms where only some of the total pool of UL12.5 remains intact during transfection and infection. The presence of multiple, protease-protected, N-terminally truncated fragments of UL12.5 in isolated mitochondria suggests that some processing of UL12.5 occurs following mitochondrial import. Despite the fact that the UL12.5 MLS has the characteristics of a mitochondrial matrix targeting presequence, the N-terminal processing of UL12.5 appears to be inconsistent with the removal of the MLS; a process which occurs for numerous mitochondrial matrix proteins. If the targeting sequence was removed in the traditional sense, one would expect that UL12.5 and $UL12_{M185}$ would co-migrate in SDS-PAGE gels; however, this was not the case. Moreover, the generation of new UL12.5 isoforms following proteinase K treatment indicates that some UL12.5 protein is not fully imported into mitochondria. Whether the proteinase K insensitive fragments are import intermediates or represent post-import isoforms of UL12.5 is currently unclear. These data presented here strongly support the conclusion that UL12.5 is a mitochondrial protein; however, it is currently unclear in which ultimate sub-mitochondrial compartment(s) this protein resides. While I favour the view that UL12.5 is within the mitochondrial matrix based on the characteristics of the MLS and the function of the protein, I cannot discount my proteinase K protection data which only loosely support this hypothesis. Therefore, additional

experiments will be required to develop a more comprehensive understanding of UL12.5 mitochondrial localization.

Chapter 4

Mitochondrial Nucleases ENDOG and EXOG Participate in Mitochondrial DNA Depletion Initiated by HSV-1 UL12.5

A version of this chapter has been published in:

Duguay BA, Smiley JR. 2013. Mitochondrial nucleases ENDOG and EXOG participate in mitochondrial DNA depletion initiated by herpes simplex virus 1 UL12.5. J Virol **87:**11787-11797. The original manuscript was written by B. Duguay with a major editorial contribution by J. Smiley.

All experiments presented within this chapter were performed by B. Duguay.

4.1 – Preface

In the preceding chapter I presented data which mapped the UL12.5 MLS to residues M185-R245 (of full-length UL12) and showed that an N-terminally truncated protein initiating at residue M185 ($UL12_{M185}$) localizes to mitochondria and depletes mtDNA (Chapter 3 and reference 475). Intriguingly, a previous study had shown that mutations in the N-terminal region of UL12 (either a L150K substitution or a deletion of residues 2-148) in residues that are absent from $UL12_{M185}$ inactivates detectable nuclease activity *in vitro* (460). These data raised the possibility that $UL12_{M185}$ lacks enzymatic activity, and by extension, that the nuclease activity of UL12.5 is not required for mtDNA depletion. Here I present data which support this hypothesis. I demonstrate that several nuclease-deficient mutants of UL12.5 retain the ability to deplete cells of mtDNA. Furthermore, I provide evidence that the mitochondrial proteins endonuclease G (ENDOG) and endonuclease G-like 1 (EXOG) contribute to the degradation of mtDNA following UL12.5 expression.

4.2 – Results

4.2.1 – Construction, expression, and mitochondrial localization of nuclease-deficient UL12.5-SPA mutants

Previously work has demonstrated that HSV-1 UL12.5 is responsible for the rapid loss of mtDNA following infection (152). To better understand the relationship between UL12.5 nuclease activity and UL12.5-mediated mtDNA depletion, I constructed a series of plasmids expressing mutant UL12.5 proteins containing known nuclease-inactivating mutations (Fig. 4.1A and references 44, 460). These included two well characterized mutations of invariant residues of conserved motif II (44), which based on the structures of the KSHV and EBV orthologs, lie in the active site of the enzyme (494, 495). Mutational analysis has demonstrated that the G336A/S338A double substitution mutation eliminates detectable exo- and endonuclease activities of UL12 whereas the D340E substitution mutation disrupts only exonuclease activity (44). Both mutations abolish the ability of UL12 to complement the growth defect of a UL12-null mutant virus (44). Mutagenesis of EBV, HCMV, and KSHV UL12 orthologs has also demonstrated that residues analogous to UL12 G336, S338, and D340 are critical for nuclease activity (293, 494, 496, 497). I included three additional mutations that have also been shown to eliminate detectable nuclease activity *in vitro* and lack the ability to complement AN-1 replication *in vivo*: ΔN (a deletion encompassing UL12.5 residues 128-148), L150K, and ΔC (a deletion of the C-terminal 49 residues) (460). A partial deletion of the UL12.5 MLS (ΔMLS) adjacent to conserved motif I (similar to the mutant shown in Fig. 3.7) was also

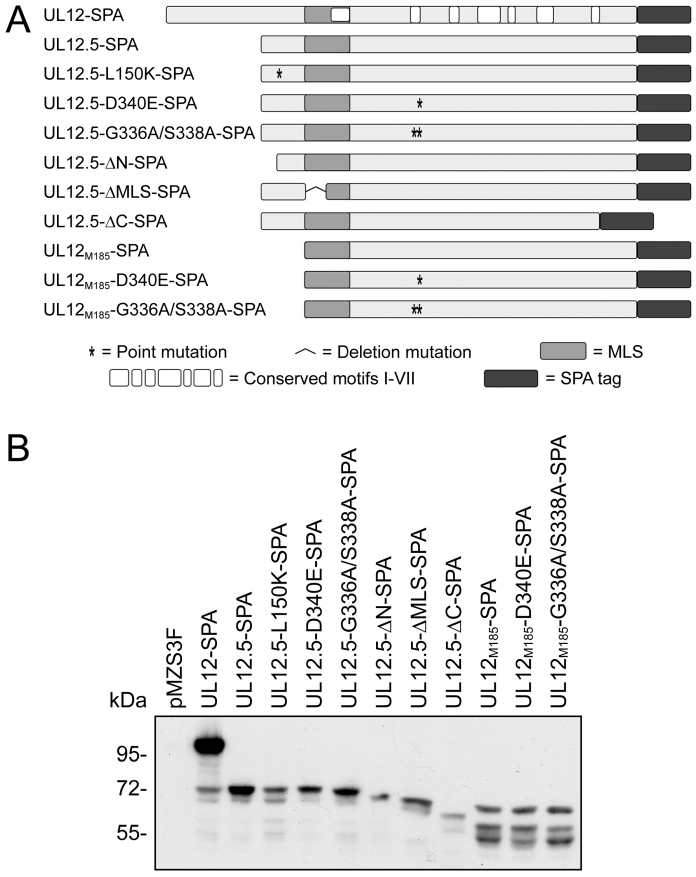

Figure 4.1. Carboxyl-terminally tagged UL12- and UL12.5-derived expression constructs. (A) Schematic of SPA-tagged proteins used in this study. The location of point and deletion mutations, the MLS, conserved alkaline nuclease motifs I-VII (43, 44), and the carboxyl-terminal sequential peptide affinity (SPA) tag are indicated. (B) Expression of SPA-tagged constructs in transfected HeLa cells. Cells were transfected with the indicated plasmids and harvested 24 hours post-transfection. Lysates were assessed for protein expression by immunoblotting with the mouse anti-FLAG M2 antibody and chemiluminescent detection.

included to assess the importance of mitochondrial localization during mtDNA depletion. *In vitro* biochemical analysis of the various nuclease-inactivating mutations in the context of UL12.5 as well as the $UL12_{M185}$ and ΔMLS mutations is described in Chapter 4A.

The mutant proteins were expressed in transfected HeLa cells and their steady-state levels were observed via western blotting (Fig. 4.1B). The largest protein product expressed from each vector migrated at the predicted mobility (UL12-SPA, ca. 100 kDa; UL12.5-SPA and UL12.5-SPA substitution mutants, ca. 70 kDa; UL12.5-ΔN-SPA and UL12.5-ΔMLS-SPA, ca. 69 kDa; UL12.5-ΔC-SPA, ca. 66 kDa; $UL12_{M185}$-SPA and $UL12_{M185}$-SPA mutants, ca. 68 kDa). The UL12-SPA expression plasmid also expressed a low level of UL12.5-SPA from the native *UL12.5* promoter contained within the *UL12* ORF (Fig. 4.1B and reference 42). Interestingly, multiple protein species can be observed for all SPA-tagged proteins (Figs. 4.1B and 4.2). Since these lysates are processed in the presence of protease inhibitors, these N-terminally truncated species are likely generated by post-translational processing of these proteins.

To determine whether the nuclease-inactivating mutations had an effect on mitochondrial targeting, I compared the localization of SPA tagged proteins (shown in red) with that of the mitochondrial protein cytochrome *c* (shown in green) using immunofluorescence microscopy. UL12-SPA demonstrated strong nuclear localization in most cells (Figs. 4.3 and 4.4A); however, a minority (ca. 20%) of cells also displayed a weak (Fig. 4.4B) or strong mitochondrial signal (Fig. 4.4C), presumably due to UL12.5 that is co-expressed from this plasmid

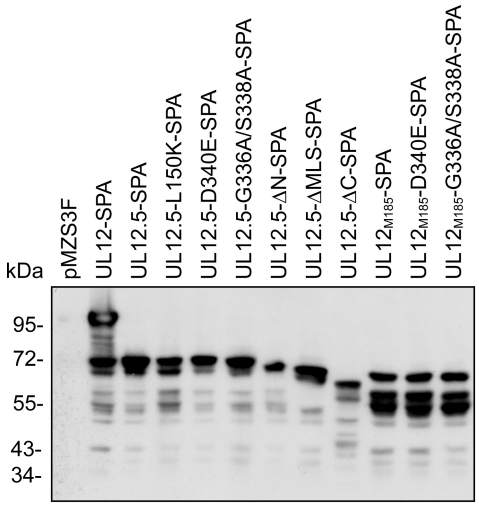

Figure 4.2. Multiple C-terminal fragments of SPA-tagged proteins are observed in transfected HeLa cells. Cells were transfected with the indicated plasmids and harvested 24 hours post-transfection. Lysates were assessed for protein expression by immunoblotting with the mouse anti-FLAG M2 antibody and chemiluminescent detection. Note: These data are the same as Figure 4.1B however this image was obtained using a longer exposure time.

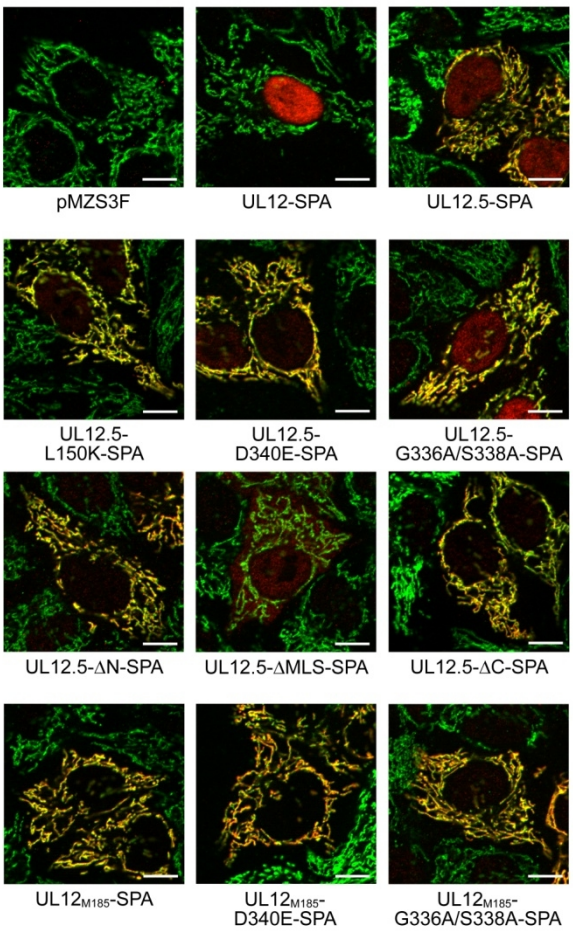

Figure 4.3. Mutations that disrupt nuclease activity do not affect mitochondrial localization. Transfected HeLa cells were co-stained with rabbit anti-FLAG (red) and mouse anti-cytochrome *c* (green) and visualized with fluorescence microscopy using a 63X objective. Colocalization of SPA-tagged (containing three FLAG epitopes) proteins with the mitochondrial protein cytochrome *c* are indicated in yellow. For clarity the DAPI channel has been omitted. Scale bars = 10 μm.

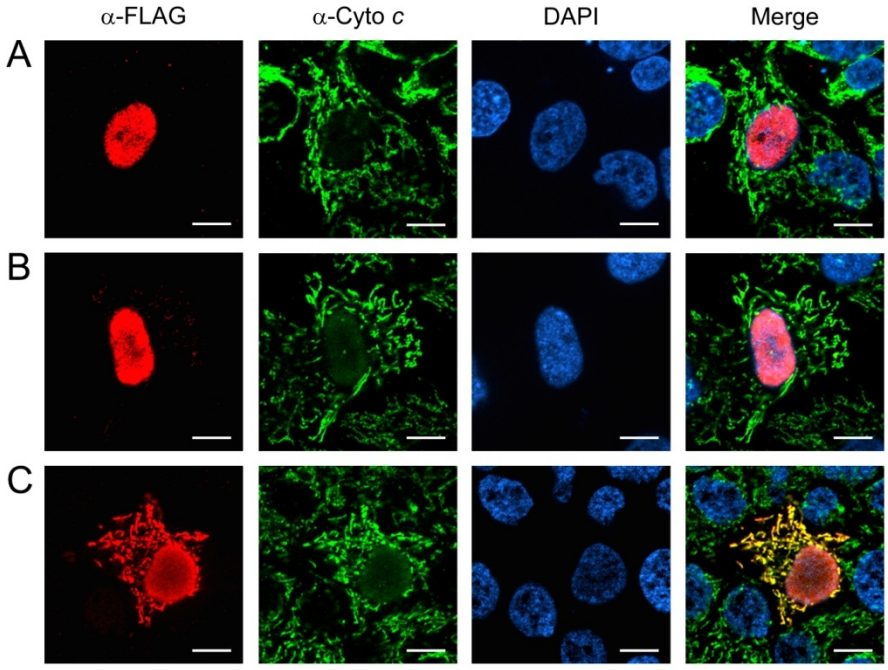

Figure 4.4. The pMZS3F UL12-SPA expression vector produces both UL12-SPA and UL12.5-SPA. HeLa cells transfected with pMZS3F UL12-SPA were co-stained with rabbit anti-FLAG (red), mouse anti-cytochrome *c* (α-Cyto *c*, green), and 4',6-diamidino-2-phenylindole (DAPI, blue) then visualized with fluorescence microscopy using a 63X objective. Expression of only UL12-SPA (A), UL12-SPA and weak UL12.5-SPA (B), and both UL12-SPA and UL12.5-SPA (C) can be observed. Colocalization of SPA-tagged proteins with the mitochondrial protein cytochrome *c* is indicated in yellow. Scale bars = 10 μm.

using the native *UL12.5* promoter. In contrast, UL12.5-SPA was predominantly mitochondrial in all cells, displaying a weaker nuclear signal than UL12 (Fig. 4.3) consistent with our previous observations (152, 475). All but one of the UL12.5 mutants displayed nuclear/mitochondrial localization similar to the wild-type UL12.5-SPA protein (Fig. 4.3). The exception was UL12.5-ΔMLS-SPA, which lacks a portion (R188-R212) of the MLS and was excluded from mitochondria. This observation supports the data highlighting the importance of N-proximal residues M185-R245 in targeting UL12.5 to mitochondria (Chapter 3 and reference 475). $UL12_{M185}$-SPA and its mutant derivatives localized exclusively to mitochondria, as did UL12.5-ΔN-SPA (Fig. 4.3). The failure of these N-terminally truncated mutants of UL12.5 to target the nucleus suggests that residues in the N-terminus of UL12.5 are needed for the partial nuclear localization of wild-type UL12.5, consistent with our previous data (Chapter 3 and reference 475). Moreover, similar observations to those mentioned above were made in immunofluorescence experiments using untagged versions of: UL12, UL12.5, UL12.5-L150K, UL12.5-ΔN, UL12.5-ΔMLS, UL12.5-ΔC, and $UL12_{M185}$, indicating that the SPA tag does not interfere with the localization of SPA-tagged UL12, UL12.5, or UL12.5 mutants (compare Figs. 4.3 and 4.5).

4.2.2 – Some nuclease-inactivating mutations do not prevent mtDNA depletion

I next determined if the nuclease-inactivating mutations eliminated mtDNA depletion using a previously described PicoGreen live cell imaging assay (152, 498). HeLa cells were co-transfected with plasmids expressing mOrange (to identify transfected cells) and UL12-SPA, UL12.5-SPA, or UL12.5-SPA mutants

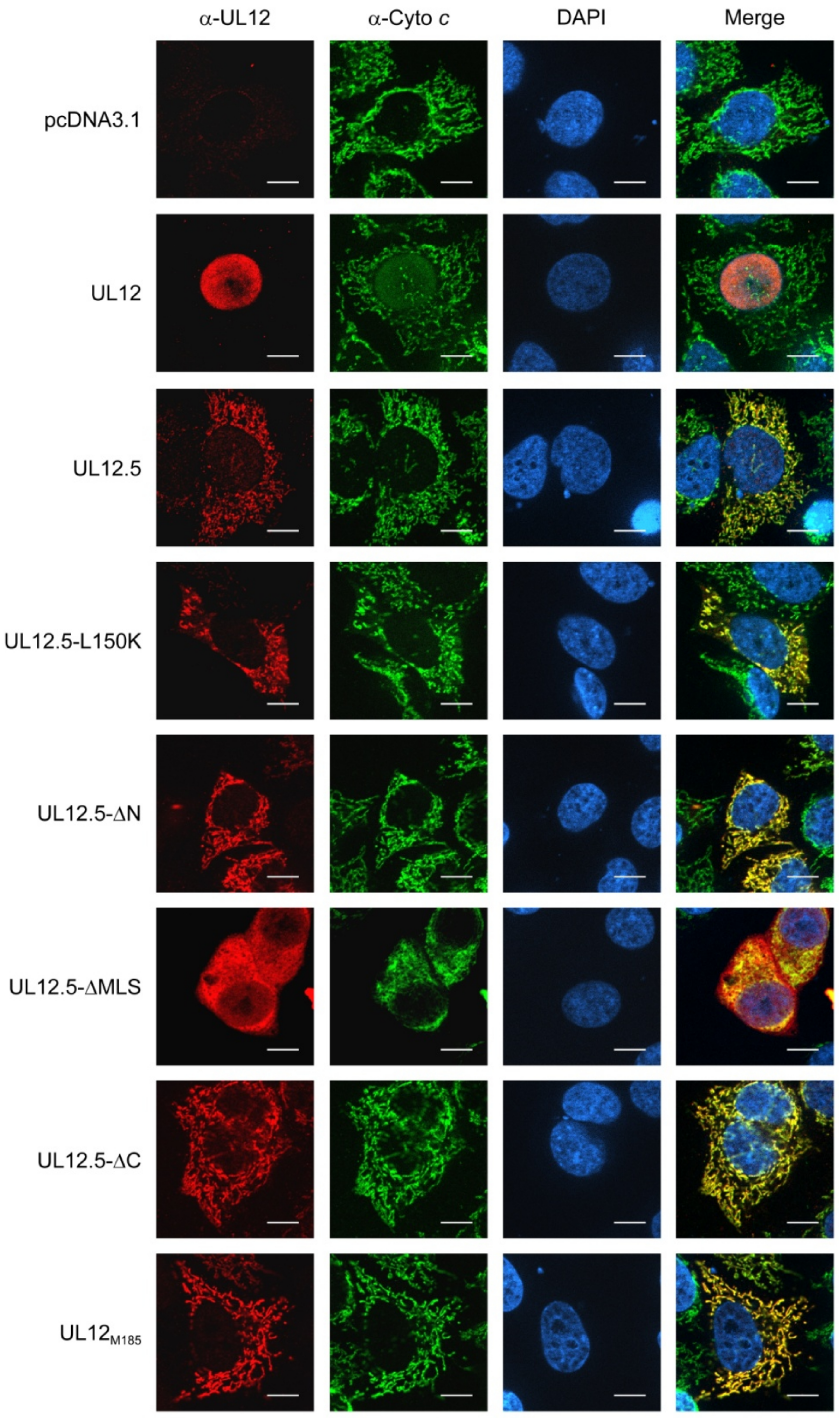

Figure 4.5. Localization of untagged UL12, UL12.5, and UL12.5-derived mutant proteins. Transfected HeLa cells were co-stained with rabbit anti-UL12 (red), mouse anti-cytochrome *c* (α-Cyto *c*, green), and 4',6-diamidino-2-phenylindole (DAPI) (blue) then visualized with fluorescence microscopy using a 63X objective. Colocalization of UL12 and UL12.5-derived proteins with the mitochondrial protein cytochrome *c* is indicated in yellow. Scale bars = 10 μm.

and stained with PicoGreen to determine the presence or absence of mtDNA. Consistent with our earlier observations (475), UL12.5-SPA and $UL12_{M185}$-SPA depleted mtDNA from the majority of transfected cells (Fig. 4.6). The UL12-SPA expression plasmid also caused mtDNA depletion in a minority of cells, likely due to expression of UL12.5-SPA from the *UL12.5* promoter in a subset of transfected cells (Figs. 4.1B and 4.4). Surprisingly, although two of the nuclease-inactivating mutations abrogated mtDNA depletion (D340E and ΔC), the L150K, G336A/S338A, and ΔN mutants retained significant activity (Fig. 4.6). Furthermore, comparable levels of expression (Fig. 4.7A) and mtDNA depletion (Fig. 4.7B) were observed in experiments using untagged versions of UL12, UL12.5, UL12.5-L150K, UL12.5-ΔN, and $UL12_{M185}$.

Purified UL12 bearing the G336A/S338A double substitution has no detectable nuclease activity (44). It is therefore striking that mutating these residues did not prevent mtDNA depletion by UL12.5 or $UL12_{M185}$ (Fig. 4.6); UL12.5-G336A/S338A-SPA caused mtDNA depletion in approximately one third as many cells as did UL12.5-SPA, while $UL12_{M185}$-G336A/S338A-SPA was as active as was $UL12_{M185}$-SPA. The enhanced ability of $UL12_{M185}$-G336A/S338A-SPA to cause mtDNA depletion relative to UL12.5-G336A/S338A-SPA may be due to its more efficient mitochondrial localization. Overall, these data indicate that neither the exonuclease or endonuclease activities of UL12.5 are required for mtDNA depletion in transfected cells.

The observation that the G336A/S338A mutations did not prevent mtDNA depletion seemed to conflict with our previous finding that a UL12.5-

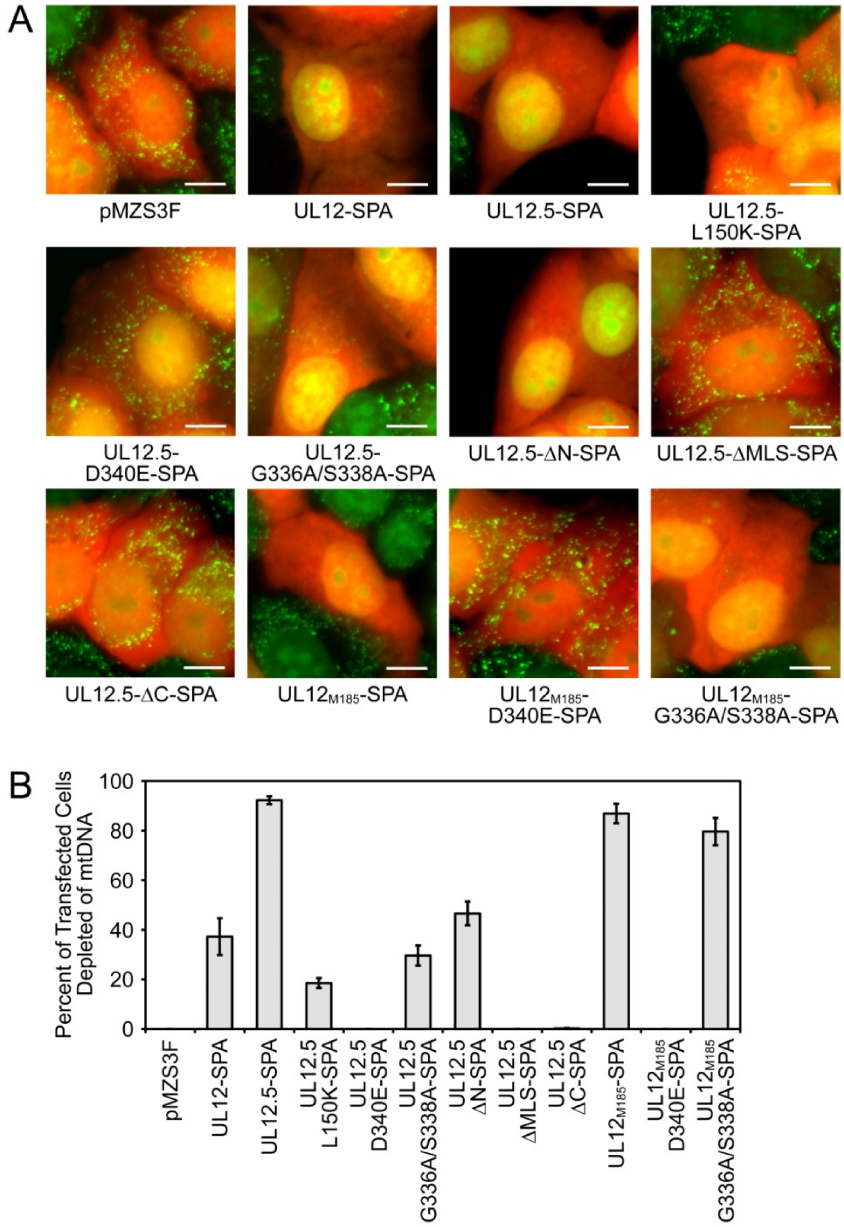

Figure 4.6. Some UL12.5 nuclease-deficient mutants retain the ability to cause mtDNA depletion. (A) HeLa cells were co-transfected with empty vector (pMZS3F), UL12-SPA, UL12.5-SPA, or UL12.5-SPA mutants and a plasmid expressing mOrange to identify transfected cells. PicoGreen staining was used to identify mtDNA foci in live cells using fluorescence microscopy at 48 hours post-transfection. Scale bars = 10 µm. (B) The extent of mtDNA depletion was determined by scoring for the presence (not depleted) or absence (depleted) of cytoplasmic PicoGreen staining in >100 randomly selected mOrange-positive cells. Data from three separate experiments were averaged and standard errors are indicated.

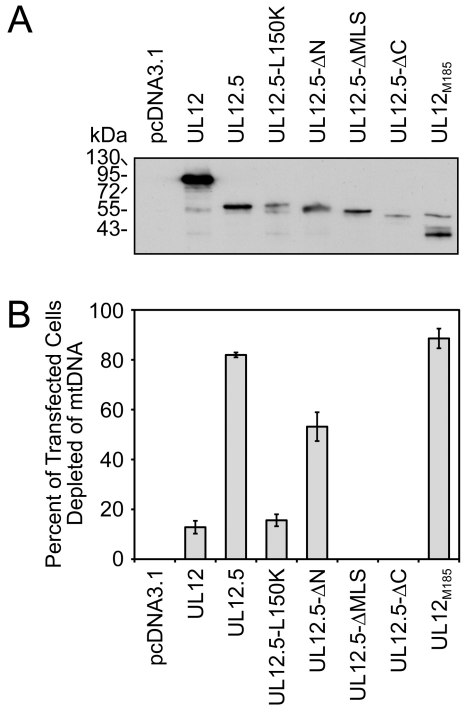

Figure 4.7. Expression and mtDNA depletion activity of untagged UL12, UL12.5, and UL12.5-derived nuclease-deficient proteins. (A) Expression of untagged constructs in transfected HeLa cells. Cells were transfected with the indicated plasmids and harvested 24 hours post-transfection. Lysates were assessed for protein expression by immunoblotting with the rabbit anti-UL12 antibody and chemiluminescent detection. (B) HeLa cells were co-transfected with empty vector (pcDNA3.1), UL12, UL12.5, or UL12.5 mutants and a plasmid expressing mOrange to identify transfected cells. PicoGreen staining was used to identify mtDNA foci in live cells using fluorescence microscopy at 48 hours post-transfection. The extent of mtDNA depletion was determined by scoring for the presence (not depleted) or absence (depleted) of cytoplasmic PicoGreen staining in >100 randomly selected mOrange-positive cells. Data from three separate experiments were averaged and standard errors are indicated.

G336A/S338A-mOrange mutant was inactive in this live cell imaging assay (475). I therefore reassessed the activity of this construct and found that it caused mtDNA depletion in a small percentage of transfected cells in some but not all experiments (Fig. 4.8). These observations were in contrast to those obtained with UL12.5-mOrange, which consistently caused mtDNA depletion, and UL12.5-D340E-mOrange, which caused no observable mtDNA depletion in transfected cells (Fig. 4.8). The reduced activity of the mOrange-tagged constructs compared to the SPA-tagged constructs may stem from the presence of the larger mOrange tag (236 residues) as compared to the 71 residue SPA tag (compare Figs. 4.5 and 4.8).

4.2.3 – Cellular endonuclease activity associates with some nuclease-deficient UL12.5 mutants

The rapid depletion of mtDNA following infection (152) argues against a defect in mtDNA replication being responsible for mtDNA loss and instead suggests that mtDNA is actively degraded by one or more nucleases. The ability of several nuclease-deficient mutants of UL12.5 to deplete mtDNA data implied that cellular nucleases are involved. Indeed, UL12 and UL12 orthologs are known to harness cellular nucleases to assist in their function. HSV-1 UL12 directly interacts with components of the MRE11-RAD50-NBS1 (MRN) complex, including the exo/endonuclease MRE11, which may facilitate viral DNA recombination during infection (466). Additionally, the KSHV shutoff and exonuclease (SOX) protein facilitates mRNA turnover in part through recruitment

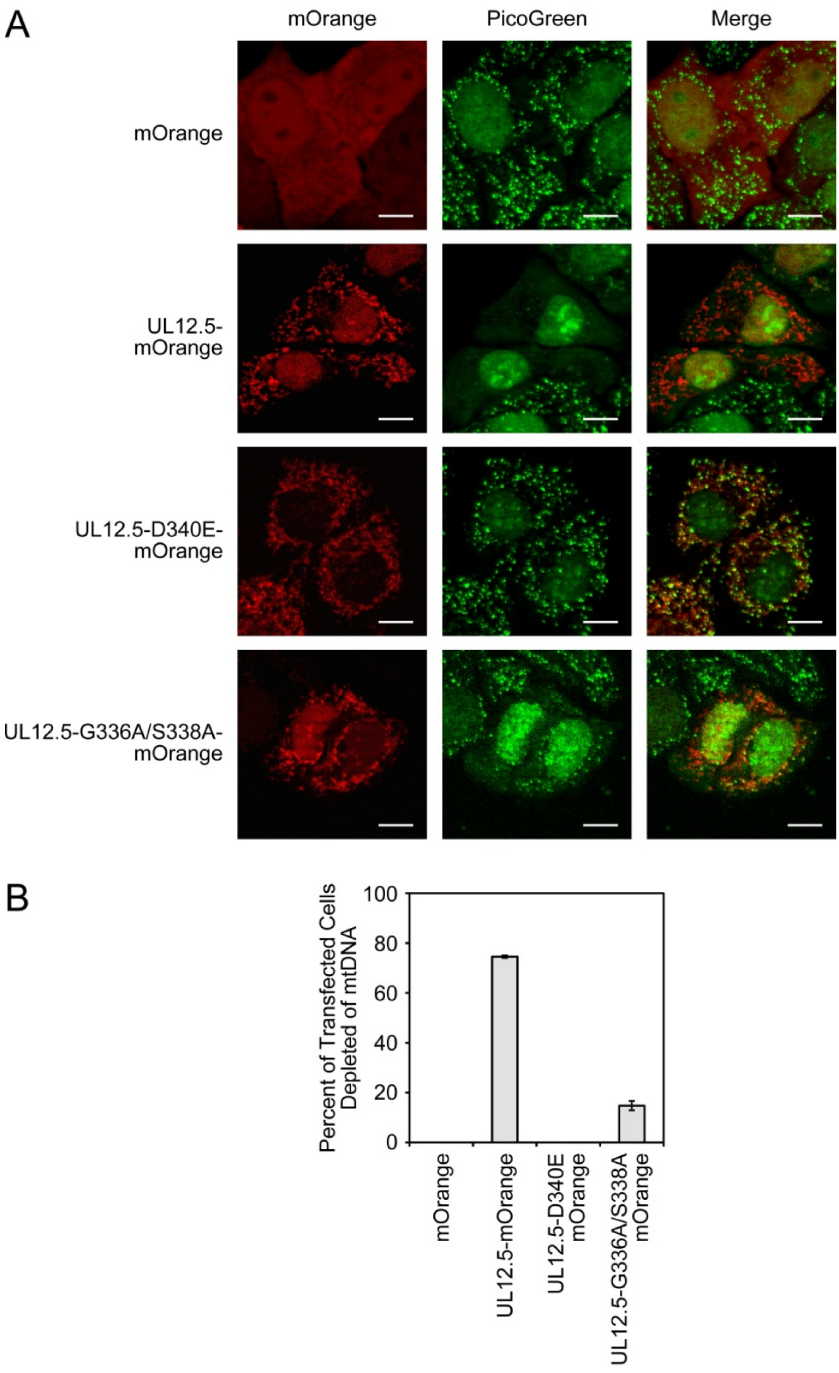

Figure 4.8. UL12.5-G336A/S338A-mOrange causes mtDNA depletion in the minority of transfected cells. (A) HeLa cells were co-transfected with empty vector (mOrange), UL12.5-mOrange, or UL12.5-mOrange mutants. PicoGreen staining was used to identify mtDNA foci in live cells using fluorescence microscopy with an ApoTome at 48 hours post-transfection. Scale bars = 10 μm. (B) The extent of mtDNA depletion in ≥100 randomly selected mOrange-positive cells was measured as described in Fig. 4.6. Data from four separate experiments were averaged and standard errors are indicated.

of the host 5'→3' exoribonuclease 1 (499). Therefore, I examined whether cellular nucleases contribute to mtDNA loss following UL12.5 expression.

As one test of this hypothesis, I expressed SPA-tagged UL12, UL12.5, and UL12.5 mutants in HeLa cells and isolated the protein complexes containing these proteins by immunoprecipitation (Figs. 4.9A and 4.9D). The resulting immunoprecipitates were tested for their ability to degrade linearized plasmid DNA or to nick circular plasmid DNA *in vitro*. These nuclease assays were performed under alkaline pH conditions that were conducive to the detection of UL12/UL12.5 nuclease activity.

As expected, immunoprecipitates containing UL12-SPA and UL12.5-SPA were capable of degrading linearized plasmid DNA consistent with their known nuclease activity, while immunoprecipitates from cells transfected with empty pMZS3F vector displayed no activity (Figs. 4.9B and 4.9E). The degradation of the linear DNA substrate could be due to exo- and/or endonuclease activity; however, it is plausible that the much stronger exonuclease activity (463) is the major contributor. In contrast, the immunoprecipitates containing $UL12_{M185}$-SPA or the SPA-tagged substitution/truncation mutants did not detectably degrade the linearized DNA substrate (Figs. 4.9B and 4.9E). These data were consistent with my observations using *in vitro* translated versions of the same proteins (Fig. 4A.1). Together, these data indicated that none of these mutant proteins possessed, or associated with, detectable nuclease activity against linear DNA substrates as measured in these assays. However it is important to note that these assays would likely not detect low levels of endonuclease activity, as a large

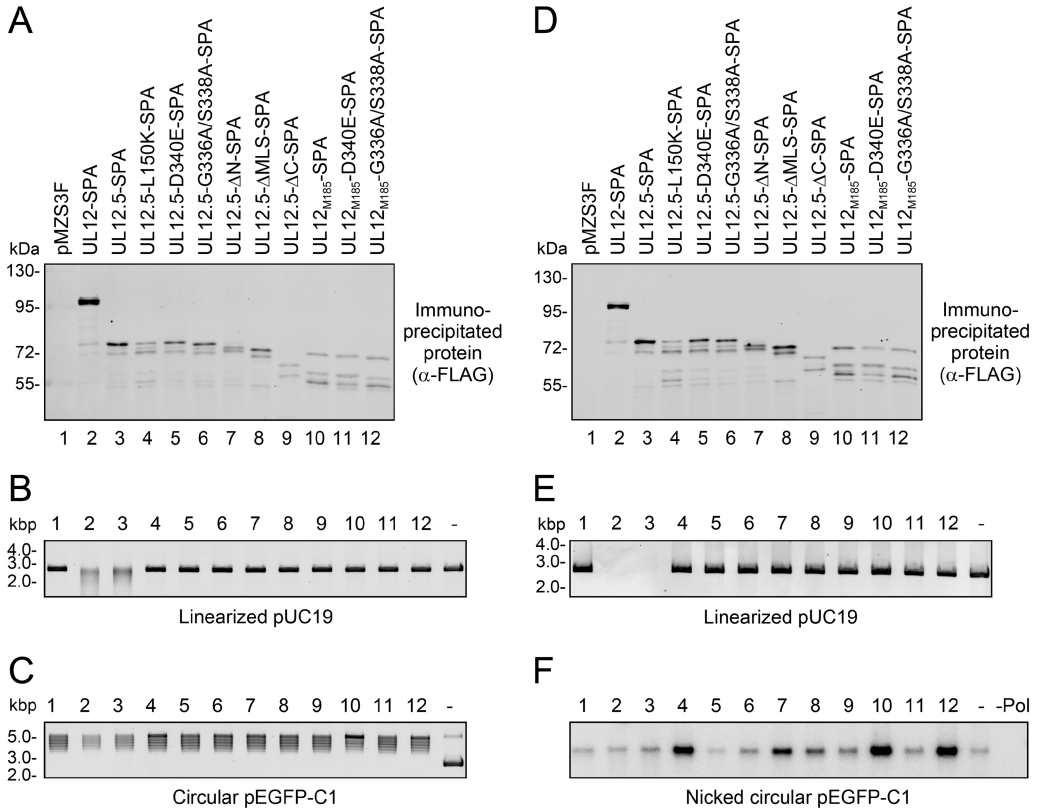

Figure 4.9. Some nuclease-deficient mutants associate with cellular endonuclease activity in transfected cells. (A) and (D) SPA-tagged proteins were immunoprecipitated from transfected HeLa cells and visualized by immunoblotting with the rabbit anti-FLAG antibody followed by infrared detection. Immunoprecipitates from panel A were incubated with 50 ng linearized pUC19 (B) or 50 ng pEGFP-C1 (C) to visualize nuclease activity. Samples in panels B and C are labelled as indicated in panel A. Plasmid DNA incubated in the absence of immunoprecipitate (DNA only) is indicated as "-". DNA was visualized using SYBR Gold staining. (E) Immunoprecipitates from panel D were incubated with 20 ng linearized pUC19 to visualize nuclease activity. Samples are labelled as indicated in panel D. Linearized pUC19 DNA incubated in the absence of immunoprecipitate (DNA only) is indicated as "-". DNA was visualized using SYBR Gold staining. (F) Immunoprecipitates from panel D were also incubated with 50 ng circular pEGFP-C1 and the resulting nicked plasmid DNA was radiolabelled using nick translation, separated by agarose gel electrophoresis, and visualized using a phosphorimager. Samples are labelled as indicated in panel D. pEGFP-C1 DNA incubated in the absence of immunoprecipitate (DNA only) is indicated as "-". Circular pEGFP-C1 DNA incubated in the absence of immunoprecipitate and processed for nick translation without *E. coli* DNA polymerase I is indicated as "-Pol".

number of nicks would be required to alter the mobility of the linear substrates in non-denaturing gels.

I also specifically tested the same immunoprecipitates for endonuclease activity using a covalently closed circular plasmid DNA substrate. The outcome was visualized by monitoring the overall loss of DNA and the generation of nicked circles using SYBR Gold staining (Fig. 4.9C) or nick translation (Fig. 4.9F). With all immunoprecipitates, the circular plasmid DNA migrated as a cluster of closely spaced bands (Figs. 4.9C and 4.10). These bands collapsed into a single linear species following restriction enzyme digestion (Fig. 4.10A), suggesting the presence of contaminating topoisomerase activity. In addition to this effect on DNA migration, a clear and consistent loss of circular DNA can be observed upon incubation with the UL12-SPA immunoprecipitate (ca. 45% loss) whereas the endonuclease activity of the UL12.5-SPA immunoprecipitates is less apparent (Fig. 4.10A). Comparable DNA laddering was detected after incubating HeLa cell lysate with protein G agarose beads in the absence of antibody which suggests that the contaminating topoisomerase activity non-specifically associates with the protein G agarose used for these immunoprecipitations (Fig. 4.10B).

As expected, immunoprecipitates containing UL12-SPA and UL12.5-SPA caused an appreciable decrease in the total amount of DNA observed by SYBR Gold staining (Fig. 4.9C), likely due to endonucleolytic nicking followed by exonuclease activity. However, when these immunoprecipitates were scored for endonuclease activity using nick translation, there was no increase compared to the controls (pMZS3F or DNA only, Fig. 4.9F), suggesting that the nicked DNA

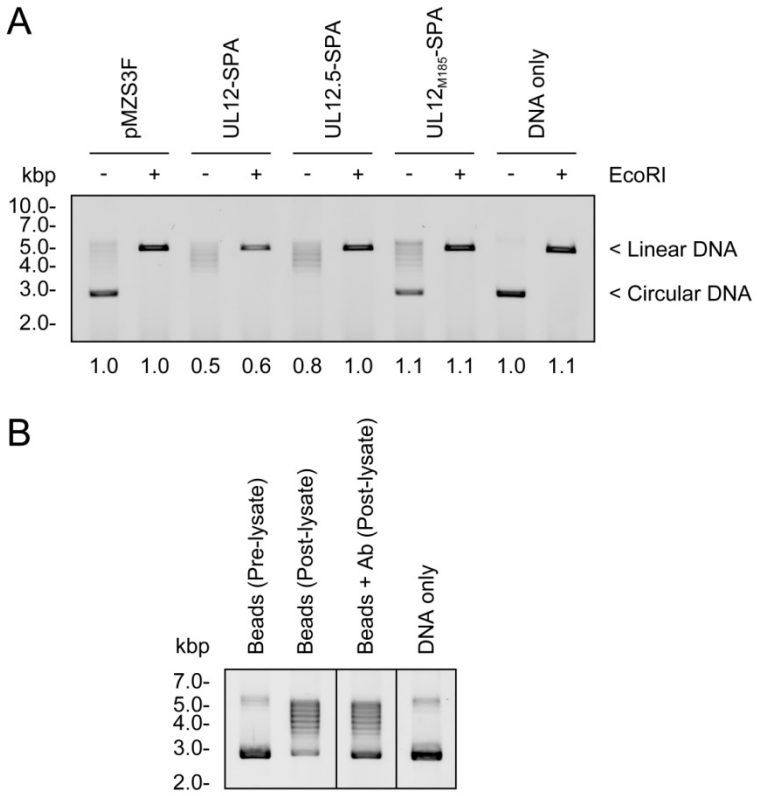

Figure 4.10. DNA laddering visible during *in vitro* nuclease assays with immunoprecipitated proteins is likely due to contaminating topoisomerase activity. (A) SPA-tagged proteins were immunoprecipitated from transfected HeLa cells and were incubated with 50 ng circular pEGFP-C1. Following the incubation, the reactions were phenol/chloroform extracted, ethanol precipitated with a tRNA carrier, then divided equally and incubated in the presence or absence of EcoRI. The migration of linear and circular isoforms of pEGFP-C1 is indicated to the right. The amount of DNA present in each sample relative to the control (DNA only, - EcoRI) is indicated below the image. (B) Protein G agarose (Beads) or protein G agarose bound to α-FLAG antibody (Beads + Ab) was incubated with pEGFP-C1 prior to (pre-lysate) or following (post-lysate) exposure to HeLa cell lysate. pEGFP-C1 DNA incubated in the absence of immunoprecipitate or lysate is labelled "DNA only".

is rapidly degraded by the powerful exonuclease activity of UL12, as previously observed (463). Interestingly, immunoprecipitates containing UL12.5-L150K-SPA, UL12.5-ΔN-SPA, $UL12_{M185}$-SPA, and $UL12_{M185}$-G336A/S338A-SPA yielded consistently higher levels of nick translation indicative of the presence of endonuclease activity (Fig. 4.9F). Some of these immunoprecipitates also generated higher levels of relaxed circles when assessed by the less sensitive SYBR Gold detection method (UL12.5-L150K-SPA, $UL12_{M185}$-SPA, and to a lesser extent $UL12_{M185}$-G336A/S338A-SPA; Fig. 4.9C). A low level of endonuclease activity was observed in immunoprecipitates containing the UL12.5-ΔMLS-SPA protein and no appreciable endonuclease activity was observed by nick translation for immunoprecipitates containing UL12.5-D340E-SPA, UL12.5-G336A/S338A-SPA, UL12.5-ΔC-SPA, or $UL12_{M185}$-D340E-SPA (Fig. 4.9F).

It might be argued that the enhanced nicking activity detected in the immunoprecipitates of some mutant proteins is due to residual UL12.5 endonuclease activity. However, the mutational sensitivity profile of the associated endonuclease activity is incompatible with this suggestion for two reasons: 1) $UL12_{M185}$-G336A/S338A-SPA immunoprecipitates were among the most active in this assay, yet purified UL12 protein bearing the G336A/S338A double substitution lacks detectable endo- and exonuclease activity (44); and 2) $UL12_{M185}$-D340E-SPA displayed only background levels of nicking in this assay, yet the D340E substitution does not greatly impair the endonuclease activity of purified UL12 (44). These considerations indicate that the immunoprecipitation

assay does not detect the weak endonuclease activity of UL12.5, and strongly argue that the nicking activity that I observe is due to one or more associated cellular endonucleases.

Interestingly, the nuclease-deficient UL12.5 mutants that associated with presumably cellular endonuclease activity tended to be those capable of causing mtDNA depletion (UL12.5-L105K-SPA, UL12.5-ΔN-SPA, $UL12_{M185}$-SPA, and $UL12_{M185}$-G336A/S338A-SPA; Figs. 4.6 and 4.9). The exceptions to this correlation were: 1) UL12.5-G336A/S338A-SPA which although capable of causing mtDNA depletion did not associate with appreciable endonuclease activity, and 2) UL12.5-ΔMLS-SPA which associated with some endonuclease activity but is unable to cause mtDNA loss (Figs. 4.6 and 4.9F). The observation that the $UL12_{M185}$ double substitution mutant exhibits stronger mitochondrial localization (Fig. 4.3), causes more mtDNA depletion (Fig. 4.6), and associates with more endonuclease activity (Fig. 4.9F) than the UL12.5 double substitution mutant is consistent with the possibility that the associated nuclease is mitochondrial.

4.2.4 – The mitochondrial nucleases ENDOG and EXOG participate in mtDNA depletion mediated by UL12.5

Mammalian mitochondria contain a small number of endonucleases including: ENDOG (500, 501), EXOG (484), APEX1/2 (400-402), FEN1 (404, 409), DNA2 (404), and the recently described endo/exonuclease Ddk1 (502). Of these, APEX1/2, FEN1, and DNA2 seemed unlikely to be involved in mtDNA loss provoked by UL12.5 since they act on specialized DNA substrates (such as

apurinic/apyrimidinic sites or DNA flaps), while Ddk1 had not been discovered at the onset of this research. I therefore examined ENDOG and EXOG as potential candidates. Unlike in *Neurospora crassa* and *Saccharomyces cerevisiae* where a single ENDOG homolog possesses both endonuclease and exonuclease activity (503-505), the majority of mammalian mitochondrial endonuclease and exonuclease activities are thought to be due to the combined action of ENDOG and its highly related paralog EXOG (484). For this reason I considered the possibility that ENDOG and EXOG may play redundant roles in UL12.5-SPA mediated-mtDNA depletion.

ENDOG is a sugar non-specific, magnesium-dependent endonuclease which preferentially introduces single-stranded nicks adjacent to guanine residues (506, 507). The biochemical properties of ENDOG are remarkably similar to UL12.5 in that ENDOG functions in the presence of magnesium, alkaline pH, and low ionic strength (459, 507). Aside from its role in apoptosis, ENDOG is responsible for the majority of mammalian mitochondrial nuclease activity and has been observed to associate with mtDNA via chromatin immunoprecipitation (390, 500, 501). Interestingly, ENDOG has already been shown to participate in HSV-1 biology from its proposed role in HSV-1 *a* sequence recombination (508, 509). EXOG differs from ENDOG in that it possesses both endonuclease and weak 5'→3' exonuclease activity and exhibits a preference for single-stranded DNA (484).

As one approach to assessing the potential roles of ENDOG and EXOG in UL12.5-mediated mtDNA depletion, I examined the effect of overexpressing

mutant forms of ENDOG and EXOG along with the mtDNA depletion-competent and nuclease-deficient mutant $UL12_{M185}$-G336A/S338A-SPA in the live cell mtDNA depletion assay. I created plasmids which express C-terminally c-myc/His-tagged (hereafter referred to as myc-tagged) wild-type and catalytically inactive forms (483, 484) of ENDOG and EXOG. As a negative control for these experiments, I obtained a plasmid which expresses a catalytically-inactive version of the mitochondrial matrix protein sirtuin 3 (Sirt3-H248Y) (477, 510) which was presumed to be unlikely to affect $UL12_{M185}$-G336A/S338A-SPA mtDNA depletion activity. The expression and apparent molecular masses of all myc-tagged proteins were confirmed by Western blotting (Fig. 4.11). The larger and smaller protein species observed following transfection of the ENDOG and Sirt3 plasmids likely correspond to previously described precursor and mature forms of the proteins, respectively (Fig. 4.11 and references 328, 510). Wild-type and mutant EXOG-myc proteins also appeared to migrate as two species during SDS-PAGE. All myc-tagged proteins also displayed the expected mitochondrial localization as observed by their co-localization with the mitochondrial protein cytochrome *c* during immunofluorescence experiments (Fig. 4.12). The addition of a C-terminal epitope tag does not interfere with the enzymatic activity of ENDOG or EXOG (484, 507, 511), and I verified in preliminary co-immunoprecipitation experiments that the catalytically inactive mutants (ENDOG-H141A and EXOG-H140A) retained the ability to form homomultimers with their wild-type counterparts (Fig. 4.13 and references 483, 484, 512); this suggests that the ENDOG-H141A and EXOG-H140A proteins may act as

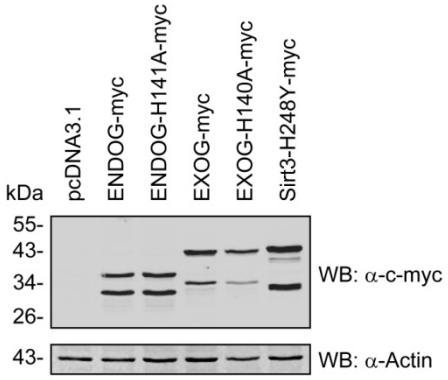

Figure 4.11. Expression of c-myc-tagged wild-type and mutant ENDOG and EXOG and Sirt3-H248Y proteins in HeLa cells. Cells were transfected with the indicated plasmids and harvested 48 hours post-transfection. Lysates were assessed for protein expression by immunoblotting using antibodies against the c-myc epitope tag (α-c-myc) and actin (α-Actin) followed by infrared detection.

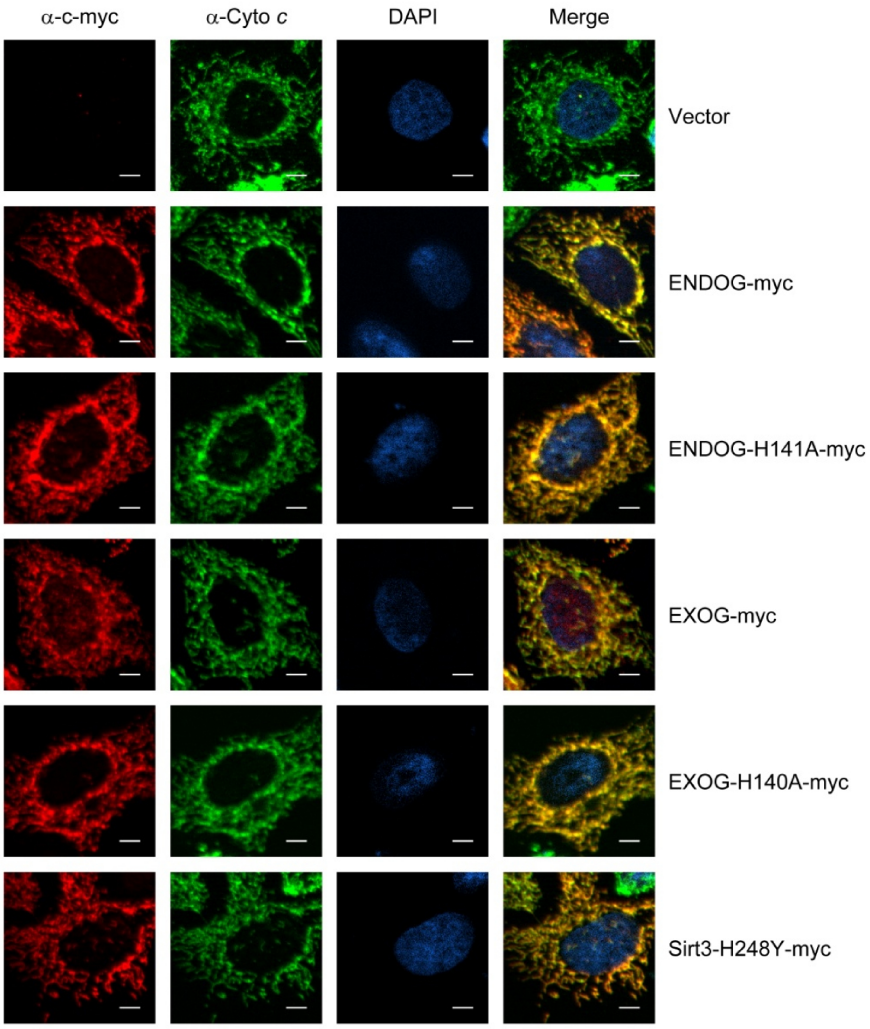

Figure 4.12. Localization of myc-tagged ENDOG, EXOG, and Sirt3 proteins in HeLa cells. Transfected HeLa cells were co-stained with rabbit anti-c-myc (α-c-myc, red), mouse anti-cytochrome *c* (α-Cyto *c*, green), and 4',6-diamidino-2-phenylindole (DAPI) (blue) then visualized with fluorescence microscopy using a 40X objective. Colocalization of myc-tagged proteins with the mitochondrial protein cytochrome *c* is indicated in yellow. Scale bars = 5 μm.

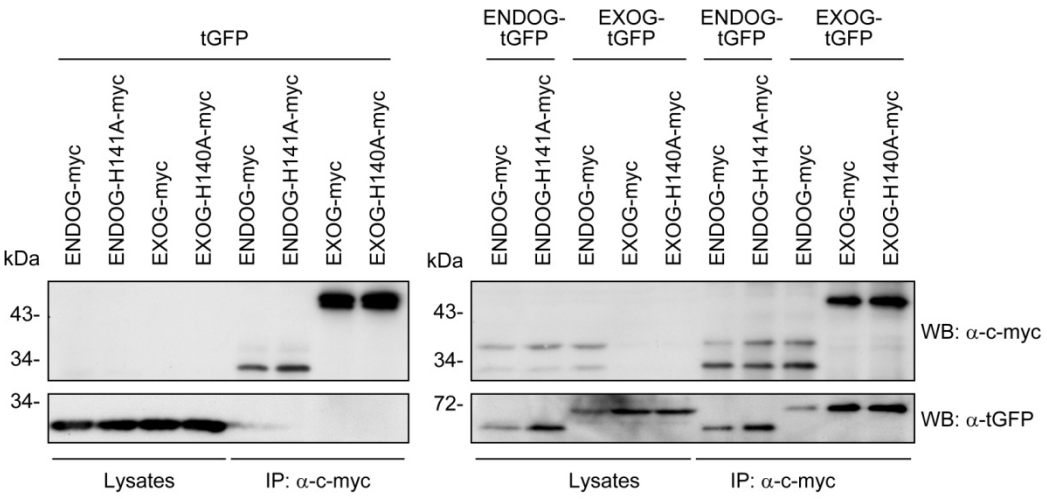

Figure 4.13. Overexpressed ENDOG and EXOG form homo- and heteromultimers in transfected cells. HeLa cells expressing the indicated combinations of proteins were lysed and processed for immunoprecipitation (IP) using an antibody against the c-myc epitope tag (α-c-myc). Both lysates and immunoprecipitates were analyzed by western blotting using antibodies against the c-myc and tGFP (α-tGFP) epitope tags. tGFP, turbo green fluorescent protein.

dominant-negative regulators of ENDOG and EXOG enzymatic activity, respectively. As an aside, I also observed that ENDOG and EXOG formed heteromultimers in transfected cells in preliminary experiments (Fig. 4.13). Although, more experiments are needed to support these findings, it is interesting that these two highly related enzymes may form a complex in higher eukaryotes.

Expression of EXOG, EXOG-H140A, or Sirt3-H248Y on their own had no observable effect on mtDNA levels in the live cell mtDNA depletion assay (Fig. 4.14). However, expression of ENDOG or ENDOG-H141A caused mtDNA depletion in approximately 8% of transfected cells (Fig. 4.14A). In the case of wild-type ENDOG this effect was eliminated by co-transfecting ENDOG siRNA (Fig. 4.15). Co-transfecting ENDOG with negative control (N.C.) siRNA had no observable affect on ENDOG-mediated mtDNA loss (compare Figs. 4.14A and 4.15). The observation that overexpression of wild-type or mutant ENDOG causes mtDNA depletion is novel and very intriguing. Although it is currently the subject of debate, several studies support a role of ENDOG in mtDNA maintenance (389, 390, 513-515). These observations suggest that although the nuclease activity of ENDOG is not responsible for mtDNA loss following overexpression, ENDOG is involved in regulating mtDNA metabolism.

Expression of wild-type or mutant ENDOG or EXOG had no significant effects on $UL12_{M185}$-G336A/S338A-SPA-mediated mtDNA depletion (Fig. 4.14A). However, when cells simultaneously expressed ENDOG-H141A and EXOG-H140A mtDNA depletion was reduced by 38% ($p = 0.029$, Fig. 4.14A). In contrast, overexpression of the unrelated mitochondrial protein Sirt3-H248Y had

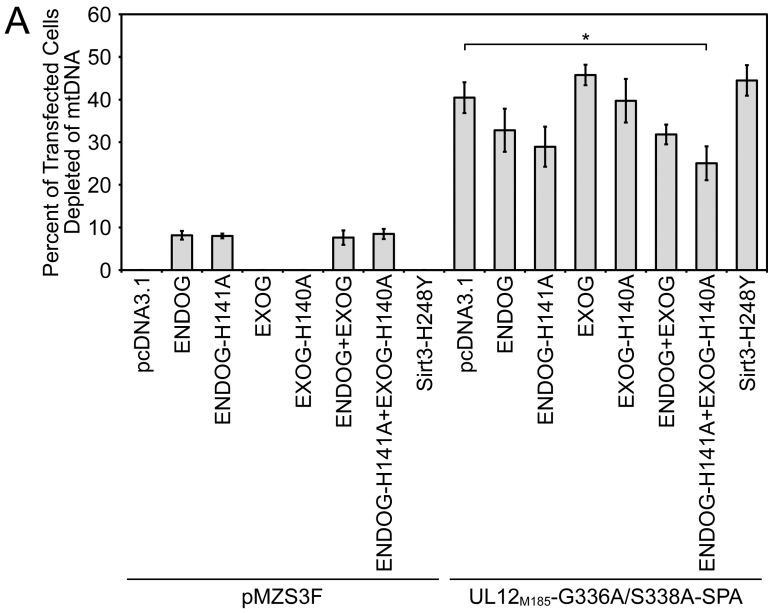
A
Percent of Transfected Cells Depleted of mtDNA
60
50
40
30
20
10
0
*
pcDNA3.1
ENDOG
ENDOG-H141A
EXOG
EXOG-H140A
ENDOG+EXOG
ENDOG-H141A+EXOG-H140A
Sirt3-H248Y
pcDNA3.1
ENDOG
ENDOG-H141A
EXOG
EXOG-H140A
ENDOG+EXOG
ENDOG-H141A+EXOG-H140A
Sirt3-H248Y
pMZS3F
UL12M185-G336A/S338A-SPA

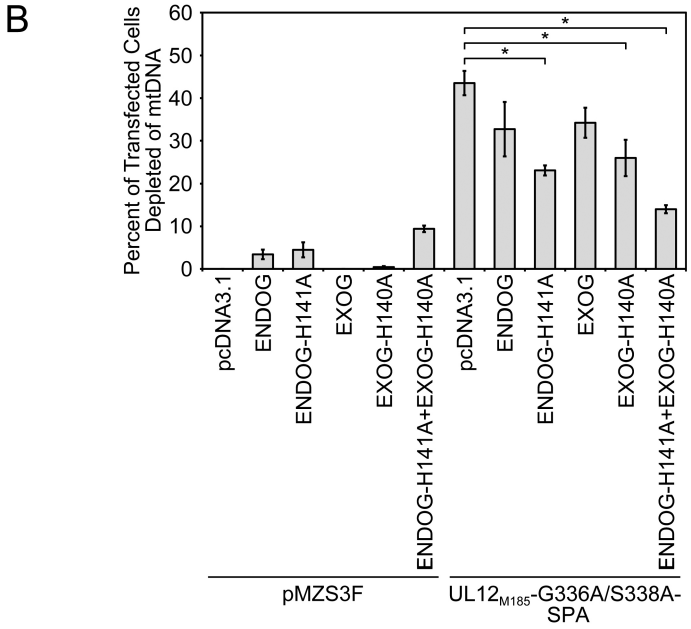
B
Percent of Transfected Cells Depleted of mtDNA
60
50
40
30
20
10
0
*
*
*
pcDNA3.1
ENDOG
ENDOG-H141A
EXOG
EXOG-H140A
ENDOG-H141A+EXOG-H140A
pcDNA3.1
ENDOG
ENDOG-H141A
EXOG
EXOG-H140A
ENDOG-H141A+EXOG-H140A
pMZS3F
UL12M185-G336A/S338A-SPA

Figure 4.14. Concurrent overexpression of nuclease-deficient ENDOG and EXOG inhibits mtDNA depletion by a mutant UL12.5-SPA protein. HeLa cells were co-transfected for 48 hours with a 2:1:1 ratio (A) or a 5:1:1 ratio (B) of total pcDNA3.1 DNA to pMZS3F DNA to pcDNA-mOrange DNA. pcDNA3.1 DNA = Empty vector (pcDNA3.1) or plasmids expressing myc-tagged ENDOG, ENDOG-H141A, EXOG, EXOG-H140A, or Sirt3-H248Y. pMZS3F DNA = Empty vector (pMZS3F) or a plasmid expressing $UL12_{M185}$-G336A/S338A-SPA. MtDNA depletion was measured as described in Fig. 4.4. Data in panel A are from four separate experiments (except those including the Sirt3 mutant which are from three separate experiments) while data in panel B are from three separate experiments. All data were averaged and standard errors are indicated. Data denoted with * indicate statistical significance ($P < 0.05$) when compared to the control ($UL12_{M185}$-G336A/S338A-SPA/pcDNA).

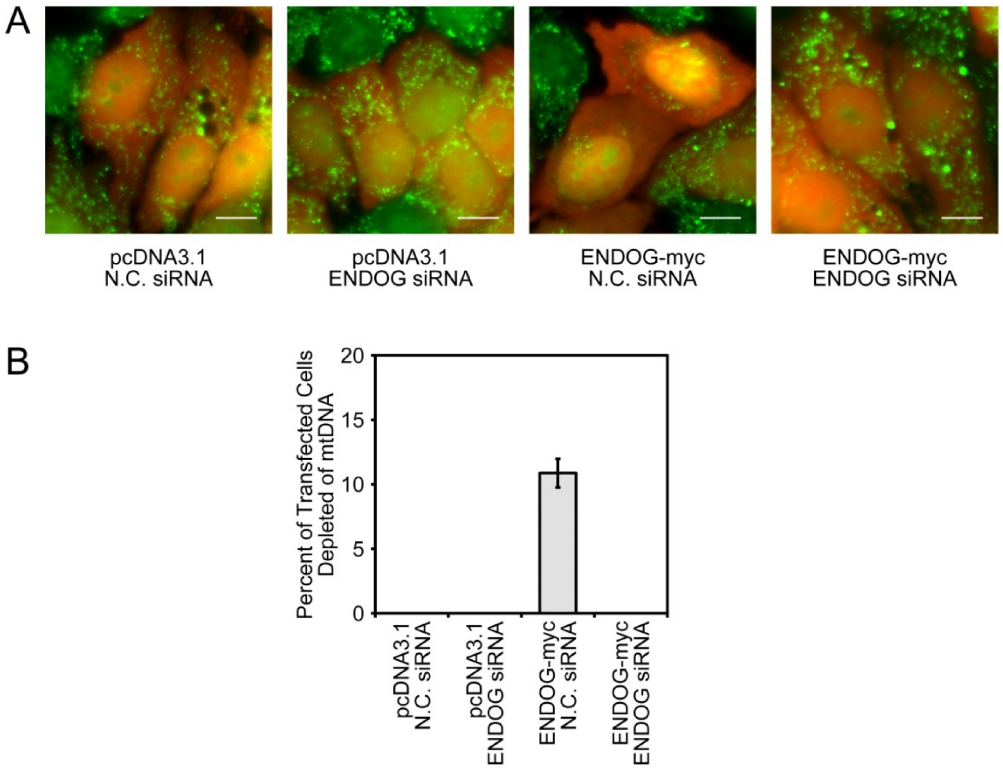

Figure 4.15. MtDNA depletion observed following ENDOG-myc overexpression is eliminated by treatment with ENDOG siRNA. (A) HeLa cells were co-transfected with empty vector (pcDNA3.1) or pcDNA3.1-ENDOG-myc, negative control (N.C.) siRNA or ENDOG siRNA, and a plasmid expressing mOrange to identify transfected cells. PicoGreen staining was used to identify mtDNA foci in live cells using fluorescence microscopy at 48 hours post-transfection. Scale bars = 10 μm. (B) The extent of mtDNA depletion was measured as described in Fig. 4.6. Data are from four separate experiments. All data were averaged and standard errors are indicated.

no effect on mtDNA depletion by $UL12_{M185}$-G336A/S338A-SPA (Fig. 4.14A). Interestingly, overexpression of both mutant ENDOG and mutant EXOG was needed to significantly impair mtDNA depletion by $UL12_{M185}$-G336A/S338A-SPA. Therefore, ENDOG and EXOG likely play at least partially redundant roles in the mtDNA degradation pathway that is stimulated following the expression of $UL12_{M185}$-G336A/S338A-SPA. The inhibitory effect of the combination of ENDOG-H141A and EXOG-H140A appeared to be dose dependent, as increasing the amount of ENDOG-H141A/EXOG-H140A plasmid DNA 2.5-fold reduced mtDNA depletion by ca. 68% ($p = 0.001$) in a separate series of experiments (Fig. 4.14B). Furthermore, significant inhibition of $UL12_{M185}$-G336A/S338A-SPA-mediated mtDNA depletion could be achieved when greater amounts of ENDOG-H141A or EXOG-H140A encoding plasmids were co-transfected into cells (Fig. 13B). Although the percent inhibition of mtDNA depletion caused by ENDOG-H141A (47%, $p = 0.003$) or EXOG-H140A (40%, $p = 0.027$) expression alone did not reach the inhibitory effect of the concurrent expression of both proteins (68%) (Fig. 4.14B).

To complement the overexpression experiments described above, I employed RNA interference to reduce ENDOG and/or EXOG levels in HeLa cells prior to mtDNA depletion. Prior to performing these experiments, I confirmed that the commercially available siRNAs used in this study appropriately suppressed EXOG and ENDOG expression. Firstly, the siRNA targeting EXOG reduced total protein expression by 56% (Fig. 4.16A). Moreover, the siRNA treatment reduced EXOG levels in mitochondria by 66% (Fig. 4.16B).

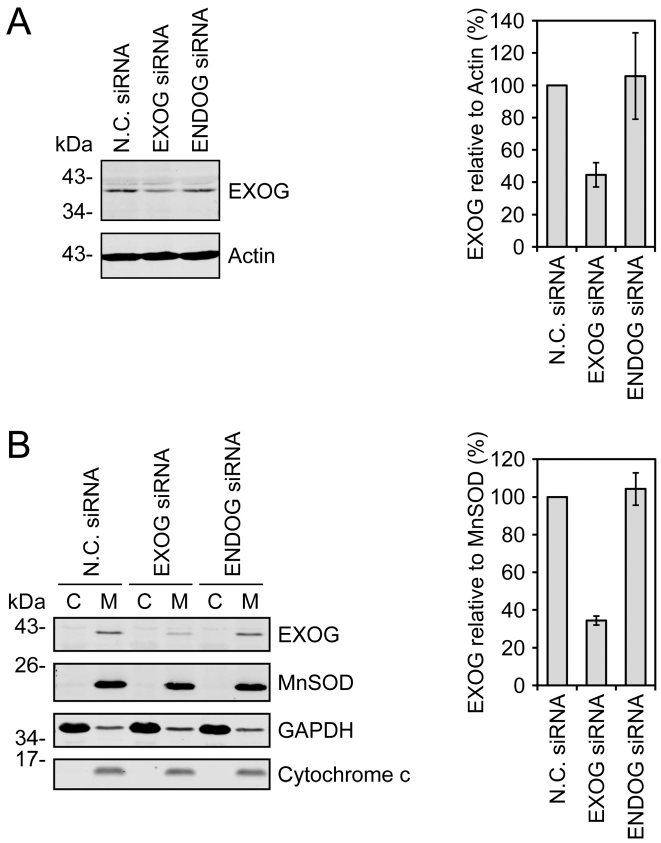

Figure 4.16. Knockdown of endogenous EXOG using siRNA. (A) Endogenous EXOG knockdown was measured in HeLa cells transfected with the indicated siRNAs. (B) Lysates from HeLa cells transfected with the indicated siRNAs were separated into cytoplasmic and mitochondrial fractions to visualize knockdown of EXOG in the mitochondrial fraction. EXOG levels were quantitated following immunoblotting and infrared detection. Data from three separate experiments were averaged, plotted relative to actin in total cell lysates (A) or MnSOD in crude mitochondrial fractions (B), and normalized to the N.C. siRNA treatment. Standard errors are indicated.

I have not been able to identify an antibody that reliably detects endogenous ENDOG and therefore tested the ENDOG siRNA for its ability to prevent *de novo* expression of exogenous myc-tagged ENDOG. Using siRNA/plasmid DNA co-transfections, I observed that the ENDOG siRNA reduced ENDOG-myc expression by 85% relative to treatment with a negative control siRNA indicating that the siRNA targets the ENDOG transcript (Fig. 4.17A). Similar suppression of EXOG-myc expression by the EXOG siRNA was also observed (68% reduction, Fig. 4.17B). Importantly, the EXOG and ENDOG siRNAs specifically target their respective transcripts (Fig. 4.17). It therefore seems likely that the ENDOG siRNA depletes endogenous ENDOG in a fashion similar to the effect of EXOG siRNA on endogenous EXOG.

For the knockdown/mtDNA depletion experiments, I pre-treated HeLa cells with N.C. siRNA, ENDOG siRNA, EXOG siRNA, or a mixture of ENDOG and EXOG siRNAs for 48 hours. Cells were then trypsinized and reverse co-transfected with additional siRNA and the indicated effector plasmids and mtDNA depletion was evaluated 24 hours later using the PicoGreen live cell imaging assay. When tested individually the ENDOG and EXOG siRNAs did not significantly affect mtDNA depletion by $UL12_{M185}$-G336A/S338A-SPA; however, concurrent knockdown of both ENDOG and EXOG led to a 41% reduction of mtDNA depletion ($p = 0.0001$, Fig. 4.18). In the case of nuclease-competent UL12.5-SPA, mtDNA depletion was significantly inhibited by both ENDOG siRNA (27% reduction, $p = 0.048$) and EXOG siRNA (17% reduction,

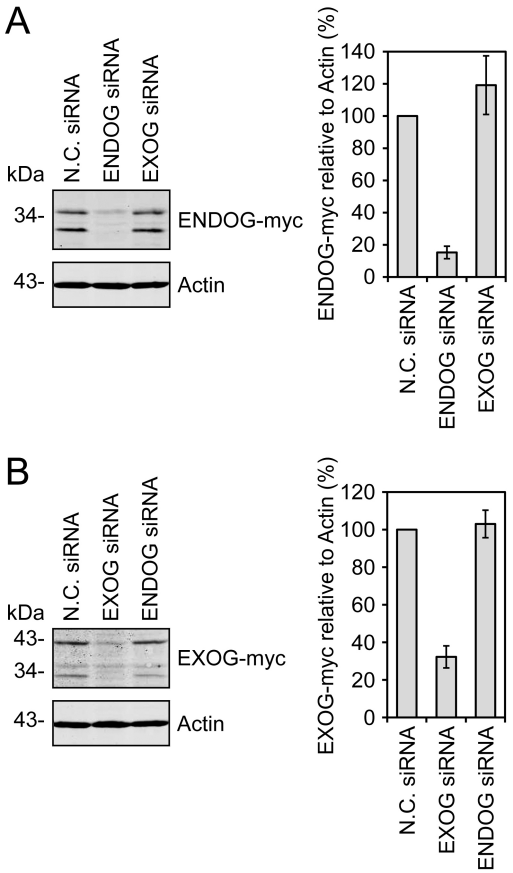

Figure 4.17. Suppression of ENDOG and EXOG overexpression using siRNA. HeLa cells were co-transfected with the indicated siRNAs and ENDOG-myc (A) or EXOG-myc (B) for 48 hours. ENDOG-myc and EXOG-myc levels were quantitated following immunoblotting and infrared detection. Data from three separate experiments were averaged, plotted relative to actin, and normalized to the N.C. siRNA treatment. Standard errors are indicated.

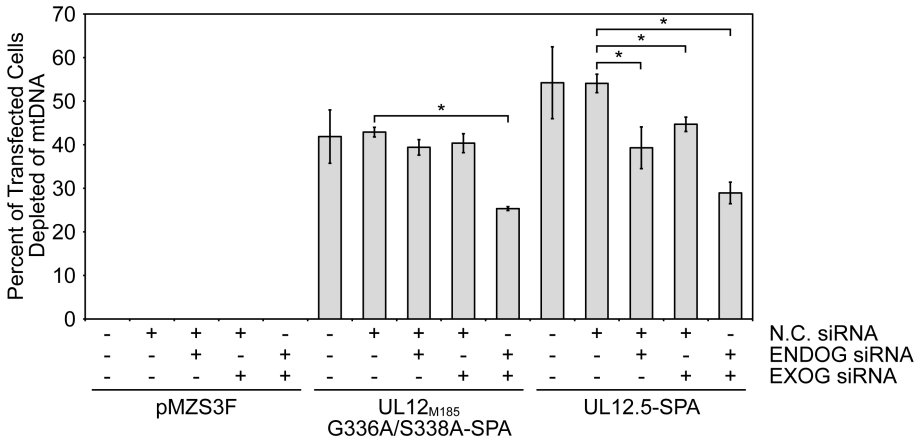

Figure 4.18. Knockdown of ENDOG and/or EXOG inhibits mtDNA depletion by UL12$_{M185}$-G336A/S338A-SPA and UL12.5-SPA. HeLa cells co-transfected with the indicated siRNAs and either empty vector (pMZS3F) or plasmids expressing UL12.5-SPA or UL12$_{M185}$-G336A/S338A-SPA were assessed for mtDNA depletion as described in Fig. 4.6. Data from three separate experiments were averaged and standard errors are indicated. Data denoted with * indicate statistical significance ($P < 0.05$) when compared to the respective control (UL12$_{M185}$-G336A/S338A-SPA/N.C. siRNA or UL12.5-SPA/N.C. siRNA).

p = 0.025), an effect that was enhanced by simultaneous knockdown of both ENDOG and EXOG (47% reduction, p = 0.0015, Fig. 4.18).

4.3 – Conclusions

As mentioned above, the observation that G336A/S338A mutations, which are known to prevent exo- and endonuclease activity of UL12 (44), did not eliminate mtDNA depletion (Fig. 4.6) provides my strongest argument for the nuclease activity of UL12.5 not being involved in mtDNA degradation. The simplest hypothesis arising from these experiments states that nucleases with access to mtDNA are aberrantly directed to degrade mtDNA in the presence of UL12.5. In support of this hypothesis, my additional data implicated ENDOG and EXOG as playing key, and at least partially overlapping, roles in mediating mtDNA loss triggered by UL12.5 (Figs. 4.14 and 4.18). While more experiments are needed to further elucidate the process of UL12.5-mediated mtDNA depletion, the data presented in this chapter support a complex and interesting mechanism employed by UL12.5 which disrupts mtDNA homeostasis in favour of the destruction of mtDNA during HSV-1 infection.

Chapter 4A

Appendix to: Mitochondrial Nucleases ENDOG and EXOG Participate in Mitochondrial DNA Depletion Initiated by HSV-1 UL12.5

All experiments presented within this chapter were performed by B. Duguay.

4A.1 – Preface

To investigate whether nuclease activity of UL12.5 was required for mtDNA depletion, I tested various substitution and deletion mutants of UL12.5 for their ability to deplete mtDNA using a live cell imaging assay (Fig. 4.6). Many of the substitution and deletion mutations utilized in my experiments have been previously characterized for their ability to inhibit UL12 nuclease activity (44, 460). I also assessed whether these mutations had the desired impact on the nuclease activity of the highly related protein UL12.5 by performing *in vitro* nuclease assays with *in vitro* translated proteins. As demonstrated in this appendix to Chapter 4, my *in vitro* nuclease assays were capable of verifying that all of the published UL12 mutations caused the expected inhibition of UL12.5 exonuclease activity. Moreover, these assays revealed that the $UL12_{M185}$ and UL12.5-ΔMLS mutants also did not possess detectable exonuclease activity *in vitro*. However, these *in vitro* nuclease assays were unable to determine if the published L150K, ΔN, ΔC, D340E, or G336A/S338A mutations (44, 460) had similar effects on UL12.5 endonuclease activity.

4A.2 – Results and Conclusions

To assess whether the L150K, ΔN, ΔC, D340E, and G336A/S338A mutations had the desired impact on UL12.5-SPA nuclease activity, I generated *in vitro* translated, ^{35}S-labelled, SPA-tagged proteins. All translation products migrated to the predicted apparent molecular masses and were consistent in size with the largest protein species observed in HeLa cells (compare Figs. 4A.1A and 4.1B). However, *in vitro* translated proteins migrated as single species (Fig. 4A.1A) unlike the respective proteins when expressed *in vivo* (Fig. 4.2). This observation is likely due to differences in protein modifications between rabbit reticulocyte lysates and cultured cells.

Using a modified version of UL12 *in vitro* nuclease assays performed by others and consistent with their published data (293, 456, 460, 497, 516, 517), I observed that *in vitro* translated UL12-SPA and UL12.5-SPA were capable of completely degrading a linearized DNA substrate (Fig. 4A.1B). All other *in vitro* translated UL12.5 mutants, including the newly characterized UL12$_{M185}$ and UL12.5-ΔMLS mutants, consistently behaved similarly to the dH_2O control demonstrating a significant impairment of exonuclease activity (Fig. 4A.1B). Additional *in vitro* nuclease assays using *in vitro* translated untagged versions of UL12, UL12.5, and UL12.5 mutants also demonstrated that linear DNA was degraded only when wild-type UL12 or UL12.5 were present (Fig. 4A.2, top).

When the *in vitro* translated proteins were tested for their ability to degrade a supercoiled, circular DNA substrate I was unable to consistently observe any appreciable loss of circular DNA for SPA-tagged or untagged

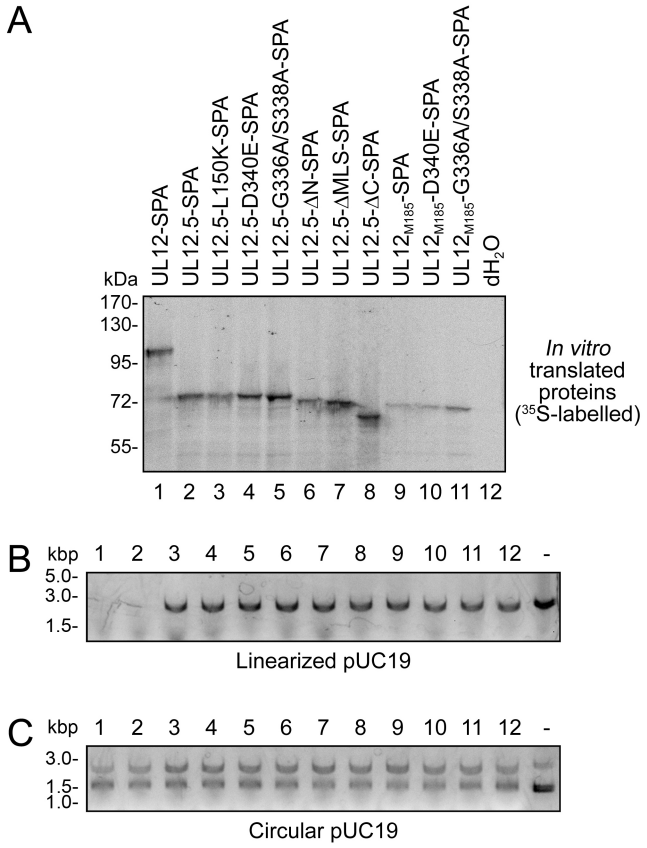

Figure 4A.1. *In vitro* translated UL12-SPA and UL12.5-SPA exhibit only exonuclease activity. (A) ^{35}S-methionine-containing *in vitro* translation products were separated by SDS-PAGE and visualized by autoradiography. *In vitro* translation reactions or unprogrammed rabbit reticulocyte cell lysate (dH_2O) were incubated with 85 ng linearized pUC19 plasmid DNA (B) or with 150 ng circular pUC19 plasmid DNA (C) to visualize nuclease activity. Samples are labelled as indicated in panel A. Plasmid DNA incubated in the absence of rabbit reticulocyte lysate is indicated as "-". DNA was visualized using ethidium bromide staining.

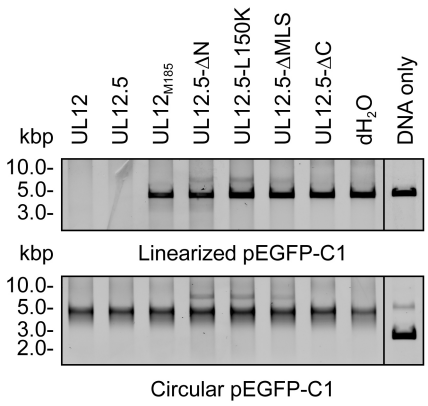

Figure 4A.2. Untagged versions of UL12 and UL12.5 exhibit only exonuclease activity *in vitro*. *In vitro* translation reactions of untagged UL12, UL12.5, or UL12.5 mutants, or unprogrammed rabbit reticulocyte cell lysate (dH_2O) were incubated with either 10 ng of linearized pEGFP-C1 plasmid DNA (top) or 10 ng of circular pEGFP-C1 plasmid DNA (bottom) to visualize nuclease activity. DNA incubated in the absence of rabbit reticulocyte lysates is labelled as "DNA only". DNA was visualized using SYBR Gold staining.

versions of UL12, UL12.5, or UL12.5 mutants (Figs. 4A.1C and 4A.2, bottom). Furthermore, no evidence of endonuclease activity was observed for the exo-/endo+ mutant UL12.5-D340E-SPA (Fig. 4A.1C).

The data presented in this appendix to Chapter 4 are consistent with the idea that the exonuclease activity of UL12.5 is significantly impaired if not abrogated by the published nuclease-inactivating mutations. However, these data provide no conclusive evidence to support a similar impairment of endonuclease activity of UL12.5 by these substitution and deletion mutations, as has been previously published for UL12 (44, 460). Published experiments examining UL12 endonuclease activity were performed using purified protein and/or radiolabelled DNA substrates which arguably enhance their sensitivity (44, 458, 460, 462, 463). Therefore, it is possible that using *in vitro* translated proteins coupled with conventional DNA staining methods does not attain the sensitivity required to detect UL12/UL12.5 endonuclease activity. Despite being unable to visualize endonuclease activity *in vitro*, published data clearly demonstrates the effects of the L150K, ΔN, ΔC, D340E, and G336A/S338A mutations on UL12 nuclease activity (44, 460). Altogether, the data presented herein, the published data characterizing the L150K, ΔN, ΔC, D340E, and G336A/S338A mutations, and the data in Chapter 4 provide a convincing argument that the nuclease activity of UL12.5 is not required for mtDNA depletion to occur.

Chapter 5

Investigating the binding partners of HSV-1 UL12.5 in transfected cells

All experiments presented within this chapter were performed by B. Duguay.

5.1 – Preface

Following infection with HSV-1, mtDNA is rapidly depleted from host cells (152) following kinetics consistent with active degradation by nucleases as opposed to a slower process of mtDNA loss due to defective mtDNA replication. While UL12.5 is needed to initiate mtDNA loss, the data in the preceding chapter document that the nuclease activity of UL12.5 is not required for this process. Moreover, I observed that nuclease-deficient versions of UL12.5 associated with cellular endonuclease activity. The discovery of a role for the nucleases ENDOG and EXOG in UL12.5-mediated mtDNA depletion implied that these cellular nucleases might be the source of the associated endonuclease activity observed *in vitro* and that these proteins may associate with UL12.5. However, the data presented hereafter demonstrate that UL12.5 does not associate with ENDOG or EXOG *in vivo*. Moreover, in transfected cells UL12.5 displays the unusual phenotype of associating with all overexpressed mitochondrial proteins tested. Interestingly, these observations were unique to UL12.5 since other overexpressed mitochondrial proteins did not form unexpected associations with unrelated mitochondrial proteins. Even though these data point toward a distinctive characteristic of the UL12.5 protein, they neither identify the source of the associated endonuclease activity observed in our assays nor do they provide conclusive evidence of physiologically relevant binding partners of UL12.5.

5.2 – Results

5.2.1 – UL12.5-SPA associates with various overexpressed mitochondrial proteins

Based on my earlier observations that both ENDOG and EXOG facilitate UL12.5-mediated mtDNA depletion (Figs. 4.14 and 4.18), it was plausible that one or both of these enzymes may be responsible for the unidentified endonuclease activity observed in my *in vitro* nuclease assays (Fig. 4.9C and 4.9F). As an initial attempt to identify the source of associated endonuclease activity, I performed immunoprecipitations in cells concurrently overexpressing turbo green fluorescent protein (tGFP)-tagged ENDOG or EXOG and UL12.5-SPA.

Cells expressing tGFP alone or one of two unrelated tGFP-tagged mitochondrial matrix proteins, inactive sirtuin 3 (Sirt3-H248Y (477, 510)) and manganese superoxide dismutase (MnSOD (518)), were used for subsequent control immunoprecipitations. All constructs were expressed in HeLa cells and migrated with the approximate expected mobility in SDS-PAGE gels (tGFP, 30 kDa; ENDOG-tGFP, 60 kDa; EXOG-tGFP, 70 kDa; MnSOD-tGFP, 60 kDa; Fig. 5.1A). For unknown reasons, the Sirt3-H248Y protein did not accumulate to the levels observed for other epitope-tagged proteins (Sirt3-H248Y-tGFP, 55 kDa) (Fig. 5.1A). I also observed that the addition of the tGFP tag did not significantly affect the mitochondrial localization of ENDOG and EXOG using live cell imaging (Fig. 5.1B). The localization of Sirt3-H248Y-tGFP or MnSOD-tGFP was not tested.

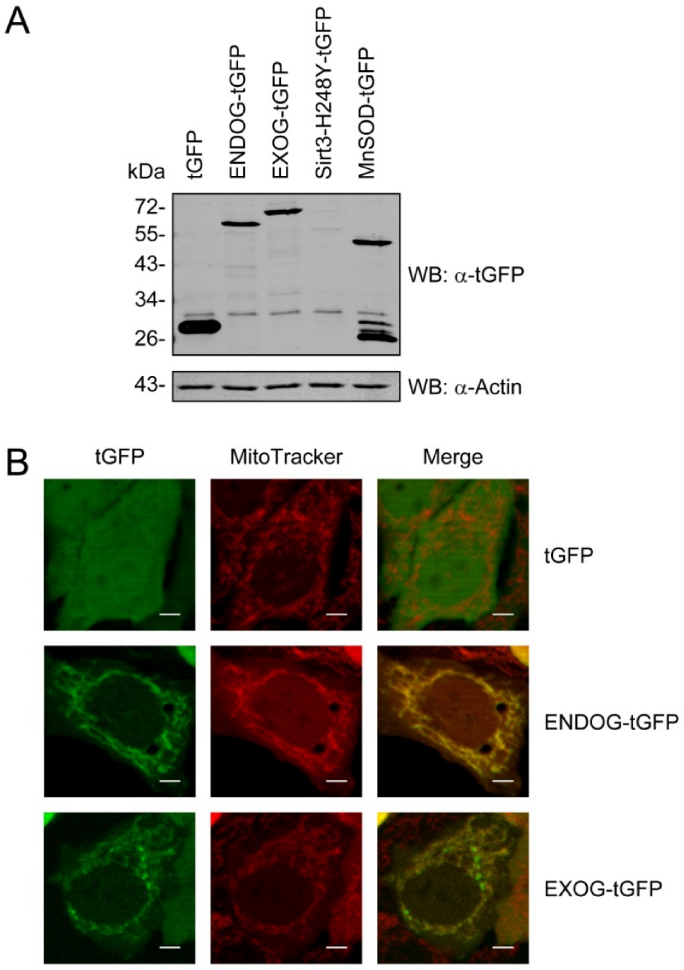

Figure 5.1. Expression of tGFP-tagged ENDOG, EXOG, Sirt3, and MnSOD proteins in HeLa cells. (A) Cells were transfected with the indicated plasmids and harvested 24 hours post-transfection. Lysates were assessed for protein expression by immunoblotting using antibodies against the turbo green fluorescent protein (tGFP) epitope tag (α-tGFP) and actin (α-Actin) followed by infrared detection. (B) HeLa cells transfected with the indicated plasmids for 48 hours were stained with MitoTracker Red and visualized using live cell fluorescence microscopy using a 40X objective and an ApoTome. Colocalization of tGFP-tagged proteins with MitoTracker Red is indicated in yellow. Scale bars = 5 μm.

When HeLa cells co-expressing UL12.5-SPA and either ENDOG-tGFP or EXOG-tGFP were used for immunoprecipitations, I observed that UL12.5-SPA formed a clear association with both overexpressed proteins (Fig. 5.2A). These associations appeared to be specific as no co-immunoprecipitation of UL12.5-SPA was observed with the more highly expressed tGFP (Fig. 5.2A). Moreover, reciprocal co-immunoprecipitation experiments using an antibody directed against the SPA tag (α-FLAG-M2) produced similar results (Fig. 5.2B). I further assessed the validity of these co-immunoprecipitation results by repeating the UL12.5-SPA/ENDOG-tGFP co-immunoprecipitation experiment under a variety of conditions (Fig. 5.2C). These data indicated that only when both ENDOG-tGFP and UL12.5-SPA were present and the α-tGFP antibody was used for the immunoprecipitation step could UL12.5-SPA be co-immunoprecipitated (Fig. 5.2C). This association was not observed in the absence of either protein, the absence of antibody, or when using an isotype control antibody (Fig. 5.2C). These co-immunoprecipitation data suggest that both ENDOG and EXOG form a complex with UL12.5.

Since the possibility existed that the associations observed in Fig. 5.2 were an artifact of an overexpression system, I also tested whether UL12.5-SPA could associate with other overexpressed mitochondrial proteins, namely MnSOD or Sirt3. These mitochondrial proteins were used for this experiment because it seemed unlikely that a mitochondrial protein other than a mitochondrial nuclease would associate with UL12.5 based on our revised hypothesis. Similar to the previous experiment (Fig. 5.2), I observed that UL12.5-SPA readily

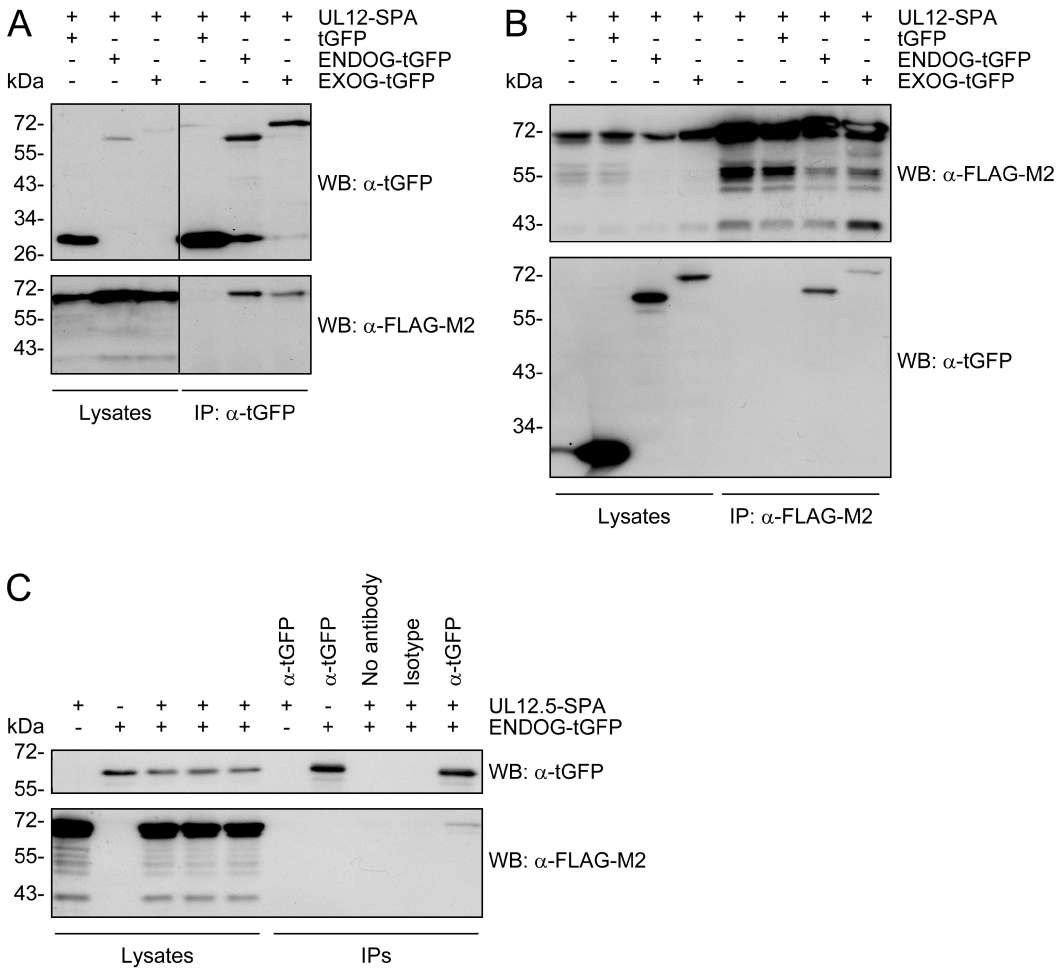

Figure 5.2. UL12.5-SPA associates with ENDOG-tGFP and EXOG-tGFP in transfected cells. HeLa cells expressing the indicated combinations of proteins were lysed and processed for immunoprecipitation (IP) using antibodies against the tGFP epitope tag (α-tGFP) (A and C), the SPA tag (α-FLAG-M2) (B), or an IgG2b control antibody (Isotype). A mock immunoprecipitation performed with protein G agarose alone is labelled "No antibody". Lysates and immuno-precipitates shown in panels A, B, and C were analyzed by western blotting using antibodies against the tGFP and SPA tags. WB, western blot; tGFP, turbo green fluorescent protein.

co-immunoprecipitated with ENDOG-tGFP (Fig. 5.3). Unexpectedly, I also detected an association between UL12.5-SPA and Sirt3-H248Y-tGFP (Fig. 5.3). Interestingly, the expression of Sirt3-H248Y-tGFP was significantly lower than all other tGFP-containing proteins in this experiment yet it was still sufficient to co-immunoprecipitate UL12.5-SPA. When MnSOD-tGFP was immuno-precipitated from the transfected cells, I also observed an association with UL12.5-SPA whether UL12.5-SPA was expressed from the CMV promoter in pMZS3F UL12.5-SPA or from the internal *UL12.5* promoter present in the pMZS3F UL12-SPA vector (Fig. 5.3). As an additional control, I examined whether MnSOD-tGFP was able to form a detectable association with a myc-tagged version of Sirt3 (Fig. 5.3). Although each of these proteins on their own associated with UL12.5-SPA, I could not observe an association between them (Fig. 5.3). This observation would suggest that characteristics inherent to UL12.5 and not all mitochondrial proteins are responsible for the observed associations during overexpression. Furthermore, the result from cells co-transfected with plasmids expressing MnSOD-tGFP and UL12-SPA indicates that the UL12.5-SPA/MnSOD-tGFP association is likely due to the fact that both of these proteins localize to mitochondria since the nuclear protein UL12-SPA (which shares the same protein sequence as UL12.5-SPA) did not co-immunoprecipitate with MnSOD-tGFP (Fig. 5.3). Also, the discord between the results using UL12-SPA and UL12.5-SPA suggests that the association between UL12.5-SPA and MnSOD-tGFP is not due to non-specific interactions during cell lysis.

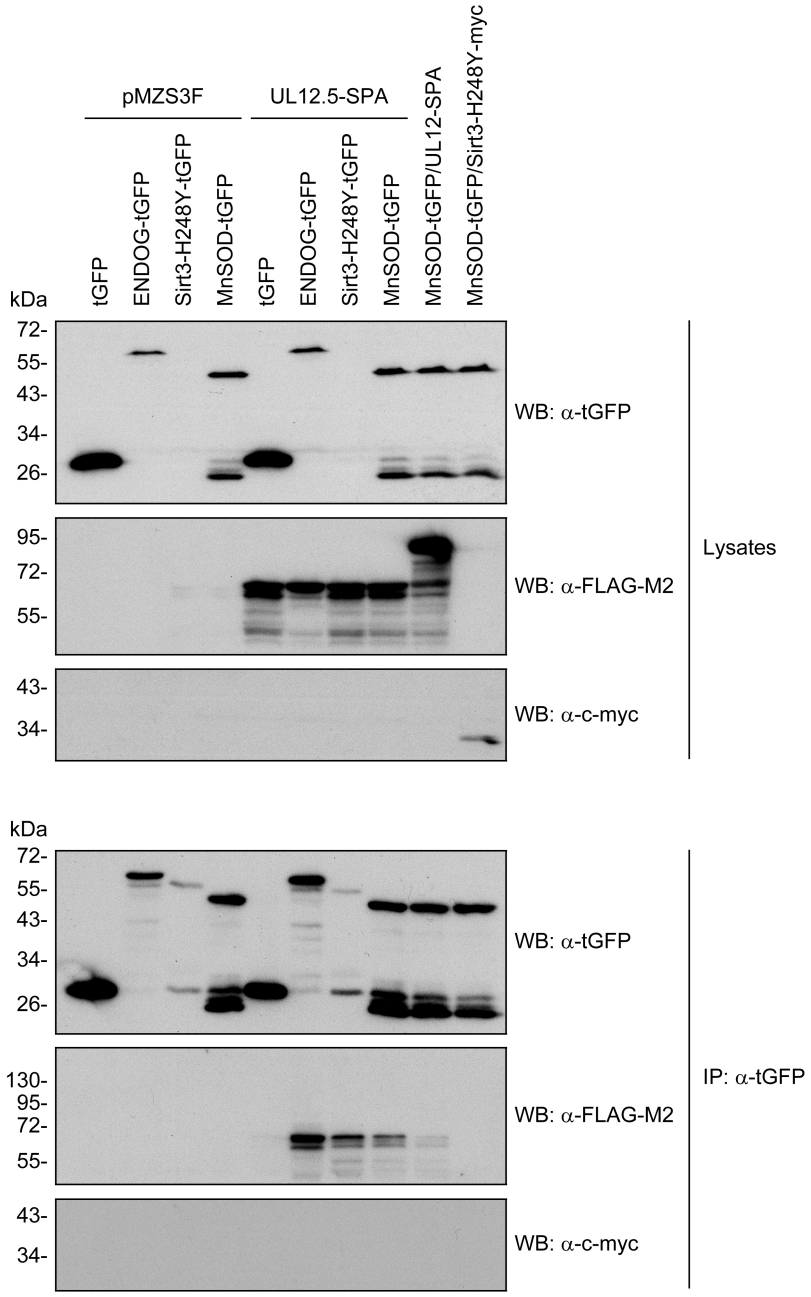

Figure 5.3. UL12.5-SPA associates with Sirt3-H248Y-tGFP and MnSOD-tGFP in transfected cells. HeLa cells expressing the indicated combinations of proteins were lysed and processed for immunoprecipitation (IP) using an antibody against the tGFP epitope tag (α-tGFP). Lysates and immunoprecipitates were analyzed by western blotting using antibodies against the tGFP, SPA (α-FLAG-M2), and c-myc (α-c-myc) tags. WB, western blot; tGFP, turbo green fluorescent protein.

As an additional experiment to test the validity of the co-immunoprecipitation data presented above, I also examined if Sirt3-H248Y-myc could associate with other overexpressed mitochondrial proteins. In these experiments Sirt3-H248Y-myc was co-expressed in HeLa cells with either tGFP, ENDOG-tGFP, EXOG-tGFP, UL12.5-SPA, a mitochondrially-targeted EGFP (M185-R245-EGFP, Fig. 3.4) or its associated control, EGFP (Fig. 5.4). Following the immunoprecipitation of Sirt3-H248Y-myc, this protein was not observed to associate with tGFP, ENDOG-tGFP, EXOG-tGFP, EGFP, or M185-R245-EGFP (Fig. 5.4). Both ENDOG-tGFP and EXOG-tGFP were not highly expressed in the cells used for these immunoprecipitations which may have influenced detecting a potential association. However, their relatively low expression did not preclude their association with UL12.5-SPA (Fig. 5.2). Moreover, the EGFP containing the UL12.5 MLS (M185-R245-EGFP) should be targeted to the same sub-mitochondrial compartment as UL12.5. Therefore, if the observed association of Sirt3-H248Y with UL12.5 (Figs. 5.3 and 5.4) was due to non-specific interactions between mitochondrial proteins then one could reasonably predict that M185-R245-EGFP and Sirt3-H248Y should also be able to form such interactions. This was not the case in these experiments indicating that simple non-specific interactions alone do not explain the observation that UL12.5-SPA associates with a variety of overexpressed mitochondrial proteins.

5.2.2 – UL12.5-SPA does not associate with endogenous ENDOG or EXOG

The data presented in section 5.2.1 suggest that UL12.5-SPA can associate with both overexpressed ENDOG and EXOG, however it was unusual that

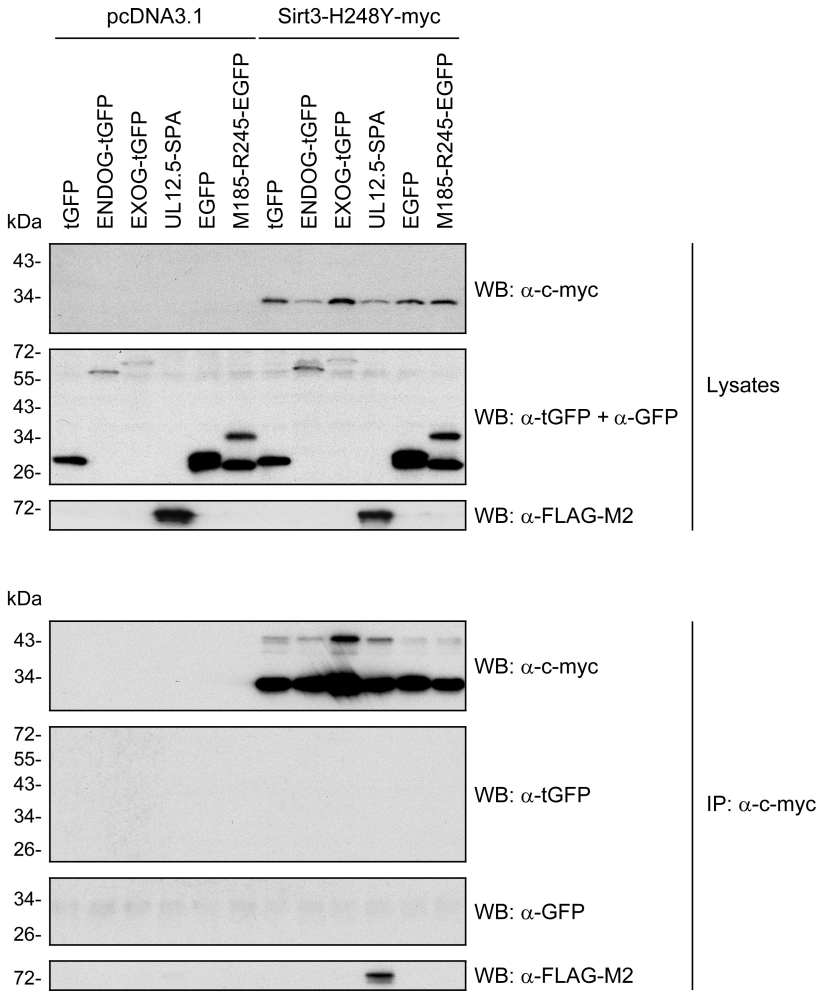

Figure 5.4. Sirt3-H248Y-myc associates with UL12.5-SPA but not other overexpressed mitochondrial proteins in transfected cells. HeLa cells expressing the indicated combinations of proteins were lysed and processed for immunoprecipitation (IP) using an antibody against the c-myc epitope tag (α-c-myc). Lysates and immunoprecipitates were analyzed by western blotting using antibodies against the c-myc, tGFP (α-tGFP), EGFP (α-GFP), and SPA (α-FLAG) tags. WB, western blot; GFP, green fluorescent protein; tGFP, turbo GFP; EGFP, enhanced GFP.

UL12.5 also was observed to associate with other overexpressed mitochondrial proteins. These observations together led me to question the validity of these observed associations. Therefore, I next tested if UL12.5-SPA could associate with endogenous ENDOG or EXOG using immunoprecipitation. In HeLa cells, the ENDOG protein had an apparent molecular weight of 34 kDa, consistent with the expected mass of human ENDOG (328), yet was inefficiently expressed (Fig. 5.5). Moreover, the commercially available antibody used in these experiments more readily detected a higher molecular mass species of unknown origin (indicated with an asterisk, Fig. 5.5). The EXOG antibody also detected two protein species, the protein species of ca. 60 kDa is of unknown origin (indicated with an asterisk, Fig. 5.5) whereas the species with the highest mobility (ca. 40 kDa) is consistent with the size of EXOG (Fig. 5.5 and reference 484). Following immunoprecipitation of UL12.5-SPA, no detectable association with either mitochondrial nuclease could be observed (Fig. 5.5). The detection of associated endonuclease activity using *in vitro* nuclease assays (Fig. 4.9C and 4.9F) is arguably more sensitive than observing a physical association using western blotting. Since it was possible that potential associations between UL12.5 and ENDOG or EXOG could be weak or transient, I also performed immunoprecipitations following treatment of transfected cells with DMSO (Fig. 5.5, -DSP) or the chemical cross-linker dithiobis(succinimidylpropionate) (DSP) dissolved in DMSO (Fig. 5.5, +DSP). In these preliminary results, I unexpectedly observed a collapse of the unidentified higher molecular mass species detected using ENDOG and EXOG antibodies into their respective lower molecular mass

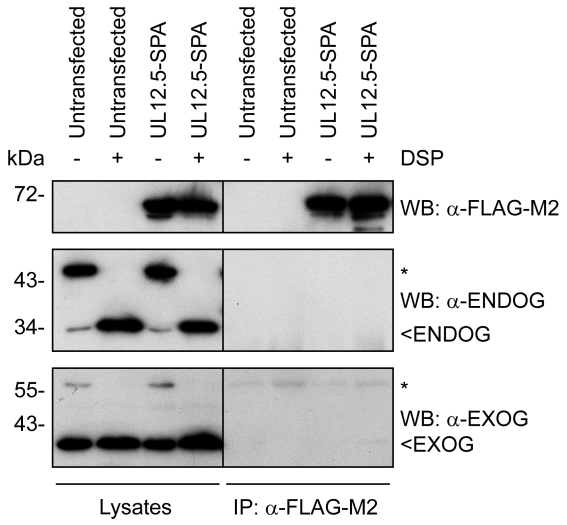

Figure 5.5. UL12.5-SPA does not associate with endogenous ENDOG or EXOG. Untransfected HeLa cells or those expressing UL12.5-SPA were treated with DMSO (-DSP) or the cross-linker DSP dissolved in DMSO (+DSP), lysed, and processed for immuno-precipitation (IP) using an antibody against the SPA tag (α-FLAG-M2). Lysates and immunoprecipitates were analyzed by western blotting (WB) using antibodies against the SPA tag, ENDOG (α-ENDOG), and EXOG (α-EXOG). DSP, dithiobis(succinimidyl propionate).

species following treatment with DSP (Fig. 5.5). It is unclear at this time why treatment with DSP would cause this effect. Regardless, even after cross-linking no association between UL12.5-SPA and ENDOG or EXOG could be observed (Fig. 5.1). The conflicting results from the co-immunoprecipitation experiments using overexpressed or endogenous forms of ENDOG or EXOG make it difficult to conclude at this time whether these mitochondrial nucleases are the source of the associated endonuclease activity observed in our *in vitro* nuclease assays.

5.3 – Conclusions

Altogether, the data presented in this chapter suggest that the overexpression of mitochondrial proteins concurrently with UL12.5-SPA is an unreliable method for identifying binding partners of UL12.5. Since UL12.5-SPA has not been observed to associate with endogenous ENDOG or EXOG yet can associate with overexpressed versions of these proteins (compare Figs. 5.2 and 5.5), it would suggest that the associations may be between newly translated proteins undergoing import into mitochondria. In a cell at any given time, the fraction of a newly translated mitochondrial protein to its mature counterpart is likely very low. However, during transient overexpression the fraction of newly synthesized protein to mature protein is likely much higher. Since mitochondrial import involves unfolding proteins during their passage through the mitochondrial membranes (519), hydrophobic interactions between partially unfolded proteins could potentially lead to non-specific associations. While this type of association could also be occurring during transient overexpression of only UL12.5-SPA or even during HSV-1 infection, the frequency of these associations is likely so low that they are undetectable in co-immunoprecipitation experiments with endogenous proteins. Based on the data presented in this chapter, this speculated mechanism would not hold true for the other mitochondrial proteins tested as no unexpected associations were observed between Sirt3 and either ENDOG, EXOG, MnSOD, or mitochondrially-targeted EGFP (Figs. 5.3 and 5.4). It is possible that unique import intermediates of the UL12.5-SPA protein could be responsible for the observed associations; however, further studies are required to examine this

possibility. More research will also be needed to identify the source of the associated endonuclease activity as well as other physiologically relevant binding partners of UL12.5. Alternative approaches to address these questions may include mass spectrometry analysis of UL12.5 containing complexes or siRNA screening for modifiers of UL12.5-mediated mtDNA depletion.

Chapter 6

Elimination of mitochondrial DNA is not required for HSV-1 replication

A version of this chapter has been published in:

Duguay BA, Saffran HA, Ponomarev A, Duley SA, Eaton HE, Smiley JR. 2014. Elimination of mitochondrial DNA is not required for herpes simplex virus type 1 replication. J Virol **88:**2967-2976. The original manuscript was written by B. Duguay with a major editorial contribution by J. Smiley.

All experiments presented within this chapter were performed by B. Duguay with the following exceptions: The data for figures 6.3B, 6.3C, 6.3D, 6.4A, 6.11, and 6.12 were generated by H. Saffran. The data for figures 6.4B and 6.4C and plasmids encoding HSV2-UL12-SPA, ORF48-SPA, and MLS-ORF48-SPA, MLS-BGLF5-SPA, and MLS-SOX-SPA were generated in collaboration with A. Ponomarev. The plasmids encoding HSV2-UL12.5-SPA, BGLF5-SPA, and SOX-SPA were generated in collaboration with S. Duley. The data for figure 6.10 was generated by H. Eaton.

6.1 – Preface

The data presented up to this point has been focused on explaining how UL12.5 localizes to mitochondria (Chapter 3) and the molecular mechanism underlying UL12.5-mediated mtDNA depletion (Chapter 4). One aspect that had yet to be addressed was whether mtDNA depletion has any impact on viral replication. To address this issue it was necessary to generate a viral mutant unable to produce UL12.5 or which eliminates its mtDNA depletion activity while preserving the nuclear functions of the related and overlapping protein, UL12. For reasons outlined in the introduction, neither a viral mutant containing one of the mutations demonstrated to abolish mtDNA depletion (Chapter 4) nor a previously generated UL12.5-null mutant virus (M127F) (468) were suitable to investigate the role of mtDNA depletion during HSV-1 replication. In this chapter, we demonstrate that the ability to mediate mtDNA depletion is not conserved among UL12 orthologs of several other human herpesviruses. This observation led us to generate an HSV-1 mutant virus in which the *UL12*/*UL12.5* ORFs were functionally replaced with the alkaline nuclease coding sequences of human cytomegalovirus (HCMV), *UL98*. This mutant virus replicated to normal titres but was severely impaired in its ability to mediate mtDNA depletion, providing evidence that the elimination of mtDNA is not required for HSV-1 replication in cell culture.

6.2 – Results

6.2.1 – Eliminating translation of UL12.5 and UL12$_{M185}$ does not prevent mtDNA depletion

Our previous work examining mtDNA depletion by HSV-1 demonstrated that the viral protein UL12.5 is sufficient for mtDNA loss in transfected cells (152). However, the M127F virus that lacks the translational initiation codon of UL12.5 (468) still causes mtDNA depletion in the absence of UL12.5 expression (475). Our evidence pointed to an N-terminally truncated version of UL12.5 termed UL12$_{M185}$ as being responsible for mtDNA loss during M127F virus infection (Chapter 3 and reference 475). We therefore asked whether eliminating translation of both UL12.5 and UL12$_{M185}$ would prevent mtDNA loss.

We generated a UL12.5/UL12$_{M185}$-null virus (F/L) containing substitutions that convert the initiator methionine codons of UL12.5 (M127) and UL12$_{M185}$ (M185) to phenylalanine and leucine codons, respectively (Fig. 6.1). The presence of these mutations in the viral genome was confirmed by two methods: Southern blotting to visualize the presence a new *Tfi*I site which was introduced adjacent to the M127F mutation during the construction of the virus (Fig. 6.2A) and DNA sequencing of the *UL12* gene present in the F/L genome (Fig. 6.2B). Western blot analysis of infected cell extracts using a polyclonal UL12 antibody revealed that these mutations had no impact on expression of full-length UL12 relative to wild-type or revertant (F/L Res) controls (Fig. 6.3A). In addition to full length UL12, the wild-type and F/L Res extracts displayed several more rapidly migrating species including a prominent band corresponding to the

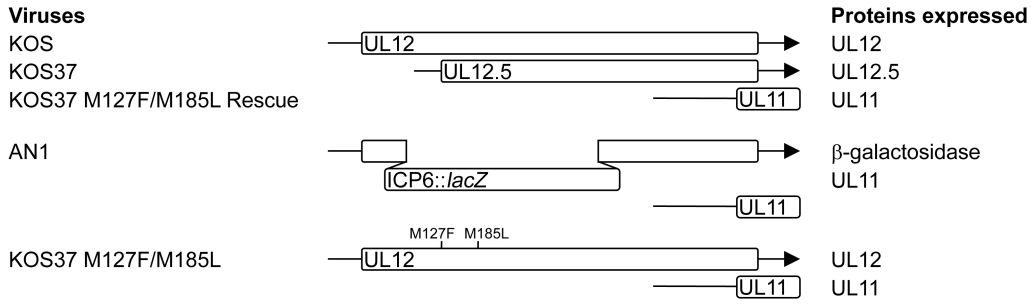

Figure 6.1. Construction of the M127F/M185L mutant virus. Schematics of the *UL12*, *UL12.5*, and *UL11* loci in HSV-1 wild-type and mutant viruses are shown. KOS, KOS37, and KOS37 M127F/M185L Rescue are wild-type viruses. AN1 possesses a partial deletion and insertion within *UL12* which eliminates UL12 and UL12.5 expression. KOS37 M127F/M185L contains two substitution mutations within the second and third in-frame methionine codons of *UL12* which prevent translation of UL12.5 and $UL12_{M185}$. The mRNA transcripts are represented by black arrows and the open reading frames are represented by boxes. All features are drawn to scale.

A

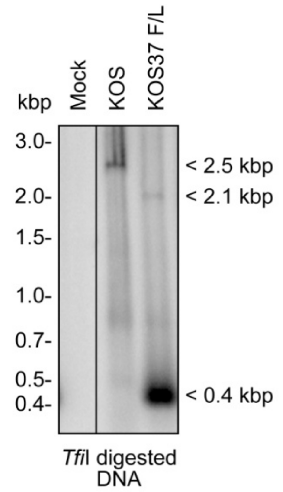

B

```
KOS     288 AGGGCCTCCGACCCCAGACATTCCGCTATCTCCTGGGGGCACCCACGCCCGCGACCCGGA
FL      288 AGGGCCTCCGACCCCAGACATTCCGCTATCTCCTGGGGGCACCCACGCCCGCGACCCGGA
            ************************************************************

KOS     348 CGCCGATCCCGACTCCCCGGACCTTGACTCTATGTGGTCGGCGTCGGTGATCCCCAACGC
FL      348 CGCCGATCCCGACTCCCCGGACCTTGATTCTTTCTGGTCGGCGTCGGTGATCCCCAACGC
            *************************** *** * ***************************

KOS     408 GCTGCCCTCCCATATACTAGCCGAGACGTTCGAGCGCCACCTGCGCGGGTTGCTGCGCGG
FL      408 GCTGCCCTCCCATATACTAGCCGAGACGTTCGAGCGCCACCTGCGCGGGTTGCTGCGCGG
            ************************************************************

KOS     468 CGTCCGCGCCCCTCTGGCCATCGGTCCCCTCTGGGCCCGCCTGGATTATCTGTGTTCCCT
FL      468 CGTCCGCGCCCCTCTGGCCATCGGTCCCCTCTGGGCCCGCCTGGATTATCTGTGTTCCCT
            ************************************************************

KOS     528 GGCCGTGGTCCTCGAGGAGGCGGGTATGGTGGACCGCGGACTCGGCCGGCACCTATGGCG
FL      528 GGCCGTGGTCCTCGAGGAGGCGGGTCTCGTGGACCGCGGACTCGGCCGGCACCTATGGCG
            ************************ * ********************************

KOS     588 CCTGACGCGCCGCGGGCCCCCGGCCGCCGCGGACGCCGTGGCGCCCCGGCCCCTCATGGG
FL      588 CCTGACGCGCCGCGGGCCCCCGGCCGCCGCGGACGCCGTGGCGCCCCGGCCCCTCATGGG
            ************************************************************
```

Figure 6.2. Validation of the M127F/M185L mutant virus. (A) Following mock infection or infection at a multiplicity of infection of one with KOS or KOS37 M127F/M185L viruses, total DNA was isolated from Vero cells harvested at twenty-four hours post-infection. The DNA was digested with *Tfi*I and screened for the presence of the M127F mutation using Southern blot hybridization with a radiolabelled probe targeting the *UL12* gene. (B) PCR amplified *UL12* from KOS and KOS37 M127F/M185L (FL) infected cell lysates was sequenced and the results compared using Clustal Omega. M127 and M185 methionine codons are in green bold italics. Restriction sites (*Tfi*I and *Bsa*I) introduced during construction of the KOS37 M127F/M185L virus are underlined. Asterisks denote conserved nucleotides. All numbering is relative to the start codon of *UL12*.

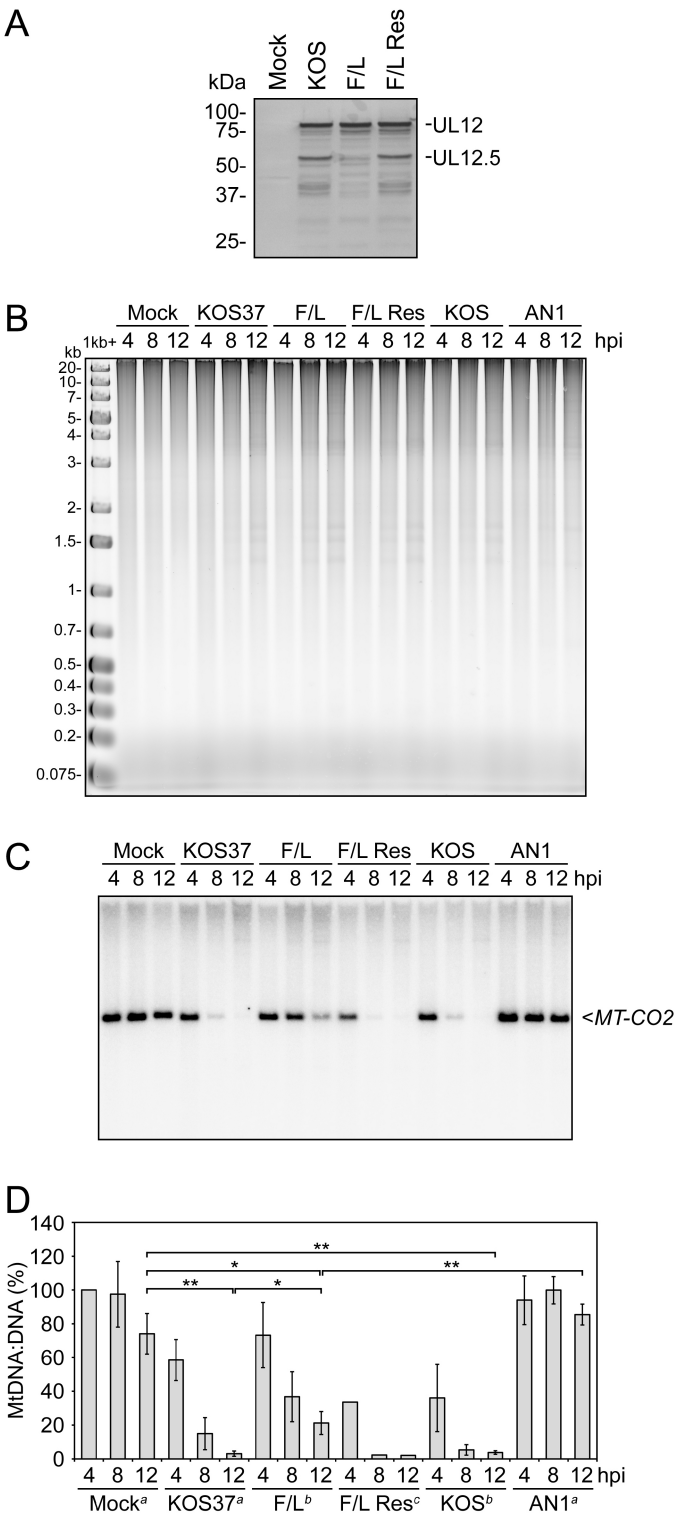
A
kDa
Mock
KOS
F/L
F/L Res
100-
75-
50-
37-
25-
-UL12
-UL12.5
B
Mock
KOS37
F/L
F/L Res
KOS
AN1
4 8 12 4 8 12 4 8 12 4 8 12 4 8 12 4 8 12 hpi
kb
1kb+
20-
10-
7-
5-
4-
3-
2-
1.5-
1-
0.7-
0.5-
0.4-
0.3-
0.2-
0.075-
C
Mock
KOS37
F/L
F/L Res
KOS
AN1
4 8 12 4 8 12 4 8 12 4 8 12 4 8 12 4 8 12 hpi
<MT-CO2
D
MtDNA:DNA (%)
140
120
100
80
60
40
20
0
**
*
**
**
*
4 8 12 4 8 12 4 8 12 4 8 12 4 8 12 4 8 12 hpi
Mock[a]
KOS37[a]
F/L[b]
F/L Res[c]
KOS[b]
AN1[a]

Figure 6.3. Preventing translation of UL12.5 and UL12$_{M185}$ impairs but does not abrogate mtDNA depletion. (A) Vero cells were mock infected or infected at a multiplicity of infection (MOI) of ten with KOS, F/L, or F/L Res viruses for eight hours. Cell lysates were assessed for viral protein expression by immunoblotting using a polyclonal anti-UL12 antibody. (B) DNA from Vero cells mock infected or infected at a MOI of ten with the indicated viruses was harvested four, eight, or twelve hours post-infection (hpi) and was visualized by SYBR Gold staining following agarose gel electrophoresis. (C) The separated DNA in panel B was transferred to nitrocellulose and mtDNA was detected following Southern blot hybridization with a radiolabelled probe targeting the mtDNA gene encoding cytochrome *c* oxidase subunit II (*MT-CO2*). (D) The MtDNA:DNA ratio from multiple Southern blots were averaged, and plotted normalized to Mock (4 hpi) with standard errors indicated. Sample sizes: ^{a}n=4, ^{b}n=3, and ^{c}n=2. Statistically significant differences are indicated as $P < 0.05$ (*) and $P < 0.01$ (**). The data for panels B, C, and D were generated by H. Saffran.

mobility of UL12.5 (Fig. 6.3A). Although the F/L mutation is predicted to prevent translation of UL12.5, the band migrating at the mobility of UL12.5 was reduced but not eliminated in extracts prepared from cells infected with the F/L mutant (Fig. 6.3A). While the source of the residual signal is uncertain, it is possible that it arises through proteolysis of full-length UL12. Because the epitopes recognized by the polyclonal antiserum have not been mapped, it is not clear whether these species are truncated at the N-terminus, the C-terminus, or at both ends. However, a similar banding pattern was obtained using whole cell lysates of cells expressing C-terminally tagged UL12-SPA and UL12.5-SPA proteins, suggesting that these additional species are N-terminally truncated (Fig. 4.2).

To determine the effect of the F/L mutation on mtDNA depletion, we examined infected cell lysates for the presence of mtDNA by Southern blotting. Equivalent amounts of DNA were loaded into agarose gels, subjected to electrophoresis, and stained with SYBR Gold (Fig. 6.3B) prior to visualization of mtDNA by hybridization with a radiolabelled probe targeting the mtDNA gene encoding cytochrome *c* oxidase subunit II (*MT-CO2*) (Fig. 6.3C). As expected on the basis of previous work (152), wild-type KOS37 and KOS reduced the amount of mtDNA by more than 95% by twelve hours post-infection ($P<0.005$, Figs. 6.3C and D), while the UL12/UL12.5/UL12$_{M185}$-null mutant AN1 had no effect (115% mtDNA relative to mock, $p = 0.43$) (Figs. 6.3C and D). The F/L mutant displayed an intermediate phenotype where mtDNA levels were reduced by 71% compared to mock-infected cells at twelve hours post-infection ($p = 0.02$, Figs. 6.3C and D), which was significantly less than the degree of depletion mediated

by KOS37 (p = 0.029, Figs. 6.3C and D). Repairing the F/L mutation in F/L Res restored wild-type levels of mtDNA depletion, confirming that the defect displayed by the F/L mutant is due to the UL12.5 mutations (Figs. 6.3C and D). Although we did observe some changes in mtDNA levels in mock infected cells over the course of these experiments these differences did not achieve statistical significance (Figs. 6.3C and D). These data indicate that inactivating the translational initiation codons of UL12.5 and $UL12_{M185}$ impairs, but does not eliminate, mtDNA depletion by HSV-1. Given that the AN1 null mutation abrogates mtDNA depletion (Figs. 6.3C and D and reference 152), one or more products of the *UL12* locus appear to retain significant depleting activity in the F/L mutant. Perhaps low levels of intact UL12 are able to localize to mitochondria; alternatively, limited proteolysis of UL12 may give rise to low levels of a UL12.5-like product (Fig. 6.3A). Further studies are required to distinguish between these possibilities. In any case, these results demonstrate that the F/L virus is not suitable for examining the role of mtDNA depletion in HSV-1 replication.

6.2.2 – UL12 orthologs from human beta- and gamma-herpesviruses do not cause mtDNA depletion in transfected cells

The alkaline nuclease orthologs produced by HSV-2 (UL12), VZV (ORF48), HCMV (UL98), EBV (BGLF5), and KSHV (SOX) are all conserved in terms of their nuclease activities (293, 452, 453, 455, 462, 520), and a previous study has shown that UL98 can at least partially substitute for UL12 in promoting HSV-1 replication (521). However, it is not yet known if UL12 orthologs other

than HSV-1 UL12.5 are capable of causing mtDNA depletion. To address this question, we created plasmids encoding C-terminally SPA-tagged versions of HSV-2 UL12, HSV-2 $UL12_{M117}$ (equivalent to HSV-1 UL12.5, (42)), VZV ORF48, HCMV UL98, EBV BGLF5, and KSHV SOX. All of the orthologs were expressed in transiently transfected HeLa cells, giving rise to products with the expected electrophoretic mobility (Fig. 6.4A); however, the levels of ORF48, BGLF5, and SOX were noticeably lower than the other orthologs. With the exception of HSV-2 $UL12_{M117}$, all of the UL12 orthologs localized predominantly to the nucleus and demonstrated no overlap with the mitochondrial protein cytochrome *c* (Fig. 6.4B). HSV-2 $UL12_{M117}$ localized to both the nucleus and mitochondria, similar to HSV-1 UL12.5 (Fig. 4.3 and reference 152). In addition to strong nuclear localization, SOX and BGLF5 displayed diffuse cytoplasmic staining, consistent with the ability of these proteins to facilitate the turnover of cytoplasmic mRNAs (293, 294).

Next, we tested the ability of the various UL12 orthologs to deplete mtDNA in transiently transfected HeLa cells using the PicoGreen live cell imaging assay. Consistent with its high degree of similarity to HSV-1 UL12.5, the HSV-2 $UL12_{M117}$ protein caused mtDNA depletion in the majority of transfected cells (Fig. 6.4C). We also observed a lower level of mtDNA depletion in cells expressing full-length HSV-2 UL12-SPA (Fig. 6.4C), likely due to expression of HSV-2 $UL12_{M117}$ from its native promoter, as observed previously for HSV-1 *UL12* (Figs. 4.1B, 4.3, 4.4, and 4.6). In contrast, ORF48, UL98, BGLF5, and SOX did not detectably deplete mtDNA in this assay (Fig. 6.4C).

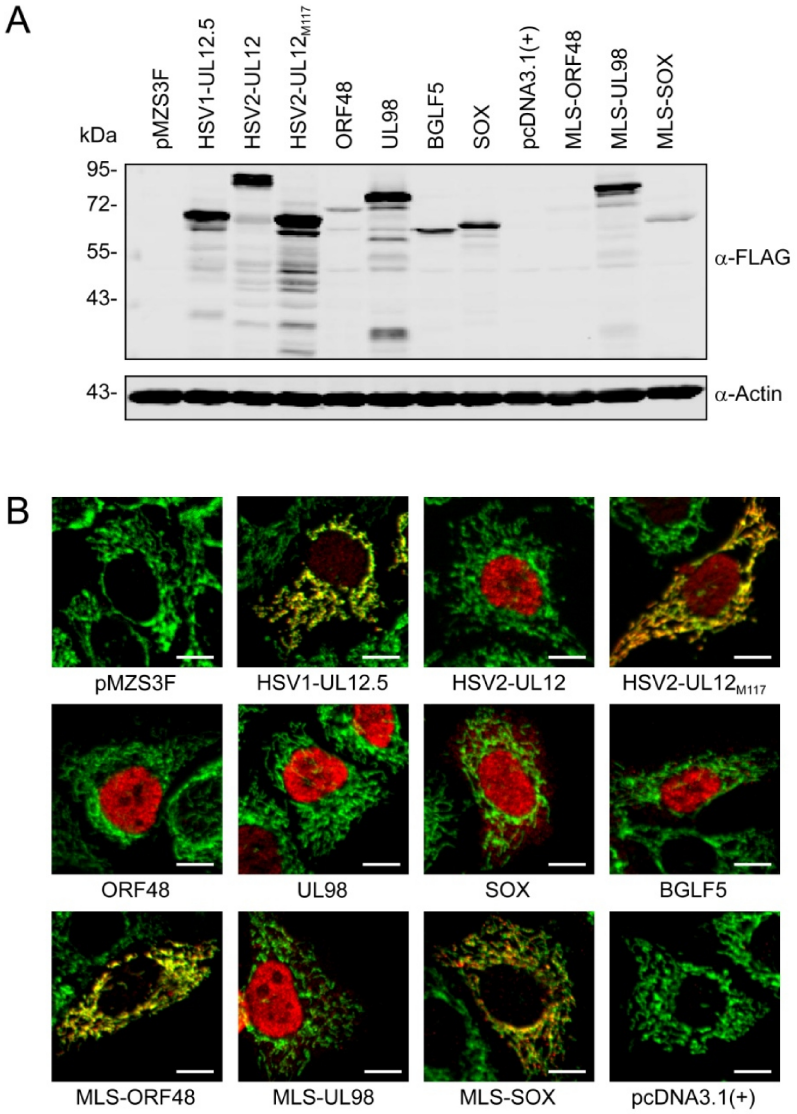
A
kDa
pMZS3F
HSV1-UL12.5
HSV2-UL12
HSV2-UL12M117
ORF48
UL98
BGLF5
SOX
pcDNA3.1(+)
MLS-ORF48
MLS-UL98
MLS-SOX
95-
72-
55-
43-
α-FLAG
43-
α-Actin
B
pMZS3F
HSV1-UL12.5
HSV2-UL12
HSV2-UL12M117
ORF48
UL98
SOX
BGLF5
MLS-ORF48
MLS-UL98
MLS-SOX
pcDNA3.1(+)
C
Percent of Transfected cells Depleted of mtDNA
100
80
60
40
20
0
pMZS3F
HSV1-UL12.5
HSV2-UL12
HSV2-UL12M117
ORF48
UL98
BGLF5
SOX
pcDNA3.1(+)
MLS-ORF48
MLS-UL98
MLS-SOX

Figure 6.4. Ability of UL12 orthologs to deplete mtDNA. (A) The indicated plasmids were transfected into HeLa cells and protein expression was visualized at 24 hours post-transfection by immunoblotting with an anti-FLAG antibody. (B) Subcellular localization of the SPA-tagged proteins was examined in transfected HeLa cells by immunofluorescence. Images were obtained using a 40X objective. The mitochondrial protein cytochrome *c* is shown in green and the SPA-tagged proteins (stained with anti-FLAG) are shown in red. Colocalization with cytochrome *c* is indicated in yellow. For clarity, the DAPI channel has been omitted. Scale bars = 10 μm. (C) The presence of absence of mtDNA in transfected HeLa cells was scored by examining cytoplasmic PicoGreen staining in ≥ 80 randomly selected mOrange-positive cells. Data from three separate experiments were averaged and standard errors are indicated. The data for panel A were generated by H. Saffran and the data for panels B and C were generated by A. Ponomarev under the supervision of B. Duguay.

In light of these results, we investigated the effect of retargeting the UL12 orthologs ORF48, UL98, and SOX to mitochondria using the MLS from the human ornithine transcarbamylase protein (486). These experiments were designed to determine if these proteins contained conserved determinants that facilitate mtDNA depletion if localized to mitochondria. Following transfection of HeLa cells, all retargeted proteins were weakly expressed in comparison to their wild-type counterparts, of which only the MLS-UL98 protein reached high levels of expression (Fig. 6.4A). When the MLS-containing proteins were examined by immunofluorescence, it was observed that both MLS-ORF48 and, to a lesser extent the MLS-SOX, were successfully retargeted to mitochondria (Fig. 6.4B). Despite containing an identical MLS, the MLS-UL98 protein only appeared to have a slight increase in diffuse cytoplasmic staining relative to the UL98 protein, indicating that the UL98 protein contains strong determinants for nuclear localization (Fig. 6.4B). Interestingly, when these proteins were subsequently assessed in the PicoGreen live cell mtDNA depletion assay we observed that the MLS-ORF48 protein was capable of reproducibly causing mtDNA depletion in 7% of transfected cells (Fig. 6.4C). The MLS-SOX and MLS-UL98 proteins were not observed to cause any depletion which is likely in part due to the inefficient relocalization of these constructs (Figs. 6.4B and C). The fact that the ORF48 protein was capable of causing mtDNA depletion upon retargeting to mitochondria despite its low expression level is intriguing. It is currently unknown whether any of these genes produce N-terminally truncated proteins targeted to mitochondria in a manner similar to the *UL12* genes of HSV-1 and

HSV-2. However, in light of our data regarding the mitochondria-localized ORF48 protein, it would be interesting to investigate if any additional ORF48-derived proteins are produced during infection and what if any impact VZV infection has on mtDNA levels. Altogether, our data demonstrate that, aside from HSV-1 and HSV-2 *UL12*, none of the full length *UL12* orthologs appear to be capable of depleting mtDNA in a transfection assay. This finding suggested that these orthologs, namely UL98 and SOX, might also be incapable of triggering mtDNA depletion during virus infection.

6.2.3 – HCMV UL98 supports wild-type levels of HSV-1 replication

A previous study demonstrated that HCMV UL98 is able to at least partially complement the growth defect of the UL12-null HSV-1 AN1 virus (521). Given that UL98 also appeared to be unable to deplete mtDNA (Fig. 6.4C), we decided to generate an HSV-1 UL12/UL12.5-null mutant that expresses UL98 from the *UL12* promoter (Fig. 6.5). Using *en passant* mutagenesis we disrupted the *UL12* and *UL12.5* ORFs by inserting *UL98* coding sequences. The resulting virus was then used to investigate the role of mtDNA depletion during infection. In this mutant virus, the *UL98-SPA* ORF was inserted in place of nucleotides 1-1152 of the *UL12* ORF (Fig. 6.5). The remaining 729 nucleotides at the 3' end of the *UL12* ORF were retained to avoid disrupting the *UL11* promoter and coding sequence (Figs. 6.5 and 6.6), which overlap with *UL12* in wild-type HSV-1 (42). The presence of the *UL98-SPA* gene and its placement in the KOS37 genome were confirmed through DNA sequencing (Fig. 6.7). To control for any effects of shifting the *UL11* gene downstream of *UL12*, we also created a virus which

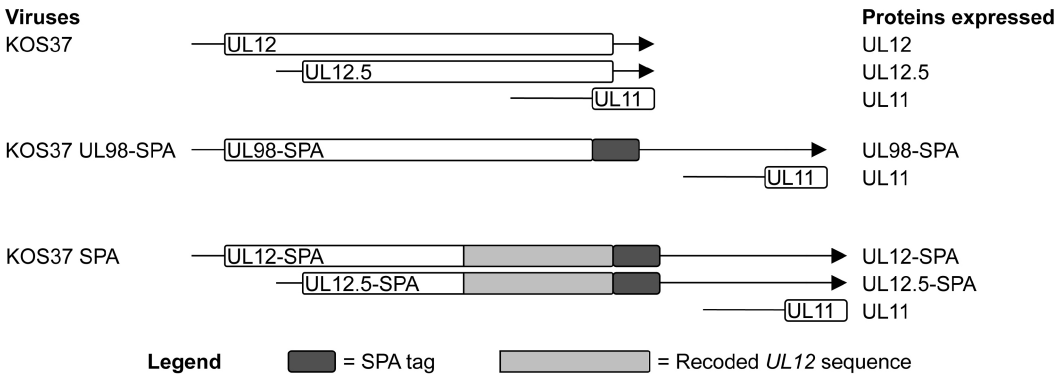

Figure 6.5. Construction of the KOS37 UL98 and KOS37 SPA mutant viruses. Schematics of the *UL12*, *UL12.5*, *UL98-SPA*, *UL12-SPA*, *UL12.5-SPA*, and *UL11* loci in HSV-1 wild-type and mutant viruses are shown. KOS37 is the wild-type parental virus. KOS37 UL98-SPA is a UL12/UL12.5-null virus which expresses a C-terminally SPA tagged version of the UL12 ortholog HCMV UL98 in a manner that does not affect UL11 expression. KOS37 SPA contains silent mutations in the 3' end of the UL12 gene which facilitate the expression of C-terminally SPA tagged UL12 and UL12.5 proteins without affecting UL11 expression. The mRNA transcripts are represented by black arrows and the open reading frames are represented by boxes. All features are drawn to scale.

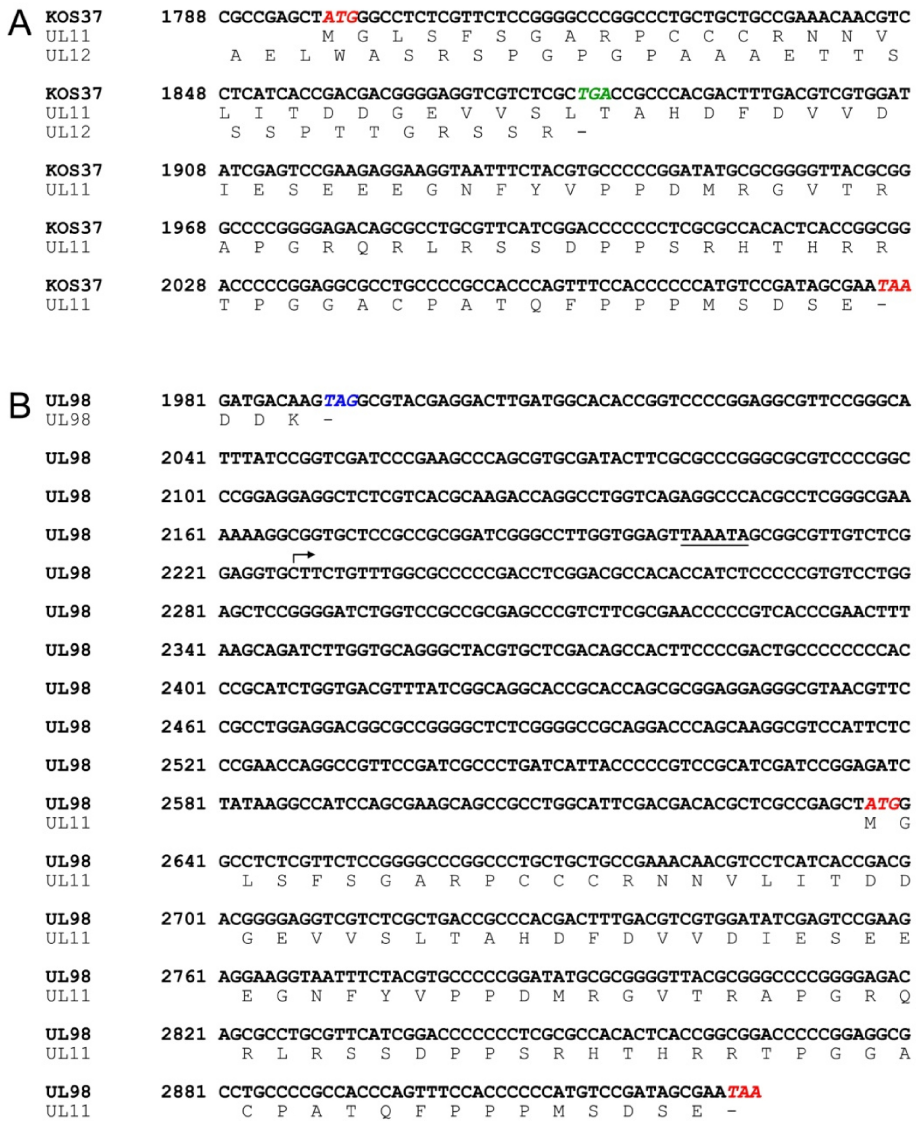

Figure 6.6. Repositioning of the *UL11* locus in the KOS37 UL98 genome. (A) Overlapping nature of *UL12* and *UL11* genes in the wild-type KOS37 viral genome. Shown are the final 31 codons of *UL12* and the entire *UL11* gene. All numbering is relative to the start codon of *UL12* (B) Position of *UL11* and its upstream untranslated region in the KOS37 UL98 viral genome. Shown are the final four codons of *UL98-SPA* and the entire *UL11* gene. The *UL11* "TATA" box is underlined and the transcript start site indicated with an arrow (42). All numbering is relative to the start codon of *UL98-SPA*. All nucleotide sequences are in bold. Start and stop codons are in bold italics with those for *UL11* in red, for *UL12* in green, and for *UL98-SPA* (UL98) in blue. The corresponding amino acids are indicated under the first nucleotide of the respective codons. SPA, sequential peptide affinity.

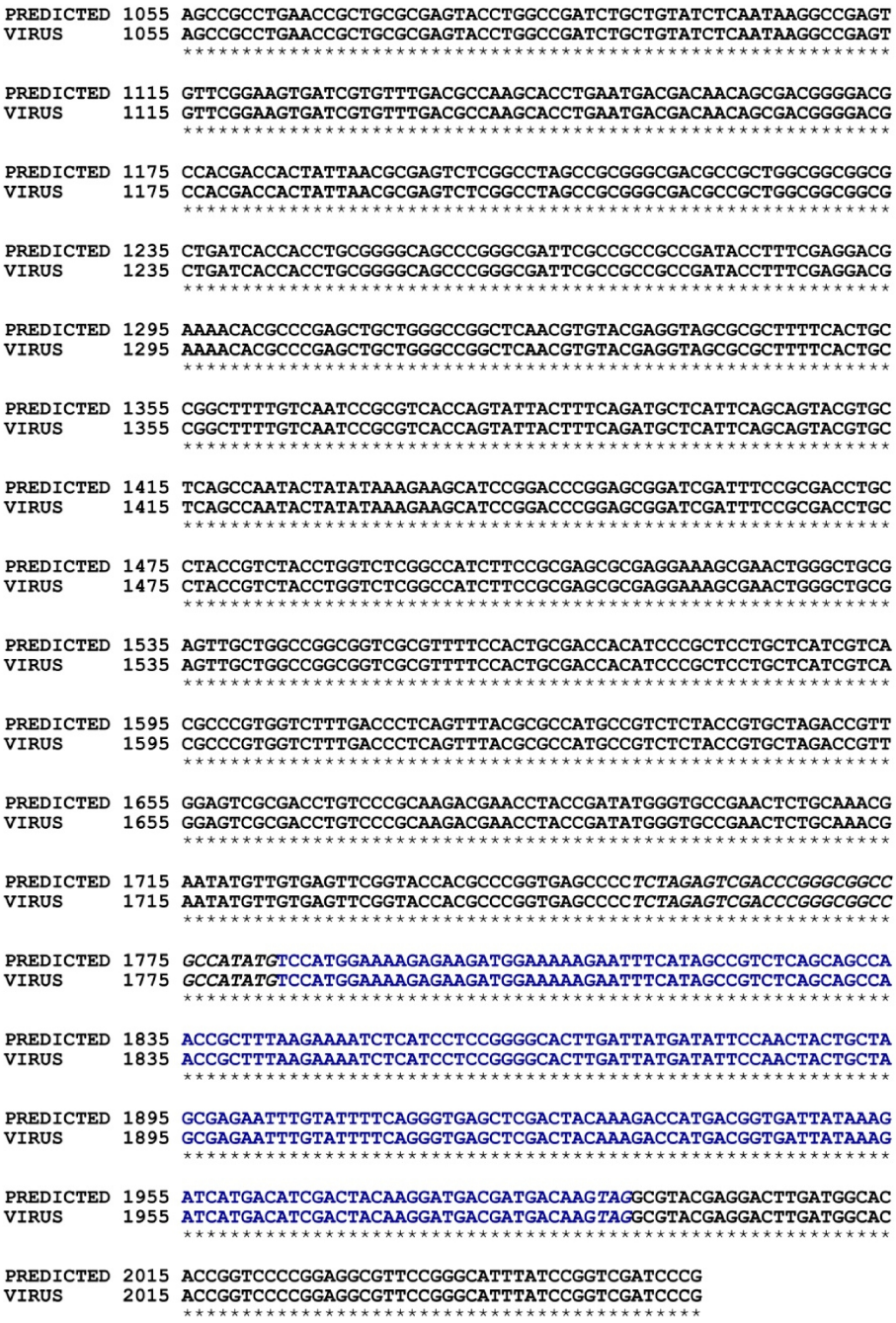

Figure 6.7. Validation of the KOS37 UL98 mutant virus. PCR amplified *UL98-SPA* from KOS37 UL98 infected cell lysates was sequenced (VIRUS) and the results compared to the predicted *UL98-SPA* sequence using Clustal Omega. Shown are nucleotides 1055 to 1992 of UL98-SPA and 66 nucleotides of viral genomic sequence downstream of *UL98-SPA*. A linker sequence (nucleotides 1753 to 1782) is shown in italics. The SPA tag coding sequence is shown in blue with the stop codon in bold italics. Asterisks indicate conserved nucleotides. All numbering is relative to the start codon of *UL98-SPA*.

expresses UL12-SPA and UL12.5-SPA (KOS37 SPA) in a similar configuration as the KOS37 UL98-SPA genome (Figs. 6.5 and 6.6). The construction of this virus required that the 729 nucleotide sequence corresponding to the 3' end of *UL12-SPA*/*UL12.5-SPA* be recoded with silent mutations to allow UL12-SPA/UL12.5-SPA expression while avoiding sequence duplication and recombination with the downstream wild-type 729 nucleotides (containing the 5' end of *UL11*) (Fig. 6.8). The KOS37 SPA *UL12-SPA* gene was used in the creation of pMZS3F UL12-SPA (see section 2.3.8.5) and as such has been verified by DNA sequencing. In these mutant viruses, UL98-SPA and UL12-SPA are under the control of the *UL12* promoter, while UL12.5-SPA is under the control of the *UL12.5* promoter.

Our next set of experiments directly examined if the M127F/M185L mutations or the expression of UL98-SPA in lieu of UL12/UL12.5 had any impact on viral replication by performing growth analyses of all viruses used in this study. To perform single-step growth curves, Vero cells were infected with five plaque forming units (PFU)/cell and viral yields were assessed at various times post-infection (Fig. 6.9A). Consistent with previous observations (149, 193), the AN1 virus was significantly impaired in replication (ca. 400-fold lower titres) compared to KOS virus by 24 hours post-infection (Fig. 6.9A). Wild-type KOS and KOS37 grew roughly comparably although KOS37 virus yielded slightly lower titres than did KOS virus (Fig. 6.9A). This minor difference in titres was also observed during the initial characterization of the KOS37 strain (473). F/L, F/L Res, and SPA viruses produced titres similar to parental KOS37

```
KOS37      1141 CCCACGGCCTCCGCGTACGAGGACTTGATGGCACACCGGTCCCCGGAGGCGTTCCGGGCA
SPA        1141 CCCACGGCCTCCGCCTATGAAGATTTGATGGCTCATCGCAGCCCCGAAGCCTTTCGCGCT
                ************** ** ** ** ******** ** **   *** ** ** ** ** **
UL12/UL12SPA    P  T  A  S  A  Y  E  D  L  M  A  H  R  S  P  E  A  F  R  A

KOS37      1201 TTTATCCGGTCGATCCCGAAGCCCAGCGTGCGATACTTCGCGCCCGGGCGCGTCCCCGGC
SPA        1201 TTCATCCGCTCAATCCCCAAACCGTCCGTCCGATATTTTGCCCCGGGACGGGTGCCGGGG
                ** ***** ** ***** ** **   *** ***** ** ** ** ** ** ** ** **
UL12/UL12SPA    F  I  R  S  I  P  K  P  S  V  R  Y  F  A  P  G  R  V  P  G

KOS37      1261 CCGGAGGAGGCTCTCGTCACGCAAGACCAGGCCTGGTCAGAGGCCCACGCCTCGGGCGAA
SPA        1261 CCCGAAGAAGCACTGGTGACCCAGGATCAAGCGTGGTCGGAAGCGCATGCGTCAGGGGAG
                ** ** ** ** ** ** ** ** ** ** ** ** ***** ** ** ** ** ** ** **
UL12/UL12SPA    P  E  E  A  L  V  T  Q  D  Q  A  W  S  E  A  H  A  S  G  E

KOS37      1321 AAAAGGCGGTGCTCCGCCGCGGATCGGGCCTTGGTGGAGTTAAATAGCGGCGTTGTCTCG
SPA        1321 AAGAGGCGCTGTAGCGCGGCCGACCGCGCGTTGGTCGAATTAAACTCCGGGGTTGTGTCA
                ** ***** **   *** ** ** ** ** ***** ** *****   *** ***** **
UL12/UL12SPA    K  R  R  C  S  A  A  D  R  A  L  V  E  L  N  S  G  V  V  S

KOS37      1381 GAGGTGCTTCTGTTTGGCGCCCCCGACCTCGGACGCCACACCATCTCCCCCGTGTCCTGG
SPA        1381 GAAGTCCTTCTCTTCGGGGCGCCGGATCTGGGACGGCATACGATCAGCCCGGTCAGCTGG
                ** ** ***** ** ** ** ** ** ** ***** ** ** ***  *** **   ****
UL12/UL12SPA    E  V  L  L  F  G  A  P  D  L  G  R  H  T  I  S  P  V  S  W

KOS37      1441 AGCTCCGGGGATCTGGTCCGCCGCGAGCCCGTCTTCGCGAACCCCCGTCACCCGAACTTT
SPA        1441 TCCAGCGGCGACCTCGTGCGGCGGGAACCGGTGTTTGCCAATCCGCGTCATCCCAATTTC
                   *  *** ** ** ** ** ** ** ** ** ** ** ** ** ***** ** ** **
UL12/UL12SPA    S  S  G  D  L  V  R  R  E  P  V  F  A  N  P  R  H  P  N  F

KOS37      1501 AAGCAGATCTTGGTGCAGGGCTACGTGCTCGACAGCCACTTCCCCGACTGCCCCCCCCAC
SPA        1501 AAACAAATCTTGGTCCAAGGGTATGTCCTGGATTCCCATTTTCCGGATTGTCCGCCGCAT
                ** ** ******** ** ** ** ** ** **   *** ** ** ** ** ** ** **
UL12/UL12SPA    K  Q  I  L  V  Q  G  Y  V  L  D  S  H  F  P  D  C  P  P  H

KOS37      1561 CCGCATCTGGTGACGTTTATCGGCAGGCACCGCACCAGCGCGGAGGAGGGCGTAACGTTC
SPA        1561 CCCCACCTCGTCACCTTCATCGGGAGGCATCGGACGTCCGCCGAAGAAGGGGTAACCTTT
                ** ** ** ** ** ** ***** ***** ** **   *** ** ** ** ***** **
UL12/UL12SPA    P  H  L  V  T  F  I  G  R  H  R  T  S  A  E  E  G  V  T  F

KOS37      1621 CGCCTGGAGGACGGCGCCGGGGCTCTCGGGGCCGCAGGACCCAGCAAGGCGTCCATTCTC
SPA        1621 CGGCTCGAAGATGGGGCGGGCGCACTGGGCGCGGCTGGACCGTCCAAAGCCAGCATCCTG
                ** ** ** ** ** ** ** ** ** ** ** ** ** *****   *** **   *** **
UL12/UL12SPA    R  L  E  D  G  A  G  A  L  G  A  A  G  P  S  K  A  S  I  L

KOS37      1681 CCGAACCAGGCCGTTCCGATCGCCCTGATCATTACCCCCGTCCGCATCGATCCGGAGATC
SPA        1681 CCCAATCAAGCGGTTCCCATCGCGCTCATCATCACGCCGGTGCGGATCGACCCCGAAATC
                ** ** ** ** ***** ***** ** ***** ** ** ** ** ***** ** ** ***
UL12/UL12SPA    P  N  Q  A  V  P  I  A  L  I  I  T  P  V  R  I  D  P  E  I

KOS37      1741 TATAAGGCCATCCAGCGAAGCAGCCGCCTGGCATTCGACGACACGCTCGCCGAGCTATGG
SPA        1741 TACAAAGCGATCCAACGATCCTCCCGGCTCGCTTTTGATGATACCCTGGCGGAACTATGG
                ** ** ** ***** ***  *  *** ** ** ** ** ** ** ** ** ** ******
UL12/UL12SPA    Y  K  A  I  Q  R  S  S  R  L  A  F  D  D  T  L  A  E  L  W

KOS37      1801 GCCTCTCGTTCTCCGGGGCCCGGCCCTGCTGCTGCCGAAACAACGTCCTCATCACCGACG
SPA        1801 GCGAGTCGTAGTCCCGGACCGGGGCCTGCAGCAGCGGAGACAACCAGCTCGTCGCCCACC
                **   ****  *** ** ** ** ***** ** ** ** *****   *** ** ** **
UL12/UL12SPA    A  S  R  S  P  G  P  G  P  A  A  A  E  T  T  S  S  S  P  T

KOS37      1861 ACGGGGAGGTCGTCTCGCTGA----------------------------------------
SPA        1861 ACCGGCAGGTCAAGTCGGGGTACCTCCATGGAAAAGAGAAGATGGAAAAAGAATTTCATA
                ** ** *****   ***  *
UL12            T  G  R  S  S  R  -
UL12SPA         T  G  R  S  S  R  G  T  S  M  E  K  R  R  W  K  K  N  F  I

KOS37           ------------------------------------------------------------
SPA        1921 GCCGTCTCAGCAGCCAACCGCTTTAAGAAAATCTCATCCTCCGGGGCACTTGATTATGAT
UL12SPA         A  V  S  A  A  N  R  F  K  K  I  S  S  S  G  A  L  D  Y  D

KOS37           ------------------------------------------------------------
SPA        1981 ATTCCAACTACTGCTAGCGAGAATTTGTATTTTCAGGGTGAGCTCGACTACAAAGACCAT
UL12SPA         I  P  T  T  A  S  E  N  L  Y  F  Q  G  E  L  D  Y  K  D  H

KOS37           ----------------------------------------------------
SPA        2041 GACGGTGATTATAAAGATCATGACATCGACTACAAGGATGACGATGACAAGTAG
UL12SPA         D  G  D  Y  K  D  H  D  I  D  Y  K  D  D  D  D  K  -
```

Figure 6.8. Design of the 3' end of the *UL12-SPA* gene for the KOS37 SPA virus. A DNA sequence alignment of the *UL12* gene of KOS37 and the recoded *UL12-SPA* gene sequence (containing 208 silent mutations and SPA tag coding sequences) of KOS37 SPA was performed using Clustal Omega. Asterisks indicate conserved nucleotides. The corresponding amino acid is indicated under the first nucleotide of the respective codon. All nucleotide sequences are in bold. Start and stop codons are in bold italics with those for *UL11* in red, for *UL12* in green, and for *UL12-SPA* (UL12SPA) in blue. All numbering is relative to the start codon of *UL12*/*UL12-SPA*. Asterisks indicate conserved nucleotides. SPA, sequential peptide affinity.

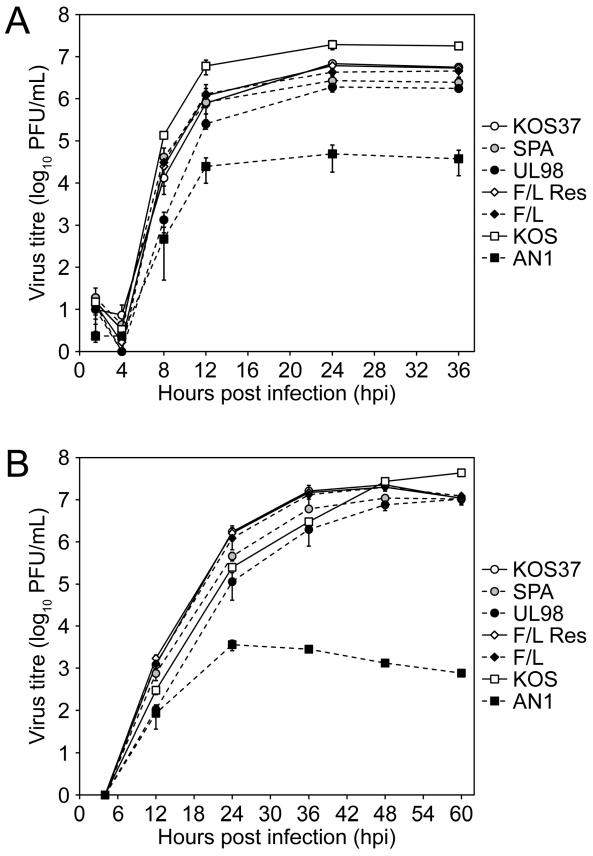

Figure 6.9. Replication of HSV-1 isolates used in this study. (A) Single-step growth curves were performed in Vero cells infected at a multiplicity of infection (MOI) of five with the indicated viruses and harvested at 1.5, 4, 8, 12, 24, and 36 hours post-infection. (B) Multi-step growth curves were performed in Vero cells infected at a MOI of 0.01 with the indicated viruses and harvested at 4, 12, 24, 36, 48, and 60 hours post-infection. All titring was performed on the UL12 complementing cell line 6-5 with the resulting titres plotted on logarithmic scales. KOS37 derived viruses are shown using circles and diamonds. KOS derived viruses are shown using squares. Wild-type viruses are indicated with solid lines and mutant viruses with dashed lines. Data are averaged from three independent experiments and standard errors are indicated.

throughout the 36 hour time course (Fig. 6.9A). Replication of the UL98 virus was delayed compared to KOS37 at early times, but the final titres were comparable to the parental virus (KOS37) and the control virus (SPA) (Fig. 6.9A).

To determine if the UL98 virus displays a defect at low multiplicities of infection compared to the KOS37 and SPA controls, we also infected Vero cells with 0.01 PFU/cell and performed a multi-step growth analysis (Fig. 6.9B). Consistent with the data presented in Fig. 6.9A, the UL98 virus exhibited somewhat reduced viral titres at early times post-infection relative to the titres produced following KOS37 and SPA infection (Fig. 6.9B). Relative to the control SPA virus, differences in viral titres were statistically significant only at the thirty-six hour time point ($p = 0.04$). However, by forty-eight hours post-infection the titres of the UL98 and SPA viruses were indistinguishable. The titres for KOS, KOS37, F/L, F/L Res, SPA, and UL98 viruses were all within one log unit throughout the entire time course (Fig. 6.9B) and the replication-defective AN1 virus never achieved titres higher than 3.6×10^3 PFU/mL (Fig. 6.9B).

Altogether, these observations are consistent with the results of complementation experiments involving UL98 during AN1 virus infection (521) and demonstrate that UL98 can restore viral replication to near wild-type levels in the absence of UL12 and UL12.5.

6.2.4 – Viral protein expression

Since the UL98 virus demonstrated a slight delay in viral replication, we examined whether this was correlated with delayed or abnormal viral protein

expression. We first examined whether the expression of the early protein UL11 was disrupted due to the gene rearrangements in the UL98 and SPA viral genomes. Vero cells were infected with five PFU/cell of the indicated viruses for four, eight, and twelve hours and the lysates were assessed for UL11 expression by western blotting (Fig. 6.10A). At four hours post-infection UL11 expression was slightly higher in cells infected with UL98, SPA, and F/L Res viruses than the other viruses; however, these differences were no longer apparent at later time points (Fig. 6.10A). UL11 expression at or around four hours post-infection is consistent with its known classification as a delayed early protein (522). An examination of additional viral proteins revealed, with the exception of some minor variations in protein expression (i.e. F/L, eight hours post-infection, ICP27), that all mutant viruses expressed the immediate early protein ICP27 and the true-late protein glycoprotein C (gC) at times consistent with their kinetic classes (Fig. 6.10B). We also observed clear expression of UL98-SPA (ca. 75 kDa) or UL12-SPA (ca. 95 kDa) and UL12.5-SPA (ca. 70 kDa) from the UL98 or SPA viruses, respectively, at times associated with early protein expression (Fig. 6.10B). These data indicate that all of the mutant viruses expressed representative immediate early, early, and true-late proteins with appropriate kinetics and that UL11 expression was not greatly affected by repositioning the *UL11* gene downstream of *UL12-SPA*/*UL12.5-SPA* or *UL98-SPA*. Thus, further experiments are required to determine the basis for the delayed replication of the UL98 virus.

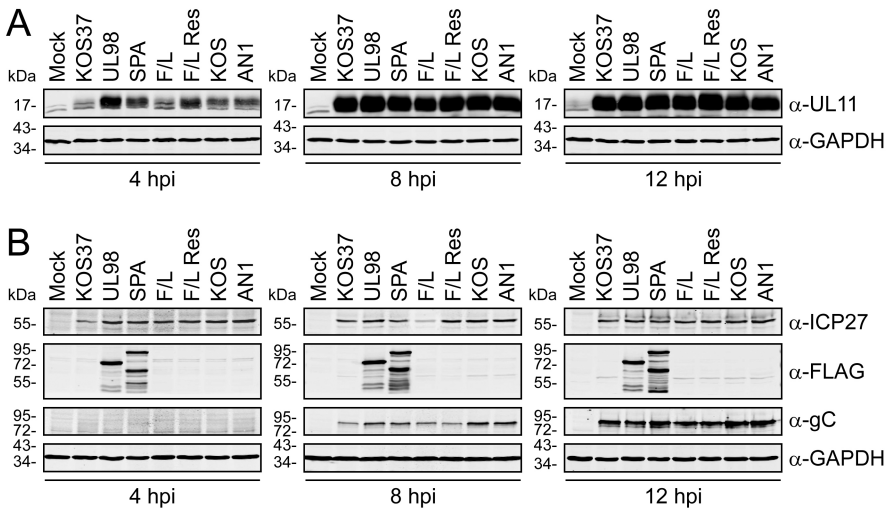

Figure 6.10. Viral protein expression is unaffected by mutations of the *UL12* gene. Vero cells were mock infected or infected at a multiplicity of infection of five with the indicated viruses and lysates for western blotting were prepared at 4, 8, or 12 hours post-infection (hpi). The expression levels of UL11 (A), ICP27 (B), glycoprotein C (gC) (B), and the FLAG-tagged proteins UL98-SPA, UL12-SPA, and UL12.5-SPA (B) are shown. GAPDH was included as a loading control in panels A and B. The data for figure 6.10 were generated by H. Eaton.

6.2.5 – MtDNA depletion is severely impaired during infection with UL98 expressing HSV-1

We next tested the ability of the UL98 and SPA viruses to deplete mtDNA using the Southern blot assay used in Fig. 6.3. Equivalent amounts of DNA isolated from mock or virus infected cells were loaded into agarose gels, subjected to electrophoresis, and stained using SYBR Gold (Fig. 6.11A) prior to visualization of mtDNA with a radiolabelled *MT-CO2* probe (Fig. 6.11B). As expected, the SPA virus reduced mtDNA content to levels similar to those observed with KOS and KOS37 by twelve hours post-infection (SPA: 2% remaining; KOS and KOS37: 5% remaining) (Figs. 6.11B and C). In contrast, the UL98 virus was severely impaired: 72% of the mtDNA remained at twelve hours post-infection (Figs. 6.11B and C) and this difference from the mock-infected values did not achieve statistical significance over the course of three independent experiments (p = 0.24). Altogether, these data indicate that replacing UL12, UL12.5, and $UL12_{M185}$ with HCMV UL98 severely impairs or inactivates the ability of HSV-1 to deplete mtDNA during productive infection and document that eliminating mtDNA is not required for efficient HSV-1 replication in cultured Vero cells (Figs. 6.9 and 6.11).

6.2.6 – Late viral protein synthesis during viral infection does not significantly influence mtDNA levels.

Although infection with the UL98 virus resulted in impaired mtDNA depletion during infection (Fig. 6.11), some of our experiments suggested that a minor loss of mtDNA may occur by twelve hours post-infection in UL98 virus

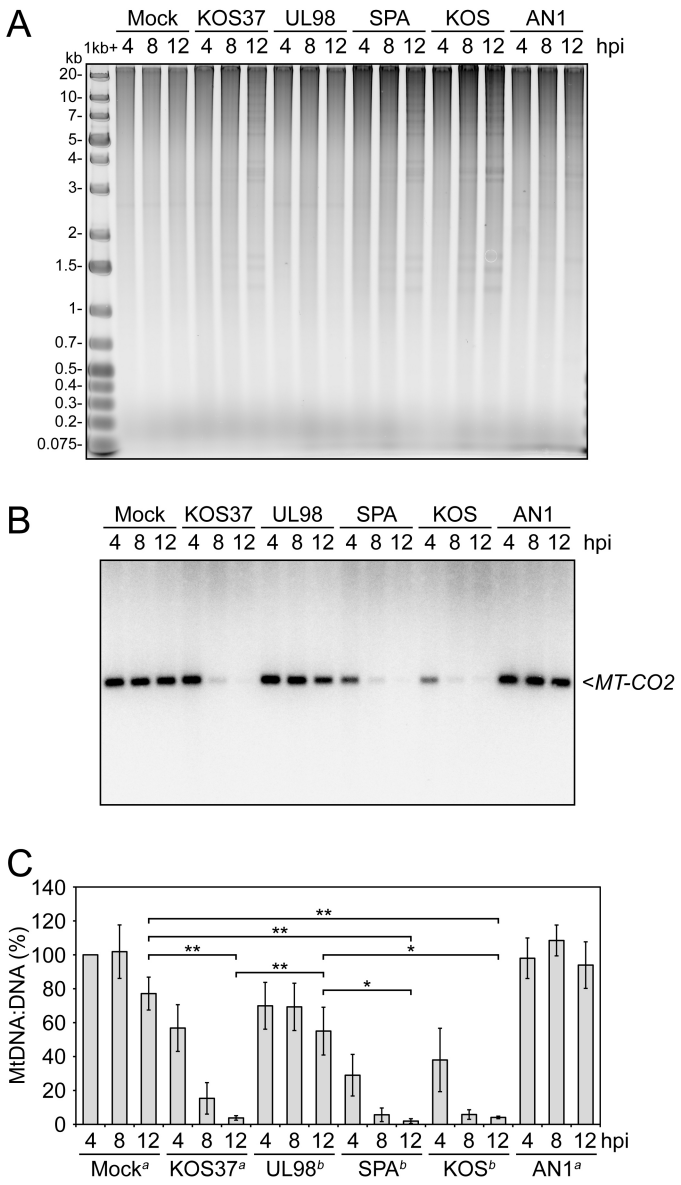

Figure 6.11. Expression of HCMV UL98 in lieu of HSV-1 UL12 severely impairs mtDNA depletion during HSV-1 infection. (A) Following mock infection or infection at a multiplicity of infection of ten with the indicated viruses, total DNA was isolated from Vero cells harvested at 4, 8, or 12 hours post-infection (hpi). Total DNA was visualized by SYBR Gold staining following agarose gel electrophoresis. (B) The separated DNA in panel A was transferred to nitrocellulose and mtDNA was detected following Southern blot hybridization with a radiolabelled probe targeting the mtDNA gene encoding cytochrome *c* oxidase subunit II (*MT-CO2*). (C) The mtDNA:DNA ratio from multiple Southern blots were averaged, and plotted normalized to Mock (4 hpi) with standard error indicated. Sample sizes: [a]n=4 and [b]n=3. Statistically significant differences are indicated for $P < 0.05$ (*) and $P < 0.01$ (**). The data for figure 6.11 were generated by H. Saffran.

infected cells; however, this difference was not observed to be statistically significant (Fig. 6.11C). It was unlikely that this loss of mtDNA was due to UL98 expression since this protein appeared unable to cause mtDNA depletion in transfected cells (Fig. 6.4C). To further investigate whether mtDNA depletion occurs in the absence of UL12.5/UL12$_{M185}$ expression at late times, we examined whether the DNA polymerase/late protein synthesis inhibitor, phosphonoacetic acid (PAA) (523-525), could have any effect on mtDNA levels in infected cells.

Vero cells were left untreated or treated with PAA at the onset of infection and harvested at twelve hours post-infection. Equivalent amounts of DNA were loaded onto agarose gels and stained using SYBR Gold (Fig. 6.12A) prior to hybridization with a radiolabelled *MT-CO2* probe (Fig. 6.12B). Following Southern blotting, we consistently observed a minor increase in mtDNA levels following the addition of PAA in KOS37, SPA, KOS, or AN1 virus infected cells compared to the respective untreated samples (Figs. 6.12B and C). However, these differences were not observed to be statistically significant in the number of replicates performed. During UL98 virus infection the level of mtDNA following PAA treatment was 41% greater compared to cells infected in the absence of PAA treatment; however, this difference also did not achieve statistical significance (Figs. 6.12B and C). Therefore, these data do not support a conclusion that late viral proteins participate in HSV-1 mtDNA depletion. Whether or not differences in mtDNA levels occur at late times post-infection, and whether or not these difference are independent of UL12.5 or UL12$_{M185}$ expression, would require more thorough examination.

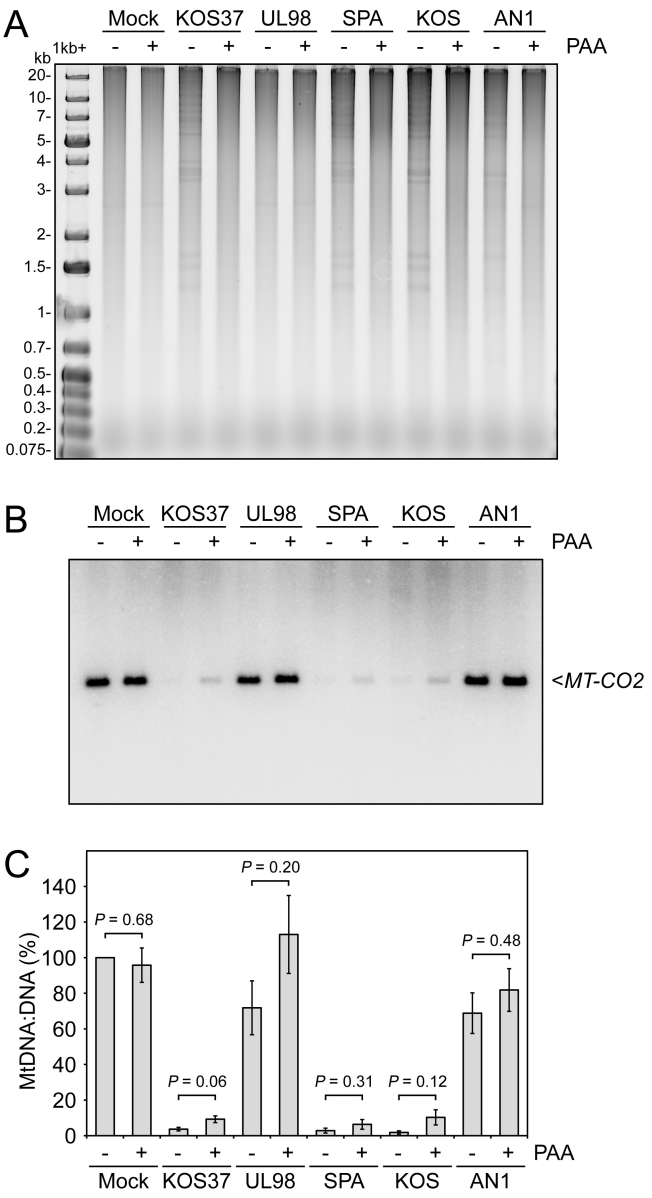

Figure 6.12. Treatment of infected cells with phosphonoacetic acid (PAA) does not have a significant impact on mtDNA depletion. (A) Vero cells were untreated (-) or treated (+) with 300 μg/mL PAA, mock infected or infected at a multiplicity of infection of ten with KOS37, UL98, SPA, KOS, or AN1 viruses, and harvested at 12 hours post-infection. Total DNA was visualized by SYBR Gold staining following agarose gel electrophoresis. (B) The separated DNA in panel A was transferred to nitrocellulose and mtDNA was detected following Southern blot hybridization with a radiolabelled probe targeting the mtDNA gene encoding cytochrome *c* oxidase subunit II (*MT-CO2*). (C) The MtDNA:DNA ratio from three Southern blots were averaged and plotted normalized to Mock infection without PAA treatment. Standard errors and *p* values are indicated. The data for figure 6.12 were generated by H. Saffran.

6.3 – Conclusions

During infection with both HSV-1 and HSV-2 mtDNA is lost rapidly following infection (152). Our hypothesis at the time of that discovery was that the *UL12* gene of HSV-2 produces a similar protein capable of causing mtDNA depletion due to the significant sequence conservation with the *UL12* gene of these viruses (42). Our data presented in this chapter provides the first direct evidence to support this hypothesis from the observation that the HSV-2 $UL12_{M117}$ protein was equally capable of causing mtDNA deletion as HSV-1 UL12.5 (Fig. 6.4C). Furthermore, when the ORF48 protein of VZV was artificially targeted to mitochondria it caused mtDNA loss in ca. 7% of transfected cells (Fig. 6.4C). This observation suggests that the protein determinants responsible for mtDNA depletion are conserved with other alphaherpesvirus UL12 orthologs; even if the full-length VZV ORF48 protein cannot localize to mitochondria. Further work is required to determine if mtDNA loss is a common aspect of alphaherpesvirus infections and to elucidate what common motifs of alphaherpesvirus UL12 orthologs facilitate mtDNA loss.

Our data herein also clearly argue that mtDNA loss is not required for HSV-1 replication in cell culture (Figs. 6.9 and 6.11). To reach this conclusion, we exploited the known ability of HCMV UL98 to compensate for UL12 loss during HSV-1 infection (521) and created a UL98-expressing, UL12-null HSV-1 mutant virus. This virus was unable to significantly affect mtDNA levels during infection compared to mock infected cells (Fig. 6.11C). These observations were in stark contrast to those made using cells infected with an HSV-1 mutant virus

containing more subtle mutations of *UL12* designed to prevent UL12.5 and $UL12_{M185}$ expression (Fig. 6.3). Future studies into the relevance of mtDNA depletion for HSV-1 infection are required but the possibility exists that this process is important for viral pathogenesis *in vivo*. The KOS37 UL98 virus created in this study, and its respective control KOS37 SPA, would be valuable for these upcoming experiments.

Chapter 7: Discussion

7.1 – Discussion

In order for herpesviruses to both productively infect cells and establish latency they must adapt to the host environment and circumvent cellular barriers to infection. Mitochondrial proteins and processes are among many of the aspects targeted by herpesviruses to facilitate pathogenesis. For alphaherpesviruses, this includes utilizing viral proteins to inhibit apoptosis, disrupt mitochondrial dynamics, alter mitochondrial energy production, and potentially affect the mitochondrial permeability-transition pore (342, 344, 345, 356, 369, 526, 527). Our recent work has added to this list by demonstrating that HSV-1 and HSV-2 dramatically affect mtDNA levels in infected cells (152), an observation which has been more recently shared with the human herpesvirus, EBV (448). However, despite understanding which viral protein was involved in HSV-1-mediated mtDNA loss, very little was known regarding the mechanism of this process. To this end, the present study sought to better elucidate the steps utilized by HSV-1 UL12.5 to deplete cells of mtDNA.

7.1.1 – UL12.5 utilizes an N-proximal mitochondrial localization sequence to traffic to mitochondria

The first step to understanding how mtDNA depletion occurred following UL12.5 expression involved determining the means by which UL12.5 localized to mitochondria. For UL12.5 to cause the destruction of mtDNA present within the mitochondrial matrix, the initial hypothesis stated that UL12.5 must also localize to the mitochondrial matrix. I clearly demonstrated that a sixty residue sequence (M185-R245) derived from the N-terminus of UL12.5 functions independently as

a MLS (Fig. 3.4). Moreover, non-conservative substitution mutations (Figs. 3.5 and 3.6) or a twenty-five residue deletion (Figs. 3.7, 4.3, and 4.5) of this sequence were sufficient to decrease the overall positive charge and disrupt mitochondrial localization of the intact protein. These observations were consistent with the known importance of positively-charged residues in mitochondrial protein presequences for recognition by one of the import receptors TOM22 (528, 529) and in facilitating the crossing of the mitochondrial inner membrane (530). However, the presence of a highly positively-charged MLS was not required for UL12.5 localization. As demonstrated in Fig. 3.6, when positively-charged arginine residues of the MLS were mutated to hydrophilic asparagine residues UL12.5 was still capable of localizing to mitochondria. The presence of asparagine resides would maintain the amphipathic nature of the predicted α-helical region of the MLS as opposed to the replacement of these residues with hydrophobic alanine residues. In the UL12.5 R→N mutant, additional histidine and arginine residues within the predicted alpha-helical regions at positions 193 and 212, respectively, may provide sufficient positive charge to compensate for the loss of the other five proximal arginine residues. Interestingly, Hammen *et al*. observed similar preservation of mitochondrial localization following arginine to glutamine mutations of the presequence of the mitochondrial matrix protein rat liver aldehyde dehydrogenase (531). The mutation of two arginine residues in conjunction with a deletion of a third arginine residue had little impact on the import of aldehyde dehydrogenase into mitochondria which was proposed to be a result of the stabilization of the α-helical presequence (531). Therefore, it is

possible that the hydrophilic nature of the UL12.5 MLS is very important for mitochondrial localization assuming additional positively-charged residues are present to facilitate mitochondrial import. It is also possible that arginine and histidine residues within predicted alpha-helical regions at positions 140, 148, 149, 151, and 169 could facilitate mitochondrial localization of the UL12.5 R→N mutant even though many of these residues on their own were not required for UL12.5 translocation to mitochondria (Jennifer Corcoran, unpublished data).

Additional experiments by Jennifer Corcoran demonstrated that significant truncation of the UL12.5 N-terminus uncovered another internal MLS at or downstream of residue M390 (475). This mutant termed $UL12_{M390}$, although able to localize to mitochondria, was unable to deplete mtDNA (475). It is possible that both the MLSs present downstream of residues M185 and M390 could contribute to the mitochondrial localization of UL12.5; however, the mutagenesis results presented in Chapter 3 do not support this hypothesis. Instead, these data support the conclusion that the sequence between residues 185 and 245 is the dominant regulator of mitochondrial localization of UL12.5. Altogether, the data in Chapter 3 and our published functional data (152) broadly support the localization of UL12.5 to the mitochondrial matrix; some aspects of the results presented in Chapter 3 do not conform to the expectations for most mitochondrial matrix-targeted proteins.

7.1.2 – Speculation regarding the ultimate sub-mitochondrial location of UL12.5

Even though the primary structure and polybasic nature of the UL12.5 MLS (Fig. 3.3) are similar to known features of cellular mitochondrial matrix

targeting sequences (317, 490), it differs in the internal positioning of these residues in the UL12.5 protein (Figs. 3.2 and 3.4). It is likely the positioning of the MLS in UL12.5 precludes its identification as a mitochondrial protein using algorithms such as MitoProt II (Fig. 3.2B). Interestingly, a global examination of the N-proteome of *Saccharomyces cerevisiae* identified proteins which localize to the mitochondrial matrix despite having low predicted probabilities of export to mitochondria (>0.322 using MitoProt II) (491). These proteins included the mitochondrial ribosomal proteins (MRP) encoded by *MRP17*, *MRP51*, *MRPL23*, and *RSM27* in addition to the mitochondrial recombinase Mhr1p and the yeast flavohemoglobin, YHb.

Often N-terminal presequences present on many proteins destined for the mitochondrial matrix are removed by the mitochondrial processing peptidase in the mitochondrial matrix (532). For UL12.5, the proteinase K protection assay data do not indicate that the MLS was cleaved following import since the full-length protein was observed in isolated mitochondria (Fig. 3.8). Furthermore, the largest UL12.5-SPA species observed in isolated mitochondria (Fig. 3.8) was equivalent in size to *in vitro* translated UL12.5-SPA (Fig. 4A.1A) , which further supports a lack of processing of the mature protein. Although uncommon, other mammalian mitochondrial matrix proteins such as rhodanese (533, 534), acetyl-CoA acyltransferase 2 (535), the β-subunit of the electron transfer flavoprotein (536), and chaperonin 10 (537, 538) as well as the *Saccharomyces cerevisiae* mitochondrial ribosomal protein YmL8 (539) have been shown to retain their targeting signals following import. Moreover, the *Saccharomyces cerevisiae*

mitochondrial matrix proteins encoded by *MRP51*, *MRPL23*, and *RSM27* as well as Mhr1p and YHb were observed using a proteomics approach to contain noncleavable MLSs (491). Therefore, it is plausible that UL12.5-SPA also localizes to the mitochondrial matrix using a noncleavable matrix targeting sequence.

The detection of prominent, significantly truncated, protease-protected, C-terminal fragments of UL12.5 and $UL12_{M185}$ in proteinase K treated mitochondria (Fig. 3.8) was at odds with expectations for mitochondrial matrix proteins. These data suggest that a significant portion of the N-termini of UL12.5 and $UL12_{M185}$ is exposed to the cytosol while the majority of the proteins reside within the mitochondrion; similar to the orientation of tail-anchored mitochondrial outer membrane proteins (540). Since I have observed full-length UL12.5 in proteinase K treated mitochondria, UL12.5 would need to be fully imported into the intermembrane space followed by reinsertion of the protein into the outer mitochondrial membrane by the sorting and assembly machinery (SAM) complex for an N_{out}-C_{in} orientation like this to occur. However, the UL12.5-SPA protein in the proteinase K protection assays does not contain any regions with sufficiently high predicted hydrophobicity to be transmembrane domains (Fig. 7.1) making it unlikely that this protein could be inserted into a membrane. Additional proteinase K protection assays using mitoplasts (mitochondria lacking outer membranes), *in vitro* import assays, or immunogold labelling would all be useful in providing a clearer understanding as to the localization of UL12.5.

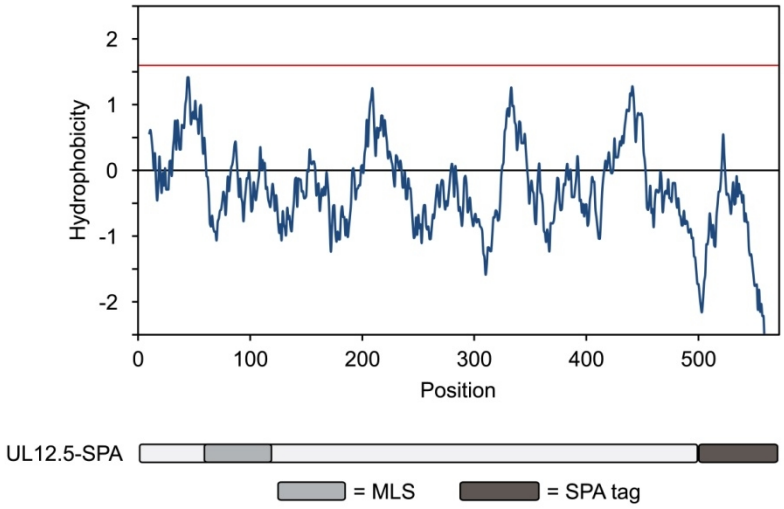

Figure 7.1. Hydropathy plot of UL12.5-SPA. A hydropathy plot of UL12.5-SPA using the Kyte and Doolittle scale was generated using ProtScale. The hydropathy window size used was 19 residues. Positive values are indicative of hydrophobic regions. The cut-off for transmembrane domains (≥1.6) is indicated with a red line (541). Amino acid position is indicated on the x-axis above a scaled schematic of the UL12.5-SPA protein.

Another aspect to consider in regards to the localization of UL12.5 is the role of both ENDOG and EXOG in UL12.5-mediated mtDNA depletion (Figs. 4.14 and 4.18). ENDOG has been shown to localize to the intermembrane space and perhaps associate with the mitochondrial inner membrane (328, 330, 542, 543). Similar results were also published regarding the localization of EXOG (484). However, these enzymes have also been implicated in the synthesis, recombination, or integrity of mtDNA (389, 390, 410, 544). ENDOG has even been found to be associated with mtDNA (390). For these two enzymes to be involved in these processes one would expect at least a fraction of the total pool of these proteins to localize to the mitochondrial matrix. In the same vein, for UL12.5 to manipulate mtDNA levels during infection it is plausible that this protein also is in close proximity to mtDNA. Such proximity would allow UL12.5 to either introduce the initial lesion in mtDNA prior to degradation by cellular nucleases or to associate with mtDNA and act as a scaffold to recruit cellular nucleases. The possibility also exists that UL12.5 redirects cellular nucleases such as ENDOG and EXOG from the intermembrane space to the mitochondrial matrix, and that it is the dysregulated localization of these proteins that leads to mtDNA degradation. A thorough investigation of the localization of ENDOG and EXOG following UL12.5 expression may further elucidate the steps leading up to the loss of mtDNA mediated by UL12.5.

7.1.3 – On the origin of endonuclease activity associated with some UL12.5 mutants and the participation of cellular nucleases in mtDNA depletion

I have been unable to demonstrate a specific association between UL12.5-SPA and endogenous ENDOG or EXOG by co-immunoprecipitation (Fig. 5.5). Therefore, I cannot say with certainty that the endonuclease activity observed in the IP nuclease assays is due to ENDOG or EXOG (Figs. 4.9C and F). While possible that UL12.5 associates with these endogenous nucleases transiently or weakly, my preliminary observations of immunoprecipitates obtained from cells exposed to the chemical cross-linker DSP would not support this hypothesis (Fig. 5.5). My additional experiments using an overexpression system to study the binding partners of UL12.5, while demonstrating some unexpected results (Figs. 5.2, 5.3, and 5.4), also did not conclusively support the presence of a physiologically relevant association between UL12.5, ENDOG, or EXOG. Therefore, the source of the associated endonuclease activity observed in Fig. 4.9 remains elusive. As mentioned earlier, the recently identified exo/endonuclease Ddk1 was not initially considered as a candidate for this activity. Ddk1 was not observed to have endonuclease activity against circular DNA substrates; instead, Ddk1 only endonucleolytically attacks double-stranded DNA with free ends (502). Therefore, it is unlikely that this enzyme is the source of the unidentified activity.

My data have demonstrated a clear and reproducible role of ENDOG and EXOG in UL12.5-mediated mtDNA depletion (Figs. 4.14 and 4.18). In the absence of a direct association with these proteins, the possibility exists that

UL12.5 may indirectly enhance the nuclease activity of ENDOG and EXOG against mtDNA. Consistent with this idea, ENDOG activity has been shown to be augmented *in vitro* due to the presence of proteins such as DNase I, exonuclease III, or heat shock protein 70 (507, 545). While these studies focus on the role of ENDOG in nuclear DNA fragmentation during apoptosis (328, 511), it is possible that while ENDOG resides within mitochondria that the presence of UL12.5 may similarly stimulate ENDOG nuclease activity resulting in mtDNA degradation. Moreover, the enhanced ability of ENDOG to degrade oxidatively damaged DNA *in vitro* supports a role for this abundant nuclease in removing extensively damaged mtDNA *in vivo* (546); a potential function that may be affected by UL12.5. Studies using purified forms of ENDOG and UL12.5 would be useful in examining if UL12.5 is capable of modulating ENDOG activity.

Recent studies on ENDOG and EXOG have proposed that these enzymes have an important role in mtDNA maintenance and repair (390, 410, 514, 515). In one particularly elegant study, ENDOG was demonstrated to be the enzyme responsible for depleting *Drosophila melanogaster* mtDNA from developing sperm which in turn promotes the maternal inheritance of mtDNA (514). This work provides a clear example of the influence of ENDOG on mtDNA maintenance. Mitochondria also contain DNA repair pathways similar to those found in the nucleus which defend against genotoxic insults and oxidative damage (547). UL12 interacts with components of the host nuclear DNA repair MRN complex (466); therefore, it would be interesting to investigate if UL12.5 directly

interacts with one or more mtDNA repair proteins other than ENDOG and EXOG.

HSV infection also leads to rapid loss of mitochondrial mRNAs (mt-mRNAs) (152, 447), a process that is at least as rapid as mtDNA loss and depends on UL12 gene products (152). Although UL12 orthologs EBV BGLF5 and KSHV SOX have been shown to mediate cytoplasmic mRNA turnover (293, 294), HSV-1 UL12 does not appear to possess this activity (293). It is interesting to note that ENDOG and EXOG both possess low levels of RNase activity (483, 484). Indeed, earlier work on ENDOG had suggested that its RNase activity generates the RNA primers for mtDNA replication (389). Thus, it is possible that ENDOG and or EXOG directly degrade mt-mRNAs during HSV infection. Further studies are required to test this possibility.

7.1.4 – Is mtDNA depletion a conserved feature of herpesvirus infections?

Our previous data demonstrated that infection with either HSV-1 or HSV-2 leads to a rapid and complete loss of mtDNA; however, the viral protein responsible for this effect in HSV-2 infected cells was not known (152). We demonstrate here that HSV-2 UL12 and $UL12_{M117}$ exhibit mtDNA depleting activity (Fig. 6.4C) similar to HSV-1 UL12 and UL12.5 (Figs. 4.6 and 4.7 and reference 475). We consider it likely that the activity of the full-length HSV-2 UL12 construct stems at least in part from the production of $UL12_{M117}$ from its internal promoter, as observed with an HSV-1 UL12 expression vector (Figs. 4.1B, 4.3, and 4.4). These data are strikingly similar to those which documented the involvement of UL12.5 in mtDNA depletion during HSV-1 infection (152,

475). Indeed, the HSV-2 *UL12* locus gives rise to a 1.9 kbp transcript with the potential to encode the $UL12_{M117}$ protein during infection (42). Due to the high degree of sequence conservation between HSV-1 and HSV-2, we propose that the HSV-2 $UL12_{M117}$ protein is responsible for mtDNA loss during HSV-2 infection (152), and suggest that it be designated UL12.5. Additional experiments are needed to confirm that UL12.5 is in fact produced during HSV-2 infection.

In contrast to HSV-1 and HSV-2, expression plasmids encoding full-length versions of the UL12 orthologs from VZV, HCMV, EBV, and KSHV are unable to cause mtDNA loss in transfected cells (Fig. 6.4C). Moreover, HMCV UL98 fails to deplete mtDNA when it is expressed from the HSV-1 genome during HSV-1 infection (Fig. 6.11). It is therefore possible that none of these *UL12* orthologs produce a mitochondrially targeted isoform analogous to HSV-1 and HSV-2 UL12.5, at least in our transfection assay. It would be interesting to determine if any of these viruses produce such an isoform during productive infection. Interestingly, when the ORF48 protein from VZV was targeted to mitochondria it resulted in the loss of mtDNA from a subset of transfected cells (Fig. 6.4C). The loss of mtDNA from MLS-ORF48-SPA expressing cells was low compared to UL12.5-SPA and could reflect either the poor expression level of this construct (Fig. 6.4A) or the inefficiency with which ORF48 mediates mtDNA loss. In either case, this observation supports the conclusion that mtDNA depletion is a conserved function among human alphaherpesvirus UL12 orthologs since ORF48 contains the appropriate features to cause this effect when targeted to mitochondria. It will be interesting to examine the relevance of any common

sequence motifs or functions that may be shared between HSV-1 UL12, HSV-2 UL12, and VZV ORF48.

It is important to note that mtDNA depletion by HSV-1 UL12.5 does not require UL12.5 nuclease activity but involves the cellular mitochondrial nucleases ENDOG and EXOG (see Chapter 4). Therefore, even nuclease-deficient truncated isoforms may be sufficient to cause mtDNA depletion provided they are localized to mitochondria. Experiments further exploring the involvement of UL12 orthologs in mtDNA depletion would be especially informative for EBV because, as noted above, EBV depletes mtDNA during lytic infection; as well, Wiedmer *et al*. noted that the Zta protein is not sufficient for this effect in transfected cells suggesting that other viral proteins may be involved (448). Taken in combination, the experiments outlined above will indicate how wide-spread mtDNA depletion is among human herpesviruses, and will clarify the potential role of UL12 orthologs in this process for viruses other than HSV-1 and HSV-2.

7.1.5 – MtDNA depletion is not required for HSV-1 replication in cell culture

Finally, our data demonstrate that HCMV UL98 is able to efficiently substitute for HSV-1 UL12 during HSV-1 replication. Gao *et al*. have previously shown that UL98 can complement the growth defect of an HSV-1 UL12-null mutant (521); however, the efficiency of such complementation compared to HSV-1 UL12 was not determined. Our results confirm their observations and further demonstrate that UL98 supports the replication of UL12-null HSV-1 to essentially wild-type levels, albeit with a detectable delay at early times (Fig. 6.9). These data suggest that UL98 is able to interface with the HSV replication system

almost as effectively as does HSV-1 UL12. UL12 forms a complex with the HSV-1 single stranded DNA binding protein ICP8 (196) and binds the host MRN complex (466). It will therefore be interesting to determine if UL98 forms similar and functional complexes during infection with the UL98 virus.

These results also indicate that mtDNA depletion is not required for efficient HSV-1 replication in cultured Vero cells. MtDNA depletion was severely impaired in cells infected with the UL98 virus (Fig. 6.11) and although a small decrease in mtDNA levels was observed at late times post-infection in some experiments, the difference was not statistically significant over repeated trials (Fig. 6.11). Our subsequent experiments using PAA treatment provided no support for the involvement of late viral proteins in facilitating mtDNA depletion either (Fig. 6.12). Therefore, we must conclude from our data that there is no late decline of mtDNA levels in the absence of UL12/UL12.5 expression. These data further support the view that mtDNA depletion is solely influenced by the presence of products of the *UL12* gene. Since the UL98 virus produced levels of progeny virus similar to those obtained with the control viruses (KOS37 and SPA) as measured using single-step and multi-step growth curves (Fig. 6.9), we can state with confidence that elimination of mtDNA is not required for HSV-1 replication.

7.1.6 – Where does mtDNA depletion fit in the pathogenesis of HSV-1 infection?

It is still unclear what benefit the loss of mtDNA serves during HSV-1 infection. The data presented here reveal that the nuclease activity of UL12.5 is dispensable for mtDNA depletion. Interestingly, a recent study came to a similar

conclusion while investigating the role of HSV-1 UL12 nuclease activity in viral replication (548). A previous report demonstrated that expression of nuclease-deficient UL12-G336A/S338A could not rescue the growth defect of a UL12-null mutant virus in a transient complementation assay (44). However, more recent data has shown that when the G336A/S338A mutations are introduced into the viral *UL12* gene within the HSV-1 genome that this mutant virus (YK665) is capable of replicating to near wild-type titres (548). These recent results demonstrate that the nuclease activities of UL12 are not required for viral replication in cell culture, much the same as the data presented above demonstrate that UL12.5 nuclease activities are not required for efficient viral replication in cell culture (Fig. 6.9). Our observation that mtDNA depletion has little impact on virus replication in Vero cells suggests that it may serve a cell type-specific role or have a more obvious function in the intact host. When survival of mice inoculated intracerebrally with the UL12-G336A/S338A-expressing mutant virus was examined, this mutant virus was observed to be 100-fold less virulent than wild-type virus (548). Therefore, it is interesting to speculate that our UL98-expressing mutant virus may also have a different phenotype in an animal model.

The results by Fujii *et al*. (548) raise some interesting questions. Is mtDNA present or absent in YK665 infected cells? Is the lack of UL12 nuclease activity the main contributor to the reduction of virulence *in vivo*, or are other ill-defined functions of UL12 important? Based on my data, I would hypothesize that YK665 infected cells would contain a reduced amount of mtDNA compared to mock infected cells since UL12.5-G336A/S338A was still capable, although

much less efficient, at mediating mtDNA depletion compared to wild-type UL12.5 (Figs. 4.6 and 4.8). However, I do not predict that mtDNA will be eliminated during infection with YK665 in the same manner as infection with wild-type virus. Alternatively, the possibility exists that *in vivo* expression or regulation of UL12.5-G336A/S338A during infection may differ from transient overexpression in a manner that results in enhanced mtDNA depletion efficiency. Future experiments will be needed to distinguish between these two possibilities. It is interesting that in the case of many mtDNA mutations associated with mitochondrial disease there is often a threshold of damage to mtDNA required prior to cause phenotypic, translational, or biochemical changes (549). While this threshold of mtDNA damage is likely exceeded during wild-type virus infection, it will be important to consider that such a threshold may also be relevant when examining phenotypes of HSV-1 mutant viruses that demonstrate less-than-wild-type levels of mtDNA depletion.

It is clear from experiments with cells lacking mtDNA (rho^0) due to long-term ethidium bromide exposure that the absence of mtDNA ultimately compromises oxidative phosphorylation (469). Therefore, loss of oxidative phosphorylation in HSV-infected cells due to mtDNA depletion likely occurs at late times post-infection. Consistent with this view, Murata *et al*. demonstrated that HSV-1 and HSV-2 cause a decline in ATP production beginning around twelve hours post-infection (356), after the viral replication cycle is largely complete. However, alterations in ATP production during HSV infection appear to be cell-type dependent (356, 360). Thus, it seems unlikely that inhibition of

oxidative phosphorylation plays a major role during productive infection. Recent work by Kramer and Enquist demonstrated that mitochondrial motility in neurons is inhibited by pseudorabies virus and HSV-1 (369). Furthermore, this alteration in mitochondrial dynamics significantly enhanced pseudorabies virus pathogenesis (369). However, the viral protein(s) required for the disruption of mitochondrial motility have yet to be identified. It will therefore be interesting to determine if UL12.5 plays a role in HSV-induced inhibition of ATP production and/or mitochondrial motility, or instead alters other mitochondrial properties such as mitochondrial membrane potential, ROS production, calcium homeostasis, or the regulation of apoptosis, innate immune responses, or mitochondrial signalling pathways. In addition, it will be important to examine how HSV-1 UL12.5 alters mitochondrial biology in a variety of cell types, including cells which undergo non-productive infection and therefore have the potential of surviving the initial infection. The UL98 virus described here will be useful for such studies in cell culture as well as for determining whether UL12.5 affects HSV-1 pathogenesis and/or latency in animal models.

7.2 – Concluding remarks and outstanding questions

During my research on mtDNA depletion mediated by HSV-1 UL12.5 I have made significant contributions to our overall understanding of this unique aspect of herpesvirus biology. Consistent with the growing literature on mtDNA regulation, my work also highlights the complexity of mtDNA depletion by UL12.5.

My initial work aided in defining the N-proximal sequence utilized by UL12.5 to target mitochondria. This work has cemented the role of UL12.5 as a mitochondrial protein; however, many questions still remain to be answered regarding the ultimate localization of UL12.5 and the effect this has on UL12.5 function. For instance, is UL12.5 in the mitochondrial matrix? Moreover, does UL12.5 associate with mtDNA? It will be interesting to explore the possibility that UL12.5 may act as a scaffold for the recruitment of cellular nucleases leading to the eventual destruction of mtDNA. This view is consistent with my data which clearly demonstrates that UL12.5 nuclease activity is not required for mtDNA depletion and that the cellular nucleases ENDOG and EXOG facilitate mtDNA loss in transfected cells. My proteinase K protection assay data, while not fully supportive of this hypothesis, does not exclude this possibility since a subset of full-length UL12.5 was protected from protease treatment. It would also need to be determined whether the nuclease-inactivating mutations employed in my work in any way affect DNA binding of UL12 or UL12.5. Altogether, these experiments highlight a newly appreciated complexity of the process of UL12.5-mediated mtDNA depletion.

Every experiment and question asked during my tenure has also been directed at ultimately understanding the relevance of mtDNA depletion to HSV-1 pathogenesis. While this has not yet been elucidated, I have made some substantial progress towards addressing this important question in HSV-1 biology. I was successful in generating an HSV-1 mutant virus that was significantly impaired in its ability to cause mtDNA depletion in cell culture. This work

eventually led to the discovery that the loss of mtDNA in Vero cells did not affect HSV-1 replication. This mutant virus will now make it possible to investigate the role of mtDNA depletion during infection in various cell lines or animal models. The observation that a viral protein is not required for viral replication in cell culture but does have a role in the intact host is not uncommon in HSV-1 research. Examples include HSV-1 mutants null for the vhs protein (550), ICP34.5 (551), VP26 (552), and the viral uracil DNA glycosylase (553). It will be interesting to observe the phenotype of the KOS37 UL98 virus *in vivo* and to determine whether mtDNA depletion contributes to the pathogenesis of HSV-1.

MtDNA has a central role in ensuring proper mitochondrial function and mtDNA loss is observed in a variety of inherited diseases (425, 554) and has been associated with human degenerative diseases such as cancer (431, 440, 442, 555-562) and Alzheimer's (563, 564). While it remains unclear if mtDNA depletion is a cause or consequence of these conditions, the association between the loss of mtDNA and human pathologies highlights the importance of mtDNA maintenance in humans. The prevalence of HSV-1 in the population, the neurotropism of this virus, and its ability to cause mtDNA depletion certainly raises the question whether HSV-1 and mtDNA loss contribute to the development or progression of human neurodegenerative diseases. In support of this possibility, some groups have proposed an association between HSV-1 infection and Alzheimer's disease (565, 566). While intriguing, the majority of these data are correlative and further investigation is warranted. Moreover, it is unclear if mtDNA depletion occurs *in vivo*, if mtDNA depletion occurs in latently

infected cells, and if latently infected cells lacking mtDNA survive. While one can only speculate as to the significance of HSV-1 infection in neurodegenerative diseases, it is certainly an intriguing proposition worthy of future study.

In conclusion, my research has enhanced our understanding of the molecular mechanisms underlying mtDNA depletion mediated by UL12.5. Moreover, this work supports a view that UL12.5 interfaces with cellular factors involved in mtDNA maintenance in order to redirect mitochondrial proteins to destroy mtDNA during infection. My findings will contribute to a more comprehensive understanding of HSV-1 biology. Furthermore, future studies into the molecular basis of UL12.5-mediated mtDNA loss may contribute to a greater understanding of the cellular regulation of mtDNA.

Bibliography

1. **Davison AJ, Eberle R, Ehlers B, Hayward GS, McGeoch DJ, Minson AC, Pellett PE, Roizman B, Studdert MJ, Thiry E.** 2009. The order Herpesvirales. Arch Virol **154:**171-177.
2. **Pellett PE, Roizman B.** 2013. Chapter 59: Herpesviridae, p. 1802-1819. *In* Knipe DM, Howley PM (ed.), Fields Virology, vol. 2. Lippincott Williams & Wilkins, Philadelphia, USA.
3. **Baringer JR.** 2008. Herpes simplex infections of the nervous system. Neurol Clin **26:**657-674, viii.
4. **Cohen JI.** 2013. Clinical practice: Herpes zoster. N Engl J Med **369:**255-263.
5. **Adams MJ, Carstens EB.** 2012. Ratification vote on taxonomic proposals to the International Committee on Taxonomy of Viruses (2012). Arch Virol **157:**1411-1422.
6. **Ablashi D, Agut H, Alvarez-Lafuente R, Clark DA, Dewhurst S, Diluca D, Flamand L, Frenkel N, Gallo R, Gompels UA, Hollsberg P, Jacobson S, Luppi M, Lusso P, Malnati M, Medveczky P, Mori Y, Pellett PE, Pritchett JC, Yamanishi K, Yoshikawa T.** 2013. Classification of HHV-6A and HHV-6B as distinct viruses. Arch Virol.
7. **Yamanishi K, Okuno T, Shiraki K, Takahashi M, Kondo T, Asano Y, Kurata T.** 1988. Identification of human herpesvirus-6 as a causal agent for exanthem subitum. Lancet **1:**1065-1067.
8. **Luppi M, Barozzi P, Marasca R, Torelli G.** 1994. Integration of human herpesvirus-6 (HHV-6) genome in chromosome 17 in two lymphoma patients. Leukemia **8 Suppl 1:**S41-45.
9. **Morissette G, Flamand L.** 2010. Herpesviruses and chromosomal integration. J Virol **84:**12100-12109.
10. **Ward KN.** 2005. Human herpesviruses-6 and -7 infections. Curr Opin Infect Dis **18:**247-252.
11. **Pattle SB, Farrell PJ.** 2006. The role of Epstein-Barr virus in cancer. Expert Opin Biol Ther **6:**1193-1205.
12. **Chang Y, Cesarman E, Pessin MS, Lee F, Culpepper J, Knowles DM, Moore PS.** 1994. Identification of herpesvirus-like DNA sequences in AIDS-associated Kaposi's sarcoma. Science **266:**1865-1869.
13. **Lieberman PM.** 2013. Keeping it quiet: chromatin control of gammaherpesvirus latency. Nat Rev Microbiol **11:**863-875.
14. **Grunewald K, Desai P, Winkler DC, Heymann JB, Belnap DM, Baumeister W, Steven AC.** 2003. Three-dimensional structure of herpes simplex virus from cryo-electron tomography. Science **302:**1396-1398.
15. **Kieff ED, Bachenheimer SL, Roizman B.** 1971. Size, composition, and structure of the deoxyribonucleic acid of herpes simplex virus subtypes 1 and 2. J Virol **8:**125-132.
16. **McGeoch DJ, Dolan A, Donald S, Rixon FJ.** 1985. Sequence determination and genetic content of the short unique region in the genome of herpes simplex virus type 1. J Mol Biol **181:**1-13.

17. **McGeoch DJ, Dolan A, Donald S, Brauer DH.** 1986. Complete DNA sequence of the short repeat region in the genome of herpes simplex virus type 1. Nucleic Acids Res **14:**1727-1745.
18. **McGeoch DJ, Dalrymple MA, Davison AJ, Dolan A, Frame MC, McNab D, Perry LJ, Scott JE, Taylor P.** 1988. The complete DNA sequence of the long unique region in the genome of herpes simplex virus type 1. J Gen Virol **69 (Pt 7):**1531-1574.
19. **Perry LJ, McGeoch DJ.** 1988. The DNA sequences of the long repeat region and adjoining parts of the long unique region in the genome of herpes simplex virus type 1. J Gen Virol **69 (Pt 11):**2831-2846.
20. **Dolan A, McKie E, MacLean AR, McGeoch DJ.** 1992. Status of the ICP34.5 gene in herpes simplex virus type 1 strain 17. J Gen Virol **73 (Pt 4):**971-973.
21. **Szpara ML, Parsons L, Enquist LW.** 2010. Sequence variability in clinical and laboratory isolates of herpes simplex virus 1 reveals new mutations. J Virol **84:**5303-5313.
22. **Macdonald SJ, Mostafa HH, Morrison LA, Davido DJ.** 2012. Genome sequence of herpes simplex virus 1 strain KOS. J Virol **86:**6371-6372.
23. **Dolan A, Jamieson FE, Cunningham C, Barnett BC, McGeoch DJ.** 1998. The genome sequence of herpes simplex virus type 2. J Virol **72:**2010-2021.
24. **Colgrove R, Diaz F, Newman R, Saif S, Shea T, Young S, Henn M, Knipe DM.** 2014. Genomic sequences of a low passage herpes simplex virus 2 clinical isolate and its plaque-purified derivative strain. Virology **450-451:**140-145.
25. **Wadsworth S, Jacob RJ, Roizman B.** 1975. Anatomy of herpes simplex virus DNA. II. Size, composition, and arrangement of inverted terminal repetitions. J Virol **15:**1487-1497.
26. **Wagner MJ, Summers WC.** 1978. Structure of the joint region and the termini of the DNA of herpes simplex virus type 1. J Virol **27:**374-387.
27. **Locker H, Frenkel N.** 1979. BamI, KpnI, and SalI restriction enzyme maps of the DNAs of herpes simplex virus strains Justin and F: occurrence of heterogeneities in defined regions of the viral DNA. J Virol **32:**429-441.
28. **Dutch RE, Bruckner RC, Mocarski ES, Lehman IR.** 1992. Herpes simplex virus type 1 recombination: role of DNA replication and viral a sequences. J Virol **66:**277-285.
29. **Hayward GS, Jacob RJ, Wadsworth SC, Roizman B.** 1975. Anatomy of herpes simplex virus DNA: evidence for four populations of molecules that differ in the relative orientations of their long and short components. Proc Natl Acad Sci U S A **72:**4243-4247.
30. **Delius H, Clements JB.** 1976. A partial denaturation map of herpes simplex virus type 1 DNA: evidence for inversions of the unique DNA regions. J Gen Virol **33:**125-133.

31. **Dutch RE, Bianchi V, Lehman IR.** 1995. Herpes simplex virus type 1 DNA replication is specifically required for high-frequency homologous recombination between repeated sequences. J Virol **69:**3084-3089.
32. **Mocarski ES, Roizman B.** 1982. Structure and role of the herpes simplex virus DNA termini in inversion, circularization and generation of virion DNA. Cell **31:**89-97.
33. **Stow ND, McMonagle EC, Davison AJ.** 1983. Fragments from both termini of the herpes simplex virus type 1 genome contain signals required for the encapsidation of viral DNA. Nucleic Acids Res **11:**8205-8220.
34. **Spaete RR, Frenkel N.** 1985. The herpes simplex virus amplicon: analyses of cis-acting replication functions. Proc Natl Acad Sci U S A **82:**694-698.
35. **Varmuza SL, Smiley JR.** 1985. Signals for site-specific cleavage of HSV DNA: maturation involves two separate cleavage events at sites distal to the recognition sequences. Cell **41:**793-802.
36. **Friedmann A, Shlomai J, Becker Y.** 1977. Electron microscopy of herpes simplex virus DNA molecules isolated from infected cells by centrifugation in CsCl density gradients. J Gen Virol **34:**507-522.
37. **Stow ND.** 1982. Localization of an origin of DNA replication within the TRS/IRS repeated region of the herpes simplex virus type 1 genome. Embo J **1:**863-867.
38. **Murchie MJ, McGeoch DJ.** 1982. DNA sequence analysis of an immediate-early gene region of the herpes simplex virus type 1 genome (map coordinates 0.950 to 0.978). J Gen Virol **62 (Pt 1):**1-15.
39. **Weller SK, Spadaro A, Schaffer JE, Murray AW, Maxam AM, Schaffer PA.** 1985. Cloning, sequencing, and functional analysis of oriL, a herpes simplex virus type 1 origin of DNA synthesis. Mol Cell Biol **5:**930-942.
40. **Roizman B, Knipe DM, Whitley RJ.** 2013. Chapter 60: Herpes Simplex Viruses, p. 1823–1892. *In* Knipe DM, Howley PM (ed.), Fields Virology, vol. 2. Lippincott Williams & Wilkins, Philadelphia, USA.
41. **Costa RH, Draper KG, Banks L, Powell KL, Cohen G, Eisenberg R, Wagner EK.** 1983. High-resolution characterization of herpes simplex virus type 1 transcripts encoding alkaline exonuclease and a 50,000-dalton protein tentatively identified as a capsid protein. J Virol **48:**591-603.
42. **Draper KG, Devi-Rao G, Costa RH, Blair ED, Thompson RL, Wagner EK.** 1986. Characterization of the genes encoding herpes simplex virus type 1 and type 2 alkaline exonucleases and overlapping proteins. J Virol **57:**1023-1036.
43. **Martinez R, Shao L, Bronstein JC, Weber PC, Weller SK.** 1996. The product of a 1.9-kb mRNA which overlaps the HSV-1 alkaline nuclease gene (UL12) cannot relieve the growth defects of a null mutant. Virology **215:**152-164.
44. **Goldstein JN, Weller SK.** 1998. The exonuclease activity of HSV-1 UL12 is required for in vivo function. Virology **244:**442-457.

45. **Gibson W, Roizman B.** 1972. Proteins specified by herpes simplex virus. 8. Characterization and composition of multiple capsid forms of subtypes 1 and 2. J Virol **10:**1044-1052.
46. **Newcomb WW, Juhas RM, Thomsen DR, Homa FL, Burch AD, Weller SK, Brown JC.** 2001. The UL6 gene product forms the portal for entry of DNA into the herpes simplex virus capsid. J Virol **75:**10923-10932.
47. **Desai P, Watkins SC, Person S.** 1994. The size and symmetry of B capsids of herpes simplex virus type 1 are determined by the gene products of the UL26 open reading frame. J Virol **68:**5365-5374.
48. **Preston VG, al-Kobaisi MF, McDougall IM, Rixon FJ.** 1994. The herpes simplex virus gene UL26 proteinase in the presence of the UL26.5 gene product promotes the formation of scaffold-like structures. J Gen Virol **75 (Pt 9):**2355-2366.
49. **Newcomb WW, Booy FP, Brown JC.** 2007. Uncoating the herpes simplex virus genome. J Mol Biol **370:**633-642.
50. **Beard PM, Taus NS, Baines JD.** 2002. DNA cleavage and packaging proteins encoded by genes U(L)28, U(L)15, and U(L)33 of herpes simplex virus type 1 form a complex in infected cells. J Virol **76:**4785-4791.
51. **Cockrell SK, Huffman JB, Toropova K, Conway JF, Homa FL.** 2011. Residues of the UL25 protein of herpes simplex virus that are required for its stable interaction with capsids. J Virol **85:**4875-4887.
52. **Loomis JS, Bowzard JB, Courtney RJ, Wills JW.** 2001. Intracellular trafficking of the UL11 tegument protein of herpes simplex virus type 1. J Virol **75:**12209-12219.
53. **Brignati MJ, Loomis JS, Wills JW, Courtney RJ.** 2003. Membrane association of VP22, a herpes simplex virus type 1 tegument protein. J Virol **77:**4888-4898.
54. **Naldinho-Souto R, Browne H, Minson T.** 2006. Herpes simplex virus tegument protein VP16 is a component of primary enveloped virions. J Virol **80:**2582-2584.
55. **Read GS, Patterson M.** 2007. Packaging of the virion host shutoff (Vhs) protein of herpes simplex virus: two forms of the Vhs polypeptide are associated with intranuclear B and C capsids, but only one is associated with enveloped virions. J Virol **81:**1148-1161.
56. **Meckes DG, Jr., Wills JW.** 2007. Dynamic interactions of the UL16 tegument protein with the capsid of herpes simplex virus. J Virol **81:**13028-13036.
57. **Desai P, Sexton GL, Huang E, Person S.** 2008. Localization of herpes simplex virus type 1 UL37 in the Golgi complex requires UL36 but not capsid structures. J Virol **82:**11354-11361.
58. **Padula ME, Sydnor ML, Wilson DW.** 2009. Isolation and preliminary characterization of herpes simplex virus 1 primary enveloped virions from the perinuclear space. J Virol **83:**4757-4765.

59. **Loret S, Lippe R.** 2012. Biochemical analysis of infected cell polypeptide (ICP)0, ICP4, UL7 and UL23 incorporated into extracellular herpes simplex virus type 1 virions. J Gen Virol **93:**624-634.
60. **Henaff D, Remillard-Labrosse G, Loret S, Lippe R.** 2013. Analysis of the early steps of herpes simplex virus 1 capsid tegumentation. J Virol **87:**4895-4906.
61. **Heine JW, Honess RW, Cassai E, Roizman B.** 1974. Proteins specified by herpes simplex virus. XII. The virion polypeptides of type 1 strains. J Virol **14:**640-651.
62. **Loret S, Guay G, Lippe R.** 2008. Comprehensive characterization of extracellular herpes simplex virus type 1 virions. J Virol **82:**8605-8618.
63. **Luxton GW, Haverlock S, Coller KE, Antinone SE, Pincetic A, Smith GA.** 2005. Targeting of herpesvirus capsid transport in axons is coupled to association with specific sets of tegument proteins. Proc Natl Acad Sci U S A **102:**5832-5837.
64. **Wolfstein A, Nagel CH, Radtke K, Dohner K, Allan VJ, Sodeik B.** 2006. The inner tegument promotes herpes simplex virus capsid motility along microtubules in vitro. Traffic **7:**227-237.
65. **Maurer UE, Sodeik B, Grunewald K.** 2008. Native 3D intermediates of membrane fusion in herpes simplex virus 1 entry. Proc Natl Acad Sci U S A **105:**10559-10564.
66. **Kelly BJ, Fraefel C, Cunningham AL, Diefenbach RJ.** 2009. Functional roles of the tegument proteins of herpes simplex virus type 1. Virus Res **145:**173-186.
67. **Vittone V, Diefenbach E, Triffett D, Douglas MW, Cunningham AL, Diefenbach RJ.** 2005. Determination of interactions between tegument proteins of herpes simplex virus type 1. J Virol **79:**9566-9571.
68. **Newcomb WW, Brown JC.** 2010. Structure and capsid association of the herpesvirus large tegument protein UL36. J Virol **84:**9408-9414.
69. **Zhu Q, Courtney RJ.** 1994. Chemical cross-linking of virion envelope and tegument proteins of herpes simplex virus type 1. Virology **204:**590-599.
70. **Gross ST, Harley CA, Wilson DW.** 2003. The cytoplasmic tail of Herpes simplex virus glycoprotein H binds to the tegument protein VP16 in vitro and in vivo. Virology **317:**1-12.
71. **Chi JH, Harley CA, Mukhopadhyay A, Wilson DW.** 2005. The cytoplasmic tail of herpes simplex virus envelope glycoprotein D binds to the tegument protein VP22 and to capsids. J Gen Virol **86:**253-261.
72. **Newcomb WW, Brown JC.** 2009. Time-dependent transformation of the herpesvirus tegument. J Virol **83:**8082-8089.
73. **van Genderen IL, Brandimarti R, Torrisi MR, Campadelli G, van Meer G.** 1994. The phospholipid composition of extracellular herpes simplex virions differs from that of host cell nuclei. Virology **200:**831-836.

74. **Honess RW, Roizman B.** 1974. Regulation of herpesvirus macromolecular synthesis. I. Cascade regulation of the synthesis of three groups of viral proteins. J Virol **14:**8-19.
75. **Banfield BW, Leduc Y, Esford L, Visalli RJ, Brandt CR, Tufaro F.** 1995. Evidence for an interaction of herpes simplex virus with chondroitin sulfate proteoglycans during infection. Virology **208:**531-539.
76. **Herold BC, WuDunn D, Soltys N, Spear PG.** 1991. Glycoprotein C of herpes simplex virus type 1 plays a principal role in the adsorption of virus to cells and in infectivity. J Virol **65:**1090-1098.
77. **Spear PG, Shieh MT, Herold BC, WuDunn D, Koshy TI.** 1992. Heparan sulfate glycosaminoglycans as primary cell surface receptors for herpes simplex virus. Adv Exp Med Biol **313:**341-353.
78. **Shieh MT, WuDunn D, Montgomery RI, Esko JD, Spear PG.** 1992. Cell surface receptors for herpes simplex virus are heparan sulfate proteoglycans. J Cell Biol **116:**1273-1281.
79. **WuDunn D, Spear PG.** 1989. Initial interaction of herpes simplex virus with cells is binding to heparan sulfate. J Virol **63:**52-58.
80. **Gruenheid S, Gatzke L, Meadows H, Tufaro F.** 1993. Herpes simplex virus infection and propagation in a mouse L cell mutant lacking heparan sulfate proteoglycans. J Virol **67:**93-100.
81. **Williams RK, Straus SE.** 1997. Specificity and affinity of binding of herpes simplex virus type 2 glycoprotein B to glycosaminoglycans. J Virol **71:**1375-1380.
82. **Oh MJ, Akhtar J, Desai P, Shukla D.** 2010. A role for heparan sulfate in viral surfing. Biochem Biophys Res Commun **391:**176-181.
83. **Montgomery RI, Warner MS, Lum BJ, Spear PG.** 1996. Herpes simplex virus-1 entry into cells mediated by a novel member of the TNF/NGF receptor family. Cell **87:**427-436.
84. **Whitbeck JC, Peng C, Lou H, Xu R, Willis SH, Ponce de Leon M, Peng T, Nicola AV, Montgomery RI, Warner MS, Soulika AM, Spruce LA, Moore WT, Lambris JD, Spear PG, Cohen GH, Eisenberg RJ.** 1997. Glycoprotein D of herpes simplex virus (HSV) binds directly to HVEM, a member of the tumor necrosis factor receptor superfamily and a mediator of HSV entry. J Virol **71:**6083-6093.
85. **Krummenacher C, Nicola AV, Whitbeck JC, Lou H, Hou W, Lambris JD, Geraghty RJ, Spear PG, Cohen GH, Eisenberg RJ.** 1998. Herpes simplex virus glycoprotein D can bind to poliovirus receptor-related protein 1 or herpesvirus entry mediator, two structurally unrelated mediators of virus entry. J Virol **72:**7064-7074.
86. **Geraghty RJ, Krummenacher C, Cohen GH, Eisenberg RJ, Spear PG.** 1998. Entry of alphaherpesviruses mediated by poliovirus receptor-related protein 1 and poliovirus receptor. Science **280:**1618-1620.
87. **Warner MS, Geraghty RJ, Martinez WM, Montgomery RI, Whitbeck JC, Xu R, Eisenberg RJ, Cohen GH, Spear PG.** 1998. A cell surface protein with herpesvirus entry activity (HveB) confers susceptibility to

infection by mutants of herpes simplex virus type 1, herpes simplex virus type 2, and pseudorabies virus. Virology **246:**179-189.

88. **Lopez M, Cocchi F, Menotti L, Avitabile E, Dubreuil P, Campadelli-Fiume G.** 2000. Nectin2alpha (PRR2alpha or HveB) and nectin2delta are low-efficiency mediators for entry of herpes simplex virus mutants carrying the Leu25Pro substitution in glycoprotein D. J Virol **74:**1267-1274.
89. **Shukla D, Liu J, Blaiklock P, Shworak NW, Bai X, Esko JD, Cohen GH, Eisenberg RJ, Rosenberg RD, Spear PG.** 1999. A novel role for 3-O-sulfated heparan sulfate in herpes simplex virus 1 entry. Cell **99:**13-22.
90. **Yoon M, Zago A, Shukla D, Spear PG.** 2003. Mutations in the N termini of herpes simplex virus type 1 and 2 gDs alter functional interactions with the entry/fusion receptors HVEM, nectin-2, and 3-O-sulfated heparan sulfate but not with nectin-1. J Virol **77:**9221-9231.
91. **Jackson JO, Longnecker R.** 2010. Reevaluating herpes simplex virus hemifusion. J Virol **84:**11814-11821.
92. **Carfi A, Willis SH, Whitbeck JC, Krummenacher C, Cohen GH, Eisenberg RJ, Wiley DC.** 2001. Herpes simplex virus glycoprotein D bound to the human receptor HveA. Mol Cell **8:**169-179.
93. **Di Giovine P, Settembre EC, Bhargava AK, Luftig MA, Lou H, Cohen GH, Eisenberg RJ, Krummenacher C, Carfi A.** 2011. Structure of herpes simplex virus glycoprotein D bound to the human receptor nectin-1. PLoS Pathog **7:**e1002277.
94. **Krummenacher C, Supekar VM, Whitbeck JC, Lazear E, Connolly SA, Eisenberg RJ, Cohen GH, Wiley DC, Carfi A.** 2005. Structure of unliganded HSV gD reveals a mechanism for receptor-mediated activation of virus entry. Embo J **24:**4144-4153.
95. **Zhang N, Yan J, Lu G, Guo Z, Fan Z, Wang J, Shi Y, Qi J, Gao GF.** 2011. Binding of herpes simplex virus glycoprotein D to nectin-1 exploits host cell adhesion. Nat Commun **2:**577.
96. **Heldwein EE, Lou H, Bender FC, Cohen GH, Eisenberg RJ, Harrison SC.** 2006. Crystal structure of glycoprotein B from herpes simplex virus 1. Science **313:**217-220.
97. **Subramanian RP, Geraghty RJ.** 2007. Herpes simplex virus type 1 mediates fusion through a hemifusion intermediate by sequential activity of glycoproteins D, H, L, and B. Proc Natl Acad Sci U S A **104:**2903-2908.
98. **Hannah BP, Cairns TM, Bender FC, Whitbeck JC, Lou H, Eisenberg RJ, Cohen GH.** 2009. Herpes simplex virus glycoprotein B associates with target membranes via its fusion loops. J Virol **83:**6825-6836.
99. **Atanasiu D, Saw WT, Cohen GH, Eisenberg RJ.** 2010. Cascade of events governing cell-cell fusion induced by herpes simplex virus glycoproteins gD, gH/gL, and gB. J Virol **84:**12292-12299.
100. **Baines JD, Jacob RJ, Simmerman L, Roizman B.** 1995. The herpes simplex virus 1 UL11 proteins are associated with cytoplasmic and

nuclear membranes and with nuclear bodies of infected cells. J Virol **69:**825-833.
101. **Kim IJ, Chouljenko VN, Walker JD, Kousoulas KG.** 2013. Herpes simplex virus 1 glycoprotein M and the membrane-associated protein UL11 are required for virus-induced cell fusion and efficient virus entry. J Virol **87:**8029-8037.
102. **Nicola AV, McEvoy AM, Straus SE.** 2003. Roles for endocytosis and low pH in herpes simplex virus entry into HeLa and Chinese hamster ovary cells. J Virol **77:**5324-5332.
103. **Gianni T, Campadelli-Fiume G, Menotti L.** 2004. Entry of herpes simplex virus mediated by chimeric forms of nectin1 retargeted to endosomes or to lipid rafts occurs through acidic endosomes. J Virol **78:**12268-12276.
104. **Clement C, Tiwari V, Scanlan PM, Valyi-Nagy T, Yue BY, Shukla D.** 2006. A novel role for phagocytosis-like uptake in herpes simplex virus entry. J Cell Biol **174:**1009-1021.
105. **Sodeik B, Ebersold MW, Helenius A.** 1997. Microtubule-mediated transport of incoming herpes simplex virus 1 capsids to the nucleus. J Cell Biol **136:**1007-1021.
106. **Mabit H, Nakano MY, Prank U, Saam B, Dohner K, Sodeik B, Greber UF.** 2002. Intact microtubules support adenovirus and herpes simplex virus infections. J Virol **76:**9962-9971.
107. **Dohner K, Wolfstein A, Prank U, Echeverri C, Dujardin D, Vallee R, Sodeik B.** 2002. Function of dynein and dynactin in herpes simplex virus capsid transport. Mol Biol Cell **13:**2795-2809.
108. **Schipke J, Pohlmann A, Diestel R, Binz A, Rudolph K, Nagel CH, Bauerfeind R, Sodeik B.** 2012. The C terminus of the large tegument protein pUL36 contains multiple capsid binding sites that function differently during assembly and cell entry of herpes simplex virus. J Virol **86:**3682-3700.
109. **Abaitua F, Hollinshead M, Bolstad M, Crump CM, O'Hare P.** 2012. A Nuclear localization signal in herpesvirus protein VP1-2 is essential for infection via capsid routing to the nuclear pore. J Virol **86:**8998-9014.
110. **Ojala PM, Sodeik B, Ebersold MW, Kutay U, Helenius A.** 2000. Herpes simplex virus type 1 entry into host cells: reconstitution of capsid binding and uncoating at the nuclear pore complex in vitro. Mol Cell Biol **20:**4922-4931.
111. **Batterson W, Furlong D, Roizman B.** 1983. Molecular genetics of herpes simplex virus. VIII. further characterization of a temperature-sensitive mutant defective in release of viral DNA and in other stages of the viral reproductive cycle. J Virol **45:**397-407.
112. **Preston VG, Murray J, Preston CM, McDougall IM, Stow ND.** 2008. The UL25 gene product of herpes simplex virus type 1 is involved in uncoating of the viral genome. J Virol **82:**6654-6666.
113. **Pasdeloup D, Blondel D, Isidro AL, Rixon FJ.** 2009. Herpesvirus capsid association with the nuclear pore complex and viral DNA release involve

the nucleoporin CAN/Nup214 and the capsid protein pUL25. J Virol **83:**6610-6623.
114. **Copeland AM, Newcomb WW, Brown JC.** 2009. Herpes simplex virus replication: roles of viral proteins and nucleoporins in capsid-nucleus attachment. J Virol **83:**1660-1668.
115. **Coller KE, Lee JI, Ueda A, Smith GA.** 2007. The capsid and tegument of the alphaherpesviruses are linked by an interaction between the UL25 and VP1/2 proteins. J Virol **81:**11790-11797.
116. **Rode K, Dohner K, Binz A, Glass M, Strive T, Bauerfeind R, Sodeik B.** 2011. Uncoupling uncoating of herpes simplex virus genomes from their nuclear import and gene expression. J Virol **85:**4271-4283.
117. **Jovasevic V, Liang L, Roizman B.** 2008. Proteolytic cleavage of VP1-2 is required for release of herpes simplex virus 1 DNA into the nucleus. J Virol **82:**3311-3319.
118. **Poffenberger KL, Roizman B.** 1985. A noninverting genome of a viable herpes simplex virus 1: presence of head-to-tail linkages in packaged genomes and requirements for circularization after infection. J Virol **53:**587-595.
119. **Garber DA, Beverley SM, Coen DM.** 1993. Demonstration of circularization of herpes simplex virus DNA following infection using pulsed field gel electrophoresis. Virology **197:**459-462.
120. **Strang BL, Stow ND.** 2005. Circularization of the herpes simplex virus type 1 genome upon lytic infection. J Virol **79:**12487-12494.
121. **Lu X, Triezenberg SJ.** 2010. Chromatin assembly on herpes simplex virus genomes during lytic infection. Biochim Biophys Acta **1799:**217-222.
122. **Placek BJ, Berger SL.** 2010. Chromatin dynamics during herpes simplex virus-1 lytic infection. Biochim Biophys Acta **1799:**223-227.
123. **Meyring-Wosten A, Hafezi W, Kuhn J, Liashkovich I, Shahin V.** 2014. Nano-visualization of viral DNA breaching the nucleocytoplasmic barrier. J Control Release **173:**96-101.
124. **Jackson SA, DeLuca NA.** 2003. Relationship of herpes simplex virus genome configuration to productive and persistent infections. Proc Natl Acad Sci U S A **100:**7871-7876.
125. **Campbell ME, Palfreyman JW, Preston CM.** 1984. Identification of herpes simplex virus DNA sequences which encode a trans-acting polypeptide responsible for stimulation of immediate early transcription. J Mol Biol **180:**1-19.
126. **Gerster T, Roeder RG.** 1988. A herpesvirus trans-activating protein interacts with transcription factor OTF-1 and other cellular proteins. Proc Natl Acad Sci U S A **85:**6347-6351.
127. **Katan M, Haigh A, Verrijzer CP, van der Vliet PC, O'Hare P.** 1990. Characterization of a cellular factor which interacts functionally with Oct-1 in the assembly of a multicomponent transcription complex. Nucleic Acids Res **18:**6871-6880.

128. **Xiao P, Capone JP.** 1990. A cellular factor binds to the herpes simplex virus type 1 transactivator Vmw65 and is required for Vmw65-dependent protein-DNA complex assembly with Oct-1. Mol Cell Biol **10:**4974-4977.
129. **Herrera FJ, Triezenberg SJ.** 2004. VP16-dependent association of chromatin-modifying coactivators and underrepresentation of histones at immediate-early gene promoters during herpes simplex virus infection. J Virol **78:**9689-9696.
130. **Mackem S, Roizman B.** 1982. Structural features of the herpes simplex virus alpha gene 4, 0, and 27 promoter-regulatory sequences which confer alpha regulation on chimeric thymidine kinase genes. J Virol **44:**939-949.
131. **Cordingley MG, Campbell ME, Preston CM.** 1983. Functional analysis of a herpes simplex virus type 1 promoter: identification of far-upstream regulatory sequences. Nucleic Acids Res **11:**2347-2365.
132. **Kristie TM, Roizman B.** 1984. Separation of sequences defining basal expression from those conferring alpha gene recognition within the regulatory domains of herpes simplex virus 1 alpha genes. Proc Natl Acad Sci U S A **81:**4065-4069.
133. **Carter KL, Roizman B.** 1996. The promoter and transcriptional unit of a novel herpes simplex virus 1 alpha gene are contained in, and encode a protein in frame with, the open reading frame of the alpha 22 gene. J Virol **70:**172-178.
134. **Everett RD.** 1984. Trans activation of transcription by herpes virus products: requirement for two HSV-1 immediate-early polypeptides for maximum activity. Embo J **3:**3135-3141.
135. **O'Hare P, Hayward GS.** 1985. Evidence for a direct role for both the 175,000- and 110,000-molecular-weight immediate-early proteins of herpes simplex virus in the transactivation of delayed-early promoters. J Virol **53:**751-760.
136. **Quinlan MP, Knipe DM.** 1985. Stimulation of expression of a herpes simplex virus DNA-binding protein by two viral functions. Mol Cell Biol **5:**957-963.
137. **Gelman IH, Silverstein S.** 1985. Identification of immediate early genes from herpes simplex virus that transactivate the virus thymidine kinase gene. Proc Natl Acad Sci U S A **82:**5265-5269.
138. **Mavromara-Nazos P, Silver S, Hubenthal-Voss J, McKnight JL, Roizman B.** 1986. Regulation of herpes simplex virus 1 genes: alpha gene sequence requirements for transient induction of indicator genes regulated by beta or late (gamma 2) promoters. Virology **149:**152-164.
139. **Gelman IH, Silverstein S.** 1986. Co-ordinate regulation of herpes simplex virus gene expression is mediated by the functional interaction of two immediate early gene products. J Mol Biol **191:**395-409.
140. **Sekulovich RE, Leary K, Sandri-Goldin RM.** 1988. The herpes simplex virus type 1 alpha protein ICP27 can act as a trans-repressor or a trans-activator in combination with ICP4 and ICP0. J Virol **62:**4510-4522.
141. **Su L, Knipe DM.** 1989. Herpes simplex virus alpha protein ICP27 can inhibit or augment viral gene transactivation. Virology **170:**496-504.

142. **Sze P, Herman RC.** 1992. The herpes simplex virus type 1 ICP6 gene is regulated by a 'leaky' early promoter. Virus Res **26:**141-152.
143. **Boehmer PE, Lehman IR.** 1997. Herpes simplex virus DNA replication. Annu Rev Biochem **66:**347-384.
144. **Dubbs DR, Kit S.** 1964. Mutant Strains of Herpes Simplex Deficient in Thymidine Kinase-Inducing Activity. Virology **22:**493-502.
145. **Frame MC, Marsden HS, Dutia BM.** 1985. The ribonucleotide reductase induced by herpes simplex virus type 1 involves minimally a complex of two polypeptides (136K and 38K). J Gen Virol **66 (Pt 7):**1581-1587.
146. **Cohen EA, Charron J, Perret J, Langelier Y.** 1985. Herpes simplex virus ribonucleotide reductase induced in infected BHK-21/C13 cells: biochemical evidence for the existence of two non-identical subunits, H1 and H2. J Gen Virol **66 (Pt 4):**733-745.
147. **Fisher FB, Preston VG.** 1986. Isolation and characterisation of herpes simplex virus type 1 mutants which fail to induce dUTPase activity. Virology **148:**190-197.
148. **Goldstein DJ, Weller SK.** 1988. Herpes simplex virus type 1-induced ribonucleotide reductase activity is dispensable for virus growth and DNA synthesis: isolation and characterization of an ICP6 lacZ insertion mutant. J Virol **62:**196-205.
149. **Weller SK, Seghatoleslami MR, Shao L, Rowse D, Carmichael EP.** 1990. The herpes simplex virus type 1 alkaline nuclease is not essential for viral DNA synthesis: isolation and characterization of a lacZ insertion mutant. J Gen Virol **71 (Pt 12):**2941-2952.
150. **Martinez R, Sarisky RT, Weber PC, Weller SK.** 1996. Herpes simplex virus type 1 alkaline nuclease is required for efficient processing of viral DNA replication intermediates. J Virol **70:**2075-2085.
151. **Bogani F, Chua CN, Boehmer PE.** 2009. Reconstitution of uracil DNA glycosylase-initiated base excision repair in herpes simplex virus-1. J Biol Chem **284:**16784-16790.
152. **Saffran HA, Pare JM, Corcoran JA, Weller SK, Smiley JR.** 2007. Herpes simplex virus eliminates host mitochondrial DNA. EMBO Rep **8:**188-193.
153. **Wilcock D, Lane DP.** 1991. Localization of p53, retinoblastoma and host replication proteins at sites of viral replication in herpes-infected cells. Nature **349:**429-431.
154. **Rice SA, Long MC, Lam V, Spencer CA.** 1994. RNA polymerase II is aberrantly phosphorylated and localized to viral replication compartments following herpes simplex virus infection. J Virol **68:**988-1001.
155. **LaBoissiere S, O'Hare P.** 2000. Analysis of HCF, the cellular cofactor of VP16, in herpes simplex virus-infected cells. J Virol **74:**99-109.
156. **Wilkinson DE, Weller SK.** 2004. Recruitment of cellular recombination and repair proteins to sites of herpes simplex virus type 1 DNA replication is dependent on the composition of viral proteins within prereplicative

sites and correlates with the induction of the DNA damage response. J Virol **78:**4783-4796.
157. **Taylor TJ, Knipe DM.** 2004. Proteomics of herpes simplex virus replication compartments: association of cellular DNA replication, repair, recombination, and chromatin remodeling proteins with ICP8. J Virol **78:**5856-5866.
158. **Elias P, O'Donnell ME, Mocarski ES, Lehman IR.** 1986. A DNA binding protein specific for an origin of replication of herpes simplex virus type 1. Proc Natl Acad Sci U S A **83:**6322-6326.
159. **Olivo PD, Nelson NJ, Challberg MD.** 1988. Herpes simplex virus DNA replication: the UL9 gene encodes an origin-binding protein. Proc Natl Acad Sci U S A **85:**5414-5418.
160. **Hardwicke MA, Schaffer PA.** 1995. Cloning and characterization of herpes simplex virus type 1 oriL: comparison of replication and protein-DNA complex formation by oriL and oriS. J Virol **69:**1377-1388.
161. **Fierer DS, Challberg MD.** 1992. Purification and characterization of UL9, the herpes simplex virus type 1 origin-binding protein. J Virol **66:**3986-3995.
162. **Boehmer PE, Dodson MS, Lehman IR.** 1993. The herpes simplex virus type-1 origin binding protein. DNA helicase activity. J Biol Chem **268:**1220-1225.
163. **Crute JJ, Tsurumi T, Zhu LA, Weller SK, Olivo PD, Challberg MD, Mocarski ES, Lehman IR.** 1989. Herpes simplex virus 1 helicase-primase: a complex of three herpes-encoded gene products. Proc Natl Acad Sci U S A **86:**2186-2189.
164. **Crute JJ, Mocarski ES, Lehman IR.** 1988. A DNA helicase induced by herpes simplex virus type 1. Nucleic Acids Res **16:**6585-6596.
165. **Crute JJ, Lehman IR.** 1991. Herpes simplex virus-1 helicase-primase. Physical and catalytic properties. J Biol Chem **266:**4484-4488.
166. **Sherman G, Gottlieb J, Challberg MD.** 1992. The UL8 subunit of the herpes simplex virus helicase-primase complex is required for efficient primer utilization. J Virol **66:**4884-4892.
167. **Purifoy DJ, Lewis RB, Powell KL.** 1977. Identification of the herpes simplex virus DNA polymerase gene. Nature **269:**621-623.
168. **Crute JJ, Lehman IR.** 1989. Herpes simplex-1 DNA polymerase. Identification of an intrinsic 5'----3' exonuclease with ribonuclease H activity. J Biol Chem **264:**19266-19270.
169. **Gottlieb J, Marcy AI, Coen DM, Challberg MD.** 1990. The herpes simplex virus type 1 UL42 gene product: a subunit of DNA polymerase that functions to increase processivity. J Virol **64:**5976-5987.
170. **Falkenberg M, Lehman IR, Elias P.** 2000. Leading and lagging strand DNA synthesis in vitro by a reconstituted herpes simplex virus type 1 replisome. Proc Natl Acad Sci U S A **97:**3896-3900.
171. **Muylaert I, Elias P.** 2007. Knockdown of DNA ligase IV/XRCC4 by RNA interference inhibits herpes simplex virus type I DNA replication. J Biol Chem **282:**10865-10872.

172. **Severini A, Morgan AR, Tovell DR, Tyrrell DL.** 1994. Study of the structure of replicative intermediates of HSV-1 DNA by pulsed-field gel electrophoresis. Virology **200:**428-435.
173. **Severini A, Scraba DG, Tyrrell DL.** 1996. Branched structures in the intracellular DNA of herpes simplex virus type 1. J Virol **70:**3169-3175.
174. **Lilley CE, Carson CT, Muotri AR, Gage FH, Weitzman MD.** 2005. DNA repair proteins affect the lifecycle of herpes simplex virus 1. Proc Natl Acad Sci U S A **102:**5844-5849.
175. **Shirata N, Kudoh A, Daikoku T, Tatsumi Y, Fujita M, Kiyono T, Sugaya Y, Isomura H, Ishizaki K, Tsurumi T.** 2005. Activation of ataxia telangiectasia-mutated DNA damage checkpoint signal transduction elicited by herpes simplex virus infection. J Biol Chem **280:**30336-30341.
176. **Long MC, Leong V, Schaffer PA, Spencer CA, Rice SA.** 1999. ICP22 and the UL13 protein kinase are both required for herpes simplex virus-induced modification of the large subunit of RNA polymerase II. J Virol **73:**5593-5604.
177. **Godowski PJ, Knipe DM.** 1985. Identification of a herpes simplex virus function that represses late gene expression from parental viral genomes. J Virol **55:**357-365.
178. **Gao M, Knipe DM.** 1991. Potential role for herpes simplex virus ICP8 DNA replication protein in stimulation of late gene expression. J Virol **65:**2666-2675.
179. **Chen YM, Knipe DM.** 1996. A dominant mutant form of the herpes simplex virus ICP8 protein decreases viral late gene transcription. Virology **221:**281-290.
180. **McNamee EE, Taylor TJ, Knipe DM.** 2000. A dominant-negative herpesvirus protein inhibits intranuclear targeting of viral proteins: effects on DNA replication and late gene expression. J Virol **74:**10122-10131.
181. **Conley AJ, Knipe DM, Jones PC, Roizman B.** 1981. Molecular genetics of herpes simplex virus. VII. Characterization of a temperature-sensitive mutant produced by in vitro mutagenesis and defective in DNA synthesis and accumulation of gamma polypeptides. J Virol **37:**191-206.
182. **Guzowski JF, Singh J, Wagner EK.** 1994. Transcriptional activation of the herpes simplex virus type 1 UL38 promoter conferred by the cis-acting downstream activation sequence is mediated by a cellular transcription factor. J Virol **68:**7774-7789.
183. **Chen S, Mills L, Perry P, Riddle S, Wobig R, Lown R, Millette RL.** 1992. Transactivation of the major capsid protein gene of herpes simplex virus type 1 requires a cellular transcription factor. J Virol **66:**4304-4314.
184. **Mills LK, Shi Y, Millette RL.** 1994. YY1 is the cellular factor shown previously to bind to regulatory regions of several leaky-late (beta gamma, gamma 1) genes of herpes simplex virus type 1. J Virol **68:**1234-1238.
185. **Lieu PT, Wagner EK.** 2000. Two leaky-late HSV-1 promoters differ significantly in structural architecture. Virology **272:**191-203.
186. **Petroski MD, Wagner EK.** 1998. Purification and characterization of a cellular protein that binds to the downstream activation sequence of the

strict late UL38 promoter of herpes simplex virus type 1. J Virol **72:**8181-8190.
187. **Sethna M, Weir JP.** 1993. Mutational analysis of the herpes simplex virus type 1 glycoprotein E promoter. Virology **196:**532-540.
188. **Huang CJ, Wagner EK.** 1994. The herpes simplex virus type 1 major capsid protein (VP5-UL19) promoter contains two cis-acting elements influencing late expression. J Virol **68:**5738-5747.
189. **Newcomb WW, Homa FL, Brown JC.** 2005. Involvement of the portal at an early step in herpes simplex virus capsid assembly. J Virol **79:**10540-10546.
190. **Newcomb WW, Homa FL, Thomsen DR, Booy FP, Trus BL, Steven AC, Spencer JV, Brown JC.** 1996. Assembly of the herpes simplex virus capsid: characterization of intermediates observed during cell-free capsid formation. J Mol Biol **263:**432-446.
191. **Booy FP, Newcomb WW, Trus BL, Brown JC, Baker TS, Steven AC.** 1991. Liquid-crystalline, phage-like packing of encapsidated DNA in herpes simplex virus. Cell **64:**1007-1015.
192. **Roos WH, Radtke K, Kniesmeijer E, Geertsema H, Sodeik B, Wuite GJ.** 2009. Scaffold expulsion and genome packaging trigger stabilization of herpes simplex virus capsids. Proc Natl Acad Sci U S A **106:**9673-9678.
193. **Shao L, Rapp LM, Weller SK.** 1993. Herpes simplex virus 1 alkaline nuclease is required for efficient egress of capsids from the nucleus. Virology **196:**146-162.
194. **Porter IM, Stow ND.** 2004. Virus particles produced by the herpes simplex virus type 1 alkaline nuclease null mutant ambUL12 contain abnormal genomes. J Gen Virol **85:**583-591.
195. **Goldstein JN, Weller SK.** 1998. In vitro processing of herpes simplex virus type 1 DNA replication intermediates by the viral alkaline nuclease, UL12. J Virol **72:**8772-8781.
196. **Thomas MS, Gao M, Knipe DM, Powell KL.** 1992. Association between the herpes simplex virus major DNA-binding protein and alkaline nuclease. J Virol **66:**1152-1161.
197. **Reuven NB, Staire AE, Myers RS, Weller SK.** 2003. The herpes simplex virus type 1 alkaline nuclease and single-stranded DNA binding protein mediate strand exchange in vitro. J Virol **77:**7425-7433.
198. **Reuven NB, Willcox S, Griffith JD, Weller SK.** 2004. Catalysis of strand exchange by the HSV-1 UL12 and ICP8 proteins: potent ICP8 recombinase activity is revealed upon resection of dsDNA substrate by nuclease. J Mol Biol **342:**57-71.
199. **Schumacher AJ, Mohni KN, Kan Y, Hendrickson EA, Stark JM, Weller SK.** 2012. The HSV-1 exonuclease, UL12, stimulates recombination by a single strand annealing mechanism. PLoS Pathog **8:**e1002862.
200. **Conway JF, Homa FL.** 2011. Chapter 10: Nucleocapsid Structure, Assembly and DNA Packaging of Herpes Simplex Virus, p. 175-193. *In*

Weller SK (ed.), Alphaheresviruses: Molecular Virology. Caister Academic Press, Norfolk, UK.
201. **White CA, Stow ND, Patel AH, Hughes M, Preston VG.** 2003. Herpes simplex virus type 1 portal protein UL6 interacts with the putative terminase subunits UL15 and UL28. J Virol **77:**6351-6358.
202. **Yang K, Homa F, Baines JD.** 2007. Putative terminase subunits of herpes simplex virus 1 form a complex in the cytoplasm and interact with portal protein in the nucleus. J Virol **81:**6419-6433.
203. **Yu D, Weller SK.** 1998. Herpes simplex virus type 1 cleavage and packaging proteins UL15 and UL28 are associated with B but not C capsids during packaging. J Virol **72:**7428-7439.
204. **Deiss LP, Chou J, Frenkel N.** 1986. Functional domains within the a sequence involved in the cleavage-packaging of herpes simplex virus DNA. J Virol **59:**605-618.
205. **Feiss M, Sippy J, Miller G.** 1985. Processive action of terminase during sequential packaging of bacteriophage lambda chromosomes. J Mol Biol **186:**759-771.
206. **Scheffczik H, Savva CG, Holzenburg A, Kolesnikova L, Bogner E.** 2002. The terminase subunits pUL56 and pUL89 of human cytomegalovirus are DNA-metabolizing proteins with toroidal structure. Nucleic Acids Res **30:**1695-1703.
207. **Nadal M, Mas PJ, Blanco AG, Arnan C, Sola M, Hart DJ, Coll M.** 2010. Structure and inhibition of herpesvirus DNA packaging terminase nuclease domain. Proc Natl Acad Sci U S A **107:**16078-16083.
208. **Selvarajan Sigamani S, Zhao H, Kamau YN, Baines JD, Tang L.** 2013. The structure of the herpes simplex virus DNA-packaging terminase pUL15 nuclease domain suggests an evolutionary lineage among eukaryotic and prokaryotic viruses. J Virol **87:**7140-7148.
209. **Reynolds AE, Liang L, Baines JD.** 2004. Conformational changes in the nuclear lamina induced by herpes simplex virus type 1 require genes U(L)31 and U(L)34. J Virol **78:**5564-5575.
210. **Simpson-Holley M, Baines J, Roller R, Knipe DM.** 2004. Herpes simplex virus 1 U(L)31 and U(L)34 gene products promote the late maturation of viral replication compartments to the nuclear periphery. J Virol **78:**5591-5600.
211. **Mou F, Forest T, Baines JD.** 2007. US3 of herpes simplex virus type 1 encodes a promiscuous protein kinase that phosphorylates and alters localization of lamin A/C in infected cells. J Virol **81:**6459-6470.
212. **Park R, Baines JD.** 2006. Herpes simplex virus type 1 infection induces activation and recruitment of protein kinase C to the nuclear membrane and increased phosphorylation of lamin B. J Virol **80:**494-504.
213. **Leach NR, Roller RJ.** 2010. Significance of host cell kinases in herpes simplex virus type 1 egress and lamin-associated protein disassembly from the nuclear lamina. Virology **406:**127-137.
214. **Reynolds AE, Ryckman BJ, Baines JD, Zhou Y, Liang L, Roller RJ.** 2001. U(L)31 and U(L)34 proteins of herpes simplex virus type 1 form a

complex that accumulates at the nuclear rim and is required for envelopment of nucleocapsids. J Virol **75:**8803-8817.
215. **Reynolds AE, Wills EG, Roller RJ, Ryckman BJ, Baines JD.** 2002. Ultrastructural localization of the herpes simplex virus type 1 UL31, UL34, and US3 proteins suggests specific roles in primary envelopment and egress of nucleocapsids. J Virol **76:**8939-8952.
216. **Yang K, Baines JD.** 2011. Selection of HSV capsids for envelopment involves interaction between capsid surface components pUL31, pUL17, and pUL25. Proc Natl Acad Sci U S A **108:**14276-14281.
217. **Wills E, Mou F, Baines JD.** 2009. The U(L)31 and U(L)34 gene products of herpes simplex virus 1 are required for optimal localization of viral glycoproteins D and M to the inner nuclear membranes of infected cells. J Virol **83:**4800-4809.
218. **Granzow H, Klupp BG, Fuchs W, Veits J, Osterrieder N, Mettenleiter TC.** 2001. Egress of alphaherpesviruses: comparative ultrastructural study. J Virol **75:**3675-3684.
219. **Remillard-Labrosse G, Guay G, Lippe R.** 2006. Reconstitution of herpes simplex virus type 1 nuclear capsid egress in vitro. J Virol **80:**9741-9753.
220. **Skepper JN, Whiteley A, Browne H, Minson A.** 2001. Herpes simplex virus nucleocapsids mature to progeny virions by an envelopment --> deenvelopment --> reenvelopment pathway. J Virol **75:**5697-5702.
221. **Farnsworth A, Wisner TW, Webb M, Roller R, Cohen G, Eisenberg R, Johnson DC.** 2007. Herpes simplex virus glycoproteins gB and gH function in fusion between the virion envelope and the outer nuclear membrane. Proc Natl Acad Sci U S A **104:**10187-10192.
222. **Browne H, Bell S, Minson T, Wilson DW.** 1996. An endoplasmic reticulum-retained herpes simplex virus glycoprotein H is absent from secreted virions: evidence for reenvelopment during egress. J Virol **70:**4311-4316.
223. **Harley CA, Dasgupta A, Wilson DW.** 2001. Characterization of herpes simplex virus-containing organelles by subcellular fractionation: role for organelle acidification in assembly of infectious particles. J Virol **75:**1236-1251.
224. **Turcotte S, Letellier J, Lippe R.** 2005. Herpes simplex virus type 1 capsids transit by the trans-Golgi network, where viral glycoproteins accumulate independently of capsid egress. J Virol **79:**8847-8860.
225. **Sugimoto K, Uema M, Sagara H, Tanaka M, Sata T, Hashimoto Y, Kawaguchi Y.** 2008. Simultaneous tracking of capsid, tegument, and envelope protein localization in living cells infected with triply fluorescent herpes simplex virus 1. J Virol **82:**5198-5211.
226. **Jayachandra S, Baghian A, Kousoulas KG.** 1997. Herpes simplex virus type 1 glycoprotein K is not essential for infectious virus production in actively replicating cells but is required for efficient envelopment and translocation of infectious virions from the cytoplasm to the extracellular space. J Virol **71:**5012-5024.

227. **Desai P, Sexton GL, McCaffery JM, Person S.** 2001. A null mutation in the gene encoding the herpes simplex virus type 1 UL37 polypeptide abrogates virus maturation. J Virol **75:**10259-10271.
228. **Farnsworth A, Goldsmith K, Johnson DC.** 2003. Herpes simplex virus glycoproteins gD and gE/gI serve essential but redundant functions during acquisition of the virion envelope in the cytoplasm. J Virol **77:**8481-8494.
229. **Foster TP, Melancon JM, Baines JD, Kousoulas KG.** 2004. The herpes simplex virus type 1 UL20 protein modulates membrane fusion events during cytoplasmic virion morphogenesis and virus-induced cell fusion. J Virol **78:**5347-5357.
230. **Fulmer PA, Melancon JM, Baines JD, Kousoulas KG.** 2007. UL20 protein functions precede and are required for the UL11 functions of herpes simplex virus type 1 cytoplasmic virion envelopment. J Virol **81:**3097-3108.
231. **Leege T, Fuchs W, Granzow H, Kopp M, Klupp BG, Mettenleiter TC.** 2009. Effects of simultaneous deletion of pUL11 and glycoprotein M on virion maturation of herpes simplex virus type 1. J Virol **83:**896-907.
232. **Johnson DC, Wisner TW, Wright CC.** 2011. Herpes simplex virus glycoproteins gB and gD function in a redundant fashion to promote secondary envelopment. J Virol **85:**4910-4926.
233. **Chouljenko DV, Kim IJ, Chouljenko VN, Subramanian R, Walker JD, Kousoulas KG.** 2012. Functional hierarchy of herpes simplex virus 1 viral glycoproteins in cytoplasmic virion envelopment and egress. J Virol **86:**4262-4270.
234. **Jambunathan N, Chouljenko D, Desai P, Charles AS, Subramanian R, Chouljenko VN, Kousoulas KG.** 2014. The Herpes Simplex Virus Type-1 UL37 Protein Interacts with Viral Glycoprotein gK and Membrane Protein UL20 and Functions in Cytoplasmic Virion Envelopment. J Virol.
235. **Negatsch A, Granzow H, Maresch C, Klupp BG, Fuchs W, Teifke JP, Mettenleiter TC.** 2010. Ultrastructural analysis of virion formation and intraaxonal transport of herpes simplex virus type 1 in primary rat neurons. J Virol **84:**13031-13035.
236. **Wisner TW, Sugimoto K, Howard PW, Kawaguchi Y, Johnson DC.** 2011. Anterograde transport of herpes simplex virus capsids in neurons by both separate and married mechanisms. J Virol **85:**5919-5928.
237. **Stevens JG, Wagner EK, Devi-Rao GB, Cook ML, Feldman LT.** 1987. RNA complementary to a herpesvirus alpha gene mRNA is prominent in latently infected neurons. Science **235:**1056-1059.
238. **Rock DL, Nesburn AB, Ghiasi H, Ong J, Lewis TL, Lokensgard JR, Wechsler SL.** 1987. Detection of latency-related viral RNAs in trigeminal ganglia of rabbits latently infected with herpes simplex virus type 1. J Virol **61:**3820-3826.
239. **Spivack JG, Fraser NW.** 1987. Detection of herpes simplex virus type 1 transcripts during latent infection in mice. J Virol **61:**3841-3847.

240. **Kristie TM, Roizman B.** 1988. Differentiation and DNA contact points of host proteins binding at the cis site for virion-mediated induction of alpha genes of herpes simplex virus 1. J Virol **62:**1145-1157.
241. **Kolb G, Kristie TM.** 2008. Association of the cellular coactivator HCF-1 with the Golgi apparatus in sensory neurons. J Virol **82:**9555-9563.
242. **Lakin ND, Palmer R, Lillycrop KA, Howard MK, Burke LC, Thomas NS, Latchman DS.** 1995. Down regulation of the octamer binding protein Oct-1 during growth arrest and differentiation of a neuronal cell line. Brain Res Mol Brain Res **28:**47-54.
243. **Kubat NJ, Tran RK, McAnany P, Bloom DC.** 2004. Specific histone tail modification and not DNA methylation is a determinant of herpes simplex virus type 1 latent gene expression. J Virol **78:**1139-1149.
244. **Kubat NJ, Amelio AL, Giordani NV, Bloom DC.** 2004. The herpes simplex virus type 1 latency-associated transcript (LAT) enhancer/rcr is hyperacetylated during latency independently of LAT transcription. J Virol **78:**12508-12518.
245. **Thompson RL, Sawtell NM.** 1997. The herpes simplex virus type 1 latency-associated transcript gene regulates the establishment of latency. J Virol **71:**5432-5440.
246. **Wang QY, Zhou C, Johnson KE, Colgrove RC, Coen DM, Knipe DM.** 2005. Herpesviral latency-associated transcript gene promotes assembly of heterochromatin on viral lytic-gene promoters in latent infection. Proc Natl Acad Sci U S A **102:**16055-16059.
247. **Cliffe AR, Garber DA, Knipe DM.** 2009. Transcription of the herpes simplex virus latency-associated transcript promotes the formation of facultative heterochromatin on lytic promoters. J Virol **83:**8182-8190.
248. **Thompson RL, Sawtell NM.** 2001. Herpes simplex virus type 1 latency-associated transcript gene promotes neuronal survival. J Virol **75:**6660-6675.
249. **Akhova O, Bainbridge M, Misra V.** 2005. The neuronal host cell factor-binding protein Zhangfei inhibits herpes simplex virus replication. J Virol **79:**14708-14718.
250. **Lu R, Misra V.** 2000. Potential role for luman, the cellular homologue of herpes simplex virus VP16 (alpha gene trans-inducing factor), in herpesvirus latency. J Virol **74:**934-943.
251. **Theil D, Derfuss T, Paripovic I, Herberger S, Meinl E, Schueler O, Strupp M, Arbusow V, Brandt T.** 2003. Latent herpesvirus infection in human trigeminal ganglia causes chronic immune response. Am J Pathol **163:**2179-2184.
252. **Khanna KM, Bonneau RH, Kinchington PR, Hendricks RL.** 2003. Herpes simplex virus-specific memory CD8+ T cells are selectively activated and retained in latently infected sensory ganglia. Immunity **18:**593-603.
253. **Knickelbein JE, Khanna KM, Yee MB, Baty CJ, Kinchington PR, Hendricks RL.** 2008. Noncytotoxic lytic granule-mediated CD8+ T cell

inhibition of HSV-1 reactivation from neuronal latency. Science **322:**268-271.
254. **Roizman B, Whitley RJ.** 2013. An inquiry into the molecular basis of HSV latency and reactivation. Annu Rev Microbiol **67:**355-374.
255. **Kosz-Vnenchak M, Jacobson J, Coen DM, Knipe DM.** 1993. Evidence for a novel regulatory pathway for herpes simplex virus gene expression in trigeminal ganglion neurons. J Virol **67:**5383-5393.
256. **Tal-Singer R, Lasner TM, Podrzucki W, Skokotas A, Leary JJ, Berger SL, Fraser NW.** 1997. Gene expression during reactivation of herpes simplex virus type 1 from latency in the peripheral nervous system is different from that during lytic infection of tissue cultures. J Virol **71:**5268-5276.
257. **Cai W, Astor TL, Liptak LM, Cho C, Coen DM, Schaffer PA.** 1993. The herpes simplex virus type 1 regulatory protein ICP0 enhances virus replication during acute infection and reactivation from latency. J Virol **67:**7501-7512.
258. **Halford WP, Schaffer PA.** 2001. ICP0 is required for efficient reactivation of herpes simplex virus type 1 from neuronal latency. J Virol **75:**3240-3249.
259. **Thompson RL, Preston CM, Sawtell NM.** 2009. De novo synthesis of VP16 coordinates the exit from HSV latency in vivo. PLoS Pathog **5:**e1000352.
260. **Sawtell NM, Triezenberg SJ, Thompson RL.** 2011. VP16 serine 375 is a critical determinant of herpes simplex virus exit from latency in vivo. J Neurovirol **17:**546-551.
261. **Browne EP, Wing B, Coleman D, Shenk T.** 2001. Altered cellular mRNA levels in human cytomegalovirus-infected fibroblasts: viral block to the accumulation of antiviral mRNAs. J Virol **75:**12319-12330.
262. **Aravalli RN, Hu S, Rowen TN, Gekker G, Lokensgard JR.** 2006. Differential apoptotic signaling in primary glial cells infected with herpes simplex virus 1. J Neurovirol **12:**501-510.
263. **Chandriani S, Ganem D.** 2007. Host transcript accumulation during lytic KSHV infection reveals several classes of host responses. PLoS One **2:**e811.
264. **Kamakura M, Nawa A, Ushijima Y, Goshima F, Kawaguchi Y, Kikkawa F, Nishiyama Y.** 2008. Microarray analysis of transcriptional responses to infection by herpes simplex virus types 1 and 2 and their US3-deficient mutants. Microbes Infect **10:**405-413.
265. **Spencer CA, Dahmus ME, Rice SA.** 1997. Repression of host RNA polymerase II transcription by herpes simplex virus type 1. J Virol **71:**2031-2040.
266. **Guo L, Wu WJ, Liu LD, Wang LC, Zhang Y, Wu LQ, Guan Y, Li QH.** 2012. Herpes simplex virus 1 ICP22 inhibits the transcription of viral gene promoters by binding to and blocking the recruitment of P-TEFb. PLoS One **7:**e45749.

267. **Sandri-Goldin RM, Mendoza GE.** 1992. A herpesvirus regulatory protein appears to act post-transcriptionally by affecting mRNA processing. Genes Dev **6:**848-863.
268. **Sandri-Goldin RM.** 1998. ICP27 mediates HSV RNA export by shuttling through a leucine-rich nuclear export signal and binding viral intronless RNAs through an RGG motif. Genes Dev **12:**868-879.
269. **Ruvolo V, Wang E, Boyle S, Swaminathan S.** 1998. The Epstein-Barr virus nuclear protein SM is both a post-transcriptional inhibitor and activator of gene expression. Proc Natl Acad Sci U S A **95:**8852-8857.
270. **Hocine S, Singer RH, Grunwald D.** 2010. RNA processing and export. Cold Spring Harb Perspect Biol **2:**a000752.
271. **McGeoch DJ.** 1987. The genome of herpes simplex virus: structure, replication and evolution. J Cell Sci Suppl **7:**67-94.
272. **Gatherer D, Seirafian S, Cunningham C, Holton M, Dargan DJ, Baluchova K, Hector RD, Galbraith J, Herzyk P, Wilkinson GW, Davison AJ.** 2011. High-resolution human cytomegalovirus transcriptome. Proc Natl Acad Sci U S A **108:**19755-19760.
273. **Davison AJ, Scott JE.** 1986. The complete DNA sequence of varicella-zoster virus. J Gen Virol **67 (Pt 9):**1759-1816.
274. **Moss WN, Steitz JA.** 2013. Genome-wide analyses of Epstein-Barr virus reveal conserved RNA structures and a novel stable intronic sequence RNA. BMC Genomics **14:**543.
275. **Hardwicke MA, Sandri-Goldin RM.** 1994. The herpes simplex virus regulatory protein ICP27 contributes to the decrease in cellular mRNA levels during infection. J Virol **68:**4797-4810.
276. **Sandri-Goldin RM, Hibbard MK.** 1996. The herpes simplex virus type 1 regulatory protein ICP27 coimmunoprecipitates with anti-Sm antiserum, and the C terminus appears to be required for this interaction. J Virol **70:**108-118.
277. **Bryant HE, Wadd SE, Lamond AI, Silverstein SJ, Clements JB.** 2001. Herpes simplex virus IE63 (ICP27) protein interacts with spliceosome-associated protein 145 and inhibits splicing prior to the first catalytic step. J Virol **75:**4376-4385.
278. **Lindberg A, Kreivi JP.** 2002. Splicing inhibition at the level of spliceosome assembly in the presence of herpes simplex virus protein ICP27. Virology **294:**189-198.
279. **Sciabica KS, Dai QJ, Sandri-Goldin RM.** 2003. ICP27 interacts with SRPK1 to mediate HSV splicing inhibition by altering SR protein phosphorylation. Embo J **22:**1608-1619.
280. **Chen IH, Sciabica KS, Sandri-Goldin RM.** 2002. ICP27 interacts with the RNA export factor Aly/REF to direct herpes simplex virus type 1 intronless mRNAs to the TAP export pathway. J Virol **76:**12877-12889.
281. **Chen IH, Li L, Silva L, Sandri-Goldin RM.** 2005. ICP27 recruits Aly/REF but not TAP/NXF1 to herpes simplex virus type 1 transcription sites although TAP/NXF1 is required for ICP27 export. J Virol **79:**3949-3961.

282. **Stern-Ginossar N, Elefant N, Zimmermann A, Wolf DG, Saleh N, Biton M, Horwitz E, Prokocimer Z, Prichard M, Hahn G, Goldman-Wohl D, Greenfield C, Yagel S, Hengel H, Altuvia Y, Margalit H, Mandelboim O.** 2007. Host immune system gene targeting by a viral miRNA. Science **317:**376-381.
283. **Grey F, Tirabassi R, Meyers H, Wu G, McWeeney S, Hook L, Nelson JA.** 2010. A viral microRNA down-regulates multiple cell cycle genes through mRNA 5'UTRs. PLoS Pathog **6:**e1000967.
284. **Kim S, Lee S, Shin J, Kim Y, Evnouchidou I, Kim D, Kim YK, Kim YE, Ahn JH, Riddell SR, Stratikos E, Kim VN, Ahn K.** 2011. Human cytomegalovirus microRNA miR-US4-1 inhibits CD8(+) T cell responses by targeting the aminopeptidase ERAP1. Nat Immunol **12:**984-991.
285. **Kim Y, Lee S, Kim S, Kim D, Ahn JH, Ahn K.** 2012. Human cytomegalovirus clinical strain-specific microRNA miR-UL148D targets the human chemokine RANTES during infection. PLoS Pathog **8:**e1002577.
286. **Jurak I, Silverstein LB, Sharma M, Coen DM.** 2012. Herpes simplex virus is equipped with RNA- and protein-based mechanisms to repress expression of ATRX, an effector of intrinsic immunity. J Virol **86:**10093-10102.
287. **Wu W, Guo Z, Zhang X, Guo L, Liu L, Liao Y, Wang J, Wang L, Li Q.** 2013. A microRNA encoded by HSV-1 inhibits a cellular transcriptional repressor of viral immediate early and early genes. Sci China Life Sci **56:**373-383.
288. **Zhu Y, Haecker I, Yang Y, Gao SJ, Renne R.** 2013. gamma-Herpesvirus-encoded miRNAs and their roles in viral biology and pathogenesis. Curr Opin Virol **3:**266-275.
289. **Inglis SC.** 1982. Inhibition of host protein synthesis and degradation of cellular mRNAs during infection by influenza and herpes simplex virus. Mol Cell Biol **2:**1644-1648.
290. **Schek N, Bachenheimer SL.** 1985. Degradation of cellular mRNAs induced by a virion-associated factor during herpes simplex virus infection of Vero cells. J Virol **55:**601-610.
291. **Waterboer T, Rahaus M, Wolff MH.** 2002. Varicella-zoster virus (VZV) mediates a delayed host shutoff independent of open reading frame (ORF) 17 expression. Virus Genes **24:**49-56.
292. **Everly DN, Jr., Feng P, Mian IS, Read GS.** 2002. mRNA degradation by the virion host shutoff (Vhs) protein of herpes simplex virus: genetic and biochemical evidence that Vhs is a nuclease. J Virol **76:**8560-8571.
293. **Glaunsinger B, Ganem D.** 2004. Lytic KSHV infection inhibits host gene expression by accelerating global mRNA turnover. Mol Cell **13:**713-723.
294. **Rowe M, Glaunsinger B, van Leeuwen D, Zuo J, Sweetman D, Ganem D, Middeldorp J, Wiertz EJ, Ressing ME.** 2007. Host shutoff during productive Epstein-Barr virus infection is mediated by BGLF5 and may contribute to immune evasion. Proc Natl Acad Sci U S A **104:**3366-3371.

295. **Doepker RC, Hsu WL, Saffran HA, Smiley JR.** 2004. Herpes simplex virus virion host shutoff protein is stimulated by translation initiation factors eIF4B and eIF4H. J Virol **78:**4684-4699.
296. **Feng P, Everly DN, Jr., Read GS.** 2005. mRNA decay during herpes simplex virus (HSV) infections: protein-protein interactions involving the HSV virion host shutoff protein and translation factors eIF4H and eIF4A. J Virol **79:**9651-9664.
297. **Page HG, Read GS.** 2010. The virion host shutoff endonuclease (UL41) of herpes simplex virus interacts with the cellular cap-binding complex eIF4F. J Virol **84:**6886-6890.
298. **Suzutani T, Nagamine M, Shibaki T, Ogasawara M, Yoshida I, Daikoku T, Nishiyama Y, Azuma M.** 2000. The role of the UL41 gene of herpes simplex virus type 1 in evasion of non-specific host defence mechanisms during primary infection. J Gen Virol **81:**1763-1771.
299. **Murphy JA, Duerst RJ, Smith TJ, Morrison LA.** 2003. Herpes simplex virus type 2 virion host shutoff protein regulates alpha/beta interferon but not adaptive immune responses during primary infection in vivo. J Virol **77:**9337-9345.
300. **Ferreira VH, Nazli A, Mossman KL, Kaushic C.** 2013. Proinflammatory cytokines and chemokines - but not interferon-beta - produced in response to HSV-2 in primary human genital epithelial cells are associated with viral replication and the presence of the virion host shutoff protein. Am J Reprod Immunol **70:**199-212.
301. **Yao XD, Rosenthal KL.** 2011. Herpes simplex virus type 2 virion host shutoff protein suppresses innate dsRNA antiviral pathways in human vaginal epithelial cells. J Gen Virol **92:**1981-1993.
302. **Sciortino MT, Parisi T, Siracusano G, Mastino A, Taddeo B, Roizman B.** 2013. The virion host shutoff RNase plays a key role in blocking the activation of protein kinase R in cells infected with herpes simplex virus 1. J Virol **87:**3271-3276.
303. **Cotter CR, Kim WK, Nguyen ML, Yount JS, Lopez CB, Blaho JA, Moran TM.** 2011. The virion host shutoff protein of herpes simplex virus 1 blocks the replication-independent activation of NF-kappaB in dendritic cells in the absence of type I interferon signaling. J Virol **85:**12662-12672.
304. **Zenner HL, Mauricio R, Banting G, Crump CM.** 2013. Herpes simplex virus 1 counteracts tetherin restriction via its virion host shutoff activity. J Virol **87:**13115-13123.
305. **Samady L, Costigliola E, MacCormac L, McGrath Y, Cleverley S, Lilley CE, Smith J, Latchman DS, Chain B, Coffin RS.** 2003. Deletion of the virion host shutoff protein (vhs) from herpes simplex virus (HSV) relieves the viral block to dendritic cell activation: potential of vhs- HSV vectors for dendritic cell-mediated immunotherapy. J Virol **77:**3768-3776.
306. **Cotter CR, Nguyen ML, Yount JS, Lopez CB, Blaho JA, Moran TM.** 2010. The virion host shut-off (vhs) protein blocks a TLR-independent pathway of herpes simplex virus type 1 recognition in human and mouse dendritic cells. PLoS One **5:**e8684.

307. **Kwong AD, Frenkel N.** 1987. Herpes simplex virus-infected cells contain a function(s) that destabilizes both host and viral mRNAs. Proc Natl Acad Sci U S A **84:**1926-1930.
308. **Oroskar AA, Read GS.** 1989. Control of mRNA stability by the virion host shutoff function of herpes simplex virus. J Virol **63:**1897-1906.
309. **Smibert CA, Popova B, Xiao P, Capone JP, Smiley JR.** 1994. Herpes simplex virus VP16 forms a complex with the virion host shutoff protein vhs. J Virol **68:**2339-2346.
310. **Lam Q, Smibert CA, Koop KE, Lavery C, Capone JP, Weinheimer SP, Smiley JR.** 1996. Herpes simplex virus VP16 rescues viral mRNA from destruction by the virion host shutoff function. Embo J **15:**2575-2581.
311. **Dauber B, Pelletier J, Smiley JR.** 2011. The herpes simplex virus 1 vhs protein enhances translation of viral true late mRNAs and virus production in a cell type-dependent manner. J Virol **85:**5363-5373.
312. **Martin W, Hoffmeister M, Rotte C, Henze K.** 2001. An overview of endosymbiotic models for the origins of eukaryotes, their ATP-producing organelles (mitochondria and hydrogenosomes), and their heterotrophic lifestyle. Biol Chem **382:**1521-1539.
313. **Galluzzi L, Kepp O, Trojel-Hansen C, Kroemer G.** 2012. Mitochondrial control of cellular life, stress, and death. Circ Res **111:**1198-1207.
314. **Palade GE.** 1952. The fine structure of mitochondria. The Anatomical Record **114:**427-451.
315. **Palade GE.** 1953. An electron microscope study of the mitochondrial structure. J Histochem Cytochem **1:**188-211.
316. **Pfanner N, Craig EA, Honlinger A.** 1997. Mitochondrial preprotein translocase. Annu Rev Cell Dev Biol **13:**25-51.
317. **Neupert W, Herrmann JM.** 2007. Translocation of proteins into mitochondria. Annu Rev Biochem **76:**723-749.
318. **Colombini M.** 1979. A candidate for the permeability pathway of the outer mitochondrial membrane. Nature **279:**643-645.
319. **Colombini M.** 1980. Structure and mode of action of a voltage dependent anion-selective channel (VDAC) located in the outer mitochondrial membrane. Ann N Y Acad Sci **341:**552-563.
320. **Clemencon B, Babot M, Trezeguet V.** 2013. The mitochondrial ADP/ATP carrier (SLC25 family): pathological implications of its dysfunction. Mol Aspects Med **34:**485-493.
321. **Stuart R.** 2002. Insertion of proteins into the inner membrane of mitochondria: the role of the Oxa1 complex. Biochim Biophys Acta **1592:**79-87.
322. **Vartak R, Porras CA, Bai Y.** 2013. Respiratory supercomplexes: structure, function and assembly. Protein Cell **4:**582-590.
323. **Herrmann JM, Riemer J.** 2010. The intermembrane space of mitochondria. Antioxid Redox Signal **13:**1341-1358.

324. **Susin SA, Lorenzo HK, Zamzami N, Marzo I, Snow BE, Brothers GM, Mangion J, Jacotot E, Costantini P, Loeffler M, Larochette N, Goodlett DR, Aebersold R, Siderovski DP, Penninger JM, Kroemer G.** 1999. Molecular characterization of mitochondrial apoptosis-inducing factor. Nature **397:**441-446.
325. **Matlib MA, O'Brien PJ.** 1976. Properties of rat liver mitochondria with intermembrane Cytochrome c. Arch Biochem Biophys **173:**27-33.
326. **Liu X, Kim CN, Yang J, Jemmerson R, Wang X.** 1996. Induction of apoptotic program in cell-free extracts: requirement for dATP and cytochrome c. Cell **86:**147-157.
327. **Li P, Nijhawan D, Budihardjo I, Srinivasula SM, Ahmad M, Alnemri ES, Wang X.** 1997. Cytochrome c and dATP-dependent formation of Apaf-1/caspase-9 complex initiates an apoptotic protease cascade. Cell **91:**479-489.
328. **Li LY, Luo X, Wang X.** 2001. Endonuclease G is an apoptotic DNase when released from mitochondria. Nature **412:**95-99.
329. **van Loo G, Schotte P, van Gurp M, Demol H, Hoorelbeke B, Gevaert K, Rodriguez I, Ruiz-Carrillo A, Vandekerckhove J, Declercq W, Beyaert R, Vandenabeele P.** 2001. Endonuclease G: a mitochondrial protein released in apoptosis and involved in caspase-independent DNA degradation. Cell Death Differ **8:**1136-1142.
330. **Ohsato T, Ishihara N, Muta T, Umeda S, Ikeda S, Mihara K, Hamasaki N, Kang D.** 2002. Mammalian mitochondrial endonuclease G. Digestion of R-loops and localization in intermembrane space. Eur J Biochem **269:**5765-5770.
331. **Verhagen AM, Ekert PG, Pakusch M, Silke J, Connolly LM, Reid GE, Moritz RL, Simpson RJ, Vaux DL.** 2000. Identification of DIABLO, a mammalian protein that promotes apoptosis by binding to and antagonizing IAP proteins. Cell **102:**43-53.
332. **Burri L, Strahm Y, Hawkins CJ, Gentle IE, Puryer MA, Verhagen A, Callus B, Vaux D, Lithgow T.** 2005. Mature DIABLO/Smac is produced by the IMP protease complex on the mitochondrial inner membrane. Mol Biol Cell **16:**2926-2933.
333. **Suzuki Y, Imai Y, Nakayama H, Takahashi K, Takio K, Takahashi R.** 2001. A serine protease, HtrA2, is released from the mitochondria and interacts with XIAP, inducing cell death. Mol Cell **8:**613-621.
334. **Hegde R, Srinivasula SM, Zhang Z, Wassell R, Mukattash R, Cilenti L, DuBois G, Lazebnik Y, Zervos AS, Fernandes-Alnemri T, Alnemri ES.** 2002. Identification of Omi/HtrA2 as a mitochondrial apoptotic serine protease that disrupts inhibitor of apoptosis protein-caspase interaction. J Biol Chem **277:**432-438.
335. **Verhagen AM, Silke J, Ekert PG, Pakusch M, Kaufmann H, Connolly LM, Day CL, Tikoo A, Burke R, Wrobel C, Moritz RL, Simpson RJ, Vaux DL.** 2002. HtrA2 promotes cell death through its serine protease activity and its ability to antagonize inhibitor of apoptosis proteins. J Biol Chem **277:**445-454.

336. **van Loo G, van Gurp M, Depuydt B, Srinivasula SM, Rodriguez I, Alnemri ES, Gevaert K, Vandekerckhove J, Declercq W, Vandenabeele P.** 2002. The serine protease Omi/HtrA2 is released from mitochondria during apoptosis. Omi interacts with caspase-inhibitor XIAP and induces enhanced caspase activity. Cell Death Differ **9:**20-26.
337. **Nass S, Nass MM.** 1963. Intramitochondrial Fibers with DNA Characteristics. Ii. Enzymatic and Other Hydrolytic Treatments. J Cell Biol **19:**613-629.
338. **Nass MM, Nass S.** 1963. Intramitochondrial Fibers with DNA Characteristics. I. Fixation and Electron Staining Reactions. J Cell Biol **19:**593-611.
339. **Satoh M, Kuroiwa T.** 1991. Organization of multiple nucleoids and DNA molecules in mitochondria of a human cell. Exp Cell Res **196:**137-140.
340. **Cavelier L, Johannisson A, Gyllensten U.** 2000. Analysis of mtDNA copy number and composition of single mitochondrial particles using flow cytometry and PCR. Exp Cell Res **259:**79-85.
341. **Legros F, Malka F, Frachon P, Lombes A, Rojo M.** 2004. Organization and dynamics of human mitochondrial DNA. J Cell Sci **117:**2653-2662.
342. **Munger J, Roizman B.** 2001. The US3 protein kinase of herpes simplex virus 1 mediates the posttranslational modification of BAD and prevents BAD-induced programmed cell death in the absence of other viral proteins. Proc Natl Acad Sci U S A **98:**10410-10415.
343. **Cartier A, Komai T, Masucci MG.** 2003. The Us3 protein kinase of herpes simplex virus 1 blocks apoptosis and induces phosporylation of the Bcl-2 family member Bad. Exp Cell Res **291:**242-250.
344. **Ogg PD, McDonell PJ, Ryckman BJ, Knudson CM, Roller RJ.** 2004. The HSV-1 Us3 protein kinase is sufficient to block apoptosis induced by overexpression of a variety of Bcl-2 family members. Virology **319:**212-224.
345. **Javouhey E, Gibert B, Arrigo AP, Diaz JJ, Diaz-Latoud C.** 2008. Protection against heat and staurosporine mediated apoptosis by the HSV-1 US11 protein. Virology **376:**31-41.
346. **Goldmacher VS, Bartle LM, Skaletskaya A, Dionne CA, Kedersha NL, Vater CA, Han JW, Lutz RJ, Watanabe S, Cahir McFarland ED, Kieff ED, Mocarski ES, Chittenden T.** 1999. A cytomegalovirus-encoded mitochondria-localized inhibitor of apoptosis structurally unrelated to Bcl-2. Proc Natl Acad Sci U S A **96:**12536-12541.
347. **Reeves MB, Davies AA, McSharry BP, Wilkinson GW, Sinclair JH.** 2007. Complex I binding by a virally encoded RNA regulates mitochondria-induced cell death. Science **316:**1345-1348.
348. **Henderson S, Huen D, Rowe M, Dawson C, Johnson G, Rickinson A.** 1993. Epstein-Barr virus-coded BHRF1 protein, a viral homologue of Bcl-2, protects human B cells from programmed cell death. Proc Natl Acad Sci U S A **90:**8479-8483.
349. **Hickish T, Robertson D, Clarke P, Hill M, di Stefano F, Clarke C, Cunningham D.** 1994. Ultrastructural localization of BHRF1: an Epstein-

Barr virus gene product which has homology with bcl-2. Cancer Res **54:**2808-2811.
350. **Kawanishi M, Tada-Oikawa S, Kawanishi S.** 2002. Epstein-Barr virus BHRF1 functions downstream of Bid cleavage and upstream of mitochondrial dysfunction to inhibit TRAIL-induced apoptosis in BJAB cells. Biochem Biophys Res Commun **297:**682-687.
351. **Cheng EH, Nicholas J, Bellows DS, Hayward GS, Guo HG, Reitz MS, Hardwick JM.** 1997. A Bcl-2 homolog encoded by Kaposi sarcoma-associated virus, human herpesvirus 8, inhibits apoptosis but does not heterodimerize with Bax or Bak. Proc Natl Acad Sci U S A **94:**690-694.
352. **Sharp TV, Wang HW, Koumi A, Hollyman D, Endo Y, Ye H, Du MQ, Boshoff C.** 2002. K15 protein of Kaposi's sarcoma-associated herpesvirus is latently expressed and binds to HAX-1, a protein with antiapoptotic function. J Virol **76:**802-816.
353. **Wang HW, Sharp TV, Koumi A, Koentges G, Boshoff C.** 2002. Characterization of an anti-apoptotic glycoprotein encoded by Kaposi's sarcoma-associated herpesvirus which resembles a spliced variant of human survivin. Embo J **21:**2602-2615.
354. **Feng P, Park J, Lee BS, Lee SH, Bram RJ, Jung JU.** 2002. Kaposi's sarcoma-associated herpesvirus mitochondrial K7 protein targets a cellular calcium-modulating cyclophilin ligand to modulate intracellular calcium concentration and inhibit apoptosis. J Virol **76:**11491-11504.
355. **Xing J, Wang S, Lin R, Mossman KL, Zheng C.** 2012. Herpes simplex virus 1 tegument protein US11 downmodulates the RLR signaling pathway via direct interaction with RIG-I and MDA-5. J Virol **86:**3528-3540.
356. **Murata T, Goshima F, Daikoku T, Inagaki-Ohara K, Takakuwa H, Kato K, Nishiyama Y.** 2000. Mitochondrial distribution and function in herpes simplex virus-infected cells. J Gen Virol **81:**401-406.
357. **Derakhshan M, Willcocks MM, Salako MA, Kass GE, Carter MJ.** 2006. Human herpesvirus 1 protein US3 induces an inhibition of mitochondrial electron transport. J Gen Virol **87:**2155-2159.
358. **Delgado T, Carroll PA, Punjabi AS, Margineantu D, Hockenbery DM, Lagunoff M.** 2010. Induction of the Warburg effect by Kaposi's sarcoma herpesvirus is required for the maintenance of latently infected endothelial cells. Proc Natl Acad Sci U S A **107:**10696-10701.
359. **Lund K, Ziola B.** 1985. Cell sonicates used in the analysis of how measles and herpes simplex type 1 virus infections influence Vero cell mitochondrial calcium uptake. Can J Biochem Cell Biol **63:**1194-1197.
360. **Aubert M, Chen Z, Lang R, Dang CH, Fowler C, Sloan DD, Jerome KR.** 2008. The antiapoptotic herpes simplex virus glycoprotein J localizes to multiple cellular organelles and induces reactive oxygen species formation. J Virol **82:**617-629.
361. **Thurau M, Marquardt G, Gonin-Laurent N, Weinlander K, Naschberger E, Jochmann R, Alkharsah KR, Schulz TF, Thome M, Neipel F, Sturzl M.** 2009. Viral inhibitor of apoptosis vFLIP/K13 protects

endothelial cells against superoxide-induced cell death. J Virol **83:**598-611.
362. **Munger J, Bajad SU, Coller HA, Shenk T, Rabinowitz JD.** 2006. Dynamics of the cellular metabolome during human cytomegalovirus infection. PLoS Pathog **2:**e132.
363. **Kaarbo M, Ager-Wick E, Osenbroch PO, Kilander A, Skinnes R, Muller F, Eide L.** 2011. Human cytomegalovirus infection increases mitochondrial biogenesis. Mitochondrion **11:**935-945.
364. **Poncet D, Pauleau AL, Szabadkai G, Vozza A, Scholz SR, Le Bras M, Briere JJ, Jalil A, Le Moigne R, Brenner C, Hahn G, Wittig I, Schagger H, Lemaire C, Bianchi K, Souquere S, Pierron G, Rustin P, Goldmacher VS, Rizzuto R, Palmieri F, Kroemer G.** 2006. Cytopathic effects of the cytomegalovirus-encoded apoptosis inhibitory protein vMIA. J Cell Biol **174:**985-996.
365. **Seo JY, Yaneva R, Hinson ER, Cresswell P.** 2011. Human cytomegalovirus directly induces the antiviral protein viperin to enhance infectivity. Science **332:**1093-1097.
366. **McCormick AL, Smith VL, Chow D, Mocarski ES.** 2003. Disruption of mitochondrial networks by the human cytomegalovirus UL37 gene product viral mitochondrion-localized inhibitor of apoptosis. J Virol **77:**631-641.
367. **LaJeunesse DR, Brooks K, Adamson AL.** 2005. Epstein-Barr virus immediate-early proteins BZLF1 and BRLF1 alter mitochondrial morphology during lytic replication. Biochem Biophys Res Commun **333:**438-442.
368. **Yeo WM, Isegawa Y, Chow VT.** 2008. The U95 protein of human herpesvirus 6B interacts with human GRIM-19: silencing of U95 expression reduces viral load and abrogates loss of mitochondrial membrane potential. J Virol **82:**1011-1020.
369. **Kramer T, Enquist LW.** 2012. Alphaherpesvirus infection disrupts mitochondrial transport in neurons. Cell Host Microbe **11:**504-514.
370. **Timmis JN, Ayliffe MA, Huang CY, Martin W.** 2004. Endosymbiotic gene transfer: organelle genomes forge eukaryotic chromosomes. Nat Rev Genet **5:**123-135.
371. **Radloff R, Bauer W, Vinograd J.** 1967. A dye-buoyant-density method for the detection and isolation of closed circular duplex DNA: the closed circular DNA in HeLa cells. Proc Natl Acad Sci U S A **57:**1514-1521.
372. **Anderson S, Bankier AT, Barrell BG, de Bruijn MH, Coulson AR, Drouin J, Eperon IC, Nierlich DP, Roe BA, Sanger F, Schreier PH, Smith AJ, Staden R, Young IG.** 1981. Sequence and organization of the human mitochondrial genome. Nature **290:**457-465.
373. **Rorbach J, Minczuk M.** 2012. The post-transcriptional life of mammalian mitochondrial RNA. Biochem J **444:**357-373.
374. **Barrell BG, Bankier AT, Drouin J.** 1979. A different genetic code in human mitochondria. Nature **282:**189-194.

375. **Chomyn A, Mariottini P, Cleeter MW, Ragan CI, Matsuno-Yagi A, Hatefi Y, Doolittle RF, Attardi G.** 1985. Six unidentified reading frames of human mitochondrial DNA encode components of the respiratory-chain NADH dehydrogenase. Nature **314:**592-597.
376. **Chomyn A, Cleeter MW, Ragan CI, Riley M, Doolittle RF, Attardi G.** 1986. URF6, last unidentified reading frame of human mtDNA, codes for an NADH dehydrogenase subunit. Science **234:**614-618.
377. **Fernandez-Silva P, Enriquez JA, Montoya J.** 2003. Replication and transcription of mammalian mitochondrial DNA. Exp Physiol **88:**41-56.
378. **Hensen F, Cansiz S, Gerhold JM, Spelbrink JN.** 2014. To be or not to be a nucleoid protein: A comparison of mass-spectrometry based approaches in the identification of potential mtDNA-nucleoid associated proteins. Biochimie **100:**219-226.
379. **Bogenhagen D, Clayton DA.** 1977. Mouse L cell mitochondrial DNA molecules are selected randomly for replication throughout the cell cycle. Cell **11:**719-727.
380. **Holt IJ, Reyes A.** 2012. Human mitochondrial DNA replication. Cold Spring Harb Perspect Biol **4**.
381. **McKinney EA, Oliveira MT.** 2013. Replicating animal mitochondrial DNA. Genet Mol Biol **36:**308-315.
382. **Yang MY, Bowmaker M, Reyes A, Vergani L, Angeli P, Gringeri E, Jacobs HT, Holt IJ.** 2002. Biased incorporation of ribonucleotides on the mitochondrial L-strand accounts for apparent strand-asymmetric DNA replication. Cell **111:**495-505.
383. **Korhonen JA, Pham XH, Pellegrini M, Falkenberg M.** 2004. Reconstitution of a minimal mtDNA replisome in vitro. Embo J **23:**2423-2429.
384. **Cerritelli SM, Frolova EG, Feng C, Grinberg A, Love PE, Crouch RJ.** 2003. Failure to produce mitochondrial DNA results in embryonic lethality in Rnaseh1 null mice. Mol Cell **11:**807-815.
385. **Ruhanen H, Ushakov K, Yasukawa T.** 2011. Involvement of DNA ligase III and ribonuclease H1 in mitochondrial DNA replication in cultured human cells. Biochim Biophys Acta **1813:**2000-2007.
386. **De A, Campbell C.** 2007. A novel interaction between DNA ligase III and DNA polymerase gamma plays an essential role in mitochondrial DNA stability. Biochem J **402:**175-186.
387. **Zhang H, Pommier Y.** 2008. Mitochondrial topoisomerase I sites in the regulatory D-loop region of mitochondrial DNA. Biochemistry **47:**11196-11203.
388. **Fuste JM, Wanrooij S, Jemt E, Granycome CE, Cluett TJ, Shi Y, Atanassova N, Holt IJ, Gustafsson CM, Falkenberg M.** 2010. Mitochondrial RNA polymerase is needed for activation of the origin of light-strand DNA replication. Mol Cell **37:**67-78.
389. **Cote J, Ruiz-Carrillo A.** 1993. Primers for mitochondrial DNA replication generated by endonuclease G. Science **261:**765-769.

390. **McDermott-Roe C, Ye J, Ahmed R, Sun XM, Serafin A, Ware J, Bottolo L, Muckett P, Canas X, Zhang J, Rowe GC, Buchan R, Lu H, Braithwaite A, Mancini M, Hauton D, Marti R, Garcia-Arumi E, Hubner N, Jacob H, Serikawa T, Zidek V, Papousek F, Kolar F, Cardona M, Ruiz-Meana M, Garcia-Dorado D, Comella JX, Felkin LE, Barton PJ, Arany Z, Pravenec M, Petretto E, Sanchis D, Cook SA.** 2011. Endonuclease G is a novel determinant of cardiac hypertrophy and mitochondrial function. Nature **478:**114-118.
391. **Yakes FM, Van Houten B.** 1997. Mitochondrial DNA damage is more extensive and persists longer than nuclear DNA damage in human cells following oxidative stress. Proc Natl Acad Sci U S A **94:**514-519.
392. **Hudson EK, Hogue BA, Souza-Pinto NC, Croteau DL, Anson RM, Bohr VA, Hansford RG.** 1998. Age-associated change in mitochondrial DNA damage. Free Radic Res **29:**573-579.
393. **Mason PA, Matheson EC, Hall AG, Lightowlers RN.** 2003. Mismatch repair activity in mammalian mitochondria. Nucleic Acids Res **31:**1052-1058.
394. **de Souza-Pinto NC, Mason PA, Hashiguchi K, Weissman L, Tian J, Guay D, Lebel M, Stevnsner TV, Rasmussen LJ, Bohr VA.** 2009. Novel DNA mismatch-repair activity involving YB-1 in human mitochondria. DNA Repair (Amst) **8:**704-719.
395. **Sykora P, Croteau DL, Bohr VA, Wilson DM, 3rd.** 2011. Aprataxin localizes to mitochondria and preserves mitochondrial function. Proc Natl Acad Sci U S A **108:**7437-7442.
396. **Kamenisch Y, Fousteri M, Knoch J, von Thaler AK, Fehrenbacher B, Kato H, Becker T, Dolle ME, Kuiper R, Majora M, Schaller M, van der Horst GT, van Steeg H, Rocken M, Rapaport D, Krutmann J, Mullenders LH, Berneburg M.** 2010. Proteins of nucleotide and base excision repair pathways interact in mitochondria to protect from loss of subcutaneous fat, a hallmark of aging. J Exp Med **207:**379-390.
397. **Aamann MD, Sorensen MM, Hvitby C, Berquist BR, Muftuoglu M, Tian J, de Souza-Pinto NC, Scheibye-Knudsen M, Wilson DM, 3rd, Stevnsner T, Bohr VA.** 2010. Cockayne syndrome group B protein promotes mitochondrial DNA stability by supporting the DNA repair association with the mitochondrial membrane. FASEB J **24:**2334-2346.
398. **Anderson CT, Friedberg EC.** 1980. The presence of nuclear and mitochondrial uracil-DNA glycosylase in extracts of human KB cells. Nucleic Acids Res **8:**875-888.
399. **Chien CY, Chou CK, Su JY.** 2009. Ung1p-mediated uracil-base excision repair in mitochondria is responsible for the petite formation in thymidylate deficient yeast. FEBS Lett **583:**1499-1504.
400. **Tell G, Crivellato E, Pines A, Paron I, Pucillo C, Manzini G, Bandiera A, Kelley MR, Di Loreto C, Damante G.** 2001. Mitochondrial localization of APE/Ref-1 in thyroid cells. Mutat Res **485:**143-152.
401. **Tsuchimoto D, Sakai Y, Sakumi K, Nishioka K, Sasaki M, Fujiwara T, Nakabeppu Y.** 2001. Human APE2 protein is mostly localized in the

nuclei and to some extent in the mitochondria, while nuclear APE2 is partly associated with proliferating cell nuclear antigen. Nucleic Acids Res **29:**2349-2360.

402. **Chattopadhyay R, Wiederhold L, Szczesny B, Boldogh I, Hazra TK, Izumi T, Mitra S.** 2006. Identification and characterization of mitochondrial abasic (AP)-endonuclease in mammalian cells. Nucleic Acids Res **34:**2067-2076.
403. **Vogel KS, Perez M, Momand JR, Acevedo-Torres K, Hildreth K, Garcia RA, Torres-Ramos CA, Ayala-Torres S, Prihoda TJ, McMahan CA, Walter CA.** 2011. Age-related instability in spermatogenic cell nuclear and mitochondrial DNA obtained from Apex1 heterozygous mice. Mol Reprod Dev **78:**906-919.
404. **Liu P, Qian L, Sung JS, de Souza-Pinto NC, Zheng L, Bogenhagen DF, Bohr VA, Wilson DM, 3rd, Shen B, Demple B.** 2008. Removal of oxidative DNA damage via FEN1-dependent long-patch base excision repair in human cell mitochondria. Mol Cell Biol **28:**4975-4987.
405. **Kalifa L, Beutner G, Phadnis N, Sheu SS, Sia EA.** 2009. Evidence for a role of FEN1 in maintaining mitochondrial DNA integrity. DNA Repair (Amst) **8:**1242-1249.
406. **Zheng L, Zhou M, Guo Z, Lu H, Qian L, Dai H, Qiu J, Yakubovskaya E, Bogenhagen DF, Demple B, Shen B.** 2008. Human DNA2 is a mitochondrial nuclease/helicase for efficient processing of DNA replication and repair intermediates. Mol Cell **32:**325-336.
407. **Duxin JP, Dao B, Martinsson P, Rajala N, Guittat L, Campbell JL, Spelbrink JN, Stewart SA.** 2009. Human Dna2 is a nuclear and mitochondrial DNA maintenance protein. Mol Cell Biol **29:**4274-4282.
408. **Das BB, Dexheimer TS, Maddali K, Pommier Y.** 2010. Role of tyrosyl-DNA phosphodiesterase (TDP1) in mitochondria. Proc Natl Acad Sci U S A **107:**19790-19795.
409. **Szczesny B, Tann AW, Longley MJ, Copeland WC, Mitra S.** 2008. Long patch base excision repair in mammalian mitochondrial genomes. J Biol Chem **283:**26349-26356.
410. **Tann AW, Boldogh I, Meiss G, Qian W, Van Houten B, Mitra S, Szczesny B.** 2011. Apoptosis induced by persistent single-strand breaks in mitochondrial genome: critical role of EXOG (5'-EXO/endonuclease) in their repair. J Biol Chem **286:**31975-31983.
411. **Randahl H, Elliott GC, Linn S.** 1988. DNA-repair reactions by purified HeLa DNA polymerases and exonucleases. J Biol Chem **263:**12228-12234.
412. **Pinz KG, Bogenhagen DF.** 1998. Efficient repair of abasic sites in DNA by mitochondrial enzymes. Mol Cell Biol **18:**1257-1265.
413. **Pinz KG, Bogenhagen DF.** 2000. Characterization of a catalytically slow AP lyase activity in DNA polymerase gamma and other family A DNA polymerases. J Biol Chem **275:**12509-12514.
414. **Lakshmipathy U, Campbell C.** 1999. The human DNA ligase III gene encodes nuclear and mitochondrial proteins. Mol Cell Biol **19:**3869-3876.

415. **Lakshmipathy U, Campbell C.** 2001. Antisense-mediated decrease in DNA ligase III expression results in reduced mitochondrial DNA integrity. Nucleic Acids Res **29:**668-676.
416. **Simsek D, Furda A, Gao Y, Artus J, Brunet E, Hadjantonakis AK, Van Houten B, Shuman S, McKinnon PJ, Jasin M.** 2011. Crucial role for DNA ligase III in mitochondria but not in Xrcc1-dependent repair. Nature **471:**245-248.
417. **Gao Y, Katyal S, Lee Y, Zhao J, Rehg JE, Russell HR, McKinnon PJ.** 2011. DNA ligase III is critical for mtDNA integrity but not Xrcc1-mediated nuclear DNA repair. Nature **471:**240-244.
418. **Shokolenko IN, Wilson GL, Alexeyev MF.** 2013. Persistent damage induces mitochondrial DNA degradation. DNA Repair (Amst) **12:**488-499.
419. **Bridges EG, Jiang Z, Cheng YC.** 1999. Characterization of a dCTP transport activity reconstituted from human mitochondria. J Biol Chem **274:**4620-4625.
420. **Ferraro P, Nicolosi L, Bernardi P, Reichard P, Bianchi V.** 2006. Mitochondrial deoxynucleotide pool sizes in mouse liver and evidence for a transport mechanism for thymidine monophosphate. Proc Natl Acad Sci U S A **103:**18586-18591.
421. **Berk AJ, Clayton DA.** 1973. A genetically distinct thymidine kinase in mammalian mitochondria. Exclusive labeling of mitochondrial deoxyribonucleic acid. J Biol Chem **248:**2722-2729.
422. **Gower WR, Jr., Carr MC, Ives DH.** 1979. Deoxyguanosine kinase. Distinct molecular forms in mitochondria and cytosol. J Biol Chem **254:**2180-2183.
423. **Copeland WC.** 2008. Inherited mitochondrial diseases of DNA replication. Annu Rev Med **59:**131-146.
424. **Rotig A, Poulton J.** 2009. Genetic causes of mitochondrial DNA depletion in humans. Biochim Biophys Acta **1792:**1103-1108.
425. **Copeland WC.** 2012. Defects in mitochondrial DNA replication and human disease. Crit Rev Biochem Mol Biol **47:**64-74.
426. **Liang BC, Ullyatt E.** 1998. Increased sensitivity to cis-diamminedichloroplatinum induced apoptosis with mitochondrial DNA depletion. Cell Death Differ **5:**694-701.
427. **Kessel D, Sun HH.** 1999. Enhanced responsiveness to photodynamic therapy-induced apoptosis after mitochondrial DNA depletion. Photochem Photobiol **70:**937-940.
428. **Liu CY, Lee CF, Hong CH, Wei YH.** 2004. Mitochondrial DNA mutation and depletion increase the susceptibility of human cells to apoptosis. Ann N Y Acad Sci **1011:**133-145.
429. **Biswas G, Anandatheerthavarada HK, Avadhani NG.** 2005. Mechanism of mitochondrial stress-induced resistance to apoptosis in mitochondrial DNA-depleted C2C12 myocytes. Cell Death Differ **12:**266-278.

430. **Yen HC, Tang YC, Chen FY, Chen SW, Majima HJ.** 2005. Enhancement of cisplatin-induced apoptosis and caspase 3 activation by depletion of mitochondrial DNA in a human osteosarcoma cell line. Ann N Y Acad Sci **1042:**516-522.
431. **Higuchi M, Kudo T, Suzuki S, Evans TT, Sasaki R, Wada Y, Shirakawa T, Sawyer JR, Gotoh A.** 2006. Mitochondrial DNA determines androgen dependence in prostate cancer cell lines. Oncogene **25:**1437-1445.
432. **Jacques C, Chevrollier A, Loiseau D, Lagoutte L, Savagner F, Malthiery Y, Reynier P.** 2006. mtDNA controls expression of the Death Associated Protein 3. Exp Cell Res **312:**737-745.
433. **Yu M, Shi Y, Wei X, Yang Y, Zhou Y, Hao X, Zhang N, Niu R.** 2007. Depletion of mitochondrial DNA by ethidium bromide treatment inhibits the proliferation and tumorigenesis of T47D human breast cancer cells. Toxicol Lett **170:**83-93.
434. **Suzuki S, Naito A, Asano T, Evans TT, Reddy SA, Higuchi M.** 2008. Constitutive activation of AKT pathway inhibits TNF-induced apoptosis in mitochondrial DNA-deficient human myelogenous leukemia ML-1a. Cancer Lett **268:**31-37.
435. **Ivanov VN, Ghandhi SA, Zhou H, Huang SX, Chai Y, Amundson SA, Hei TK.** 2011. Radiation response and regulation of apoptosis induced by a combination of TRAIL and CHX in cells lacking mitochondrial DNA: a role for NF-kappaB-STAT3-directed gene expression. Exp Cell Res **317:**1548-1566.
436. **Marin JJ, Hernandez A, Revuelta IE, Gonzalez-Sanchez E, Gonzalez-Buitrago JM, Perez MJ.** 2013. Mitochondrial genome depletion in human liver cells abolishes bile acid-induced apoptosis: Role of the Akt/mTOR survival pathway and Bcl-2 family proteins. Free Radic Biol Med **61C:**218-228.
437. **Cloos CR, Daniels DH, Kalen A, Matthews K, Du J, Goswami PC, Cullen JJ.** 2009. Mitochondrial DNA depletion induces radioresistance by suppressing G2 checkpoint activation in human pancreatic cancer cells. Radiat Res **171:**581-587.
438. **Crider DG, Garcia-Rodriguez LJ, Srivastava P, Peraza-Reyes L, Upadhyaya K, Boldogh IR, Pon LA.** 2012. Rad53 is essential for a mitochondrial DNA inheritance checkpoint regulating G1 to S progression. J Cell Biol **198:**793-798.
439. **Cavalli LR, Varella-Garcia M, Liang BC.** 1997. Diminished tumorigenic phenotype after depletion of mitochondrial DNA. Cell Growth Differ **8:**1189-1198.
440. **Moro L, Arbini AA, Marra E, Greco M.** 2008. Mitochondrial DNA depletion reduces PARP-1 levels and promotes progression of the neoplastic phenotype in prostate carcinoma. Cell Oncol **30:**307-322.
441. **Hamer I, Delaive E, Dieu M, Abdel-Sater F, Mercy L, Jadot M, Arnould T.** 2009. Up-regulation of cathepsin B expression and enhanced

secretion in mitochondrial DNA-depleted osteosarcoma cells. Biol Cell **101:**31-41.

442. **Moro L, Arbini AA, Yao JL, di Sant'Agnese PA, Marra E, Greco M.** 2009. Mitochondrial DNA depletion in prostate epithelial cells promotes anoikis resistance and invasion through activation of PI3K/Akt2. Cell Death Differ **16:**571-583.
443. **Soejima A, Inoue K, Takai D, Kaneko M, Ishihara H, Oka Y, Hayashi JI.** 1996. Mitochondrial DNA is required for regulation of glucose-stimulated insulin secretion in a mouse pancreatic beta cell line, MIN6. J Biol Chem **271:**26194-26199.
444. **Kennedy ED, Maechler P, Wollheim CB.** 1998. Effects of depletion of mitochondrial DNA in metabolism secretion coupling in INS-1 cells. Diabetes **47:**374-380.
445. **Park KS, Nam KJ, Kim JW, Lee YB, Han CY, Jeong JK, Lee HK, Pak YK.** 2001. Depletion of mitochondrial DNA alters glucose metabolism in SK-Hep1 cells. Am J Physiol Endocrinol Metab **280:**E1007-1014.
446. **Park SY, Lee W.** 2007. The depletion of cellular mitochondrial DNA causes insulin resistance through the alteration of insulin receptor substrate-1 in rat myocytes. Diabetes Res Clin Pract **77 Suppl 1:**S165-171.
447. **Latchman DS.** 1988. Effect of herpes simplex virus type 2 infection on mitochondrial gene expression. J Gen Virol **69 (Pt 6):**1405-1410.
448. **Wiedmer A, Wang P, Zhou J, Rennekamp AJ, Tiranti V, Zeviani M, Lieberman PM.** 2008. Epstein-Barr virus immediate-early protein Zta co-opts mitochondrial single-stranded DNA binding protein to promote viral and inhibit mitochondrial DNA replication. J Virol **82:**4647-4655.
449. **Bujnicki JM, Rychlewski L.** 2001. The herpesvirus alkaline exonuclease belongs to the restriction endonuclease PD-(D/E)XK superfamily: insight from molecular modeling and phylogenetic analysis. Virus Genes **22:**219-230.
450. **Keir HM, Gold E.** 1963. Deoxyrbionucleic acid nucleotidyltransferase and deoxyribonuclease from cultured cells infected with herpes simplex virus. Biochimica et Biophysica Acta (BBA) - Specialized Section on Nucleic Acids and Related Subjects **72:**263-276.
451. **Francke B, Moss H, Timbury MC, Hay J.** 1978. Alkaline DNase activity in cells infected with a temperature-sensitive mutant of herpes simplex virus type 2. J Virol **26:**209-213.
452. **Hoffmann PJ, Cheng YC.** 1978. The deoxyribonuclease induced after infection of KB cells by herpes simplex virus type 1 or type 2. I. Purification and characterization of the enzyme. J Biol Chem **253:**3557-3562.
453. **Baylis SA, Purifoy DJ, Littler E.** 1989. The characterization of the EBV alkaline deoxyribonuclease cloned and expressed in E. coli. Nucleic Acids Res **17:**7609-7622.

454. **Chee MS, Bankier AT, Beck S, Bohni R, Brown CM, Cerny R, Horsnell T, Hutchison CA, 3rd, Kouzarides T, Martignetti JA, et al.** 1990. Analysis of the protein-coding content of the sequence of human cytomegalovirus strain AD169. Curr Top Microbiol Immunol **154:**125-169.
455. **Sheaffer AK, Weinheimer SP, Tenney DJ.** 1997. The human cytomegalovirus UL98 gene encodes the conserved herpesvirus alkaline nuclease. J Gen Virol **78 (Pt 11):**2953-2961.
456. **Mueller NH, Gilden D, Cohrs RJ.** 2013. Varicella-Zoster virus open reading frame 48 encodes an active nuclease. J Virol **87:**11936-11938.
457. **Strobel-Fidler M, Francke B.** 1980. Alkaline deoxyribonuclease induced by herpes simplex virus type 1: composition and properties of the purified enzyme. Virology **103:**493-501.
458. **Banks L, Purifoy DJ, Hurst PF, Killington RA, Powell KL.** 1983. Herpes simplex virus non-structural proteins. IV. Purification of the virus-induced deoxyribonuclease and characterization of the enzyme using monoclonal antibodies. J Gen Virol **64 (Pt 10):**2249-2260.
459. **Bronstein JC, Weller SK, Weber PC.** 1997. The product of the UL12.5 gene of herpes simplex virus type 1 is a capsid-associated nuclease. J Virol **71:**3039-3047.
460. **Henderson JO, Ball-Goodrich LJ, Parris DS.** 1998. Structure-function analysis of the herpes simplex virus type 1 UL12 gene: correlation of deoxyribonuclease activity in vitro with replication function. Virology **243:**247-259.
461. **Reuven NB, Antoku S, Weller SK.** 2004. The UL12.5 gene product of herpes simplex virus type 1 exhibits nuclease and strand exchange activities but does not localize to the nucleus. J Virol **78:**4599-4608.
462. **Hoffmann PJ, Cheng YC.** 1979. DNase induced after infection of KB cells by herpes simplex virus type 1 or type 2. II. Characterization of an associated endonuclease activity. J Virol **32:**449-457.
463. **Bronstein JC, Weber PC.** 1996. Purification and characterization of herpes simplex virus type 1 alkaline exonuclease expressed in Escherichia coli. J Virol **70:**2008-2013.
464. **Banks LM, Halliburton IW, Purifoy DJ, Killington RA, Powell KL.** 1985. Studies on the herpes simplex virus alkaline nuclease: detection of type-common and type-specific epitopes on the enzyme. J Gen Virol **66 (Pt 1):**1-14.
465. **Daikoku T, Yamashita Y, Tsurumi T, Nishiyama Y.** 1995. The US3 protein kinase of herpes simplex virus type 2 is associated with phosphorylation of the UL12 alkaline nuclease in vitro. Arch Virol **140:**1637-1644.
466. **Balasubramanian N, Bai P, Buchek G, Korza G, Weller SK.** 2010. Physical interaction between the herpes simplex virus type 1 exonuclease, UL12, and the DNA double-strand break-sensing MRN complex. J Virol **84:**12504-12514.

467. **Mohni KN, Mastrocola AS, Bai P, Weller SK, Heinen CD.** 2011. DNA mismatch repair proteins are required for efficient herpes simplex virus 1 replication. J Virol **85:**12241-12253.
468. **Martinez R, Goldstein JN, Weller SK.** 2002. The product of the UL12.5 gene of herpes simplex virus type 1 is not essential for lytic viral growth and is not specifically associated with capsids. Virology **298:**248-257.
469. **King MP, Attardi G.** 1989. Human cells lacking mtDNA: repopulation with exogenous mitochondria by complementation. Science **246:**500-503.
470. **Scherer WF, Syverton JT, Gey GO.** 1953. Studies on the propagation in vitro of poliomyelitis viruses. IV. Viral multiplication in a stable strain of human malignant epithelial cells (strain HeLa) derived from an epidermoid carcinoma of the cervix. J Exp Med **97:**695-710.
471. **Jacobs JP, Jones CM, Baille JP.** 1970. Characteristics of a human diploid cell designated MRC-5. Nature **227:**168-170.
472. **Miller G, Shope T, Lisco H, Stitt D, Lipman M.** 1972. Epstein-Barr virus: transformation, cytopathic changes, and viral antigens in squirrel monkey and marmoset leukocytes. Proc Natl Acad Sci U S A **69:**383-387.
473. **Gierasch WW, Zimmerman DL, Ward SL, Vanheyningen TK, Romine JD, Leib DA.** 2006. Construction and characterization of bacterial artificial chromosomes containing HSV-1 strains 17 and KOS. J Virol Methods **135:**197-206.
474. **Heckman KL, Pease LR.** 2007. Gene splicing and mutagenesis by PCR-driven overlap extension. Nat Protoc **2:**924-932.
475. **Corcoran JA, Saffran HA, Duguay BA, Smiley JR.** 2009. Herpes simplex virus UL12.5 targets mitochondria through a mitochondrial localization sequence proximal to the N terminus. J Virol **83:**2601-2610.
476. **Zeghouf M, Li J, Butland G, Borkowska A, Canadien V, Richards D, Beattie B, Emili A, Greenblatt JF.** 2004. Sequential Peptide Affinity (SPA) system for the identification of mammalian and bacterial protein complexes. J Proteome Res **3:**463-468.
477. **Ahn BH, Kim HS, Song S, Lee IH, Liu J, Vassilopoulos A, Deng CX, Finkel T.** 2008. A role for the mitochondrial deacetylase Sirt3 in regulating energy homeostasis. Proc Natl Acad Sci U S A **105:**14447-14452.
478. **Warming S, Costantino N, Court DL, Jenkins NA, Copeland NG.** 2005. Simple and highly efficient BAC recombineering using galK selection. Nucleic Acids Res **33:**e36.
479. **Kozak M.** 1984. Compilation and analysis of sequences upstream from the translational start site in eukaryotic mRNAs. Nucleic Acids Res **12:**857-872.
480. **Hwang PM, Bunz F, Yu J, Rago C, Chan TA, Murphy MP, Kelso GF, Smith RA, Kinzler KW, Vogelstein B.** 2001. Ferredoxin reductase affects p53-dependent, 5-fluorouracil-induced apoptosis in colorectal cancer cells. Nat Med **7:**1111-1117.

481. **Falcone D, Andrews DW.** 1991. Both the 5' untranslated region and the sequences surrounding the start site contribute to efficient initiation of translation in vitro. Mol Cell Biol **11:**2656-2664.
482. **Wang W, Malcolm BA.** 1999. Two-stage PCR protocol allowing introduction of multiple mutations, deletions and insertions using QuikChange Site-Directed Mutagenesis. Biotechniques **26:**680-682.
483. **Schafer P, Scholz SR, Gimadutdinow O, Cymerman IA, Bujnicki JM, Ruiz-Carrillo A, Pingoud A, Meiss G.** 2004. Structural and functional characterization of mitochondrial EndoG, a sugar non-specific nuclease which plays an important role during apoptosis. J Mol Biol **338:**217-228.
484. **Cymerman IA, Chung I, Beckmann BM, Bujnicki JM, Meiss G.** 2008. EXOG, a novel paralog of Endonuclease G in higher eukaryotes. Nucleic Acids Res **36:**1369-1379.
485. **Shaner NC, Campbell RE, Steinbach PA, Giepmans BN, Palmer AE, Tsien RY.** 2004. Improved monomeric red, orange and yellow fluorescent proteins derived from Discosoma sp. red fluorescent protein. Nat Biotechnol **22:**1567-1572.
486. **Horwich AL, Fenton WA, Williams KR, Kalousek F, Kraus JP, Doolittle RF, Konigsberg W, Rosenberg LE.** 1984. Structure and expression of a complementary DNA for the nuclear coded precursor of human mitochondrial ornithine transcarbamylase. Science **224:**1068-1074.
487. **Claros MG, Vincens P.** 1996. Computational method to predict mitochondrially imported proteins and their targeting sequences. Eur J Biochem **241:**779-786.
488. **Rost B, Yachdav G, Liu J.** 2004. The PredictProtein server. Nucleic Acids Res **32:**W321-326.
489. **Tischer BK, Smith GA, Osterrieder N.** 2010. En passant mutagenesis: a two step markerless red recombination system. Methods Mol Biol **634:**421-430.
490. **Chacinska A, Koehler CM, Milenkovic D, Lithgow T, Pfanner N.** 2009. Importing mitochondrial proteins: machineries and mechanisms. Cell **138:**628-644.
491. **Vogtle FN, Wortelkamp S, Zahedi RP, Becker D, Leidhold C, Gevaert K, Kellermann J, Voos W, Sickmann A, Pfanner N, Meisinger C.** 2009. Global analysis of the mitochondrial N-proteome identifies a processing peptidase critical for protein stability. Cell **139:**428-439.
492. **Freitag H, Neupert W, Benz R.** 1982. Purification and characterisation of a pore protein of the outer mitochondrial membrane from Neurospora crassa. Eur J Biochem **123:**629-636.
493. **Freitag H, Janes M, Neupert W.** 1982. Biosynthesis of mitochondrial porin and insertion into the outer mitochondrial membrane of Neurospora crassa. Eur J Biochem **126:**197-202.
494. **Buisson M, Geoui T, Flot D, Tarbouriech N, Ressing ME, Wiertz EJ, Burmeister WP.** 2009. A bridge crosses the active-site canyon of the Epstein-Barr virus nuclease with DNase and RNase activities. J Mol Biol **391:**717-728.

495. **Dahlroth SL, Gurmu D, Schmitzberger F, Engman H, Haas J, Erlandsen H, Nordlund P.** 2009. Crystal structure of the shutoff and exonuclease protein from the oncogenic Kaposi's sarcoma-associated herpesvirus. Febs J **276:**6636-6645.
496. **Kuchta AL, Parikh H, Zhu Y, Kellogg GE, Parris DS, McVoy MA.** 2012. Structural modelling and mutagenesis of human cytomegalovirus alkaline nuclease UL98. J Gen Virol **93:**130-138.
497. **Horst D, Burmeister WP, Boer IG, van Leeuwen D, Buisson M, Gorbalenya AE, Wiertz EJ, Ressing ME.** 2012. The "Bridge" in the Epstein-Barr virus alkaline exonuclease protein BGLF5 contributes to shutoff activity during productive infection. J Virol **86:**9175-9187.
498. **Ashley N, Harris D, Poulton J.** 2005. Detection of mitochondrial DNA depletion in living human cells using PicoGreen staining. Exp Cell Res **303:**432-446.
499. **Covarrubias S, Gaglia MM, Kumar GR, Wong W, Jackson AO, Glaunsinger BA.** 2011. Coordinated destruction of cellular messages in translation complexes by the gammaherpesvirus host shutoff factor and the mammalian exonuclease Xrn1. PLoS Pathog **7:**e1002339.
500. **Cummings OW, King TC, Holden JA, Low RL.** 1987. Purification and characterization of the potent endonuclease in extracts of bovine heart mitochondria. J Biol Chem **262:**2005-2015.
501. **Gerschenson M, Houmiel KL, Low RL.** 1995. Endonuclease G from mammalian nuclei is identical to the major endonuclease of mitochondria. Nucleic Acids Res **23:**88-97.
502. **Szczesny RJ, Hejnowicz MS, Steczkiewicz K, Muszewska A, Borowski LS, Ginalski K, Dziembowski A.** 2013. Identification of a novel human mitochondrial endo-/exonuclease Ddk1/c20orf72 necessary for maintenance of proper 7S DNA levels. Nucleic Acids Res **41:**3144-3161.
503. **Chow TY, Fraser MJ.** 1983. Purification and properties of single strand DNA-binding endo-exonuclease of Neurospora crassa. J Biol Chem **258:**12010-12018.
504. **Dake E, Hofmann TJ, McIntire S, Hudson A, Zassenhaus HP.** 1988. Purification and properties of the major nuclease from mitochondria of Saccharomyces cerevisiae. J Biol Chem **263:**7691-7702.
505. **Zassenhaus HP, Hofmann TJ, Uthayashanker R, Vincent RD, Zona M.** 1988. Construction of a yeast mutant lacking the mitochondrial nuclease. Nucleic Acids Res **16:**3283-3296.
506. **Ruiz-Carrillo A, Renaud J.** 1987. Endonuclease G: a (dG)n X (dC)n-specific DNase from higher eukaryotes. Embo J **6:**401-407.
507. **Widlak P, Li LY, Wang X, Garrard WT.** 2001. Action of recombinant human apoptotic endonuclease G on naked DNA and chromatin substrates: cooperation with exonuclease and DNase I. J Biol Chem **276:**48404-48409.
508. **Huang KJ, Zemelman BV, Lehman IR.** 2002. Endonuclease G, a candidate human enzyme for the initiation of genomic inversion in herpes simplex type 1 virus. J Biol Chem **277:**21071-21079.

509. **Huang KJ, Ku CC, Lehman IR.** 2006. Endonuclease G: a role for the enzyme in recombination and cellular proliferation. Proc Natl Acad Sci U S A **103:**8995-9000.
510. **Schwer B, North BJ, Frye RA, Ott M, Verdin E.** 2002. The human silent information regulator (Sir)2 homologue hSIRT3 is a mitochondrial nicotinamide adenine dinucleotide-dependent deacetylase. J Cell Biol **158:**647-657.
511. **Parrish J, Li L, Klotz K, Ledwich D, Wang X, Xue D.** 2001. Mitochondrial endonuclease G is important for apoptosis in C. elegans. Nature **412:**90-94.
512. **Cote J, Renaud J, Ruiz-Carrillo A.** 1989. Recognition of (dG)n.(dC)n sequences by endonuclease G. Characterization of the calf thymus nuclease. J Biol Chem **264:**3301-3310.
513. **Tiranti V, Rossi E, Ruiz-Carrillo A, Rossi G, Rocchi M, DiDonato S, Zuffardi O, Zeviani M.** 1995. Chromosomal localization of mitochondrial transcription factor A (TCF6), single-stranded DNA-binding protein (SSBP), and endonuclease G (ENDOG), three human housekeeping genes involved in mitochondrial biogenesis. Genomics **25:**559-564.
514. **DeLuca SZ, O'Farrell PH.** 2012. Barriers to male transmission of mitochondrial DNA in sperm development. Dev Cell **22:**660-668.
515. **Dzierzbicki P, Kaniak-Golik A, Malc E, Mieczkowski P, Ciesla Z.** 2012. The generation of oxidative stress-induced rearrangements in Saccharomyces cerevisiae mtDNA is dependent on the Nuc1 (EndoG/ExoG) nuclease and is enhanced by inactivation of the MRX complex. Mutat Res **740:**21-33.
516. **Hsiang CY, Ho TY, Chang TJ.** 1996. Identification of a pseudorabies virus UL12 (deoxyribonuclease) gene. Gene **177:**109-113.
517. **Zuo J, Thomas W, van Leeuwen D, Middeldorp JM, Wiertz EJ, Ressing ME, Rowe M.** 2008. The DNase of gammaherpesviruses impairs recognition by virus-specific CD8+ T cells through an additional host shutoff function. J Virol **82:**2385-2393.
518. **Peeters-Joris C, Vandevoorde AM, Baudhuin P.** 1975. Subcellular localization of superoxide dismutase in rat liver. Biochem J **150:**31-39.
519. **Eilers M, Schatz G.** 1986. Binding of a specific ligand inhibits import of a purified precursor protein into mitochondria. Nature **322:**228-232.
520. **Mueller NH, Gilden D, Cohrs RJ.** 2013. Varicella-zoster virus open reading frame 48 encodes an active nuclease. J Virol **87:**11936-11938.
521. **Gao M, Robertson BJ, McCann PJ, O'Boyle DR, Weller SK, Newcomb WW, Brown JC, Weinheimer SP.** 1998. Functional conservations of the alkaline nuclease of herpes simplex type 1 and human cytomegalovirus. Virology **249:**460-470.
522. **MacLean CA, Dolan A, Jamieson FE, McGeoch DJ.** 1992. The myristylated virion proteins of herpes simplex virus type 1: investigation of their role in the virus life cycle. J Gen Virol **73 (Pt 3):**539-547.

523. **Shipkowitz NL, Bower RR, Appell RN, Nordeen CW, Overby LR, Roderick WR, Schleicher JB, Von Esch AM.** 1973. Suppression of herpes simplex virus infection by phosphonoacetic acid. Appl Microbiol **26:**264-267.
524. **Overby LR, Robishaw EE, Schleicher JB, Rueter A, Shipkowitz NL, Mao JC.** 1974. Inhibition of herpes simplex virus replication by phosphonoacetic acid. Antimicrob Agents Chemother **6:**360-365.
525. **Mao JC, Robishaw EE, Overby LR.** 1975. Inhibition of DNA polymerase from herpes simplex virus-infected wi-38 cells by phosphonoacetic Acid. J Virol **15:**1281-1283.
526. **Aubert M, Pomeranz LE, Blaho JA.** 2007. Herpes simplex virus blocks apoptosis by precluding mitochondrial cytochrome c release independent of caspase activation in infected human epithelial cells. Apoptosis **12:**19-35.
527. **Tanaka M, Sata T, Kawaguchi Y.** 2008. The product of the Herpes simplex virus 1 UL7 gene interacts with a mitochondrial protein, adenine nucleotide translocator 2. Virol J **5:**125.
528. **Kiebler M, Keil P, Schneider H, van der Klei IJ, Pfanner N, Neupert W.** 1993. The mitochondrial receptor complex: a central role of MOM22 in mediating preprotein transfer from receptors to the general insertion pore. Cell **74:**483-492.
529. **Brix J, Dietmeier K, Pfanner N.** 1997. Differential recognition of preproteins by the purified cytosolic domains of the mitochondrial import receptors Tom20, Tom22, and Tom70. J Biol Chem **272:**20730-20735.
530. **Martin J, Mahlke K, Pfanner N.** 1991. Role of an energized inner membrane in mitochondrial protein import. Delta psi drives the movement of presequences. J Biol Chem **266:**18051-18057.
531. **Hammen PK, Waltner M, Hahnemann B, Heard TS, Weiner H.** 1996. The role of positive charges and structural segments in the presequence of rat liver aldehyde dehydrogenase in import into mitochondria. J Biol Chem **271:**21041-21048.
532. **Mossmann D, Meisinger C, Vogtle FN.** 2012. Processing of mitochondrial presequences. Biochim Biophys Acta **1819:**1098-1106.
533. **Boggaram V, Horowitz P, Waterman MR.** 1985. Studies on rhodanese synthesis in bovine adrenocortical cells. Biochem Biophys Res Commun **130:**407-411.
534. **Miller DM, Delgado R, Chirgwin JM, Hardies SC, Horowitz PM.** 1991. Expression of cloned bovine adrenal rhodanese. J Biol Chem **266:**4686-4691.
535. **Amaya Y, Arakawa H, Takiguchi M, Ebina Y, Yokota S, Mori M.** 1988. A noncleavable signal for mitochondrial import of 3-oxoacyl-CoA thiolase. J Biol Chem **263:**14463-14470.
536. **Finocchiaro G, Colombo I, Garavaglia B, Gellera C, Valdameri G, Garbuglio N, Didonato S.** 1993. cDNA cloning and mitochondrial import of the beta-subunit of the human electron-transfer flavoprotein. Eur J Biochem **213:**1003-1008.

537. **Rospert S, Junne T, Glick BS, Schatz G.** 1993. Cloning and disruption of the gene encoding yeast mitochondrial chaperonin 10, the homolog of E. coli groES. FEBS Lett **335:**358-360.
538. **Ryan MT, Hoogenraad NJ, Hoj PB.** 1994. Isolation of a cDNA clone specifying rat chaperonin 10, a stress-inducible mitochondrial matrix protein synthesised without a cleavable presequence. FEBS Lett **337:**152-156.
539. **Matsushita Y, Isono K.** 1993. Mitochondrial transport of mitoribosomal proteins, YmL8 and YmL20, in Saccharomyces cerevisiae. Eur J Biochem **214:**577-585.
540. **Becker T, Gebert M, Pfanner N, van der Laan M.** 2009. Biogenesis of mitochondrial membrane proteins. Curr Opin Cell Biol **21:**484-493.
541. **Kyte J, Doolittle RF.** 1982. A simple method for displaying the hydropathic character of a protein. J Mol Biol **157:**105-132.
542. **Davies AM, Hershman S, Stabley GJ, Hoek JB, Peterson J, Cahill A.** 2003. A Ca2+-induced mitochondrial permeability transition causes complete release of rat liver endonuclease G activity from its exclusive location within the mitochondrial intermembrane space. Identification of a novel endo-exonuclease activity residing within the mitochondrial matrix. Nucleic Acids Res **31:**1364-1373.
543. **Buttner S, Eisenberg T, Carmona-Gutierrez D, Ruli D, Knauer H, Ruckenstuhl C, Sigrist C, Wissing S, Kollroser M, Frohlich KU, Sigrist S, Madeo F.** 2007. Endonuclease G regulates budding yeast life and death. Mol Cell **25:**233-246.
544. **Zassenhaus HP, Denniger G.** 1994. Analysis of the role of the NUC1 endo/exonuclease in yeast mitochondrial DNA recombination. Curr Genet **25:**142-149.
545. **Kalinowska M, Garncarz W, Pietrowska M, Garrard WT, Widlak P.** 2005. Regulation of the human apoptotic DNase/RNase endonuclease G: involvement of Hsp70 and ATP. Apoptosis **10:**821-830.
546. **Ikeda S, Ozaki K.** 1997. Action of mitochondrial endonuclease G on DNA damaged by L-ascorbic acid, peplomycin, and cis-diamminedichloroplatinum (II). Biochem Biophys Res Commun **235:**291-294.
547. **Kazak L, Reyes A, Holt IJ.** 2012. Minimizing the damage: repair pathways keep mitochondrial DNA intact. Nat Rev Mol Cell Biol **13:**659-671.
548. **Fujii H, Mugitani M, Koyanagi N, Liu Z, Tsuda S, Arii J, Kato A, Kawaguchi Y.** 2014. Role of the Nuclease Activities Encoded by Herpes Simplex Virus 1 UL12 in Viral Replication and Neurovirulence. J Virol **88:**2359-2364.
549. **Rossignol R, Faustin B, Rocher C, Malgat M, Mazat JP, Letellier T.** 2003. Mitochondrial threshold effects. Biochem J **370:**751-762.
550. **Strelow LI, Leib DA.** 1995. Role of the virion host shutoff (vhs) of herpes simplex virus type 1 in latency and pathogenesis. J Virol **69:**6779-6786.

551. **Chou J, Kern ER, Whitley RJ, Roizman B.** 1990. Mapping of herpes simplex virus-1 neurovirulence to gamma 134.5, a gene nonessential for growth in culture. Science **250:**1262-1266.
552. **Desai P, DeLuca NA, Person S.** 1998. Herpes simplex virus type 1 VP26 is not essential for replication in cell culture but influences production of infectious virus in the nervous system of infected mice. Virology **247:**115-124.
553. **Pyles RB, Thompson RL.** 1994. Evidence that the herpes simplex virus type 1 uracil DNA glycosylase is required for efficient viral replication and latency in the murine nervous system. J Virol **68:**4963-4972.
554. **El-Hattab AW, Scaglia F.** 2013. Mitochondrial DNA depletion syndromes: review and updates of genetic basis, manifestations, and therapeutic options. Neurotherapeutics **10:**186-198.
555. **Lee HC, Yin PH, Lin JC, Wu CC, Chen CY, Wu CW, Chi CW, Tam TN, Wei YH.** 2005. Mitochondrial genome instability and mtDNA depletion in human cancers. Ann N Y Acad Sci **1042:**109-122.
556. **Wu CW, Yin PH, Hung WY, Li AF, Li SH, Chi CW, Wei YH, Lee HC.** 2005. Mitochondrial DNA mutations and mitochondrial DNA depletion in gastric cancer. Genes Chromosomes Cancer **44:**19-28.
557. **Tseng LM, Yin PH, Chi CW, Hsu CY, Wu CW, Lee LM, Wei YH, Lee HC.** 2006. Mitochondrial DNA mutations and mitochondrial DNA depletion in breast cancer. Genes Chromosomes Cancer **45:**629-638.
558. **Yu M, Zhou Y, Shi Y, Ning L, Yang Y, Wei X, Zhang N, Hao X, Niu R.** 2007. Reduced mitochondrial DNA copy number is correlated with tumor progression and prognosis in Chinese breast cancer patients. IUBMB Life **59:**450-457.
559. **Kulawiec M, Safina A, Desouki MM, Still I, Matsui S, Bakin A, Singh KK.** 2008. Tumorigenic transformation of human breast epithelial cells induced by mitochondrial DNA depletion. Cancer Biol Ther **7:**1732-1743.
560. **Xing J, Chen M, Wood CG, Lin J, Spitz MR, Ma J, Amos CI, Shields PG, Benowitz NL, Gu J, de Andrade M, Swan GE, Wu X.** 2008. Mitochondrial DNA content: its genetic heritability and association with renal cell carcinoma. J Natl Cancer Inst **100:**1104-1112.
561. **Correia RL, Oba-Shinjo SM, Uno M, Huang N, Marie SK.** 2011. Mitochondrial DNA depletion and its correlation with TFAM, TFB1M, TFB2M and POLG in human diffusely infiltrating astrocytomas. Mitochondrion **11:**48-53.
562. **Koochekpour S, Marlowe T, Singh KK, Attwood K, Chandra D.** 2013. Reduced mitochondrial DNA content associates with poor prognosis of prostate cancer in African American men. PLoS One **8:**e74688.
563. **Rodriguez-Santiago B, Casademont J, Nunes V.** 2001. Is mitochondrial DNA depletion involved in Alzheimer's disease? Eur J Hum Genet **9:**279-285.
564. **Podlesniy P, Figueiro-Silva J, Llado A, Antonell A, Sanchez-Valle R, Alcolea D, Lleo A, Molinuevo JL, Serra N, Trullas R.** 2013. Low

cerebrospinal fluid concentration of mitochondrial DNA in preclinical Alzheimer disease. Ann Neurol **74:**655-668.

565. **Itzhaki RF, Wozniak MA.** 2008. Herpes simplex virus type 1 in Alzheimer's disease: the enemy within. J Alzheimers Dis **13:**393-405.

566. **Agostini S, Clerici M, Mancuso R.** 2014. How plausible is a link between HSV-1 infection and Alzheimer's disease? Expert Rev Anti Infect Ther **12:**275-278.